2 mip

NASA CR-132436

AN OCCULTATION SATELLITE SYSTEM FOR DETERMINING PRESSURE LEVELS IN THE ATMOSPHERE

by

A. R. Morrison, S. G. Ungar, and B. B. Lusignan

Stanford Electronics Laboratories
Stanford University
Stanford, California

prepared for

NATIONAL AERONAUTICS AND SPACE ADMINISTRATION

NASA Langley Research Center
Hampton, Virginia

Contracts NAS1-9962 and NAS1-9963

INTRODUCTION

The potential role of an occultation satellite in the National Weather Satellite system has been investigated under NASA Contracts NAS 1-9962 and NAS 1-9963. Detailed reports of the findings are contained in the two attached volumes: "Orbit Determination for a Weather Occultation Satellite," which describes the outcome of computer simulations of orbit dynamics and data processing procedures that would be used with an occultation system, and "An Occultation Satellite System for Determining Pressure Levels in the Atmosphere," which describes the radio and atmospheric physics of the occultation system, reports on the outcome of a simulation using occultation system data together with satellite infrared sounding data to determine the atmospheric pressure reference, and describes a ground based test of the system in Hawaii and the implications for a satellite occultation system. Following is a brief discussion of these two documents and their implications. The intent is not to summarize the reports, the reports already contain adequate summaries, but rather to relate the findings to each other and to the present needs of the U.S. weather program.

The physical basis of a radio occultation satellite system is that radio waves travel more slowly in the atmosphere than they do in a vacuum. Additionally, if the atmospheric density varies across the path of the radio waves, the radio path will be bent. These two effects combine to make the effective radio path between two satellites longer if the path goes through the atmosphere. The amount of this path increase is a function of the atmospheric density and hence provides the opportunity for measurement of atmospheric variations responsible for the earth's weather.

The use of radio occultation to measure atmospheres is not new. The most precise measurements of the atmospheres of Mars, Venus, and now Jupiter have been obtained by radio occultations of Mariner and Pioneer spacecraft. The equipment used in these efforts has precision far

greater than that required for useful information on the Earth's atmosphere. The physics of radio occultation and the equipment performance have been well established. What remains to be answered is whether the information that can be provided on a continuous operational basis by an earth radio-occultation system is useful to the world's meteorologists and whether the occultation system is the least costly way of obtaining that information.

The work described in the attached reports concludes that the information supplied by an occultation system would indeed be of great use to the meteorologists. However, whether the occultation system is the least costly way of obtaining that information is still to be resolved. The authors feel that is is. But it is clear from reaction to radio occultation proposals, that the cost and performance of other systems designed to obtain equivalent information must be more clearly defined. It is hoped that the upcoming tests of global observation systems and weather prediction technique will help to better define the performance and cost of these alternatives.

.....

There are many ways the radio occultation technique could be employed to obtain useful weather information. The particular system evaluated in the following reports reflects several years of interaction between the authors and members of the meteorological community. The proposed system would provide only information that is very hard to obtain by other measurement techniques. To do this, the system makes use of data readily available from already proven satellite sensors, from existing ground based observations, and from historical records. In other words, the proposed system is intended to be a good match to other components of the weather program.

The occultation system consists of two satellites in the same orbit. One satellite, the "master" satellite, would carry the main instrumentation and data recording equipment; in an operational system this satellite would

also carry other sensors involved in the overall weather observation system. A second, much smaller "slave" satellite, would be located in the same orbit but behind the "master" satellite sufficiently far that radio signals between the two would intersect the atmosphere in the vicinity of the 500 millibar altitude. A transmitter in the "master" satellite would send a radio signal to the receiver in the "slave" satellite. The "slave" satellite would shift the signals in frequency to avoid interference and transmit them back to a raido receiver in the "master" satellite. At the "master", the radio path length would be recorded and relayed to the earth by the normal satellite telemetry system.

The system would use the orbit best suited to the other meteorological sensors, most likely a sun-synchronous polar orbit. The occultation data would provide continuous information in the subsatellite orbit track.

Used in conjunction with other information, the occultation system would provide weather prediction programs with continuous measurements of the world wide 500 millibar pressure reference level with better than 24 meter accuracy. To achieve this, information required from other sources is continuous atmospheric temperature profiles obtained from satellite infrared sounding instruments, historic seasonal averages of lower atmospheric water vapor content, and a few daily surface or upper air pressure level measurements wherever it is most convenient to obtain them.

The major concerns that have been raised about the proposed occultation system are:

- When the inaccuracies of infrared soundings are combined with the expected occultation inaccuracies and the complexities of inversion procedures, will the results have sufficient accuracy for meteorological applications?
- Will the effects of water vapor in the lower atmosphere cause serious errors in the interpretation of the occultation measurements?
- Will complex radio ray paths from inhomogenieties in the lower atmosphere cause loss of data or distortion of results?
- Can the satellites motions in orbit due to inhomogenieties in the earth's gravity field, air drag, and satellite thrusters, be separated from changes in apparent distance caused by atmospheric pressure variations?

Analyses of these questions are presented in great detail in the attached reports. The conclusions are summarized briefly below:

Inversion Accuracy

- To evaluate the accuracy of the occultation system, computer inversion techniques were used to derive pressure references using simulated infrared and occultation data. Actual atmospheric temperature profiles were used to derive infrared measurements and from these "derived" temperature profiles were obtained by inversion techniques. (The derived profiles have no absolute altitude reference.) The actual and "derived" temperature profiles were supplied by Dr. William Smith of the National Oceanic and Atmospheric Administration (NOAA). Next the actual temperature profiles were used to calculate atmospheric density profiles, and raytracing programs calculated "actual" occultation raypath measurements. To these measurements were added 0.5 M rms random errors to simulate occultation measurement errors. The noisy occultation data and "derived" temperature profiles were used in a computer inversion program to obtain estimates of the 500 mb levels. This was done for a range of longitudes and weather conditions. The estimated and actual levels were compared yielding less than 24 M rms errors, which meets the requirements of the weather program. Checks showed that the majority of the error comes from the temperature inversion inaccuracy rather than the occultation system inaccuracy and thus the occultation pressure reference results will improve as the infrared sounding techniques improve.

Water Vapor Effects

- Radio waves are effected by water vapor in the atmosphere as well as by the air density itself. At the higher altitudes water vapor density is not enough to cause a significant effect; but at lower altitudes, especially in the temperate regions in the summer, it must be considered. In the above runs the effects of water vapor were included and different methods of correction were evaluated. To include the effects, actual water vapor profiles for each test day were included in the occultation raytracing procedure. The occultation results and derived temperature profiles were obtained as before. This information was then used together with different estimates of water vapor in the inversion program to obtain estimates of the pressure level. Ignoring water vapor all together, caused systematic pressure level errors in the summer temperate regions that exceeded the desired precision by three to four times. Using the historical average seasonal water vapor profiles for these regions reduced the errors to the 24 M rms requirements. And, as might be expected, using the actual daily water vapor profiles in the inversion, reduced the errors to levels obtained with dry atmospheres.

•Thus even crude climactic data is sufficient to correct for the effect of water vapor on the occultation pressure-reference results. In an operational weather system, better than climactic water vapor information would be available from other components of the observation or forecasting system and would be used in the occultation data inversion.

Multipath

•Multiple ray paths due to water vapor layers in the lower atmosphere is a phenomenon observed during system demonstrations in Hawaii. In these demonstrations equipment similar to that proposed for the occultation measurements was operated between two islands. Amplitude and phase path length measurements were made. The phase measurements confirmed equipment precision and propagation physics. However, during a number of days deep long-term amplitude fading was observed. Computer raytracing was carried out using atmospheric refractivity profiles obtained by airplane flights during the demonstrations. These computations confirmed that on days of deep fades conditions required for persistant deep fading were satisfied. These conditions are that there be two and only two ray paths between transmitter and receiver, that the two signals be very nearly equal in amplitude, and that the paths differ in length by a small number of wavelengths. When these conditions are satisfied, two signals can precisely cancel each other periodically, causing deep fades. In the Hawaiian geometry these conditions can occur fairly often. More than two rays, unequal amplitudes, or a rapid variation of path length difference make the probability of precise cancellation very, very small.

The ray tracing programs were used with the Hawaiian atmospheric refractivity profiles to determine the probability of multipath for occultation satellite geometries. The probability of multipath occurrence will be less than that observed in Hawaii for two reasons: first the primary occultation raypaths will be much higher in the atmosphere, where there is less water vapor to distort them; and secondly, the humidity and layering conditions in Hawaii are much more severe than is typical of other geographic areas and seasons.

The probability of more than one ray path reaching the occultation satellite is thus reduced in comparison with the Hawaiian observations. Furthermore, when multiple paths do occur, the probability that they will cause deep or prolonged fading is very small; none of the three conditions for such fading is satisfied in the satellite geometry. For the satellites three or more rays are involved in any multipath occurrence not just two; this results from the transmitter and receiver being located above the refracting layers, rather than in them. Secondly the multiple rays that reach the satellite pass long distances through significantly different parts of the atmos-

phere, undergoing different focusing and absorption, which changes their relative amplitudes. Thirdly, the phase relationships between the multiple rays will change rapidly as the satellites (and ray paths between them) move at orbital speeds over the weather patterns. In the Hawaiian experiments, the weather moved through the ray paths at a much lower velocity. The probability of three or more rays arriving with the right amplitudes and phases to closely cancel each other for any length of time will thus be very, very small.

The ray tracing programs also showed that when more than one ray existed between transmitter and receiver, the difference in path lengths between the rays was typically less than one-half meter. This would indicate that if the equipment was designed to measure path length in the presence of multiple rays, it would yield usefully accurate results even when more than one ray is received. It was not clear from the ray tracing why this occurred, and more simulations should be done before a system is designed to take advantage of the phenomenon.

The analysis concluded that, while multipath could be expected to occur, it would not occur with high probability, that when it did occur, the probability of deep fading would be remote, and that results obtained during multiple rays would still meet the desired measurement accuracy.

Orbit Analysis

- In the occultation technique, the basic measurement is the effective length of the radio path between two orbiting satellites. When this path passes through the atmosphere, its effective length is increased by bending and retardation. To determine atmospheric pressure to meteorologically useful accuracy, changes in this increase have to be measured to an accuracy of 0.5 M. To accomplish this, of course, requires knowledge of the relative movement of the satellites to the same accuracy.

  To test the predictability of satellite spacing, first computer models were used to simulate the motions of the two satellites. All perturbations of consequence were included; where actual disturbances were unknown, e.g., the higher order components of the gravity field or air drag, random numbers were used to simulate the effect with the expected magnitude.

  Next this "actual" motion was used to derive the information that would be available to the proposed occultation system. In the proposal system the satellites would be launched together and then caused to drift apart over a period of two weeks until they reach the occultation separation. During this drift period, continuous path length measurement between the satellites would be available undistorted by atmospheric bending. After this time, essentially continuous data would still be available but now actual motions of the satellites would be mixed with path lengthening caused by the atmospheric bending, the data for the meteorologists.

Orbit modeling programs then used the drift period data to find coefficients for the orbit elements of both satellites, for all significant elements of the geopotential field and for other factors (such as air drag) effecting the satellite motions. These coefficients were used in the prediction of satellite motion during occultation. The predicted and "actual" were compared to find the kind of errors that would result with this technique. The resulting errors were all acceptable for the meteorological application, but for different reasons.

Perturbations due to the high order components of the earth's gravitational field were predictable well within the 0.5 M accuracy. The drift-period data (actually accurate to 0.03 M) was sufficient to determine the geopotential coefficients to much better accuracy than required. Once these fixed coefficients are determined, relatively crude knowledge of the satellites' positions in the geopotential field during occultation is sufficient to predict the geopotential perturbations of both satellites.

On the other hand, relative drifts of the two satellites due to different drag coefficients could easily accumulate to a steadily increasing separation error exceeding several meters in days. However, there is no way to confuse such a steady increase in path length with an actual meteorological phenomenon. (Is the atmosphere all over the globe expanding at a steady rate?) Data obtained during occultation could be processed so as to attribute any such steady path length growth to drift in the orbit and the data corrected accordingly.

In a similar way, worst-case unknown air drag variation can cause an error in prediction of variation of the orbits' eccentricities, which can amount to a meter or so once-per-orbit oscillation error in the satellite separation prediction. Again, there is not an atmospheric phenomena that would cause a worldwide smooth atmospheric bulge of the form indicated by the eccentricity variation. The data would be processed to filter out the eccentricity harmonics from the path length measurement and to correct eccentricity predictions.

It is assumed that the satellites would use attitude control systems that would fire gas jets only rarely (unloading the momentum in a momentum wheel for instance). Furthermore, control of relative positioning of the satellites would be accomplished by gas thrusters similar to those used for synchronous communications satellites. In this event, changes in relative satellite drift rates from these causes would occur at known times and could also be easily filtered from the data.

For any of these systematic errors, in actual operation it may be advantageous to determine the corrections by comparing occultation measurements against known atmospheric conditions rather than by statistical filtering. Such calibration data is readily available from rawinsonde measurements over the populated areas of the northern hemisphere.

These simulations thus showed that an occultation system can detect the variations caused by the weather patterns with the required 0.5 M accuracy. All errors larger than this are systematic and of a form that can readily be separated from actual meteorological information.

.....

The work in the following reports thus indicates that an occultation system would be able to obtain worldwide pressure reference information to the accuracy required by meteorological forecasters.

The original intent of the study was to proceed from this analysis to an interface analysis for including the occultation system in existing satellite projects. The conclusions, however, are that the configuration proposed originally in 1968 (Report no. RL 5-68) were an adequate solution. It would serve no purpose to conduct further engineering design tradeoffs unless a specific mission was identified. While the occultation equipment is simple, the details of including the equipment on a mission is very much dependent on the design of the spacecraft and launch vehicle. Antenna sizes and transmitter powers on both master and slave satellites depend on the spacecraft attitude control technique and precision, orbit adjustment needs, and on space, power, and weight capabilities.

Judging from past design exercises and from knowledge of present transponder costs, launch vehicle cost, and cost of minisatellites, the cost to add occultation to an operational weather satellite may be expected to be in the $4 to $6 million dollar range. But a study of an actual implementation is needed for an accurate estimate.

For the transponder design two guidelines have resulted from the research. The originally proposed equipment had two techniques for measuring the path length, a coherent phase path counter accurate to 0.03 M change in path length, and a modulation technique determining absolute group path length to 0.5 M accuracy. (Both techniques are used in current spacecraft tracking equipment.) It is recommended that ambiguities of 100 meters or more be allowed in the group path measurement if this simplifies equipment design. Ground information will be able to resolve such ambiguities.

In addition, the group path measurement should account for the expected characteristics of multipath when it does occur; namely, that the lengths of the different paths will differ by several wavelengths but by less than the desired 0.5 M accuracy. Thus a modulation technique that under these conditions will measure the group path length of the strongest signal or of any average of the signals will give useful results even during multipath. Amplitude modulation techniques will yield this result, frequency or phase modulation will not.

°°°°°

The above comments summarize the status of information on the occultation techniques. The attached reports in extensive detail show that it is feasible for these techniques to obtain meteorlogically useful information. This technique should be compared in cost and accuracy with other means available to obtain similar data.

PRECEDING PAGE BLANK NOT FILMED

ABSTRACT

The microwave occultation technique has proven useful in sensing the neutral atmosphere of terrestrial planets such as Mars and Venus. An adaptation of this technique can provide meteorological information for the Earth.

A two-satellite microwave occultation system is described that will fix as an absolute function of altitude the pressure-temperature profile generated by a passive infrared sounder. This method would be successful in determining the altitude of the 300 mb pressure level to within 24 m rms, assuming the temperature errors produced by the IR sensor are not greater than 2°K rms. Error caused by water vapor in the radio path can be corrected by climatological adjustments (by use of mean water-vapor profiles) if accurate water-vapor sensors are not available.

A ground test of the proposed system is described. A microwave signal propagating between two mountain tops was found to be subject to periods of intense fading. Computer analysis of the raypath between the transmitting and receiving stations indicates that multipath and defocusing were responsible for this fading. Because these phenomena are associated with lower altitudes than the closest approach altitude of an occultation-system raypath, it is unlikely that an operational pressure-reference-level system will be subject to the deep fades observed in the ground test.

CONTENTS

ILLUSTRATIONS

ILLUSTRATIONS (Cont)

TABLES

ACKNOWLEDGMENTS

The author wishes to thank the following people for their valuable assistance: Dr. Bruce B. Lusignan, under whose guidance this research was pursued, for his help and encouragement over the years; Dr. M. C. Thompson and his group at the Institute for Telecommunications Sciences in Boulder, Colorado, who provided the data for the Hawaii portion of this study; Dr. William Smith of the NOAA, who provided the data for the final error analysis of the occultation system; my colleague, Dr. Angus Morrison, for his help throughout this project; Dr. Willebrord Snell whose pioneering work made the occultation technique a reality; Mr. Kinji Ono for his assistance in processing the Hawaii data.

"In all things of nature there is something of the marvelous."

--Aristotle

Chapter I

INTRODUCTION

"Every science and every inquiry, and similarly every activity and pursuit, is thought to aim at some good."

--Aristotle

To achieve 10-day weather forecasts with 80 percent accuracy (the same accuracy now available for overnight forecasts), new techniques must be developed. The partial differential equations that describe the behavior of the atmosphere must be written in a form that permits their solution by digital computers; faster computers must be developed to solve these equations in an acceptably short time. Data-acquisition systems must be designed and implemented, which will sense important atmospheric variables on a global basis and report their findings in essentially real time.

In 1966, Stanford University published a report [1] that described a possible meteorological data-acquisition system. One of the proposed techniques described was the application of microwave occultation to the Earth's atmosphere. Occultation (which is based on the fact that the atmosphere will bend and retard a radio wave passing through it) had been demonstrated with Mariner IV, the space probe that flew past Mars; an occultation system had received a microwave signal from Earth as the spacecraft moved behind the planet. When the line of sight between Mariner IV and Earth passed through the Martian atmosphere, the radio signal was bent and retarded (Fig. 1). By analyzing this bending and retardation, researchers at Stanford and at the Jet Propulsion Laboratory were able to deduce the density of the Martian atmosphere [2]; model matching enabled them to estimate the atmospheric composition and the pressure and temperature profiles.

SPINMAP [1] proposed that a similar system be utilized to sense the density of the Earth's atmosphere, and thus supply meteorologists with temperature and pressure profiles of the atmosphere on a global basis. The SPINMAP configuration (Fig. 2) consisted of a mother satellite and several daughter satellites, all in the same near-polar orbit. The satellites would be spaced such that the radio path between the

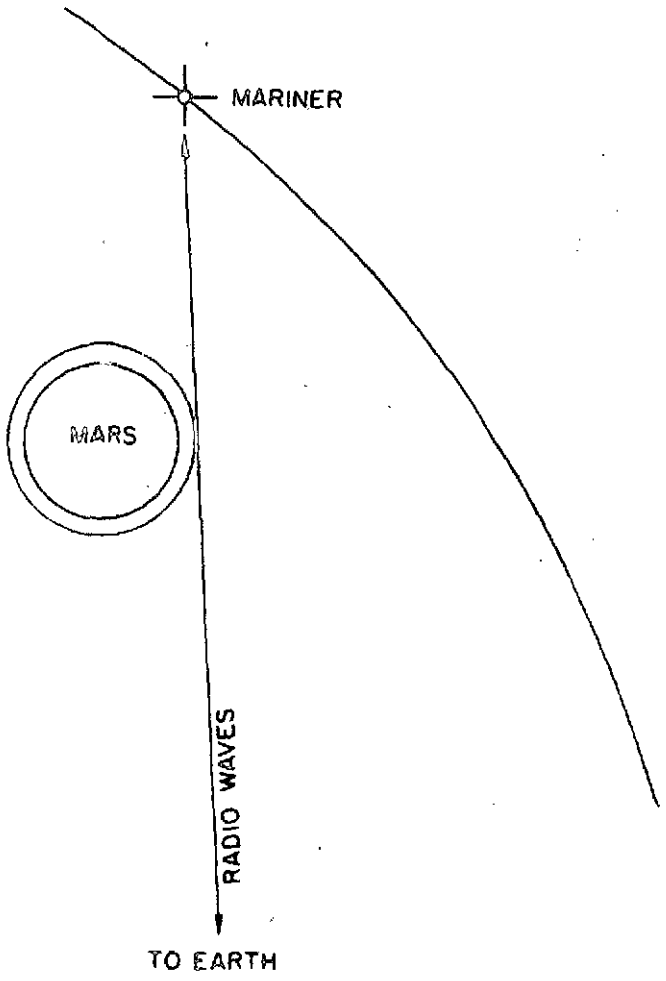

Fig. 1. THE MARINER IV OCCULTATION EXPERIMENT.

mother and each of the daughters passed through the Earth's atmosphere. The fact that there was more than one daughter allowed the atmosphere to be "sampled" by rays that had different minimum altitudes; thus, a continuous "occultation" could be achieved. As the satellites proceeded in their orbit, they would continuously sense the atmosphere. The results could be telemetered back to Earth, the data inverted, and pressure and temperature profiles generated.

Because the Earth's atmosphere is more complex than that of Mars (or even that of Venus whose atmosphere was sensed by an occultation experiment on board Mariner V in 1968), objections were raised as to the desirability of using occultation satellites in preference to other

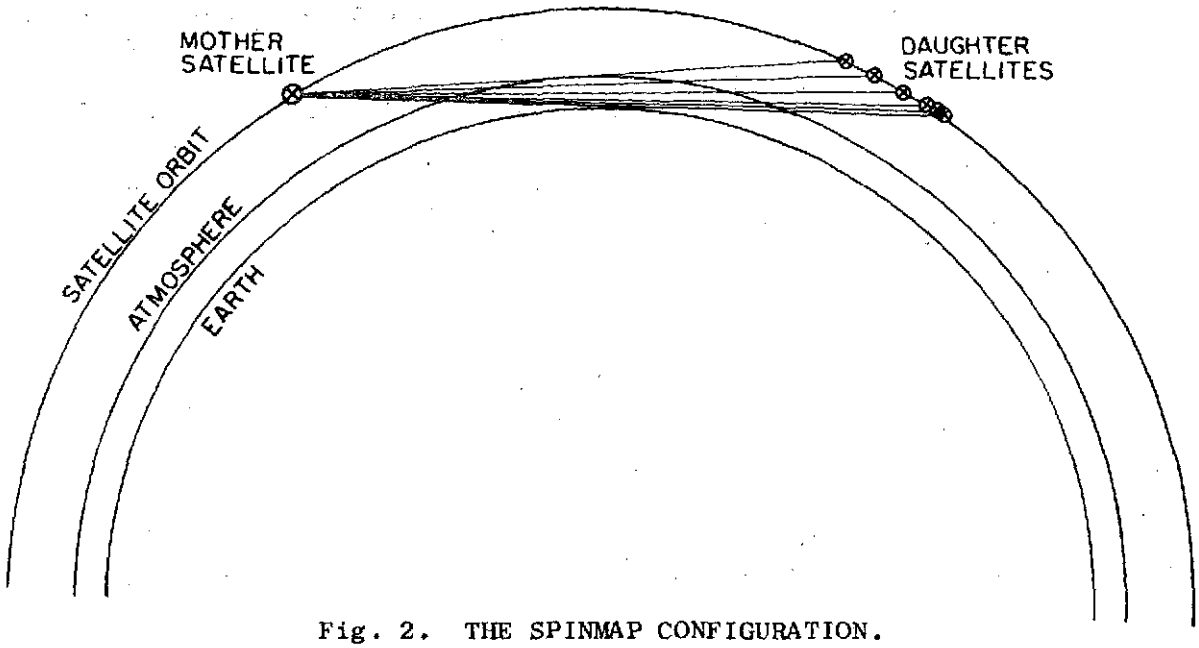

Fig. 2. THE SPINMAP CONFIGURATION.

simpler techniques, such as passive infrared sounders. Pomalaza [3] discussed many of the objections and showed how empirical orthogonal functions can be used to invert occultation data to yield pressure profiles accurate to within 0.3 mb at the surface.

In 1969, an infrared sensor was flown successfully aboard a NIMBUS satellite. The SIRS instrument (satellite infrared sounder) provided, as output, temperature as a function of pressure for values between 0.1 and 1000 mb (the sensor actually provides only nine parameters, but empirical orthogonal functions are used to develop a least-squares temperature-pressure profile). The SIRS instrument, however, did not provide an altitude reference that would fix the temperature-pressure profile as a function of height. Although the hypsometric formula could be used to determine the relative altitude between any two pressure levels, a reference value was required that would permit these relative altitudes to be expressed as absolute altitudes.

At a meeting of the Radio Occultation Working Group in Washington in September 1969, it was suggested that occultation satellites could be used to provide this pressure-reference altitude. This report will demonstrate the feasibility of a two-satellite occultation technique to

supplement the infrared sensor system by providing an accurate altitude reference that will serve to fix, as a function of height, the temperature profile of the SIRS instrument.

The results of ground tests made in Hawaii during June 1970 also will be described. These tests were conducted to estimate the likely effects of scintillation and fading on an occultation system. It was found that the microwave signal suffered periods of intense fading; however, it will be shown that the probable cause of the fading was multipath, which is a low-altitude phenomenon and, therefore, is not apt to affect the proposed pressure-reference system which operates at a relatively high altitude (≈ 8 km).

Chapter II

BASIC PRINCIPLES

"Philosophy is written in this grand book--I mean the universe--which stands continually open to our gaze, but it cannot be understood unless one first learns to comprehend the language and interpret the characters in which it is written. It is written in the language of mathematics..."

--Galileo Galilei

A. Refraction

The occultation technique is based on the fact that when a radio wave passes through the atmosphere it is bent and retarded. This happens because the atmosphere has an index of refraction n that is greater than 1, and this parameter will vary from place to place.

The index of refraction, however, is not much greater than 1; a typical value at the surface of the Earth is 1.000314. Because the significant variations in the index of refraction are very small, it has been found convenient to define a quantity known as refractivity N:

$$N = (n - 1) \times 10^6 \tag{2.1}$$

In other words, N is the fractional part of n, multiplied by 10^6.

Refractivity is a function of atmospheric density and, therefore, a function of atmospheric pressure and temperature (temperature, pressure, and density are related by the equation of state or ideal gas law, $P = \rho RT$, where P = pressure, ρ = density, T = absolute temperature, and R = the universal gas constant). In terms of temperature T, atmospheric pressure P, and the partial pressure of water vapor e, refractivity can be written as [4]

$$N = 77.6 \frac{P}{T} - 5.6 \frac{e}{T} + 3.75 \times 10^5 \frac{e}{T^2} \tag{2.2}$$

where T is in degrees Kelvin, P and e are in millibars, and N is dimensionless. It can be seen from this equation that N is directly proportional to pressure and inversely proportional to some power of

temperature; in addition, it is a very strong function of water-vapor pressure because of the polar nature of the water molecule. The first term on the right-hand side of Eq. (2.2) is often called the "dry term," and the remainder are called the "wet terms." At low altitudes, where water-vapor pressures can be expected to be high, the wet terms make a significant contribution to the value of N. At higher altitudes (above 7 km), this contribution is very small and the dry term is principally responsible for the value of N.

A radio wave in the atmosphere is retarded if N is greater than zero because the index of refraction n is the ratio between the speed of light in a vacuum c and the speed of light in the medium; therefore, N represents the fractional difference between the speed of the radio wave in the atmosphere and its speed in a vacuum. The higher the value of N, the greater the retardation. (It should be noted that a monochromatic wave is being discussed and, therefore, the distinction between group velocity and phase velocity is not of concern. In any case, the atmosphere for the frequency range of interest (X-band) is essentially nondispersive. In this report, "velocity" of a wave refers to "phase velocity.")

In addition to retarding the wave, the atmosphere also causes it to bend because N (being a function of pressure, temperature, and water-vapor pressure) varies in magnitude, both horizontally and vertically. From Snell's Law, it is known that an electromagnetic "ray" tends to bend in the direction of increasing index of refraction. Mathematically, this can be written as [5]

$$\frac{d\lambda}{\lambda} = \frac{d\rho}{\rho} \tag{2.3}$$

where λ is the wavelength and ρ is the radius of curvature of the raypath (henceforth, ρ will refer to radius of curvature rather than density). The derivatives are taken in the direction of travel of the ray.

The wavelength λ is related to frequency ν by $\lambda = v/\nu$, where v is the velocity of the wave. Because $v = c/n$,

$$\lambda = \frac{c}{n\nu}$$

and

$$d\lambda = - \frac{c}{n^2 \nu} dn$$

Substituting these expressions into Eq. (2.3) and rearranging results in

$$\rho = - \frac{n}{dn/d\rho} \tag{2.4}$$

which relates the radius of curvature of a ray to the index of refraction n and the derivative $dn/d\rho$. This derivative can be expressed as the sum of two terms; one is proportional to the horizontal gradient of n, and the other is proportional to the vertical gradient:

$$\frac{dn}{d\rho} = \vec{\nabla} n \cdot \frac{\vec{\rho}}{|\rho|} = - \left|\frac{dn}{dr}\right| \cos \phi + \frac{1}{r} \frac{dn}{d\theta} \sin \phi \tag{2.5}$$

where r and θ are polar coordinates with origin at the center of the Earth, and ϕ is the angle between $\vec{\rho}$ (the radius of curvature vector) and $\vec{r}$ (the radius vector). Note that, for $\vec{r}$ pointed outward, dn/dr is negative for a normal atmosphere.

The radius of curvature ρ can now be written as

$$\rho = \frac{n}{|dn/dr| \cos \phi - (1/r)(dn/d\theta) \sin \phi} \tag{2.6}$$

Therefore, the radius of curvature of a ray is found to be proportional to the index of refraction of the medium and inversely proportional to the gradient of the index of refraction. If the gradients are large, ρ will be small and the ray will curve sharply; if they are small and if n is large, the ray will follow a "straight" trajectory.

Both the bending of the ray and its retardation tend to increase the apparent path length of the ray. If the atmosphere is not present,

the radio signal travels in a straight line at the speed of light in a vacuum. Bending and retardation caused by the atmosphere increase the time it takes for a ray to travel between the same endpoints and, thus, effectively increase the length of the raypath.

This increase in path length is called the "phase defect."[†]

B. The Occultation System

The proposed two-satellite occultation system (Fig. 3) would measure the phase defect and use it to infer the altitude of a pressure level.

The infrared sensor determines the pressure-temperature profile of the atmosphere over a particular portion of Earth; simultaneously, the occultation system propagates a radio wave through this same segment of atmosphere and measures the phase defect. This result is telemetered back to the ground

(It should be noted that, in an operational system, the IR sensor can be mounted on one of the occultation satellites instead of on a third satellite, as illustrated in Fig. 3. This sensor has a resolution cell similar in size to that of the occultation system, and the results can be correlated on the ground.)

The pressure-temperature profile is used as input for a computer program that raytraces through the index-of-refraction profile generated from the pressure-temperature curve. The results of this raytracing are compared to the phase defect measured by the satellites. The index-of-refraction profile is then adjusted the proper vertical distance until the raytracing result obtained from the computer program matches the phase defect obtained from the satellites.

Several of the parameters of the proposed system are significant and should be given special attention. Because an attempt is being made

---

[†] The origin of the term "phase defect" is obscure. It may be attributed to the fact that, as the path length and wavelength increase, the number of zero crossings registered by the receiver decreases, resulting in a phase "defect" at the receiver.

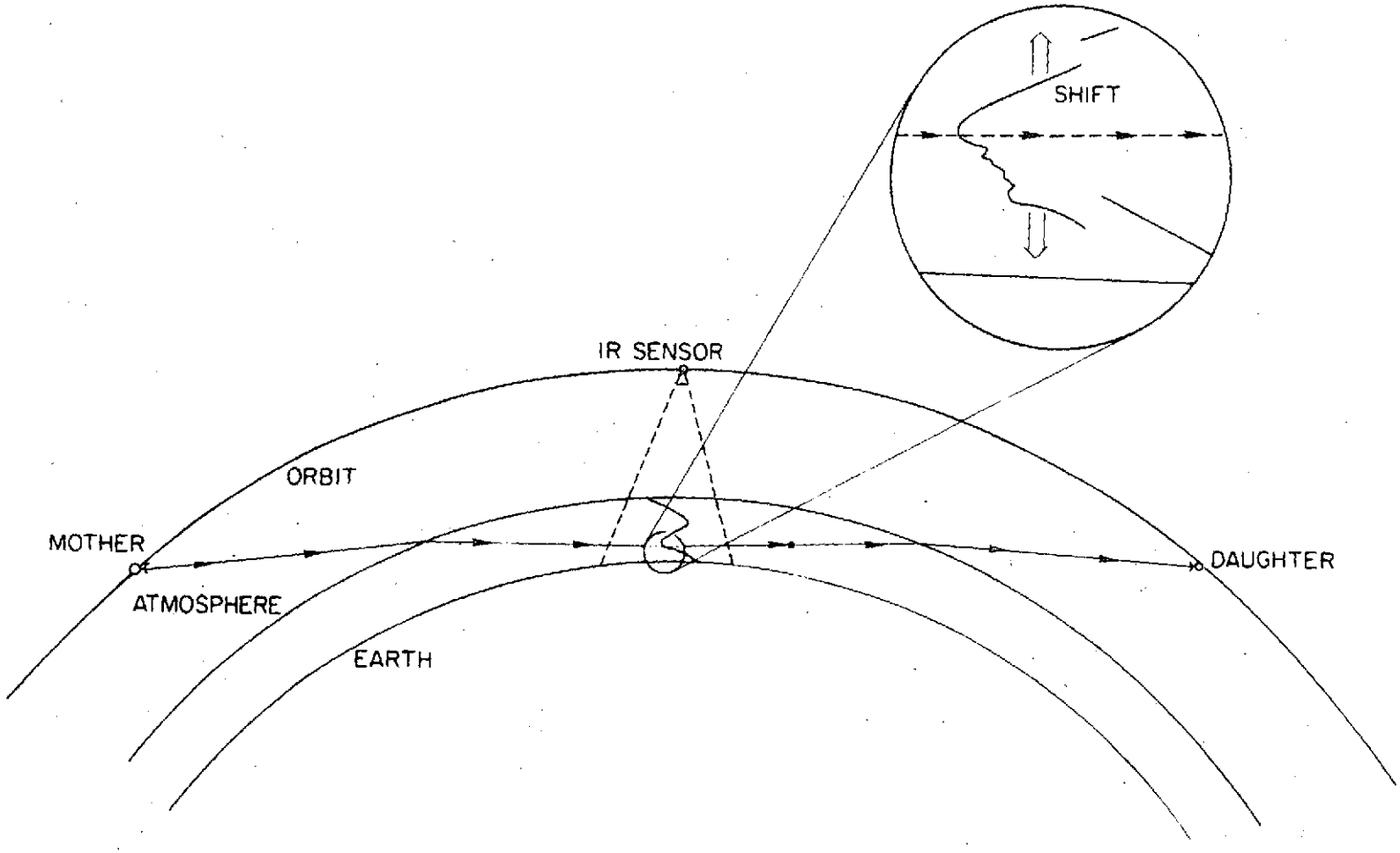

Fig. 3. THE PRESSURE-REFERENCE-LEVEL SYSTEM.

to measure an excess path length on the order of hundreds of meters over a path on the order of 8000 km, it is obvious that the system must be of high precision. In fact, only small variations (on the order of meters) in the phase defect are of interest. It is important, therefore, to be able to measure the phase defect as accurately as possible, hopefully to within 1 m or less, which means that the relative positions of the satellites must be known to within this distance.

The factors affecting satellite position are atmospheric drag, solar-radiation pressure, and perturbations in the orbit attributed to anomalies in the Earth's gravitational field. Drag and solar-radiation pressure will have periodic effects that can be removed from the data by digital filtering. The drag effect is a long-term phenomenon; the solar-radiation effect will have a period of half a revolution and should be removable without undue difficulty.

Orbital perturbations caused by anomalies in the Earth's gravitational field are a more difficult problem. Theoretical analysis [6] has shown that, by launching the mother and daughter satellites together and then letting the daughter drift away, the gravitational field can be mapped with sufficient accuracy to remove the effects of the anomalies.

Another significant parameter is the nominal separation distance between the satellites. By increasing this distance, the raypath between the satellites can be made to approach closer to the Earth's surface at its lowest altitude. In addition, the Earth is somewhat oblate; the difference in radius measured at the equator and at the pole is ≈ 20 km. As will be shown in Chapter III, satellite separation and the effects of the Earth's oblateness are important factors in system design.

Figure 4 is a block diagram of the system. The mother satellite transmits a CW signal through the Earth's atmosphere. The daughter satellite receives the signal, multiplies its frequency by some rational fraction (such as 11/10), and retransmits it phase coherently to the mother satellite where it is multiplied by the inverse of the original multiplying factor (in this case, by 10/11). The signal now beats with the original frequency, and the beats are counted and recorded. If, in passing through the atmosphere, the frequency of the signal was not affected, the result of beating will be zero; however, if the atmosphere

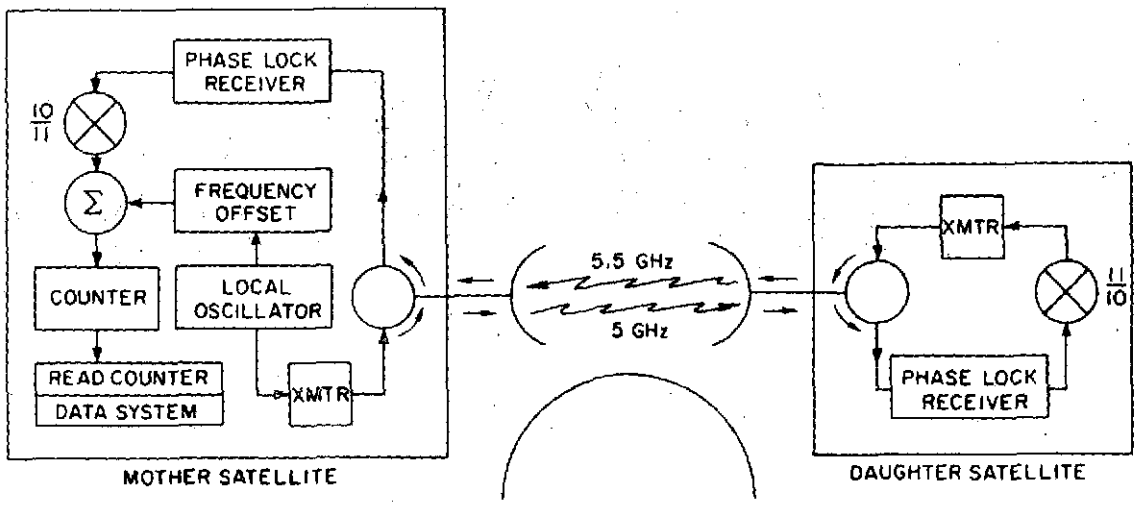

Fig. 4. BLOCK DIAGRAM OF THE OCCULTATION-SYSTEM HARDWARE.

causes the apparent distance between the satellites to change, the frequency of the signal will have shifted slightly as a result of the Doppler effect, and this shift will appear as a beat frequency. Half the number of beats/sec produces the number of wavelengths of excess path length caused by the atmosphere (or, as noted above, caused by real path-length changes resulting from variations in satellite position).

In addition to the system described above, which counts every wavelength change in distance between the satellites, the signal of the master satellite is phase modulated at ≈ 5 MHz. This modulation is carried through the repeater satellite and received back at the master. Phase comparison of the received and transmitted signals yields an absolute-distance measurement of approximately 1/2 m accuracy with a basic ambiguity of ≈ 60 m; this ambiguity can be increased to approximately 3 km by adding a second modulation frequency if system considerations so require. The absolute-distance system provides the original absolute-distance reference and reestablishes the absolute reference whenever the more precise system loses count because of interference. The possibility of signal loss from multipath is discussed extensively in later chapters.

It should be noted that hardware similar to that described above has been flight tested and proven on numerous planetary and interplanetary missions, including Mariner, Pioneer, Lunar Orbiter, and Apollo.

Chapter III

ERROR ANALYSIS OF THE PRESSURE-REFERENCE-LEVEL SYSTEM

"Errare humanum est."

--Ancient Saying

A computer simulation of the occultation system was necessary to determine the feasibility of using occultation satellites to measure the altitude of a pressure level. This chapter describes the program used and the results obtained.

A. The Pressure-Reference-Level Program

The computer program was divided into two parts. In the first, a model atmosphere, consisting of the best temperature, pressure, and water-vapor information available, was input to the computer to construct an index-of-refraction profile. A raytracing routine traced through this profile, simulating the result that would be obtained if a satellite system were to transmit through this model atmosphere. The result was a phase defect (the excess path length) and was called SR, meaning "satellite reading."

In the second, the information used to construct the index-of-refraction profile was degraded so as to simulate the errors inherent in the satellite infrared sensor (SIRS) which, in an operational system, would be the source for this data. (The particular species of degradation employed varied from one run to another and will be described later in this chapter.) All information relating pressure or temperature to altitude was discarded, and the bottom-most temperature-pressure pair was arbitrarily fixed at some starting height. The hypsometric formula was used to assign corresponding altitudes to the remaining pressure-temperature pairs, an index-of-refraction profile was constructed, and the raytracing routine was employed to generate a value of the phase defect. (This value was denoted as PD1.) The profile was then shifted vertically 1 km, the raytracing routine was again applied, and a new value (PD2) was obtained. These two values were used to calculate the derivative of the phase defect with respect to altitude $d\phi/dz$, where $d\phi/dz = PD2 - PD1$.

Now, the SR of the first part of the experiment (the phase defect "measured" by the imaginary satellite system) was employed to construct an error term,

$$\Delta\phi = SR - PD2 \tag{3.1}$$

This value $\Delta\phi$ was used in conjunction with the derivative $d\phi/dz$ to determine the shift Δz necessary to bring the error term $\Delta\phi$ to zero:

$$\Delta z = \frac{\Delta\phi}{d\phi/dz} \tag{3.2}$$

In practice, the system is somewhat nonlinear, and more than one iteration is generally necessary before $\Delta\phi$ is brought arbitrarily close to zero.

When $\Delta\phi$ had been made acceptably small through repeated raytracing, application of Eq. (3.2), and the appropriate vertical shift of the index-of-refraction profile, the altitudes of various pressure levels were compared to the altitudes of these same levels in the "measured" atmosphere profile used in the first part of the program. The differences in altitude constituted the error of the system; therefore, if the 500 mb level were at 5.005 km in the reference atmosphere and at 5.015 km in the atmosphere generated by the shifting procedure, the error at 500 mb would be 5.015 - 5.005 km = 0.010 km, or 10 m. Figure 5 is a flow chart of this program, and its listing is found in Appendix A.

In the remainder of this chapter, the results of the final error analysis are discussed, in which simulated data from the satellite infrared sounder (SIRS) were used to generate the reference atmosphere.

B. Error Analysis, Using Simulated SIRS Data

The simulated SIRS profiles [7] consisted of 206 profiles of temperature vs pressure, with temperatures at 100 pressure levels between 1000.0 and 0.1 mb. A typical data set is shown in Fig. 6. Each level presents a simulated temperature "sensed" by the SIRS, a temperature "error" (how this sensed temperature differs from the true temperature),

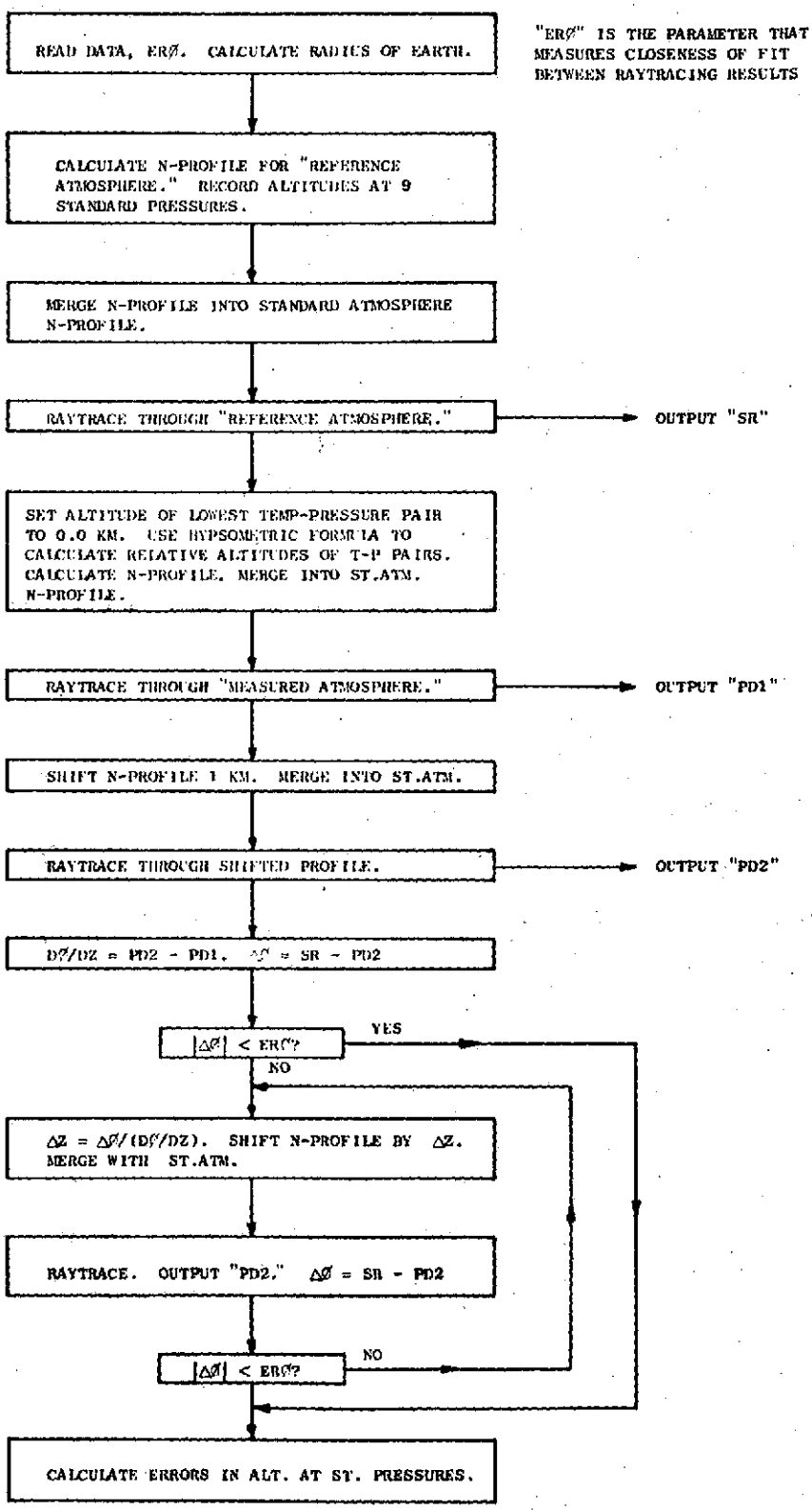

Fig. 5. FLOW CHART OF THE PRESSURE-REFERENCE-LEVEL PROGRAM.

STATION NO. 72201

PROFILE NO. 1　　CASE NO. 2　　SET NO. 2

PRESS	TEMP	TEMP DEV	H DEV	PRESS	TEMP	TEMP DEV	H DEV	PRESS	TEMP	TEMP DEV	H DEV	PRESS	TEMP	TEMP DEV	H DEV
.10	230.33	-3.67	-32.41	15.91	226.37	-1.67	-14.61	116.22	202.80	1.21	-51.41	409.83	253.27	-.11	2.87
.15	241.10	-.63	-.47	17.69	225.05	-.84	-10.45	123.42	203.90	.39	-52.84	427.44	255.56	-.06	2.97
.22	251.75	2.53	-7.96	19.59	223.72	-.03	-9.10	130.94	204.86	-.35	-52.89	445.59	257.87	.01	3.00
.32	256.79	.77	-25.46	21.63	222.35	.57	-9.85	134.78	205.99	-1.04	-51.77	464.28	260.19	.10	2.94
.43	261.34	-.74	-27.69	23.83	220.97	1.10	-12.19	146.76	207.19	-1.65	-49.49	483.52	262.51	.18	2.77
.58	265.03	-1.70	-17.86	26.18	219.56	.31	-15.19	155.47	208.46	-2.21	-46.31	503.33	264.74	.31	2.49
.75	267.05	-3.15	.40	28.70	219.00	-1.79	-12.32	164.32	209.77	-2.72	-42.37	523.71	266.48	.63	1.95
.97	267.67	-3.37	24.10	31.39	216.67	-2.55	-6.69	173.53	211.13	-3.19	-37.61	544.67	268.13	.86	1.10
1.22	266.20	-1.55	41.43	34.26	215.09	-1.99	-.85	183.11	212.53	-3.51	-32.29	566.23	269.70	1.02	.03
1.51	263.63	-.71	48.93	37.27	213.51	-1.48	3.50	193.05	213.94	-4.02	-26.37	588.39	271.21	1.11	-1.16
[illegible]	260.59	.14	50.92	40.50	212.03	-.91	6.46	203.38	215.53	-4.36	-19.95	611.16	272.63	1.12	-2.61
2.25	257.76	.66	48.79	43.92	210.56	-.27	7.86	214.09	218.16	-3.88	-13.77	634.55	273.89	.96	-3.55
[illegible]	[illegible]	.97	44.47	47.55	209.11	.35	7.79	225.20	220.90	-3.38	-6.92	658.58	274.97	.62	-4.41
[illegible]	[illegible]	1.39	39.52	51.37	207.63	.98	6.31	236.72	223.65	-2.87	-3.81	683.25	275.99	.23	-4.68
[illegible]	[illegible]	2.01	30.30	55.41	206.16	1.66	3.42	249.65	226.09	-2.38	-.02	708.57	277.15	-.02	-4.99
[illegible]	[illegible]	2.63	19.76	59.68	204.65	2.39	-.87	261.00	228.59	-1.59	2.82	734.56	278.57	.00	-4.95
5.15	243.50	3.25	6.80	64.18	203.23	2.99	-6.42	273.79	231.06	-.79	4.50	761.22	280.23	.25	-5.11
5.93	240.78	3.87	-8.25	68.91	201.75	3.67	-13.34	287.02	233.46	-.06	5.11	788.56	282.04	.67	-5.59
6.84	237.98	4.50	-25.25	73.89	200.33	2.79	-19.99	300.70	235.79	.56	4.76	816.60	283.20	.43	-6.15
7.82	235.[illegible]	2.11	-38.53	79.12	199.71	2.23	-25.03	314.83	238.30	.44	4.09	845.34	283.50	-.60	-6.03
8.90	232.82	-.28	-47.20	84.61	199.67	2.08	-29.27	329.44	240.87	.34	3.56	874.80	283.42	-1.24	-5.07
10.07	231.53	-1.61	-39.00	90.37	199.44	2.12	-33.31	344.53	243.36	.25	3.17	904.98	283.45	-1.52	-3.70
11.36	230.24	-1.75	-33.10	96.40	200.29	2.96	-38.10	360.10	245.89	.17	2.91	935.91	283.72	-1.56	-2.19
12.75	228.96	-1.90	-26.89	102.71	201.02	3.05	-43.68	376.16	248.41	.08	2.75	967.57	286.05	-1.54	-.67
14.27	227.66	-2.06	-20.39	109.32	201.88	2.10	-48.41	392.74	250.90	-.07	2.76	1000.00	296.07	.17	1.27

NO	WAVE NO.	INTENSITY	CALC.ERROR	DELTA RADIANCE	BORY.TERM	MEAN RAD.	RANDOM ERROR
1	890.0	95.0754	.00782	-2.43648	0.00009	97.62105	.10921
2	750.0	101.0281	-.01795	1.33617	.00463	99.59878	-.11450
3	735.0	81.7952	-.37166	2.82768	.02110	79.56725	-.37922
4	715.0	67.0587	-.14504	2.92283	.07286	63.82632	-.23569
5	700.0	49.1553	-.25290	1.32877	.09485	47.66588	-.06654
6	690.0	40.4864	-.19206	-1.14346	.15225	41.24376	-.23783
7	668.0	39.0309	.11112	-.39929	.12002	39.59661	.29643
8	2225.0	.4443	.00182	.06309	.00003	.38456	-.00334
9	2340.0	.1019	-.00041	-.00287	.00035	.10435	.00007

RAD.ERRORS .00182 -.00041

TEMP.ERRORS 700-1000= .74 400-700 = .46 100-400 = 1.73 10-100= 1.71 1-10 = 1.93

HGHT.ERRORS 100-1000= .46 475-1000= .43 600-1000= 1.10 300-600= .37 100-300= .94

DIFT.ERRORS 100-1000= -.31 475-1000= .48 600-1000= .05 300-600= -.15 100-300= .60

DIFH.ERRORS 100-1000= -.26 475-1000= .42 600-1000= -.72 300-600= -.28 100-300= 1.25

Fig. 6. A TYPICAL INPUT DATA SET.

STATION NO. 72201 PROFILE NO. 1 CASE NO. 2 SET NO. 2

KEY WEST/INT FLORIDA

24 33 N 81 45 W RADIUS OF EARTH AT THIS LATITUDE 6374.4727 KM.

LEVEL(MB)	
500.000	-1.32
400.000	-1.09
300.000	0.90
200.000	-25.81
150.000	-55.26
100.000	-45.30
70.000	-18.83
50.000	3.07
30.000	-13.79

STATISTICS FOR LOWER 9 PRESSURE LEVELS

MEAN	-17.50
ST. DEV.	21.15
RMS	27.45
MIN	-55.26
MAX	3.07

Fig. 7. A TYPICAL OUTPUT SAMPLE.

and the error in height resulting from the accumulated error in temperature. In addition, each set tabulates rms errors for various ranges of pressure (such as 700 to 400 mb, 400 to 100 mb).

Half of the data sets consist of simulated profiles for a 7-channel sensor; the other half consist of profiles for a 9-channel sensor, which are the only ones used in this error analysis. The data sets were divided into three groups (set 2, set 3, and set 4), according to the latitude of the stations, and these latitude ranges are indicated in Table 1.

The pressure-reference-level program was run by combining the "sensed" temperature profile and the corresponding temperature errors so as to produce the "true" temperature profile which became the "reference atmosphere." The original sensed-temperature profile was used as "measured data." An atmosphere was constructed from this profile and shifted vertically until the results of raytracing through the vertically shifted measured profile matched the results of raytracing through the reference atmosphere. In both portions of the program, a random error of absolute magnitude (0.5 m) was added to the phase defect to simulate the uncertainty in satellite spacing.

The resulting altitude error at each of nine pressure levels was recorded. Figure 7 is a typical output sample. Statistical summaries for each of the three latitude ranges are tabulated in Tables 2 through 7. Tables 2, 3, and 4 list the results for a satellite separation of 7863 km, and Tables 5, 6, and 7 list the results for 7888 km. (The greater the satellite separation, the lower is the closest approach altitude of the ray.) Table 1b lists the closest approach altitudes for each of the cases shown in Tables 2 to 7; the results are also displayed in Figs. 8 and 9.

A smaller number of profiles were run with water vapor introduced into the reference-atmosphere portion of the program. This water-vapor data consisted of the associated rawinsonde relative humidity profiles. A simplistic water-vapor correction was used in the second half (measured-data portion) of the program. This correction consisted of one of two humidity profiles, one representing a "high" value of water vapor and the other a "low" value (see Fig. 10), chosen according to the surface value of the rawinsonde water-vapor profile. All of the data sets from

Table 1

SIGNIFICANT DATA FOR PRESSURE-REFERENCE-SYSTEM ERROR ANALYSIS, EMPLOYING SIMULATED SIRS TEMPERATURE PROFILES

Latitude	Set No.		
	2	3	4
Min	25 N	38 N	51 N
Max	37 N	51 N	76 N

a. Latitude ranges

Set	Satellite Separation					
	7863 km			7888 km		
	No. Prof	Min Alt	Max Alt	No. Prof	Min Alt	Max Alt
2	14	5.78	7.86	14	3.59	5.44
3	20	7.55	9.75	19	4.85	6.81
4	18	9.59	12.56	18	7.29	9.91

b. Dry Atmosphere

Set	Satellite Separation					
	7863 km			7888 km		
	No. Prof	Min Alt	Max Alt	No. Prof	Min Alt	Max Alt
2	6	6.25	7.59	6	4.11	4.95
3	8	7.62	9.96	8	4.99	7.10
4	7	9.70	11.47	7	7.40	9.28

c. Wet atmosphere with simplistic climatic correction

Set	Satellite Separation		
	7863		
	No. Prof	Min Alt	Max Alt
2	6	6.11	7.65
3	8	7.69	10.00
4	7	9.98	11.85

d. Wet atmosphere with ideal correction

Table 2

SATELLITE SEPARATION: 7863.0000 KM (14 Stations); SET 2

Level (mb)	Mean	St. Dev.	rms	Min	Max
500.000	7.70	14.05	16.02	-16.89	28.33
400.000	8.18	16.42	18.35	-21.21	30.48
300.000	17.64	28.40	33.43	-30.50	53.93
200.000	24.65	35.57	43.28	-25.81	92.03
140.000	2.64	33.55	33.65	-55.26	61.61
100.000	0.57	27.10	27.10	-45.36	58.87
70.000	4.56	28.17	28.54	-42.50	56.64
50.000	11.02	38.20	39.76	-58.88	91.92
30.000	10.55	37.38	38.84	-49.27	58.26

Table 3

SATELLITE SEPARATION: 7863.0000 KM (20 Stations); SET 3

Level (mb)	Mean	St. Dev.	rms	Min	Max
500.000	1.21	17.67	17.71	-20.61	36.88
400.000	-3.15	12.97	13.35	-24.05	17.89
300.000	-0.07	16.47	16.47	-43.97	21.99
200.000	6.28	25.77	26.52	-51.67	41.15
140.000	4.90	42.22	42.50	-83.59	80.43
100.000	-2.32	39.53	39.59	-73.74	95.77
70.000	1.13	28.35	28.38	-33.48	87.17
50.000	9.72	24.72	26.57	-28.99	77.82
30.000	24.42	40.21	47.05	-47.99	87.49

Table 4

SATELLITE SEPARATION: 7863.0000 KM (18 Stations); SET 4

Level (mb)	Mean	St. Dev.	rms	Min	Max
500.000	12.38	22.83	25.97	-27.09	48.48
400.000	9.56	25.29	27.04	-31.75	42.22
300.000	-0.82	25.32	25.33	-49.44	38.81
200.000	12.11	22.26	25.34	-12.92	72.49
140.000	14.80	29.62	33.11	-21.11	95.06
100.000	15.39	33.36	36.74	-38.29	105.33
70.000	11.87	29.70	31.99	-41.17	76.05
50.000	1.35	19.38	19.42	-31.85	30.24
30.000	-21.75	36.20	42.23	-78.40	43.18

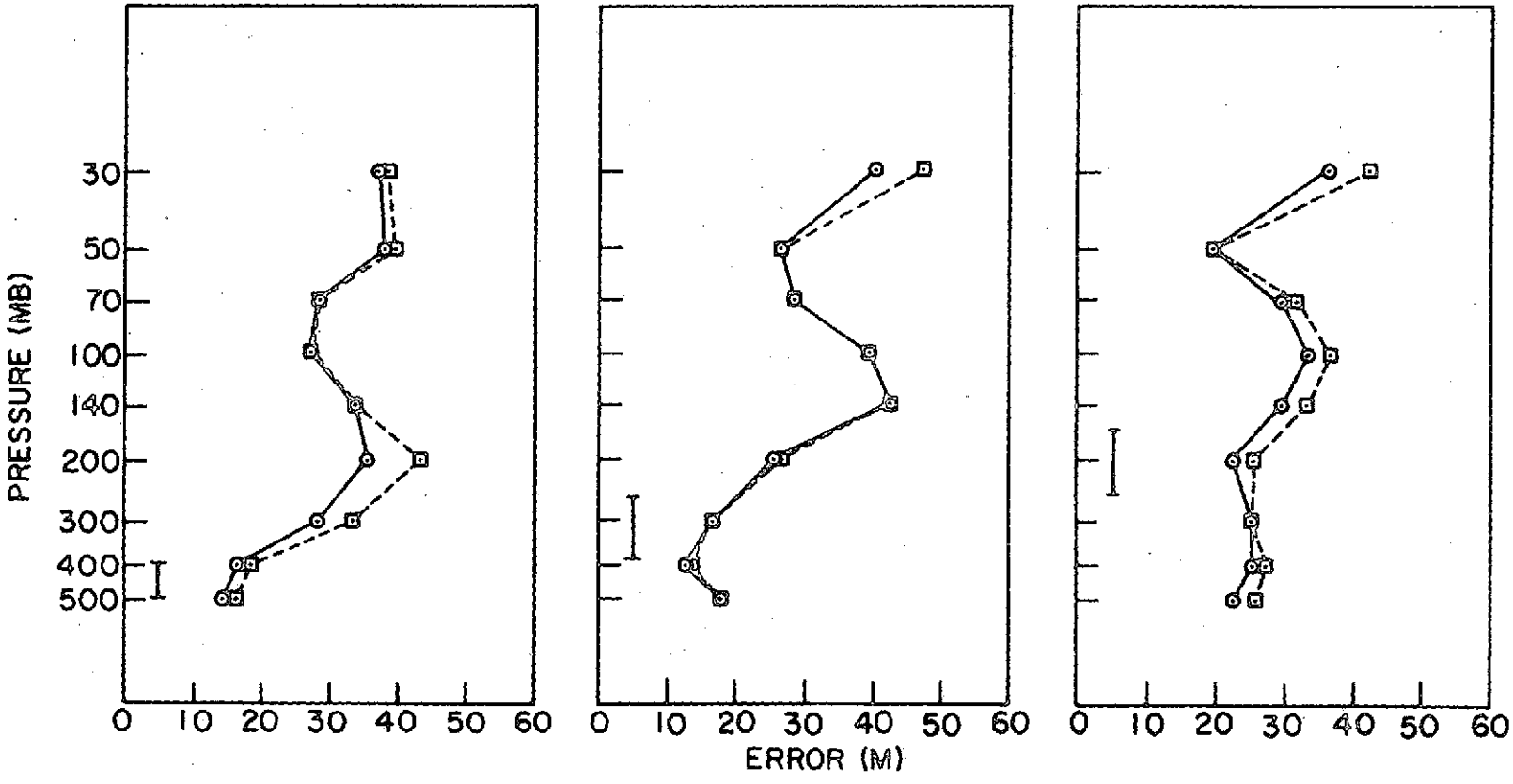

Latitude range 25°-37° N
14 profiles

Latitude range 38°-51° N
20 profiles

Latitude range 51°-76° N
18 profiles

Standard Deviation ——— RMS -----

Fig. 8. STANDARD DEVIATION AND RMS ERROR VS PRESSURE. Dry atmosphere, satellite separation: 7863.0 km. Closest approach altitude of ray indicated by vertical line.

Table 5

SATELLITE SEPARATION: 7888.0000 KM (14 Stations); SET 2

Level (mb)	Mean	St. Dev.	rms	Min	Max
500.000	2.72	16.82	17.04	-32.38	30.76
400.000	3.20	17.42	17.71	-28.07	28.50
300.000	12.66	15.84	20.27	-14.57	34.83
200.000	19.67	22.48	29.87	-13.67	59.76
140.000	-2.34	32.35	32.44	-47.95	48.25
100.000	-4.41	28.62	28.96	-62.93	42.37
70.000	-0.42	23.34	23.34	-47.52	32.24
50.000	6.04	29.24	29.86	-32.20	68.65
30.000	5.57	25.40	26.00	-44.91	44.65

Table 6

SATELLITE SEPARATION: 7888.0000 KM (19 Stations); SET 3

Level (mb)	Mean	St. Dev.	rms	Min	Max
500.000	-3.31	19.62	19.90	-43.18	27.33
400.000	-7.95	28.79	29.87	-68.50	41.94
300.000	-5.63	45.71	46.06	-96.07	69.94
200.000	-0.87	43.21	43.22	-80.68	71.70
140.000	-0.31	38.60	38.60	-68.58	68.34
100.000	-6.49	37.56	38.12	-60.89	73.51
70.000	-2.94	30.74	30.88	-51.80	72.04
50.000	4.29	25.10	25.47	-33.07	51.54
30.000	15.71	37.80	40.93	-47.12	89.89

Table 7

SATELLITE SEPARATION: 7888.0000 KM (18 Stations); SET 4

Level (mb)	Mean	St. Dev.	rms	Min	Max
500.000	14.07	35.69	38.36	-29.69	90.63
400.000	11.25	28.34	30.49	-17.20	76.93
300.000	0.87	27.49	27.51	-40.40	56.26
200.000	13.81	49.56	51.45	-56.19	103.93
140.000	16.49	58.22	60.51	-60.69	133.87
100.000	17.08	54.47	57.08	-40.43	140.75
70.000	13.56	50.62	52.40	-47.56	127.72
50.000	3.04	49.95	50.04	-79.01	109.18
30.000	-20.06	63.61	66.70	-134.16	83.86

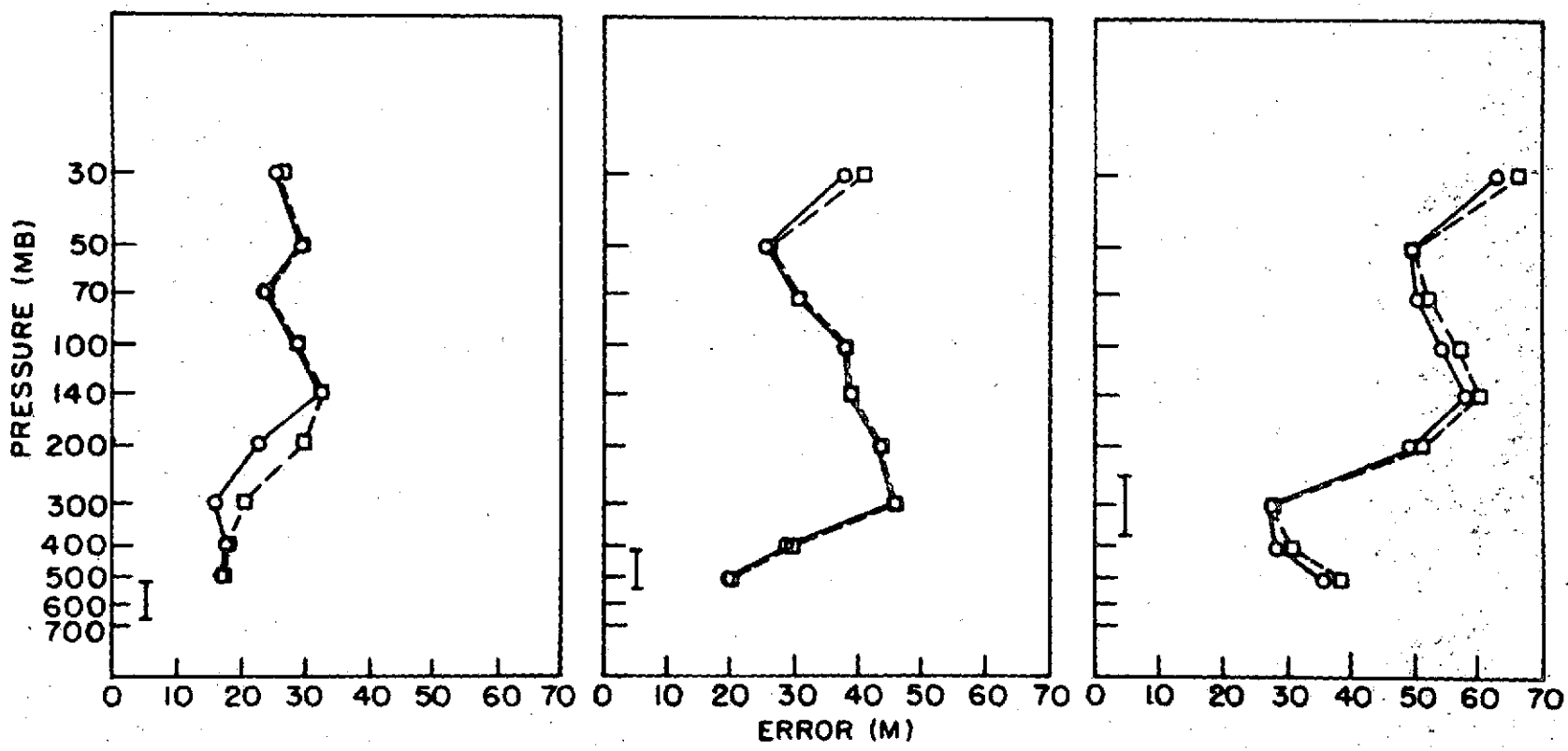

Fig. 9. STANDARD DEVIATION AND RMS ERROR VS PRESSURE. Dry atmosphere, satellite separation: 7888.0 km. Closest approach altitude of ray indicated by vertical line.

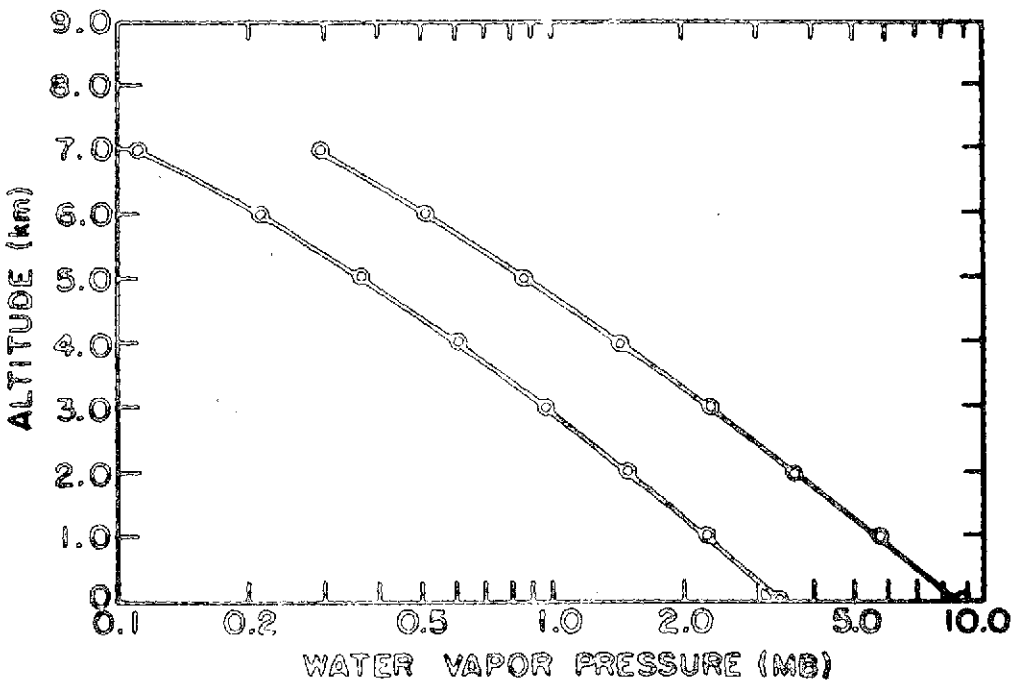

Fig. 10. WATER VAPOR PROFILES. The above profiles were extrapolated to 25 km by use of the equation $e(z) = e(7) * \exp[0.5476 * (z - 7)]$, where e is the water-vapor pressure, in millibars, and z is the altitude, in kilometers.

sets 3 and 4, and one from set 2 used the lower corrective profile; the remaining data sets in set 2 used the higher corrective profile. Tables 8, 9, and 10 summarize the results for a satellite separation of 7863 km, and Tables 11, 12, and 13 summarize the results for 7888 km. The corresponding closest approach altitudes are listed in Table 1c, and the results are illustrated in Figs. 11 and 12.

To determine the effect of an improvement in the water-vapor correction technique (a more sophisticated approach than the simplistic method described above), the same data were run with the exact rawinsonde water-vapor profile used in both the reference and measured atmospheres, which is equivalent to an ideal water-vapor correction. Results of this run (for the 7863 km satellite separation only) are tabulated in Tables 14 through 16. The corresponding closest approach altitudes are listed in Table 1d, and the results are displayed in Fig. 13.

Finally, to determine the effects of the temperature errors on the system, the analysis of six low-latitude profiles (without water) was repeated, this time using the reference temperature values (the values without error) in both the reference and measured atmospheres, which is equivalent to having an ideal-temperature sensor. The result of this run is illustrated in Fig. 14 for the 7863 km satellite separation only.

C. Analysis of Results, Using Simulated SIRS Data

In Figs. 8, 9, 11, and 12, the solid line represents the standard deviation of the error (in meters), and the dashed line represents the root mean square (rms) error; both are shown as a function of pressure. The difference between the standard deviation and the rms values at each pressure level is an indication of the size of the mean error at this level. The rms value is equal to the square root of the sum of the squares of the standard deviation and the mean (rms^2 = standard deviation^2 + mean^2).

A cursory examination of these figures reveals that the curve of altitude error vs pressure follows a typical pattern, regardless of whether the atmosphere is wet or dry or, if wet, how the water-vapor error is corrected. Typically, there are two minima and two maxima.

Table 8

SATELLITE SEPARATION: 7863.0000 KM (6 Stations); SET 2

Level (mb)	Mean	St. Dev.	rms	Min	Max
500.000	13.12	16.80	21.31	-7.95	40.43
400.000	8.31	20.21	21.85	-23.56	29.32
300.000	15.22	26.48	30.54	-27.64	40.54
200.000	34.51	34.32	48.67	-2.97	93.47
140.000	32.68	47.46	57.63	-18.32	80.53
100.000	19.16	31.17	36.59	-26.20	59.18
70.000	6.13	43.39	43.82	-56.23	46.92
50.000	11.06	59.10	60.13	-52.70	83.33
30.000	15.58	26.30	30.57	-19.93	46.52

Table 9

SATELLITE SEPARATION: 7863.0000 KM (8 Stations); SET 3

Level (mb)	Mean	St. Dev.	rms	Min	Max
500.000	39.18	33.84	51.77	-5.46	99.36
400.000	30.87	30.54	43.42	-1.78	88.95
300.000	21.53	29.34	36.39	-16.31	68.32
200.000	38.97	38.62	54.86	-3.64	94.15
140.000	50.94	48.82	70.56	-22.24	121.11
100.000	44.02	46.73	64.20	-35.13	105.45
70.000	38.30	34.71	51.69	-13.50	88.64
50.000	32.68	31.24	45.21	-21.36	70.95
30.000	43.89	40.11	59.45	-33.54	85.94

Table 10

SATELLITE SEPARATION: 7863.0000 KM (7 Stations); SET 4

Level (mb)	Mean	St. Dev.	rms	Min	Max
500.000	25.19	27.94	37.62	-20.77	66.63
400.000	23.62	25.98	35.12	-26.80	52.06
300.000	9.41	8.46	12.66	-3.93	18.65
200.000	13.59	14.00	19.51	-7.75	35.83
140.000	17.46	21.65	27.81	-13.57	41.90
100.000	25.93	25.36	36.27	-23.61	56.55
70.000	29.48	26.43	39.59	-20.16	69.11
50.000	14.41	24.78	28.66	-19.81	43.91
30.000	-30.30	47.90	56.68	-91.29	39.23

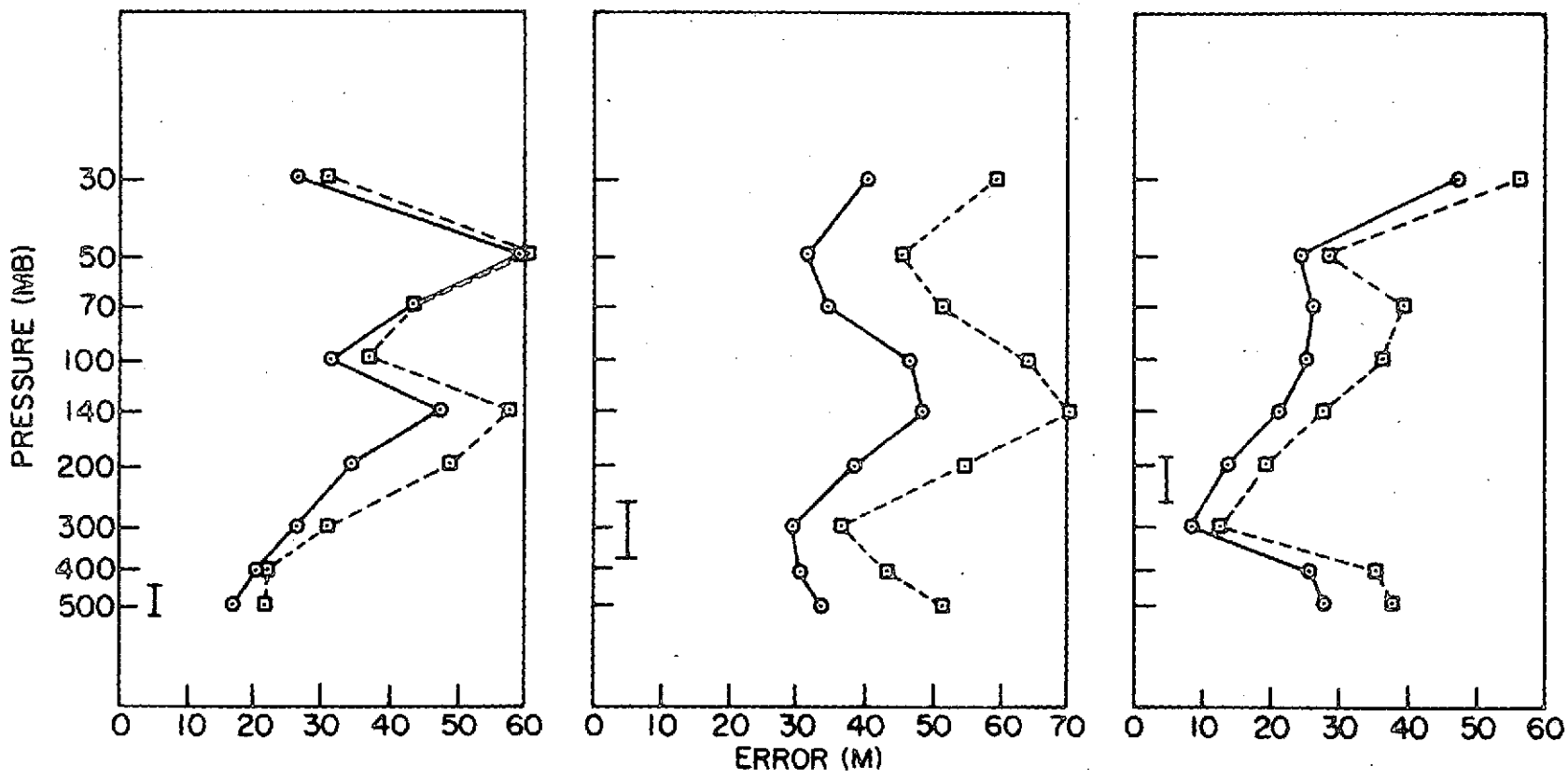

Fig. 11. STANDARD DEVIATION AND RMS ERROR VS PRESSURE. Wet atmosphere with simplistic climatic correction, satellite separation: 7863.0 km. Closest approach altitude of ray indicated by vertical line.

Table 11

SATELLITE SEPARATION: 7888.0000 KM (6 Stations); SET 2

Level (mb)	Mean	St. Dev.	rms	Min	Max
500.000	-53.11	37.21	64.85	-97.58	8.24
400.000	-57.93	41.29	71.14	-122.42	-2.86
300.000	-51.02	45.27	68.21	-126.50	0.03
200.000	-31.72	47.98	57.52	-68.77	61.28
140.000	-33.55	49.06	59.44	-89.27	48.35
100.000	-47.07	37.68	60.29	-77.58	27.00
70.000	-60.11	60.83	85.52	-142.15	9.67
50.000	-55.17	73.51	91.91	-151.57	12.85
30.000	-50.65	46.45	68.73	-118.79	5.25

Table 12

SATELLITE SEPARATION: 7888.0000 KM (8 Stations); SET 3

Level (mb)	Mean	St. Dev.	rms	Min	Max
500.000	51.29	57.44	77.00	-12.32	146.25
400.000	42.97	56.47	70.96	-31.52	135.84
300.000	33.63	58.84	67.77	-51.88	115.21
200.000	51.08	63.97	81.86	-32.43	135.99
140.000	63.04	69.96	94.18	-30.39	168.00
100.000	56.13	72.17	91.42	-43.29	150.06
70.000	50.40	63.12	80.77	-21.67	126.30
50.000	50.12	50.68	71.27	-2.69	117.84
30.000	55.99	50.55	75.44	-1.54	125.75

Table 13

SATELLITE SEPARATION: 7888.0000 KM (7 Stations); SET 4

Level (mb)	Mean	St. Dev.	rms	Min	Max
500.000	15.78	48.91	51.40	-34.20	99.85
400.000	14.21	42.20	44.53	-37.26	85.28
300.000	0.01	46.03	46.03	-67.46	67.63
200.000	4.18	64.08	64.22	-89.11	92.39
140.000	8.06	60.09	60.63	-94.93	75.12
100.000	16.53	49.55	52.23	-68.07	67.30
70.000	20.07	44.89	49.18	-41.15	72.56
50.000	5.00	59.20	59.41	-65.16	75.32
30.000	-39.71	93.34	101.44	-145.74	94.39

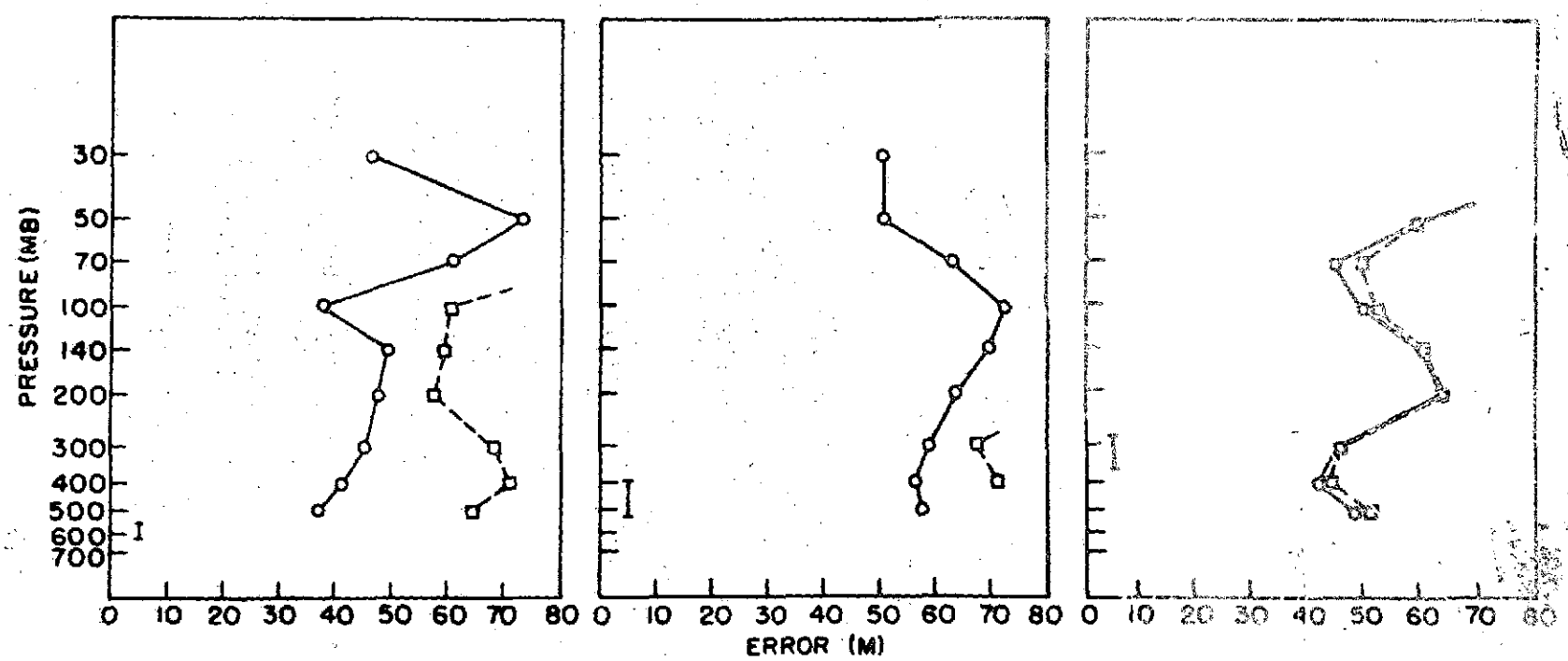

Fig. 12. STANDARD DEVIATION AND RMS ERROR VS PRESSURE. Wet atmosphere with simplistic climatic correction, satellite separation: 7888.0 km. Closest approach altitude of ray indicated by vertical line.

Table 14

SATELLITE SEPARATION: 7863.0000 KM (6 Stations); SET 2

Level (mb)	Mean	St. Dev.	rms	Min	Max
500.000	10.37	8.66	13.51	-0.26	21.08
400.000	5.56	15.49	16.45	-19.55	28.87
300.000	12.47	22.52	25.74	-23.63	45.27
200.000	31.76	27.86	42.25	1.24	71.97
140.000	29.93	45.59	54.54	-23.13	80.99
100.000	16.42	27.90	32.38	-18.49	46.27
70.000	3.38	38.68	38.83	-54.34	56.15
50.000	8.31	55.82	56.43	-49.15	92.56
30.000	12.83	24.88	28.00	-15.91	55.76

Table 15

SATELLITE SEPARATION: 7863.0000 KM (8 Stations); SET 3

Level (mb)	Mean	St. Dev.	rms	Min	Max
500.000	13.91	20.29	24.60	-18.24	38.74
400.000	5.59	17.51	18.38	-19.58	27.90
300.000	-3.74	18.36	18.74	-39.93	24.18
200.000	13.70	28.19	31.34	-20.49	66.59
140.000	25.67	39.40	47.02	-40.89	92.33
100.000	18.75	37.49	41.92	-53.79	77.89
70.000	13.02	26.43	29.47	-32.17	61.07
50.000	12.74	12.80	18.06	2.70	42.34
30.000	18.61	32.47	37.43	-46.31	67.28

Table 16

SATELLITE SEPARATION: 7863.0000 KM (7 Stations); SET 4

Level (mb)	Mean	St. Dev.	rms	Min	Max
500.000	20.38	26.00	33.03	-25.66	48.63
400.000	18.81	25.17	31.42	-31.70	45.03
300.000	4.60	11.40	12.29	-9.59	19.66
200.000	8.78	11.17	14.20	-8.24	16.14
140.000	12.65	20.65	24.22	-13.66	34.70
100.000	21.12	27.21	34.45	-28.50	58.59
70.000	24.67	29.83	38.71	-25.05	71.14
50.000	9.60	25.67	27.41	-20.39	45.94
30.000	-35.12	44.69	56.83	-100.97	18.59

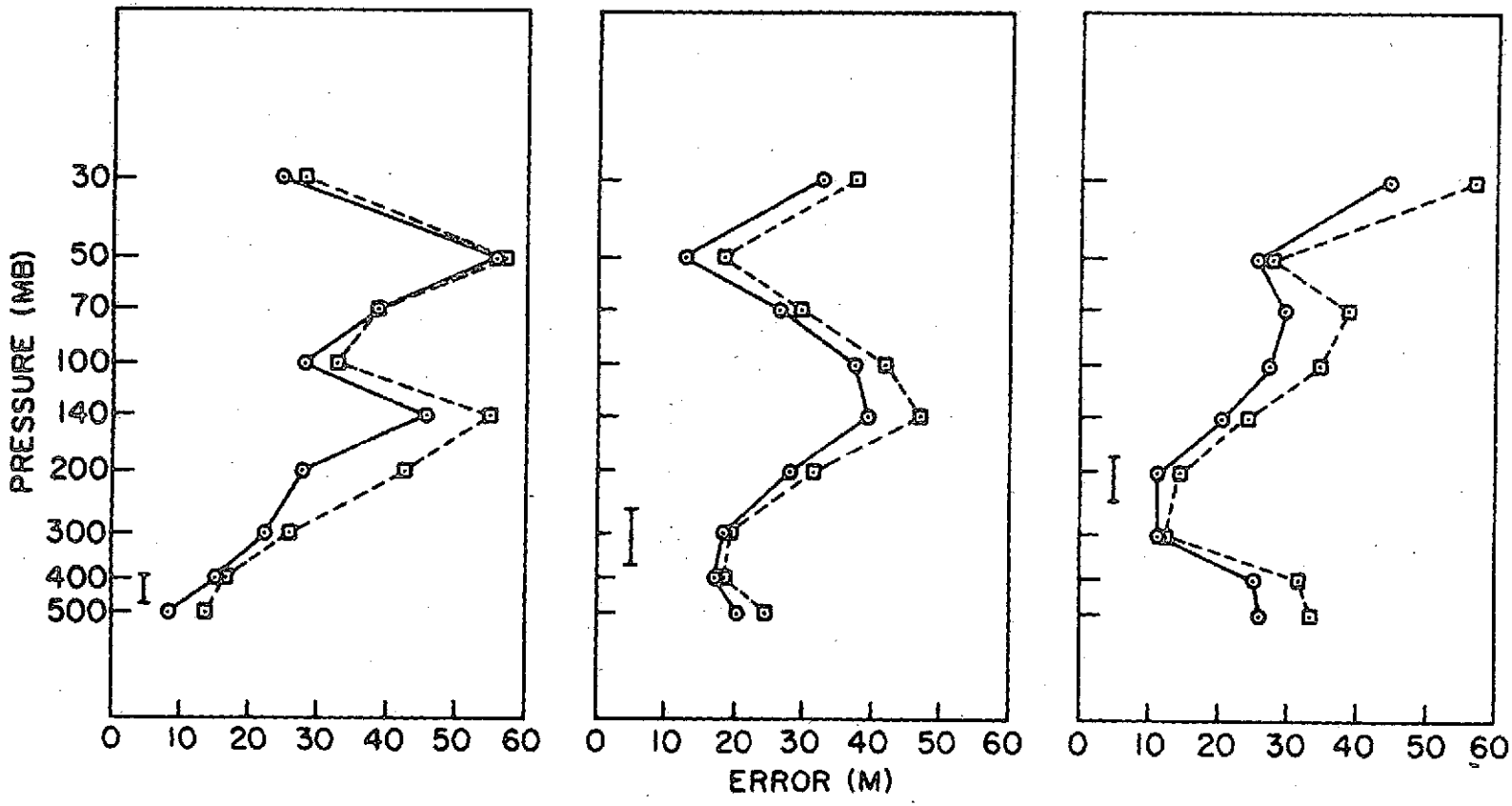

Latitude range 25°-37° N
6 profiles

Latitude range 38°-51° N
8 profiles

Latitude range 51°-76° N
7 profiles

Standard Deviation ——— RMS -------

Fig. 13. STANDARD DEVIATION AND RMS ERROR VS PRESSURE. Wet atmosphere with ideal water-vapor correction, satellite separation: 7863.0 km. Closest approach altitude of ray indicated by vertical line.

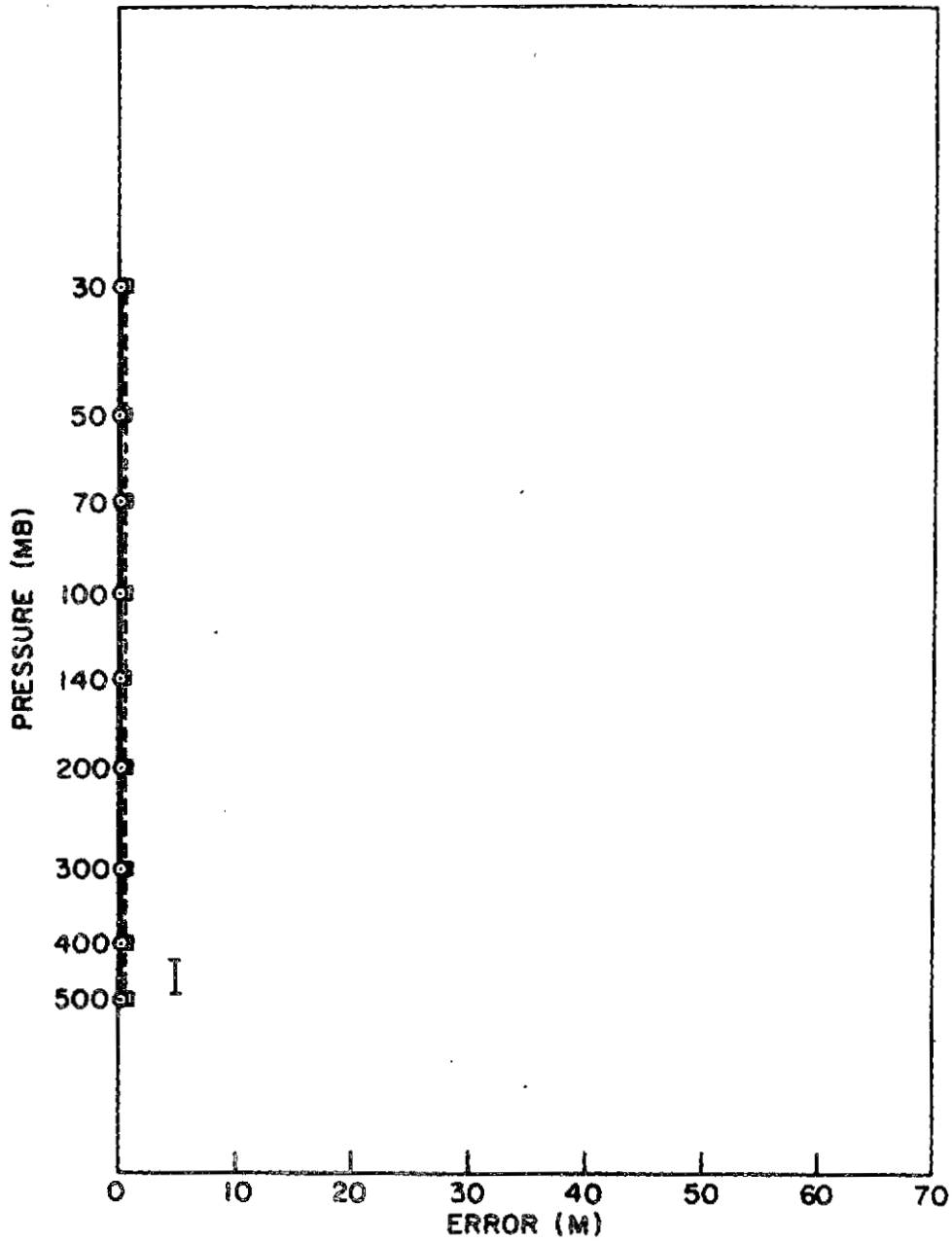

Latitude range 25°-30° N
6 profiles

Standard Deviation ——— RMS -------

Fig. 14. STANDARD DEVIATION AND RMS ERROR VS PRESSURE. Ideal temperature profile, dry atmosphere. Satellite separation: 7863.0 km.

One minima generally occurs in the neighborhood of 300 to 400 mb, and the other in the neighborhood of 50 to 70 mb. The maxima are near the 30 mb level and between 100 and 200 mb (which, for most profiles, is the pressure level of the tropopause).

The pattern can be explained by considering that the minimum at the lower altitude, near the 300 mb level, is associated with the closest approach altitude of the raypath (the vertical line in the figures). Because the system is most sensitive to atmospheric effects in approximately the lower 3 km of the raypath, the absolute value of error in this neighborhood tends to be minimized.

The overall pattern is the result of the errors in the temperature profile, which generate errors in altitude when the temperature-altitude profile is constructed using the hypsometric formula. This effect is illustrated by the absence of any extrema in the results of the ideal, temperature-profile case (Fig. 14) where each level has the same error as that of the 300 to 400 mb level. The magnitude of the error is of primary interest. It can be seen in Figs. 8 and 9 that, generally, the rms and standard deviation below 300 mb are approximately 20 to 30 m. Figure 15 shows the 300 mb error for each of the profiles used in the generation of Fig. 6, plotted as a function of rms temperature error in the 100 to 400 mb pressure range. Although there is no clear regression line, it should be noted that the upper left-hand portion of the graph is free of data points, which indicates that a low rms value of temperature error in the 100 to 400 mb range invariably results in a small altitude error at the 300 mb level. It is reasonable, therefore, to expect that improvements in the performance of the SIRS will lead to concommitant improvements in the performance of the occultation system. It should be noted also that a high rms value of temperature error does not lead necessarily to a large error in the altitude of the 300 mb level, as witnessed by the large number of points in the lower right-hand portion of the figure.

Comparison of Figs. 8 and 9 reveals that it is possible to choose a satellite separation for each of the latitude ranges such that the rms and standard deviation at the 300 mb level are less than 26 m.

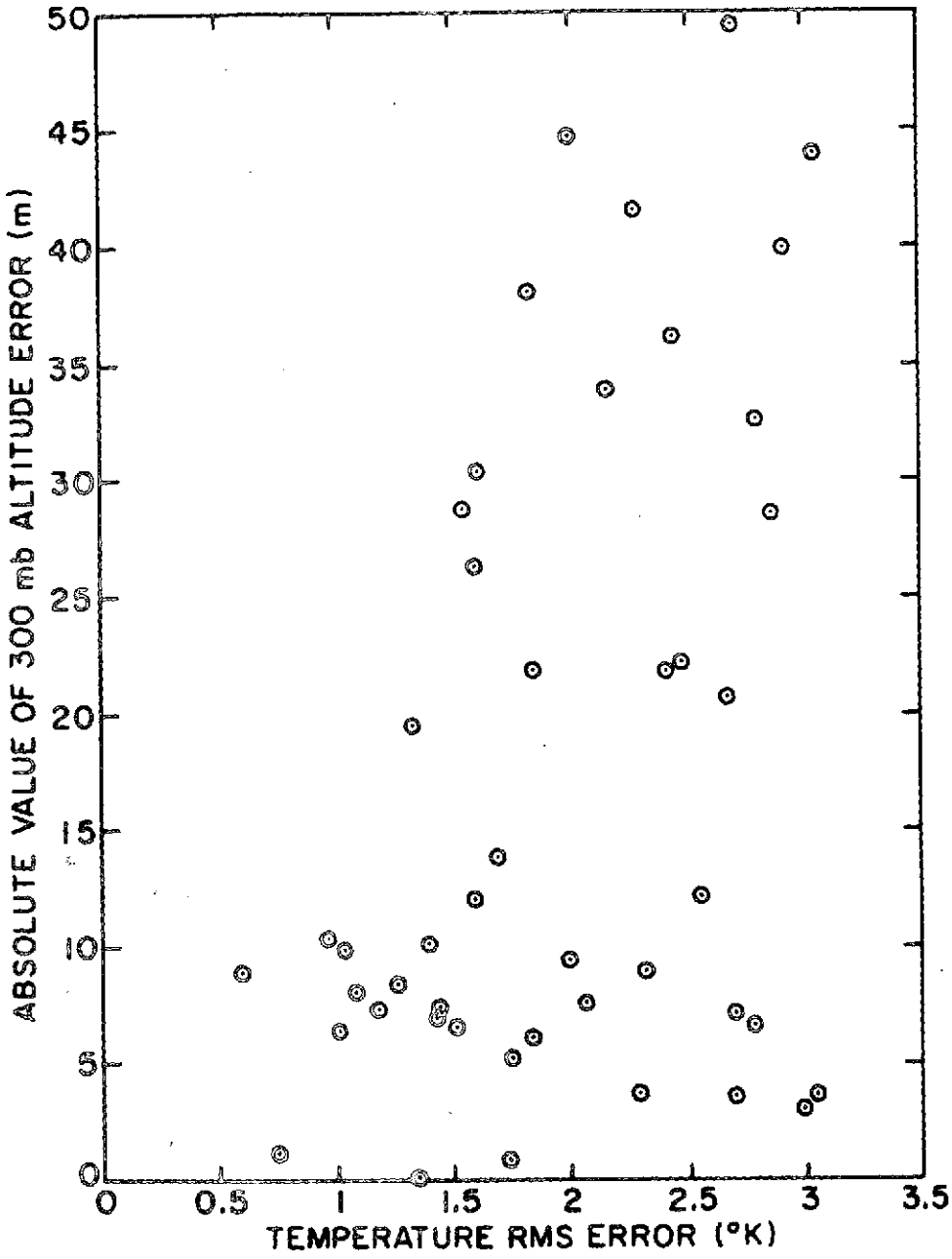

Fig. 15. ALTITUDE ERROR AT 300 mb VS TEMPERATURE RMS ERROR.
Pressure range: 100 to 400 mb.

This does not suggest necessarily that there must be more than one satellite pair in the system, but it does illustrate that minimum ray altitude is a significant parameter that should be selected in such a way as to optimize system performance. In fact, the 7863.0 km separation obtains acceptable results at all three latitude ranges. Should further analysis indicate that variable satellite separation is desirable, a small oblateness can be introduced intentionally into the satellite orbit. Note that, in each figure, the lower minimum occurs in the range of the closest approach altitude.

It can be seen in Fig. 11 that the simplistic water-vapor correction produces remarkably good results. The standard deviation and rms at the 300 mb level and below are once again in the neighborhood of 20 to 30 m. Figure 13 illustrates that the errors are caused by the failure of the corrective profile to account adequately for the water vapor, and these results should be compared to the corresponding curves in Fig. 8. Errors introduced by water vapor can be totally eliminated by properly correcting for the water vapor. If exact corrections are not available, even the most simplistic corrections (Fig. 11), in which a standard water-vapor profile corrects for water-vapor effects, can have dramatic results. Not correcting for water vapor will yield errors on the order of hundreds of meters.

The effect of varying the minimum ray height in the presence of water vapor is illustrated in Fig. 12. The system operating at the lower ray height (greater satellite separation) yields generally poorer results than the system operating at the higher ray height (smaller satellite separation). Because water-vapor concentration falls off rapidly with altitude (scale height on the order of 2 km), this is not a particularly surprising result, as proper water-vapor correction is more important as the ray passes into regions of high water-vapor content.

Chapter IV

THE HAWAII EXPERIMENT

"One would grow poor staying in one place always."

--Poem of the Cid

A major concern in the design of an occultation satellite system is the possible effect of atmospheric turbulence on system performance, consisting chiefly of scintillation of the microwave signal and the possible consequent loss of phase lock. In addition, multipath due to atmospheric water-vapor inhomogeneities could cause deep fading for several seconds or longer, again resulting in loss of phase lock. Although ambiguity resolution built into the system hardware would make it easy to reestablish the phase-path measurement after lock is regained, there will be a total loss of data while the signal is in deep fade.

To assess the problems associated with scintillation and deep fade, a ground test was performed between two mountains in Hawaii during June 1970. The choice of site was determined largely by such logistical factors as the availability of power and shelter and ease of access. The Hawaii location also provided a 150 km transmission path between stations at a relatively high altitude for a ground test (3.05 and 3.35 km above sea level).

By proper choice of antenna beamwidths, the illuminated area between the transmitter and receiver was limited to altitudes between 2 and 4 km above sea level, thus avoiding interference from surface reflection. An operational pressure-reference system will have a closest approach ray altitude in the neighborhood of 8 km, which is much higher (and dryer) than the 2 to 4 km altitude sampled in this experiment. It was necessary, therefore, to extrapolate the results obtained in Hawaii to the higher altitude so as to assess the impact of the observed phenomenon on the proposed system. Ideally, 8 km mountains were preferred. None were available.

The data acquisition and scintillation analysis were performed by a group from the U.S. Department of Commerce Office of Telecommunications [8].

A. Description of Measurements

Radio-propagation measurements were made in 1970 over a continuous two-week period from 0800 June 15 through 0500 June 29. The transmitter was located at the University of Hawaii Mees Solar Observatory, at the summit of Haleakala on the island of Maui. The receiver was located 150 km to the southeast, at the Mauna Loa Observatory (at the 11,000 ft level) on the island of Hawaii.

At the transmitter end of the path, three 1.25 m parabolic dishes (beamwidth 1.8°) transmitted signals at wavelengths very close to 3.4 cm (a slight frequency offset at each of the antennas enabled the receiver to distinguish between signals transmitted from each antenna). The antennas were spaced horizontally along a line perpendicular to the nominal transmission path, with 10 m between the first and second antennas and 100 m between the first and the third. The receiver consisted of a single 2 m parabolic dish (1.2° beamwidth) and associated electronics, and the received signals were retransmitted to the Haleakala station via a frequency-modulated telemetry link. The beamwidths of the receiving and transmitting antennas were narrow enough to ensure that the Earth's surface would not be illuminated within the half-power points of the two antennas.

Signal amplitudes from the three antennas, phase variability of the three transmission paths, and phase difference between the first and second and the first and third antennas were recorded continuously. Only the signal-amplitude measurements are discussed in this study.

In addition to the radio measurements, an instrumented aircraft equipped with a microwave refractometer was flown along the raypath to measure the refractivity of the atmosphere. Flights were made approximately twice a day, on a schedule that ensured sampling from each period of the diurnal cycle.

Figures 16 and 17 are horizontal and vertical views of the transmission path.†

†All figures in this chapter were taken from Ref. 8.

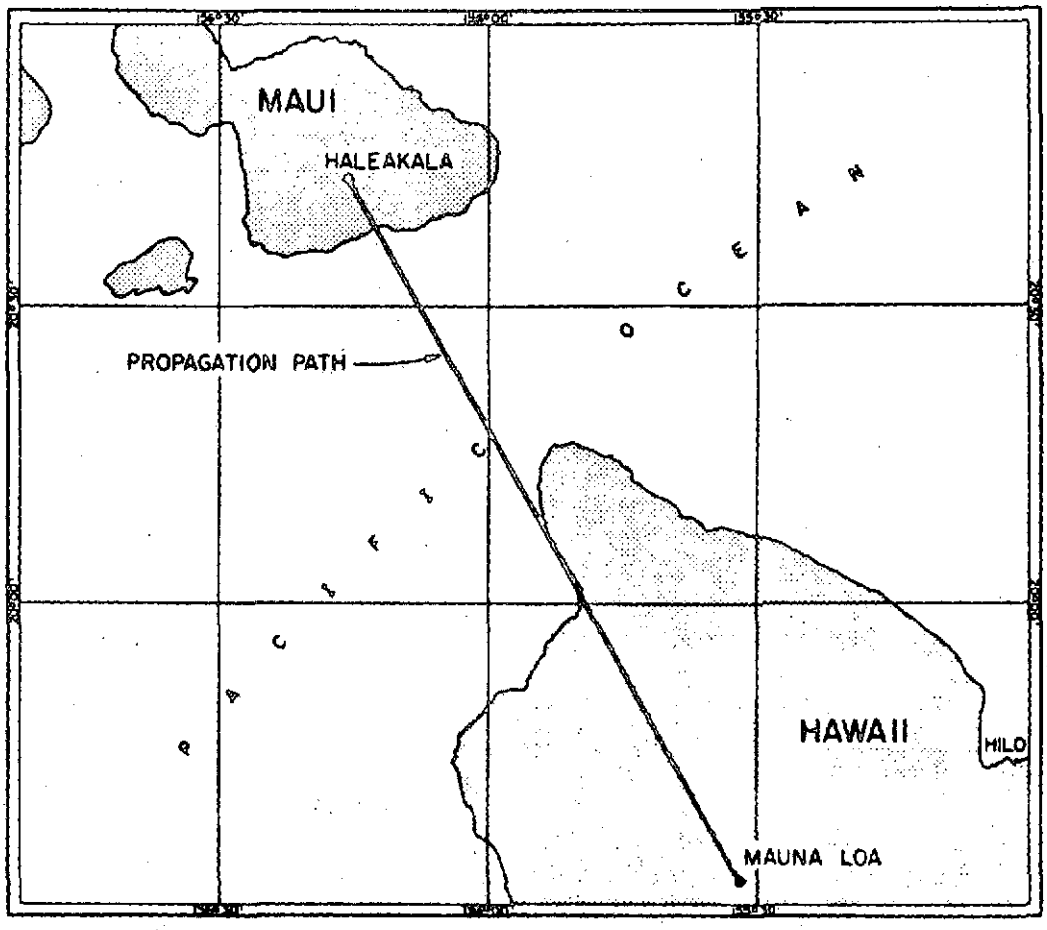

Fig. 16. HAWAII PROPAGATION PATH. The transmitter was located on Haleakala. Prevailing winds were from the northeast (upper right-hand corner).

B. Significant Observations

Perhaps the most interesting feature of the observed radio data was the presence of periods of deep fading, some as deep as -40 dB. Although these very deep fades would typically have a duration of only a few seconds, on occasion, the signal would drop below -30 dB for as long as 20 sec. Days with deep fades were also characterized by many incidents of less intense fading. Signal enhancements of up to +5 dB were occasionally observed. Typical amplitude records from a "quiet" day (one in which there was very little intense fading) and from a "noisy" day are shown in Fig. 18.

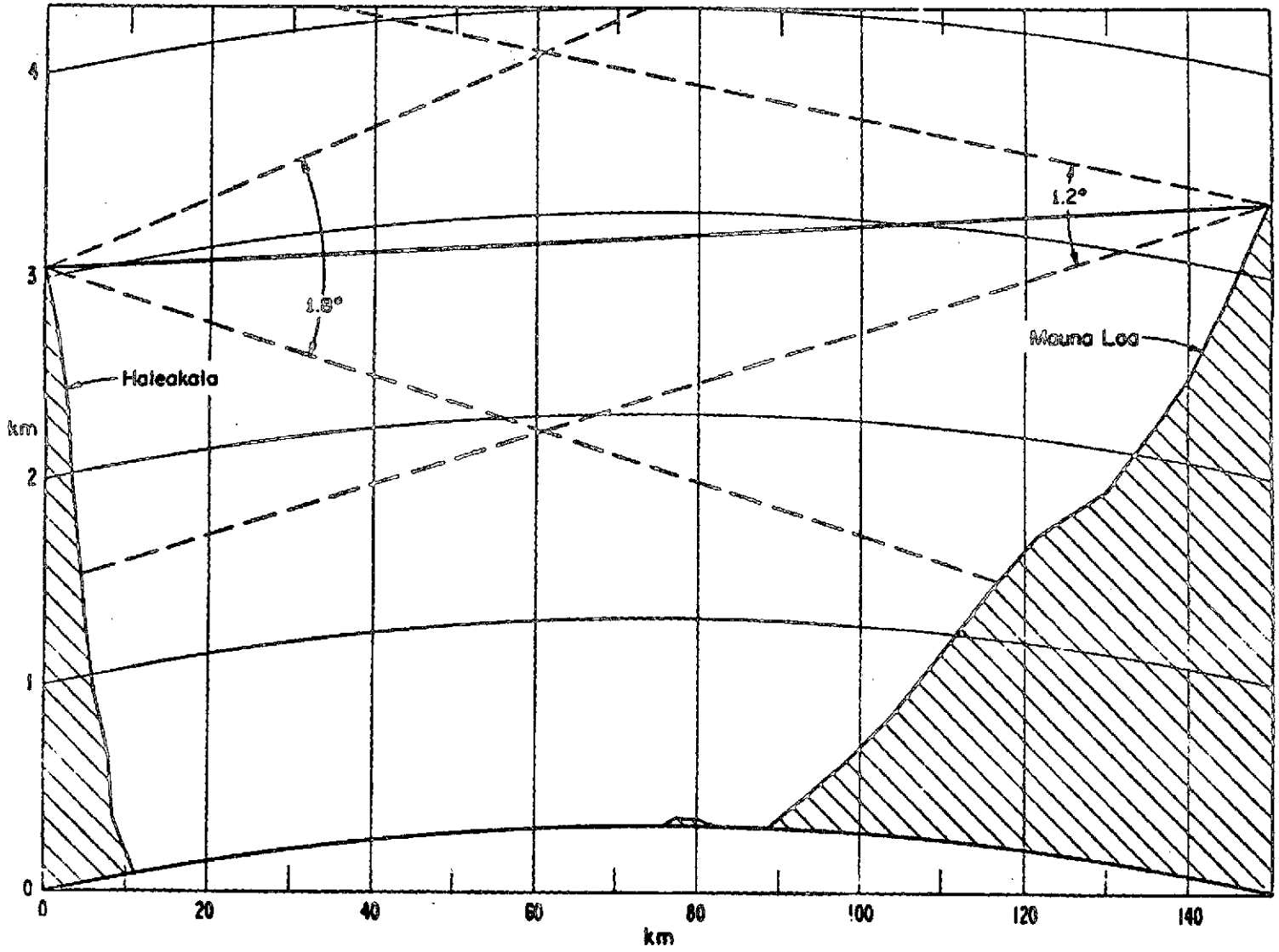

Fig. 17. VERTICAL SECTION OF THE HAWAII PROPAGATION PATH. The transmitter is on the left. The dashed lines indicate the beamwidths of the antennas. Note that only the region from 2 to 4 km above sea level is illuminated by both the transmitting and receiving antennas.

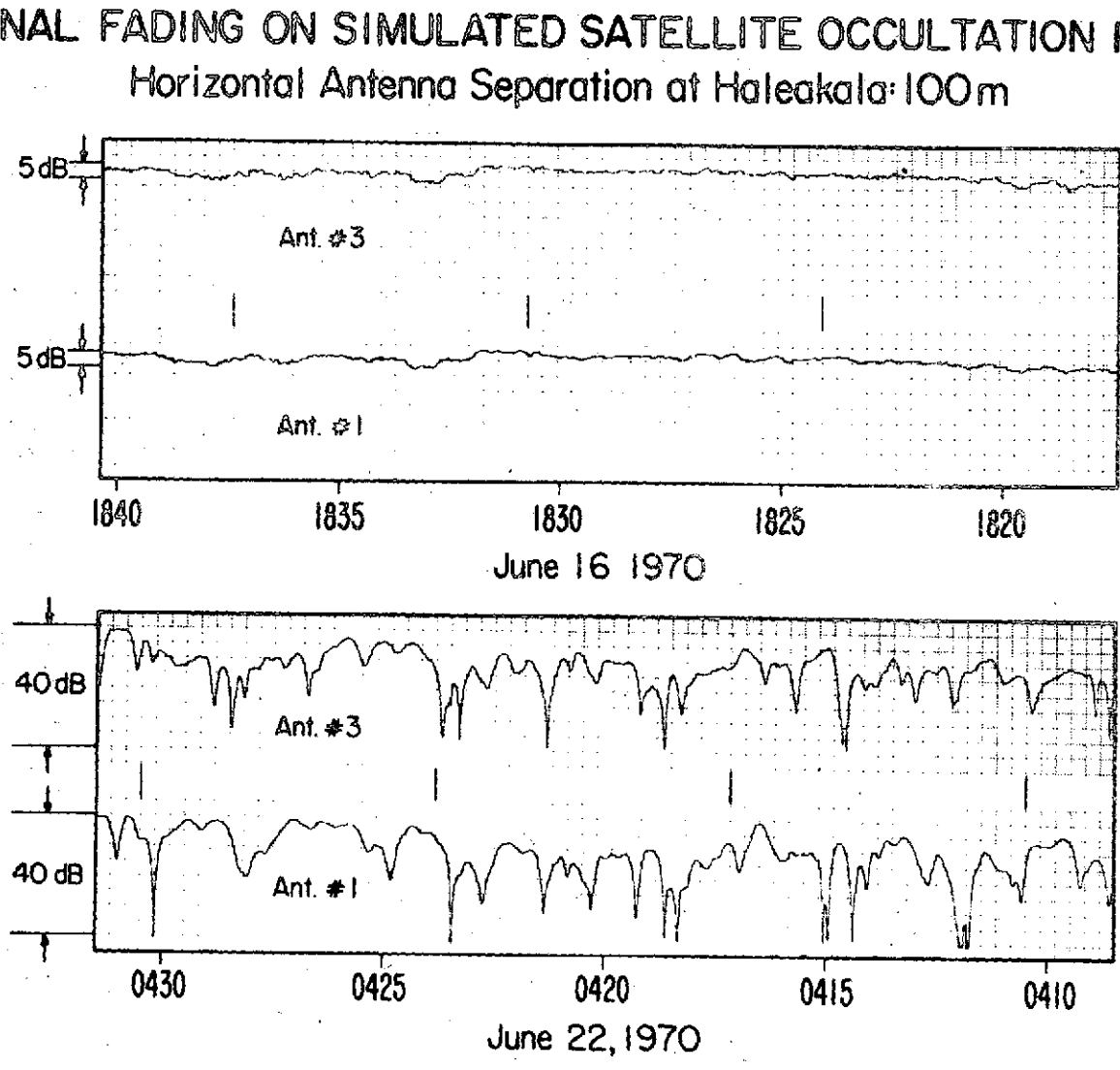

Fig. 18. TYPICAL AMPLITUDE RECORDS FOR A "QUIET" DAY (TYPE B) AND A "NOISY" DAY (TYPE D). Antennas 1 and 3 were separated by 100 m.

The amplitude record was divided into 30 min periods, each classified into one of four "fading types" designated A, B, C, and D, corresponding to

Type A: <5 dB peak-to-peak fading range

Type B: >5 dB peak-to-peak fading range

Type C: >5 dB fading range with 1 to 5 V-shaped fades >15 dB

Type D: >5 dB fading range with over 5 V-shaped fades >15 dB

The record of microwave fading over the two-week period of the experiment is summarized in Fig. 19.

It was necessary to modify the flight pattern of the instrumented aircraft because of the unexpected incidence of deep fading. The original plan ("Flight Pattern I") called for the plane to fly an H-shaped pattern, taking two vertical profiles to study ray propagation, and a horizontal profile in between to be used as data for the scintillation analysis.

Because the presence of deep fading made extra vertical profiles desirable, a second plan ("Flight Pattern II") was implemented, in which the aircraft flew a sawtooth pattern between the transmitter and the receiver.

The flight patterns are also summarized in Fig. 19. Figures 20 and 21 are typical N-profile records; flight 4 (Fig. 20) was made during a type B fading period and flight 12 (Fig. 21) during a type D fading period.

C. Analysis of the Data

The primary objective in analyzing the data was to identify the mechanism responsible for the deep fades and, if possible, to determine whether this mechanism will be active at the 8 km altitude at which the pressure-reference-level system will operate. The method chosen was to raytrace through the refractivity profiles (N-profiles) recorded by the aircraft and to establish correlations between raytracing results and signal properties.

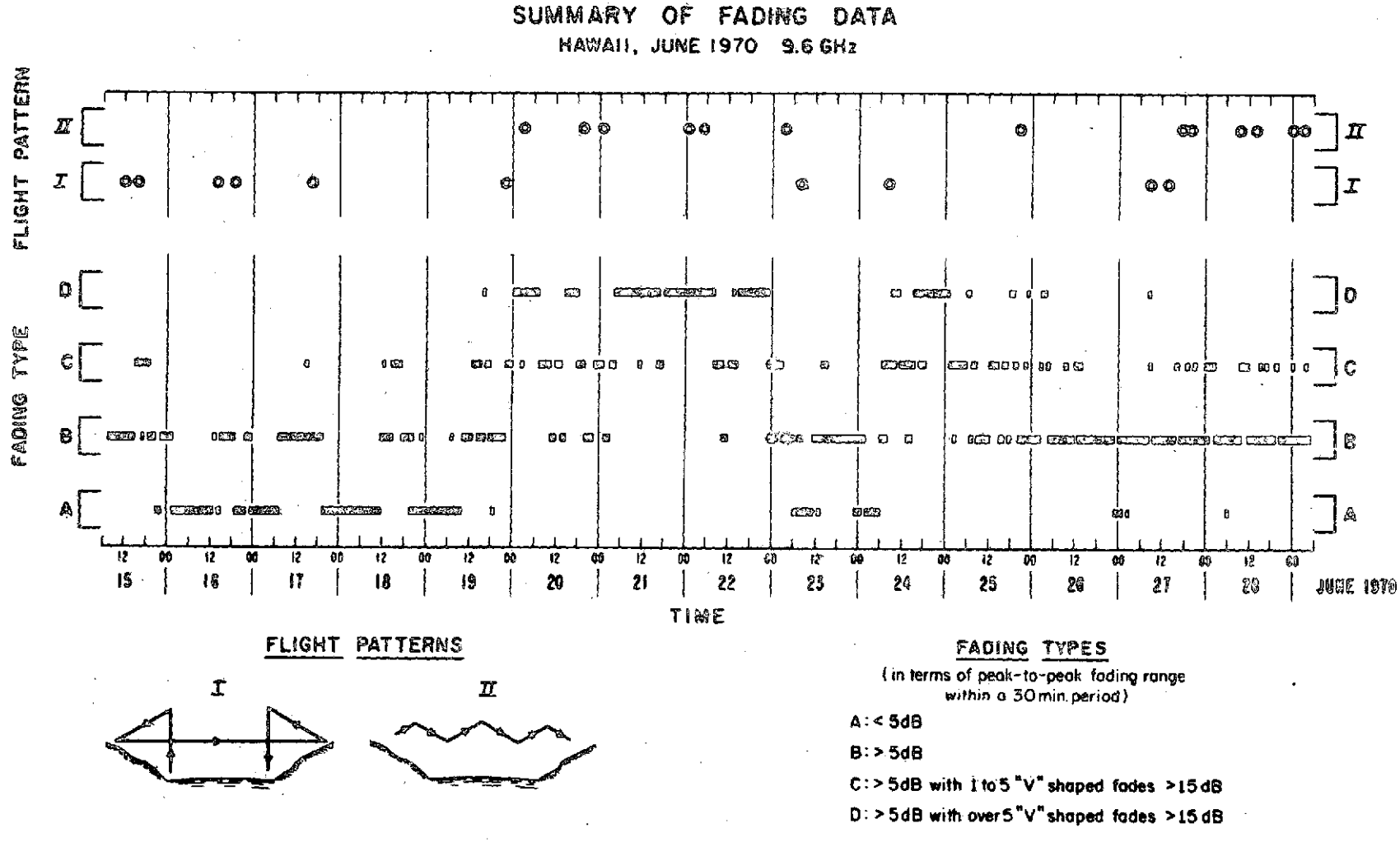

Fig. 19. RECORD OF MICROWAVE FADING AND INSTRUMENTED AIRCRAFT FLIGHTS.

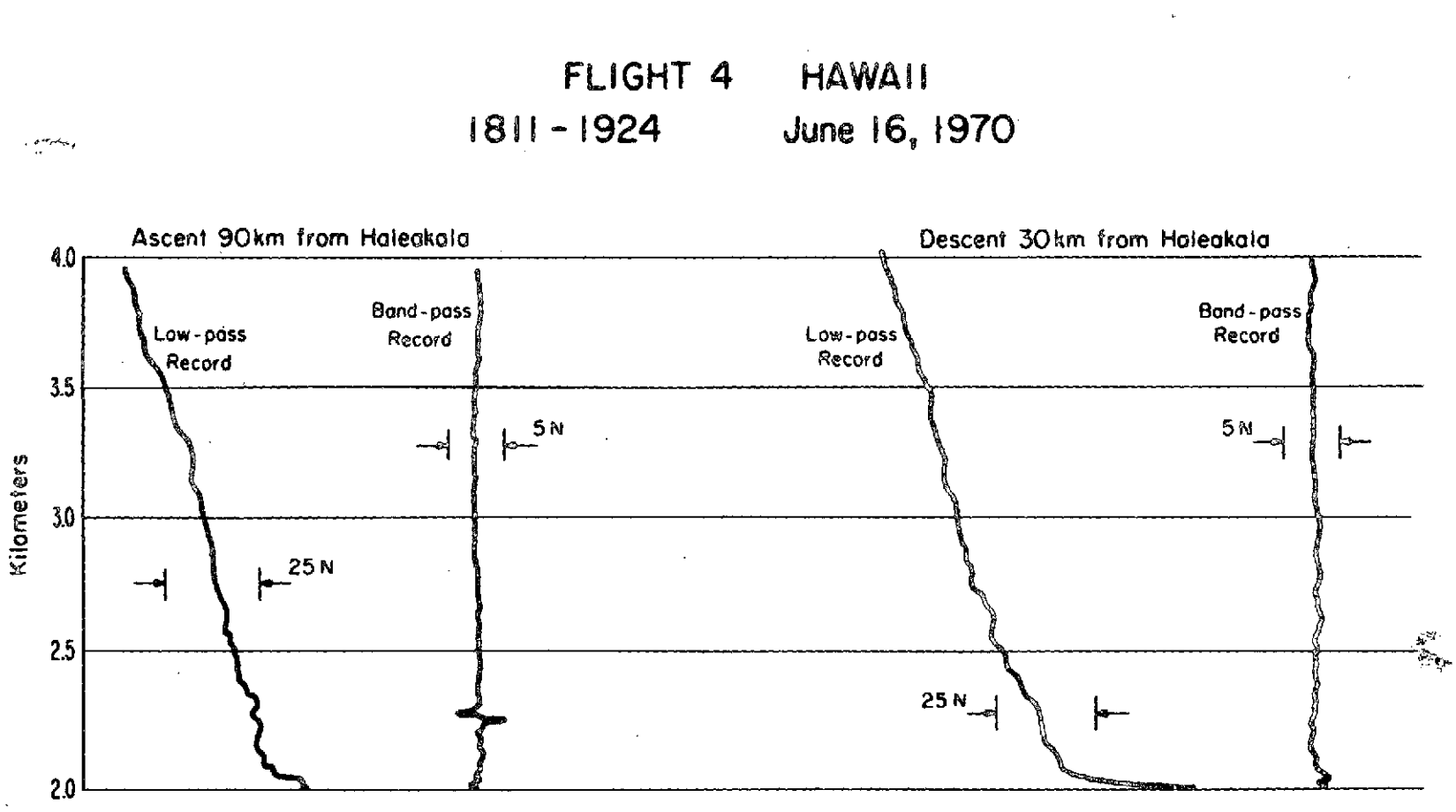

Fig. 20. TYPICAL N-PROFILES TAKEN BY THE AIRCRAFT ON A QUIET DAY. The nearly vertical lines are high-frequency residuals that result from applying a low-frequency filter to the adjacent N-profiles.

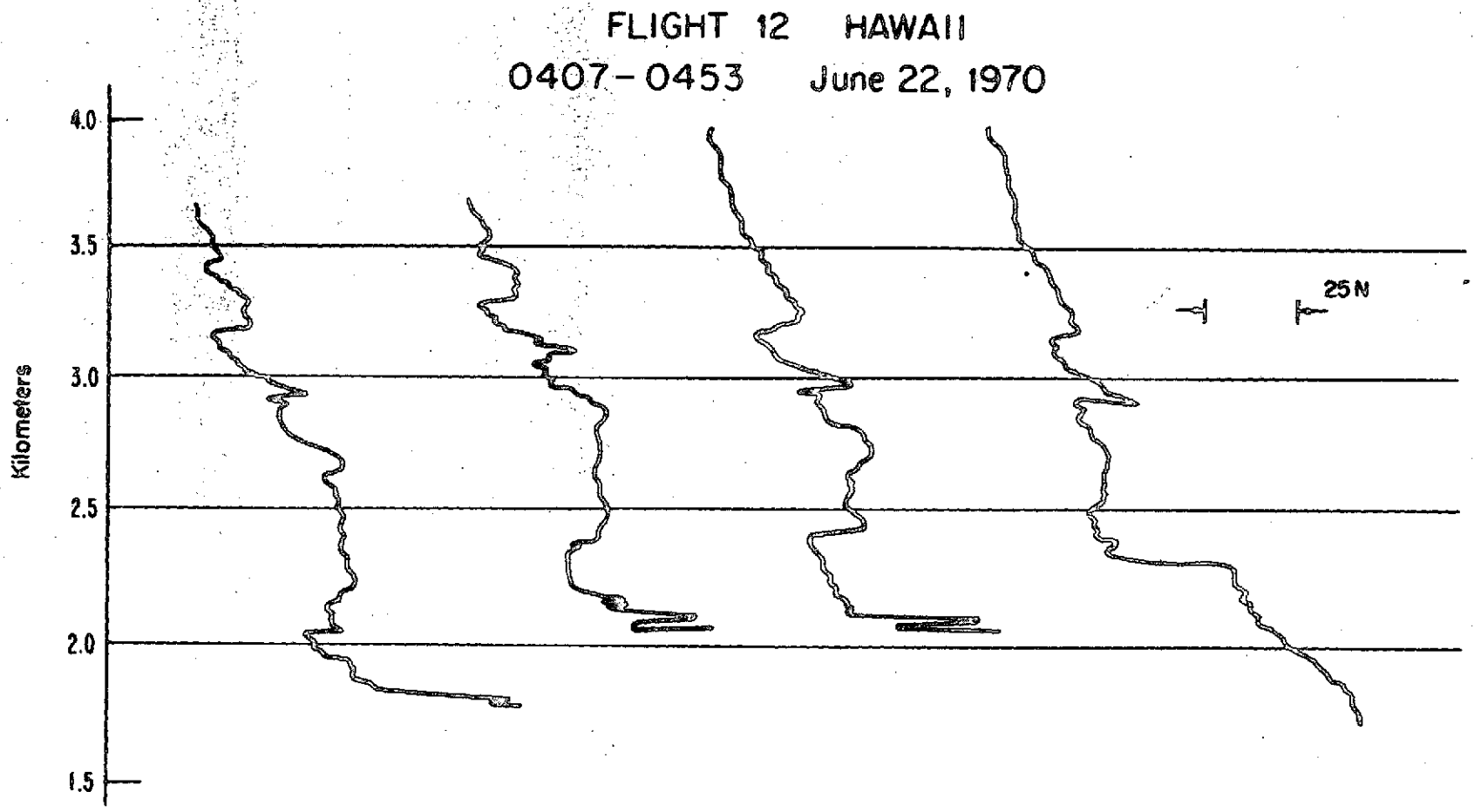

Fig. 21. TYPICAL N-PROFILES TAKEN BY THE AIRCRAFT ON A NOISY DAY.

To raytrace through the Hawaii data, a raytracing program was required that could accommodate a nonsymmetric atmosphere with data points at varied spacing (variable resolution data). A similar program had been developed several years ago, called RAYTRACE, based on Snell's Law (see Chapter II). This early program was capable of raytracing through a nonsymmetric atmosphere (one in which horizontal gradients were nonzero), with relatively low-resolution data.

To adapt RAYTRACE to the Hawaii data, a new mode of raytracing was required. RAYTRACE began tracing at an arbitrary "center" of a raypath, where the ray was assumed horizontal, and then traced its way out, first to the left and then to the right, stopping when it reached "satellite altitude." For the Hawaii analysis, it was necessary for the raytracing program to begin at a "transmitter" and then follow a raypath through to the neighborhood of the "receiver," each located on a "mountain" at a given range and altitude.

It was desirable, also, for the program to raytrace from satellite-to-satellite through an atmosphere whose lower portion consisted of the Hawaii data. The variable-resolution feature of the program was needed for this phase of the analysis because it was necessary to supplement the Hawaii data at altitudes above 4 km with relatively low-resolution Standard Atmosphere data.

Details of the resulting programs, HAWAII (station-to-station) and THRUWAY (satellite-to-satellite), and the original RAYTRACE are described in Appendix C, with a listing of THRUWAY in Appendix B.

The N-profile data were analyzed in four stages.

(1) Each available vertical profile was expanded spherically symmetrically, and the HAWAII program (station-to-station, raytrace between two mountains) simulated the performance of the propagation experiment.

(2) A small but representative sample of these profiles was also expanded spherically symmetrically and used in the THRUWAY program (satellite-to-satellite) to simulate the performance of a satellite system transmitting through spherically symmetric atmospheres whose vertical profiles were the same as those obtained in the Hawaii experiment.

(3) The vertical profiles from five of the airplane flights were combined to form nonsymmetric atmospheres (atmospheres with nonzero horizontal gradients).

(4) These nonsymmetric atmospheres were used with both the HAWAII and THRUWAY programs.

Details of these analyses are presented in the following chapters.

Chapter V

RAYTRACING STATION-TO-STATION THROUGH SYMMETRIC HAWAII PROFILES

"If a man will begin with certainties, he shall end in doubts; but if he will be content to begin with doubts, he shall end in certainties."

--Francis Bacon

The first stage in the raytracing analysis of the Hawaii data was to expand each of the refractivity profiles generated by the airplane into a spherically symmetric "atmosphere," and raytrace through this stratified profile using the mountain-to-mountain raytracing program HAWAII (see Chapter IV).

The program traces raypaths, beginning at the transmitter and continuing to some point at the range (150 km) of the receiver, thereby simulating the configuration of the Hawaii experiment (Figs. 16 and 17). The starting angle of the ray at the transmitter is varied by 45 mrad, in 1 mrad steps, thus generating an image of the raypaths for signals leaving the transmitting antenna across its main lobe.

The HAWAII program output is a computer-generated plot of the raypaths between the two stations (at 3.05 and 3.35 km altitudes and separated by 150 km in range), and plots of received power and integrated phase defect (excess path length caused by bending and retardation), both as functions of altitude at the range of the receiver (see Figs. 22 to 37). If the program detects a multipath, it will determine the magnitude and phase of the resultant phasor at the range of the receiver. This program was run on an XDS Sigma-5 computer, and the plots were drawn on-line on a 10 in. Calcomp plotter.

A total of 77 refractivity profiles were available for raytracing. The profiles were transcribed from analog tape onto graph paper. Values of refractivity were read onto computer cards at 40 altitudes between 6500 and 13,000 ft (corresponding to 2 and 4 km). These cards were used as input to a data-conversion program on an IBM 360/67 computer which gave 40 values of refractivity as output, interpolated at 50 m intervals between 2 and 3.95 km. This interpolated data formed the input for the raytracing program on the XDS Sigma-5 computer.

As seen in Figs. 26 and 27, the refractivity profiles made by the aircraft produced only relative values of N. To generate realistic values of excess path length caused by retardation, absolute values were required. The excess path length resulting from bending, and the shape of the raypath, are both functions of the gradient in N and, therefore, can be computed given only relative values of refractivity.

The value of N at 4.0 km was taken arbitrarily as 0.0, and a standard value of refractivity was added to each of the 40 points on the profile. This standard value was determined from the temperature and pressure values at 4.0 km in the U.S. Standard Atmosphere Supplement, 1966, 15° N Annual profile [9], along with a value of water-vapor pressure obtained from a standard profile [10], using Eq. (2.2) to determine N given the values of T, p, and e.

As a result, the refractivity data progressed through several stages of transcribing, reading, and interpolating before it was incorporated into the raytracing routine. Visual comparison was made between the data sent from Boulder and the final refractivity profile to ensure that the input presented to the computer was reasonably accurate in that no gross features had been overlooked or spurious features introduced along the line.

As described in Chapter IV, the received microwave signals were divided into four fading types, according to the amount of fading present during a 30 min period:

Type A: peak-to-peak fading range <5 dB, one profile

Type B: peak-to-peak fading range >5 dB, 49 profiles

Type C: 1 to 5 V-shaped fades >15 dB, 12 profiles

Type D: >5 V-shaped fades >15 dB, 15 profiles

The atmospheric effects generally held responsible for radio fading are (1) multipath propagation in which more than one path is available to the radio wave between the transmitter and receiver, resulting in destructive interference at the receiver, and (2) defocusing in which the radio signal is "spread out" over the transmission path (the loss is greater than the $1/R^2$ loss associated with spherically propagating waves).

The results of this portion of the raytracing study are listed in Table 17, in which the incidence of multipath and/or defocusing is compared to the signal fading type. (For this study, defocusing is defined

Table 17

FRACTION OF PROFILES EXHIBITING MULTIPATH OR DEFOCUSING

Flight No.	Fading Types							
	A		B		C		D	
	Multi-path	Defocus-ing Only†	MP	DF	MP	DF	MP	DF
1			1/2					
2			--		1/2			
3			--	1/2				
4			0/2					
5			0/2					
7			1/1		0/1			
8			--				1/3	1/3
10			--	1/2		1/1		
11			--				4/4	
12			--				6/6	
13			1/6	2/6				
14	0/1		0/1					
15					2/2			
16			3/4	1/4				
17					0/1		1/1	
18			2/2					
19			3/4	1/2				
20			1/5					
21				1/3	2/2			
22			3/4		1/3			
23			1/3		1/3			
24			3/6					
Total Count	0/1	0/1	19/49	7/49	6/12	1/12	12/15	1/15

Fraction Profiles	Fading Types			
	A	B	C	D
With multipath	0.000	0.388	0.500	0.800
With defocusing only	0.00	0.143	0.083	0.067
With multipath and/ or defocusing	0.00	0.531	0.583	0.867

† Refers to profiles lacking multipath but exhibiting defocusing; defocusing is also present when multipath is present.

as a power variation greater than 15 dB when measured as a function of altitude at the receiver range.) There appears to be a definite correlation between the amount and intensity of fading and the existence of multipath or defocusing. Although both multipath and defocusing are present in slightly more than half of the type-B profiles, they are present in 87 percent of the type-D profiles. It appears likely, therefore, that multipath and defocusing are responsible to some extent for the fading observed in the Hawaii experiment.

The "shape" of the fades in the record illustrated in Fig. 18 suggests that multipath is at least partially responsible for the fading; this shape very strongly resembles the result obtained by adding two rotating phasors, as illustrated in Fig. 38. The distinguishing parameter in Fig. 38 is the relative amplitude of the two adding phasors. The two rotating phasors whose amplitudes differ by 0.1 dB or less will produce a "fade" that is very similar to the deeper fades in Fig. 18. This suggests that the observed fading in the Hawaii data may have been caused by rotating phasors of very close amplitude adding at the receiving antenna (a multipath situation).

It is important to understand the limitations of this portion of the study. First, we are treating the atmosphere between the Hawaiian mountains as spherically symmetric which, of course, is not the case. The validity of this approximation is uncertain for the scale sizes considered.

Second, the refractivity data taken by the aircraft represent a "smoothed" value over a considerable horizontal distance (the plane flies essentially horizontally, not vertically); therefore, the "vertical" profile of refractivity is not a vertical profile in the sense of a rawinsonde profile being vertical. In addition, the measurements go through various stages of reading and transcribing, as described above, before they reach the Sigma-5 computer. As a result, although the refractivity profile probably is a good representation of the Hawaii atmosphere on some gross scale, individual features of a small scale are necessarily eliminated. It is uncertain how important these features may be in explaining the behavior of the microwave signal but, if they exist, their presence is not inferable from the data, so their effect can only be hypothesized.

Third, it must be emphasized that the raypaths obtained by tracing through this "smoothed" profile are "average" raypaths (the actual raypaths between the two mountain tops in Hawaii probably never looked exactly like the raypaths drawn by the computer). In addition to being spatially smoothed, the refractivity profile also represents a time sample because it takes the airplane a finite amount of time to generate the profile (on the order of half an hour). It is futile, therefore, to attempt to match any specific feature in the microwave signal, such as a particularly deep fade, with any one raypath configuration. In addition, because the raypaths are essentially an average picture of the situation that existed in the atmosphere, it is quite reasonable to treat the entire raypath pattern as a whole and not be overly concerned with multipaths or defocusing that occur very close to the receiver altitude. A slight vertical shift in the refractivity profile was found to change the position of multipaths and focuses by a much greater amount than the actual shift in the profile.

The results of the raytracing program indicate that phase defect is a very strong function, not of path configuration or of path length, but of altitude at the range of the receiver. In other words, even in a multipath situation, the signals that arrive at a particular altitude at the receiver range tend to have phases that are very nearly equal, on the scale of several centimeters (see, for example, Fig. 33 or 37).

At first, one might be tempted to attribute this phenomenon to Fermat's Principle but, in fact, this is not the case. According to this principle, the optical length of an actual ray between any two points P_1 and P_2

$$\int_{P_1}^{P_2} n \, ds$$

is shorter than the optical length of any other curve that joins these points and lies in a certain regular neighborhood of it. (Here, n is the index of refraction of the medium and ds is an elemental distance along the raypath.) "Regular neighborhood" refers to a region that may be covered by rays in such a way that one (and only one) ray passes

through each point [11]. Fermat's Principle, therefore, specifically excludes media that give rise to multipath situations.

Figures 39 and 40 illustrate the dependence of phase and power on altitude at the receiver range and are expansions of Figs. 36 and 37 in the region of 3.4 km. Note that the phase difference between the multipath signals is on the order of a wavelength. Figures 41 and 42 plot the power difference and phase difference between the multipath signals as a function of altitude at the receiver range. The curve in Fig. 42 has a slope of 0.1 wavelength/m in the region between 3.402 and 3.405 km and an average slope of -0.3 wavelength/m between 3.405 and 3.4085 km. Figure 42 shows that a vertical shift of 6 m in the antenna position, or in the index-of-refraction profile relative to the two antennas, causes the phase difference to vary only 1.2 wavelengths.

Inspection of the amplitude record of the microwave signal during periods of deep fade shows that incidents of deep fade (< -30 dB) are occasionally interspersed with an incident of signal enhancement. It is much more common, however, for incidents of deep fade or enhancement to be clustered in groups, which indicates that, if the received signal is the sum of two rotating phasors, the phasors tend to oscillate relative to one another rather than swing through full circles of 360°. This is consistent with the situation illustrated in Fig. 42, in which the phase difference between two multipath signals is less than a wavelength. Note that the phase of the detected signal may vary considerably relative to some arbitrary value, while the phase difference of its two component signals remains small.

Figure 41 shows the power difference over the same region. The average slope over the interval below 3.407 km is 0.86 dB/m, and the maximum variation over the 6 m interval between 3.402 and 3.408 km is ≈ 4.5 dB.

The intensity distribution of the deep fades indicates that 27 percent of the fades are caused by signals with amplitude difference greater than 0.8 dB, 51 percent are caused by signals that differ by more than 0.5 dB, 67 percent by signals that differ by more than 0.3 dB, and 75 percent by signals that differ by more than 0.2 dB. Thus, 25 percent of the deep fades are attributable to the sum of two signals that differ by not more than 0.2 dB in amplitude.

The results of the raytracing study indicate that there is a definite correlation between observed multipath and defocusing in the spherically symmetric profiles and the fading observed in the microwave signals. The very brief statistical study of the incidents of deep fade corroborates this hypothesis. Clearly, opportunities are plentiful for further statistical analysis of these data. Thompson et al [8] present some interesting studies of amplitude and phase distributions.

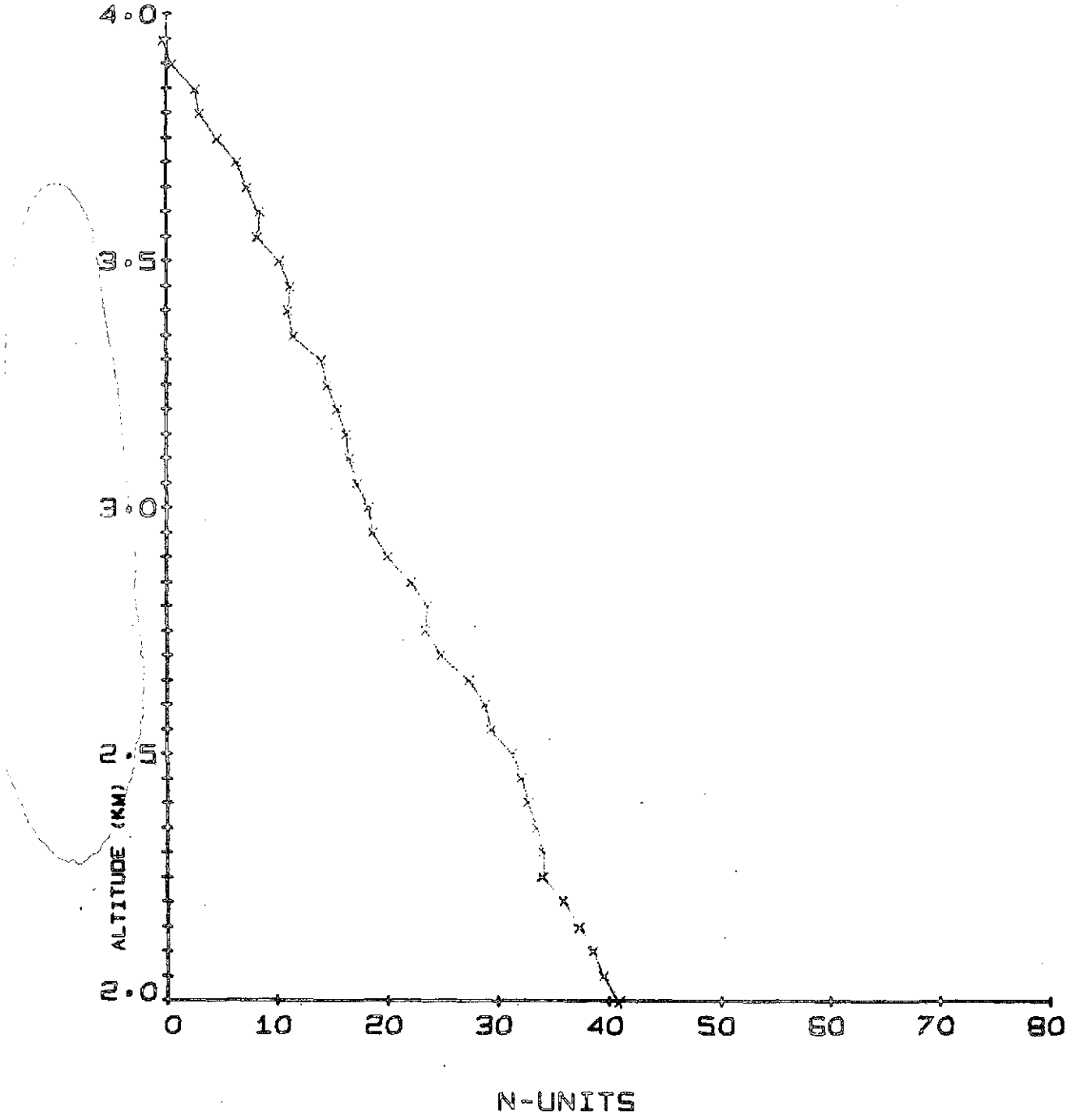

Fig. 22. N-PROFILE FOR FLIGHT 03A1, AS DRAWN BY THE SIGMA-5 COMPUTER. The number 03A1 refers to the first ascent made on the third flight. This profile was taken during a type-B period.

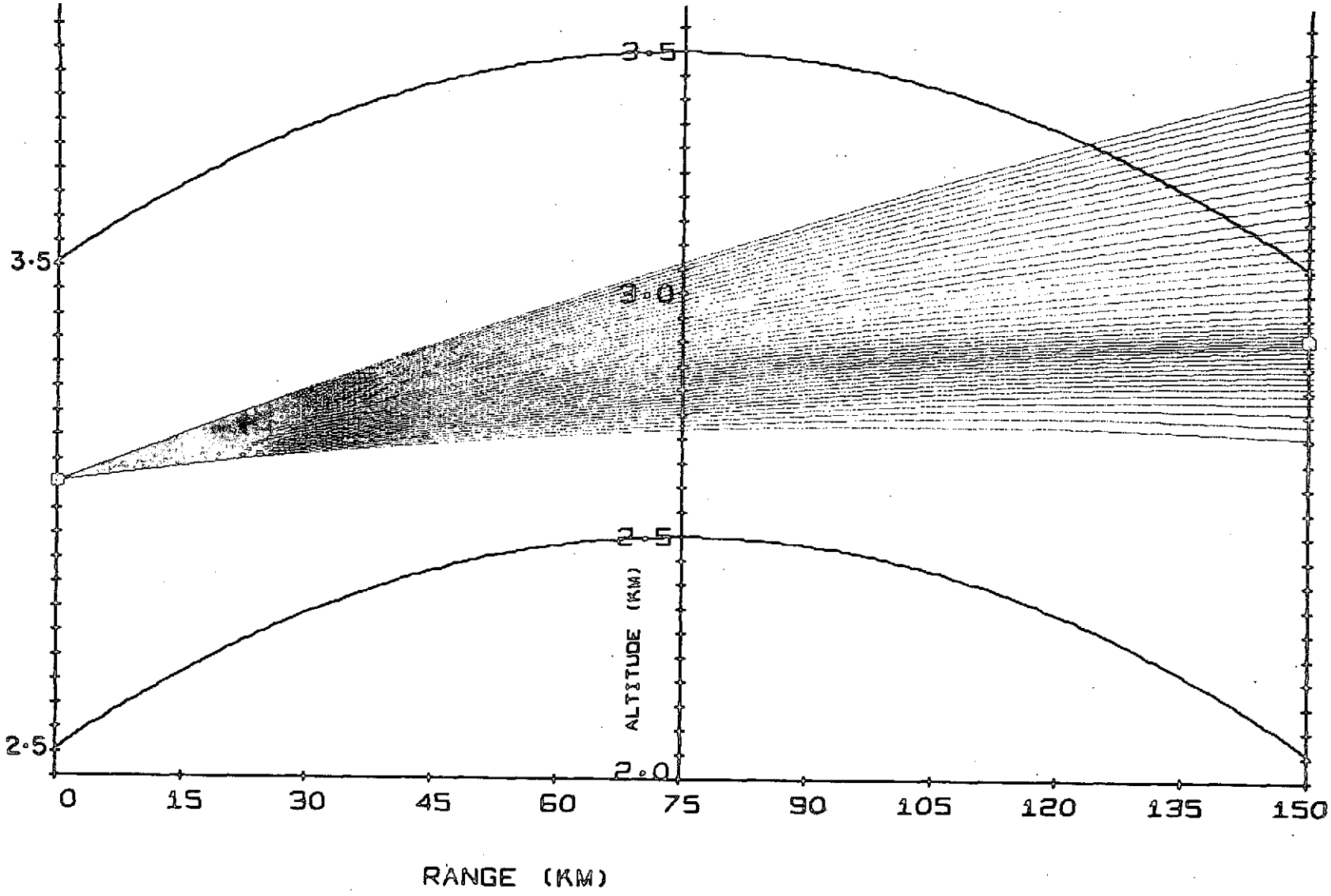

Fig. 23. COMPUTER-DRAWN RAYPATHS FOR PROFILE 03A1. Profile of Fig. 22 was expanded spherically symmetrically and used with the raytracing program to develop this diagram. Box on left = Haleakala transmitter; box on right = Mauna Loa receiver. Vertical scale is greatly expanded.

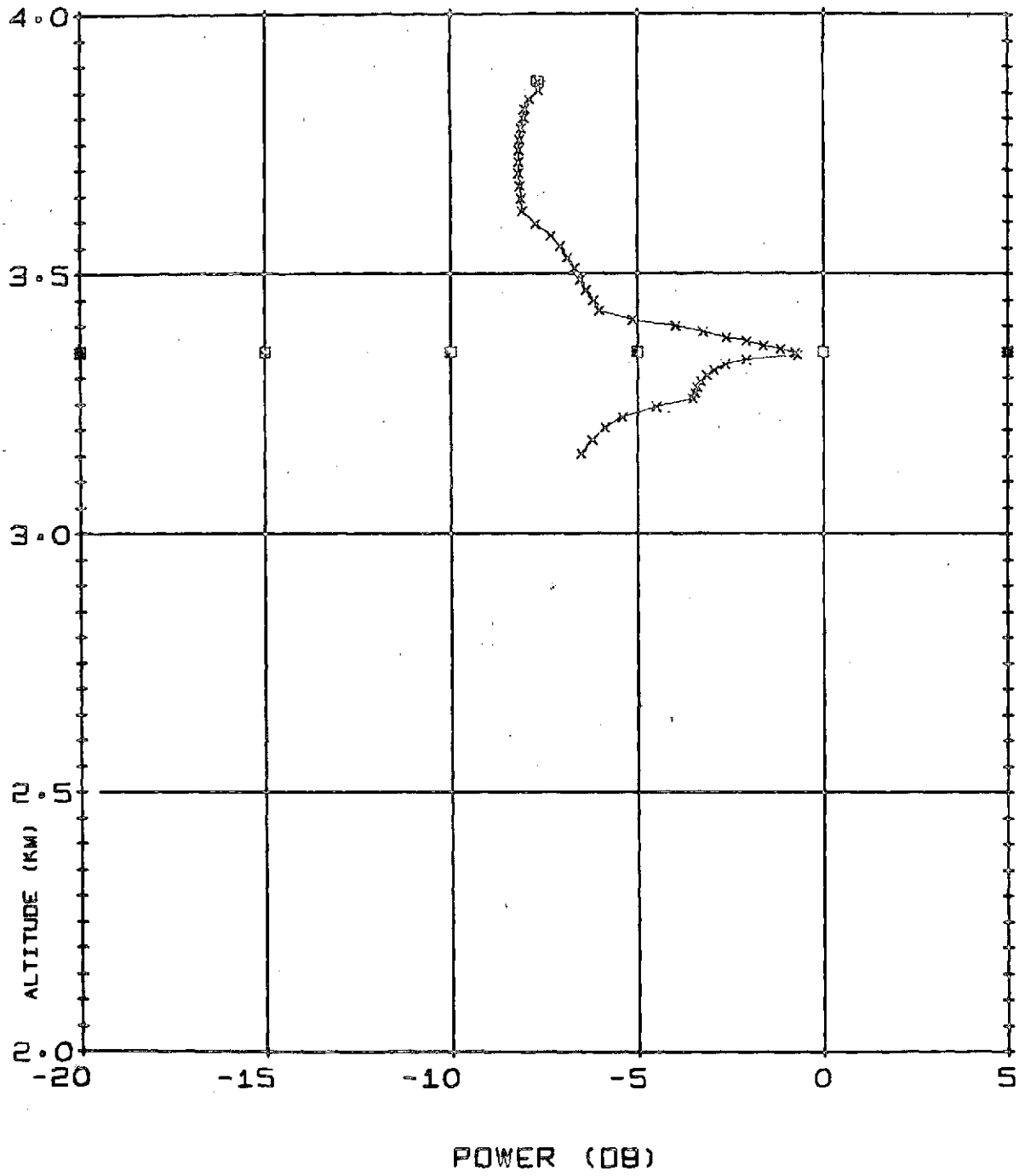

Fig. 24. POWER VS ALTITUDE AT THE RECEIVER RANGE FOR PROFILE 03A1. This figure illustrates the power that would be detected by a receiver if the receiver moves vertically along the right-hand axis of Fig. 23.

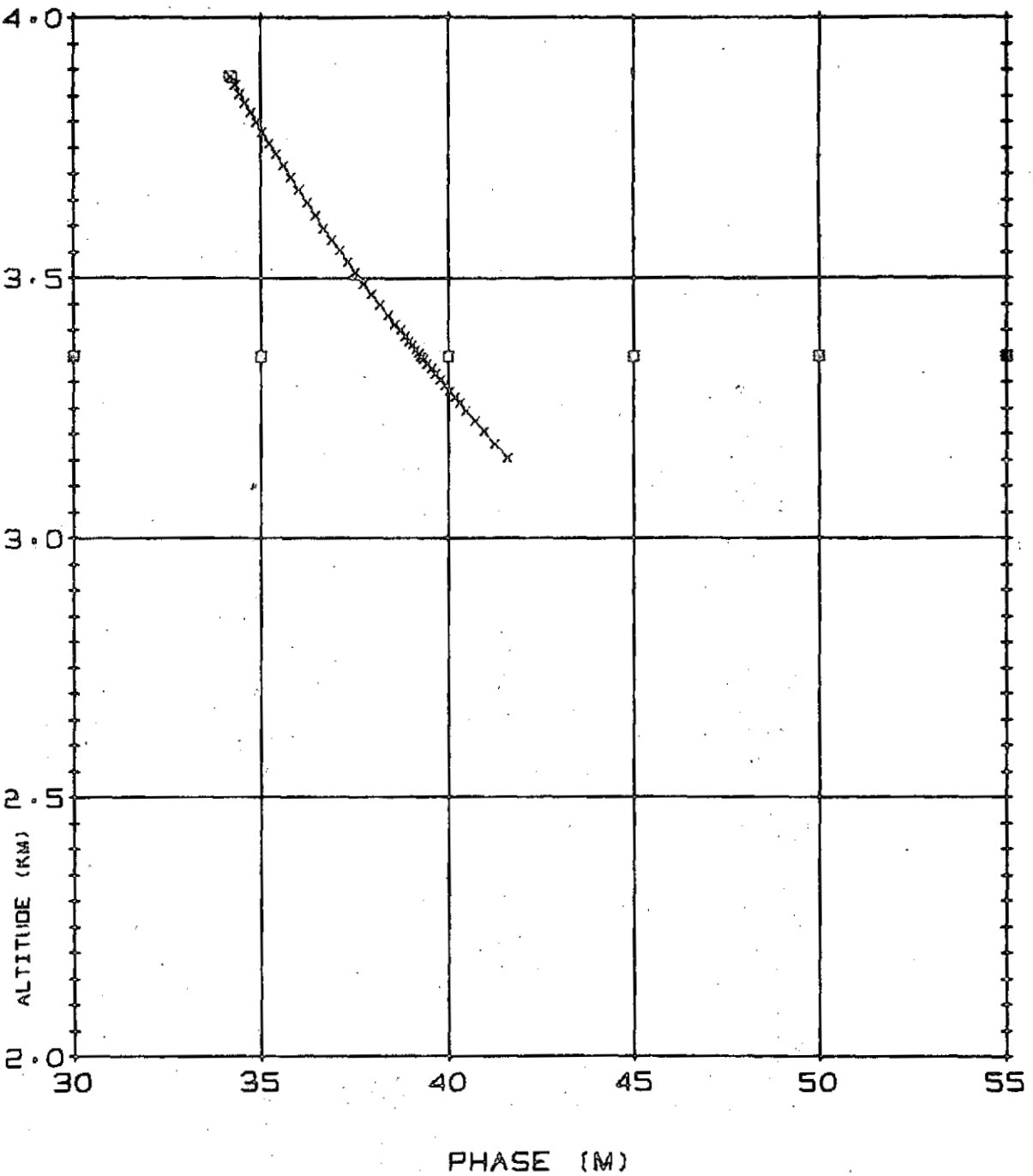

Fig. 25. PHASE VS ALTITUDE AT THE RECEIVER RANGE FOR PROFILE 03A1. This figure illustrates the phase that would be detected by a receiver if the receiver moves vertically along the right-hand axis of Fig. 23.

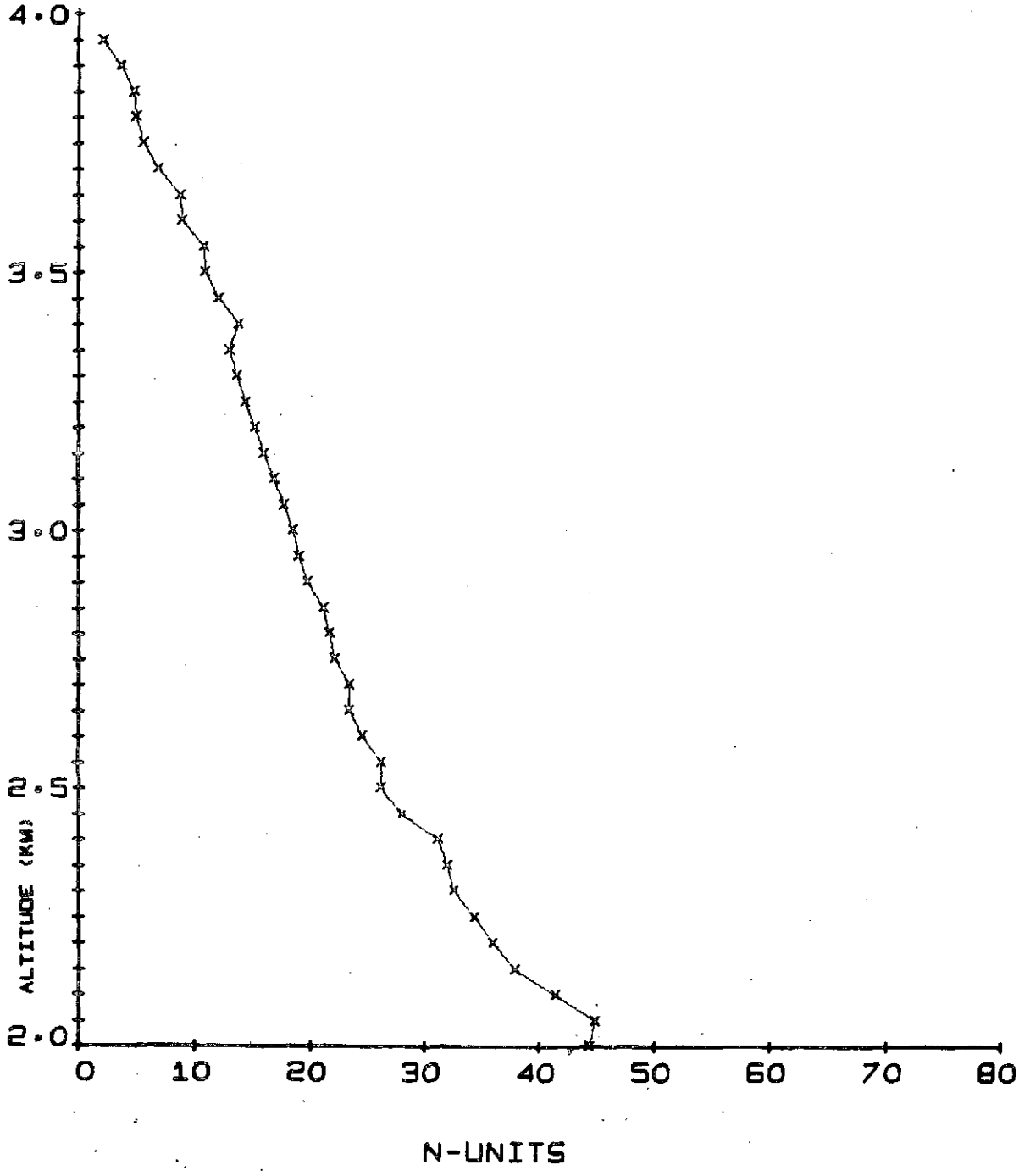

Fig. 26. N-PROFILE FOR FLIGHT 04D1, AS DRAWN BY THE SIGMA-5 COMPUTER. The 04D1 refers to the first descent made on the fourth flight. This profile was taken during a type-B period.

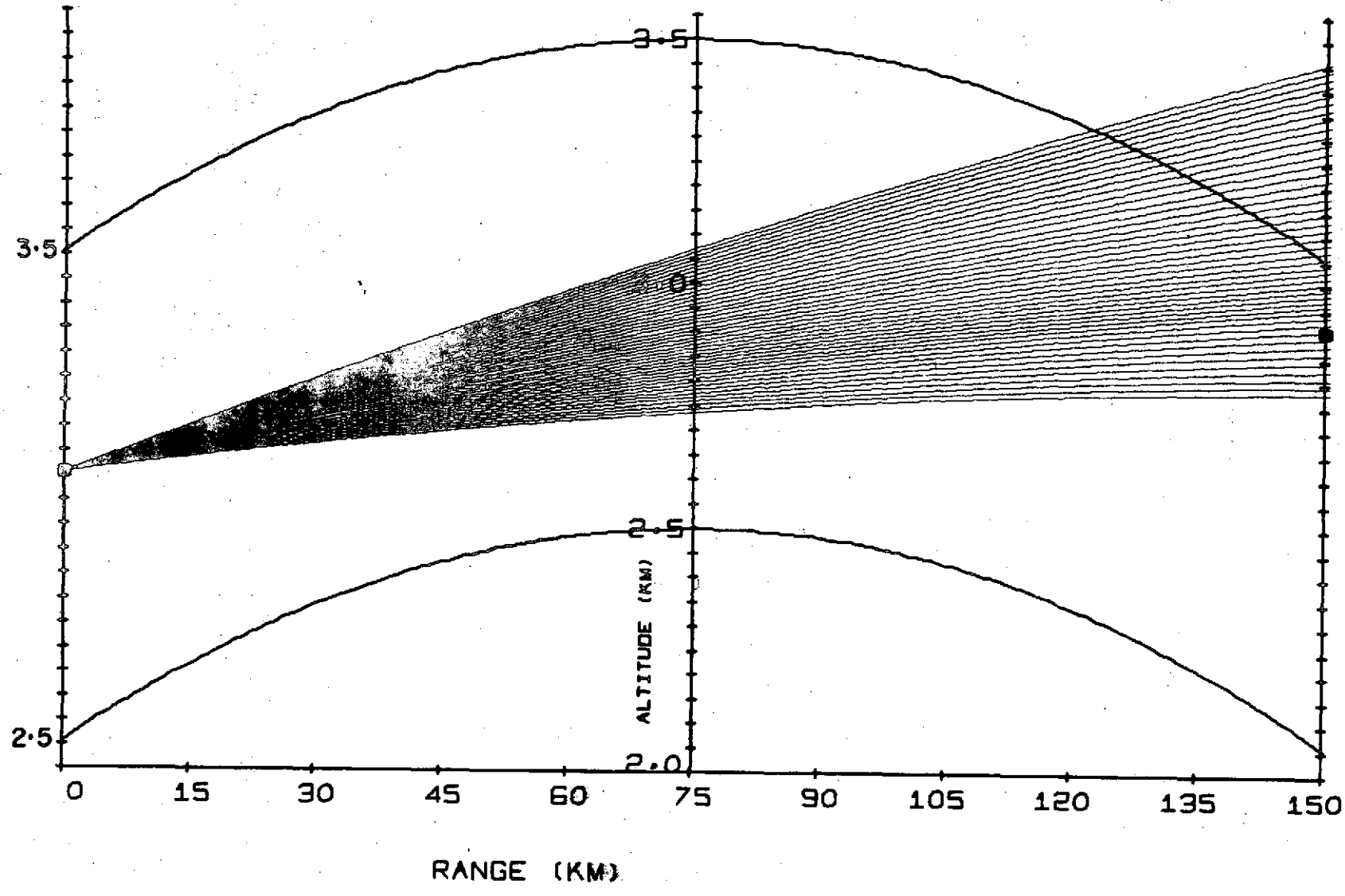

Fig. 27. COMPUTER-DRAWN RAYPATHS FOR PROFILE 04D1.

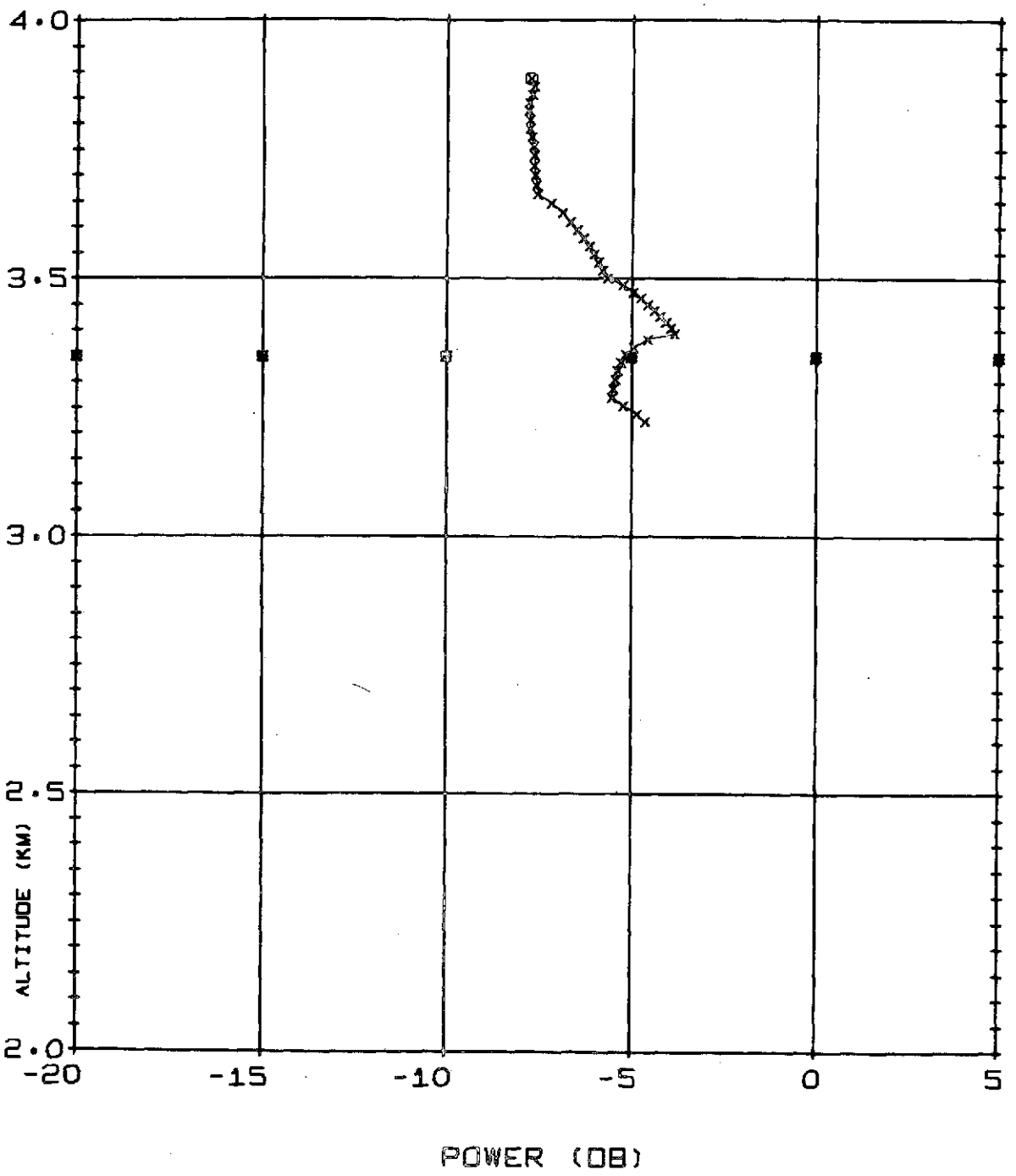

Fig. 28. POWER VS ALTITUDE AT THE RECEIVER RANGE FOR PROFILE 04D1.

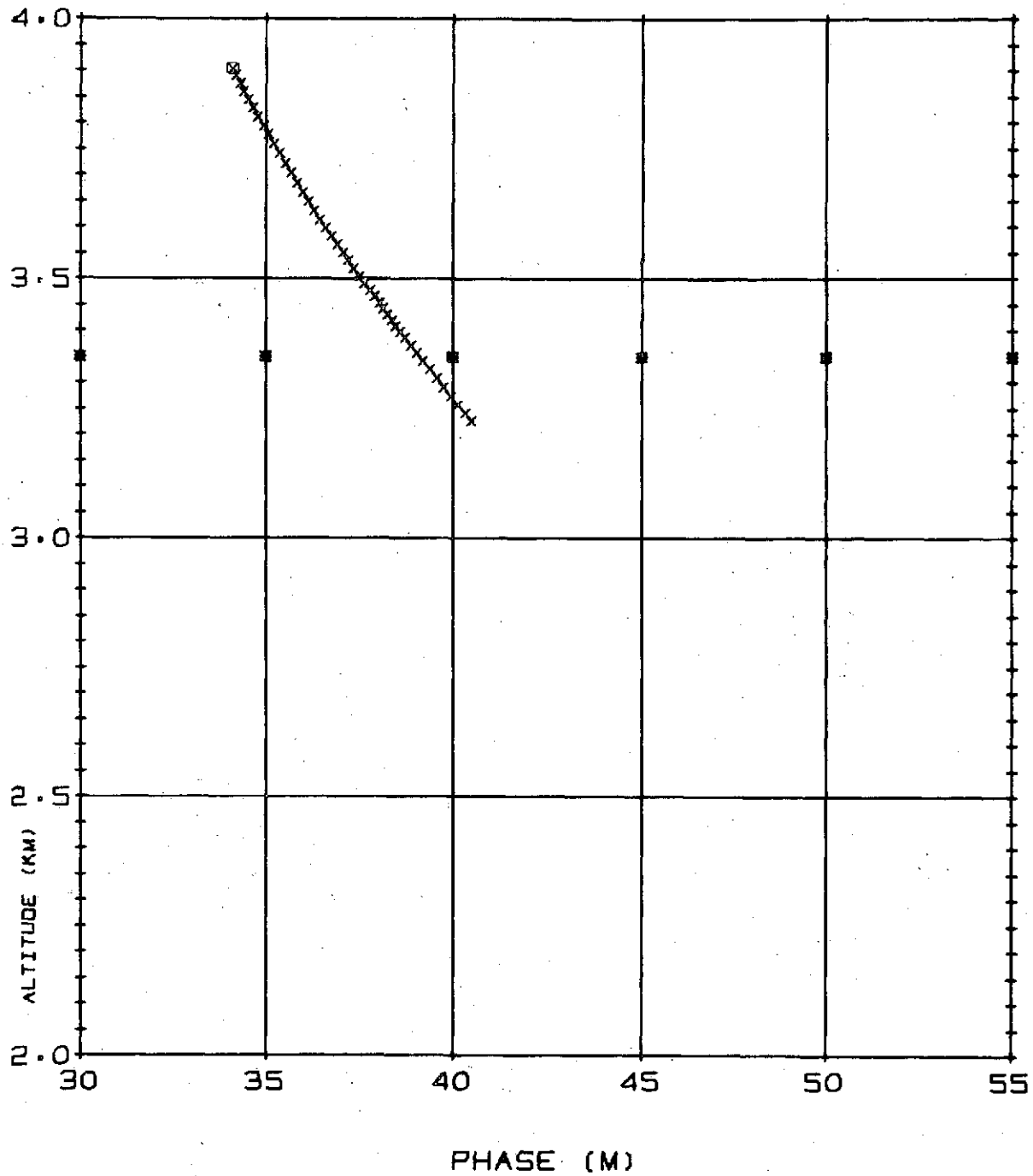

Fig. 29. PHASE VS ALTITUDE AT THE RECEIVER RANGE FOR PROFILE 04D1.

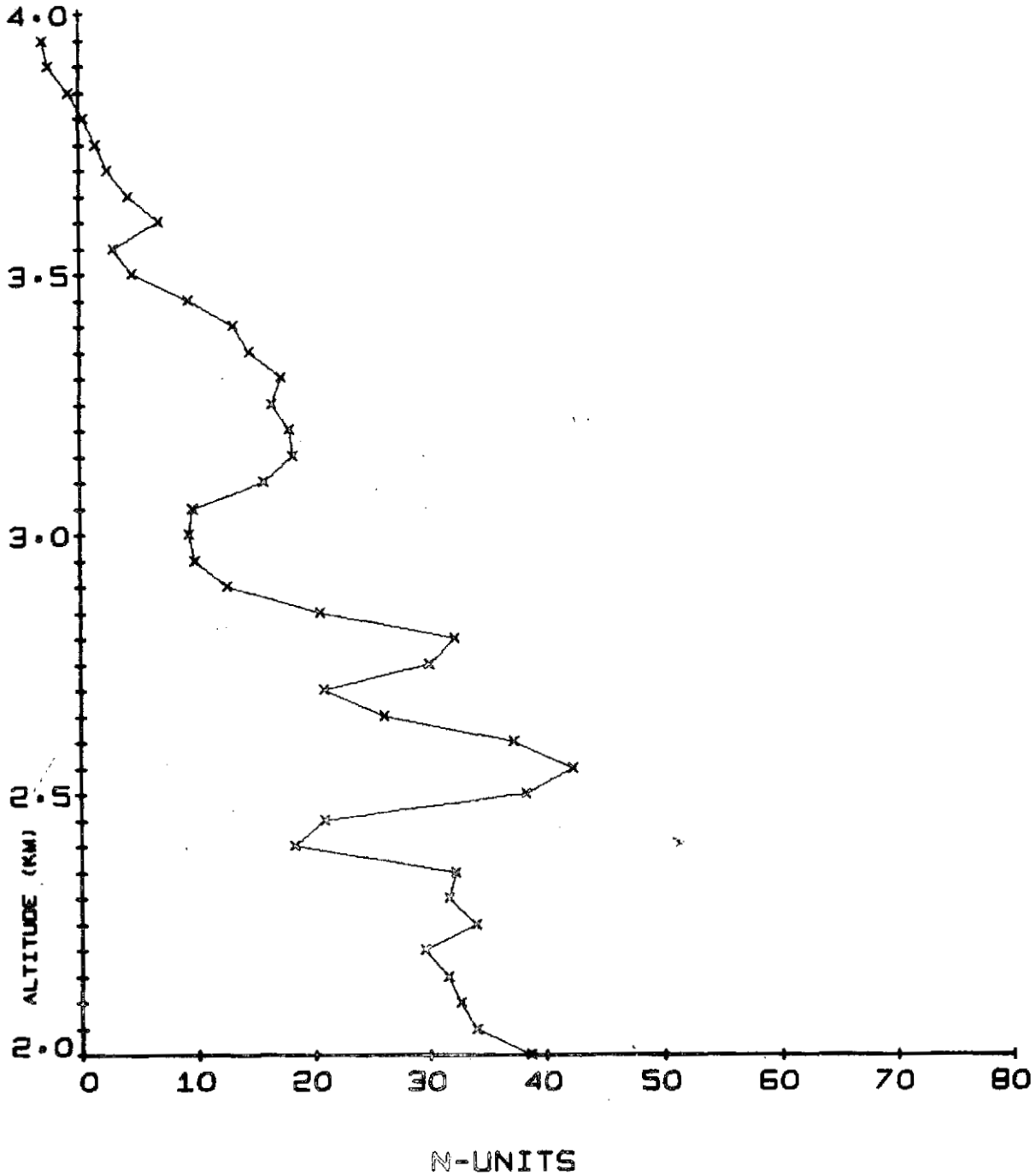

Fig. 30. N-PROFILE FOR FLIGHT 11D2, AS DRAWN BY THE SIGMA-5 COMPUTER. 11D2 refers to the second descent made on the eleventh flight. This profile was taken during a type-D period.

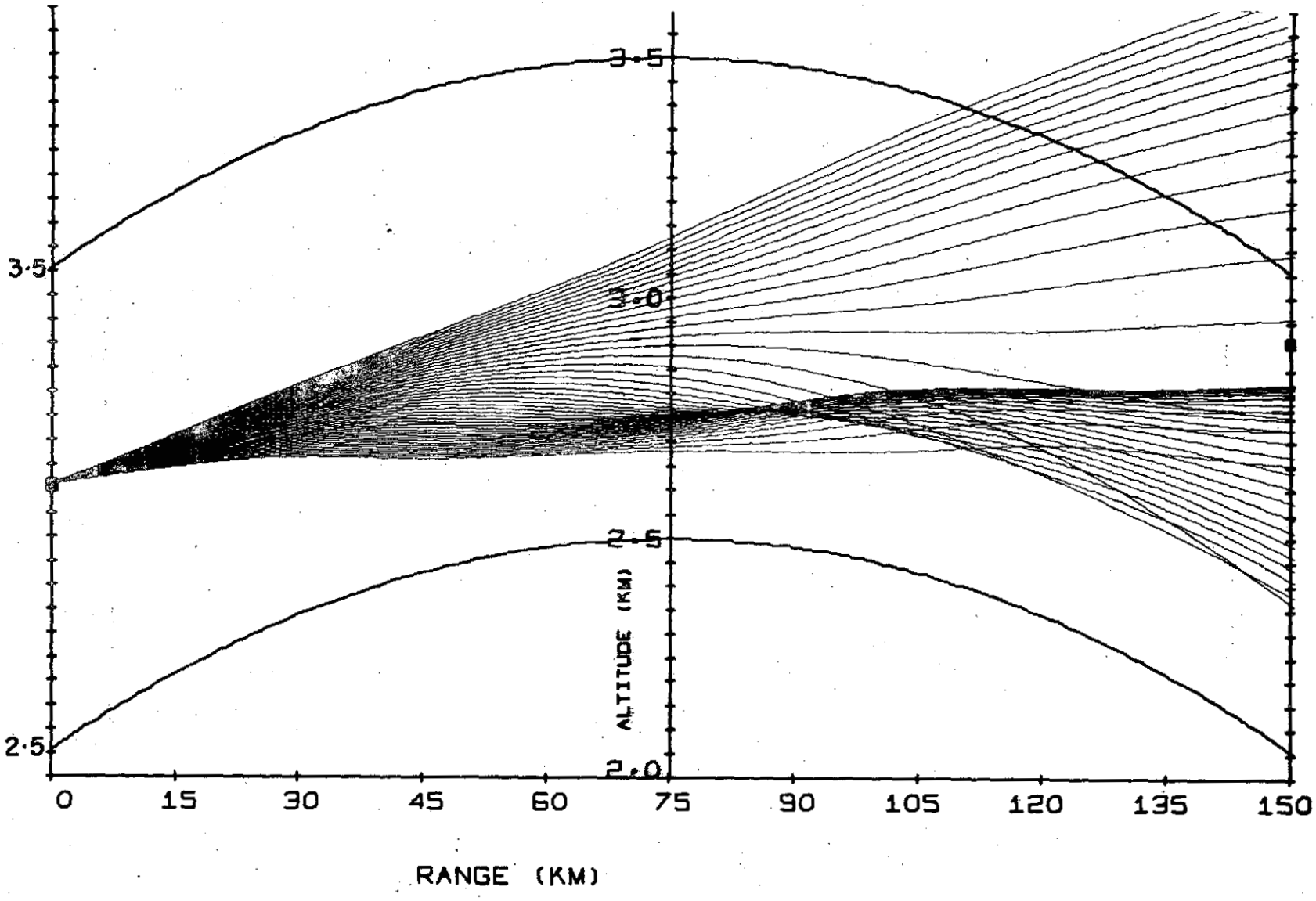

Fig. 31. COMPUTER-DRAWN RAYPATHS FOR PROFILE 11D2. Note the extensive multipath.

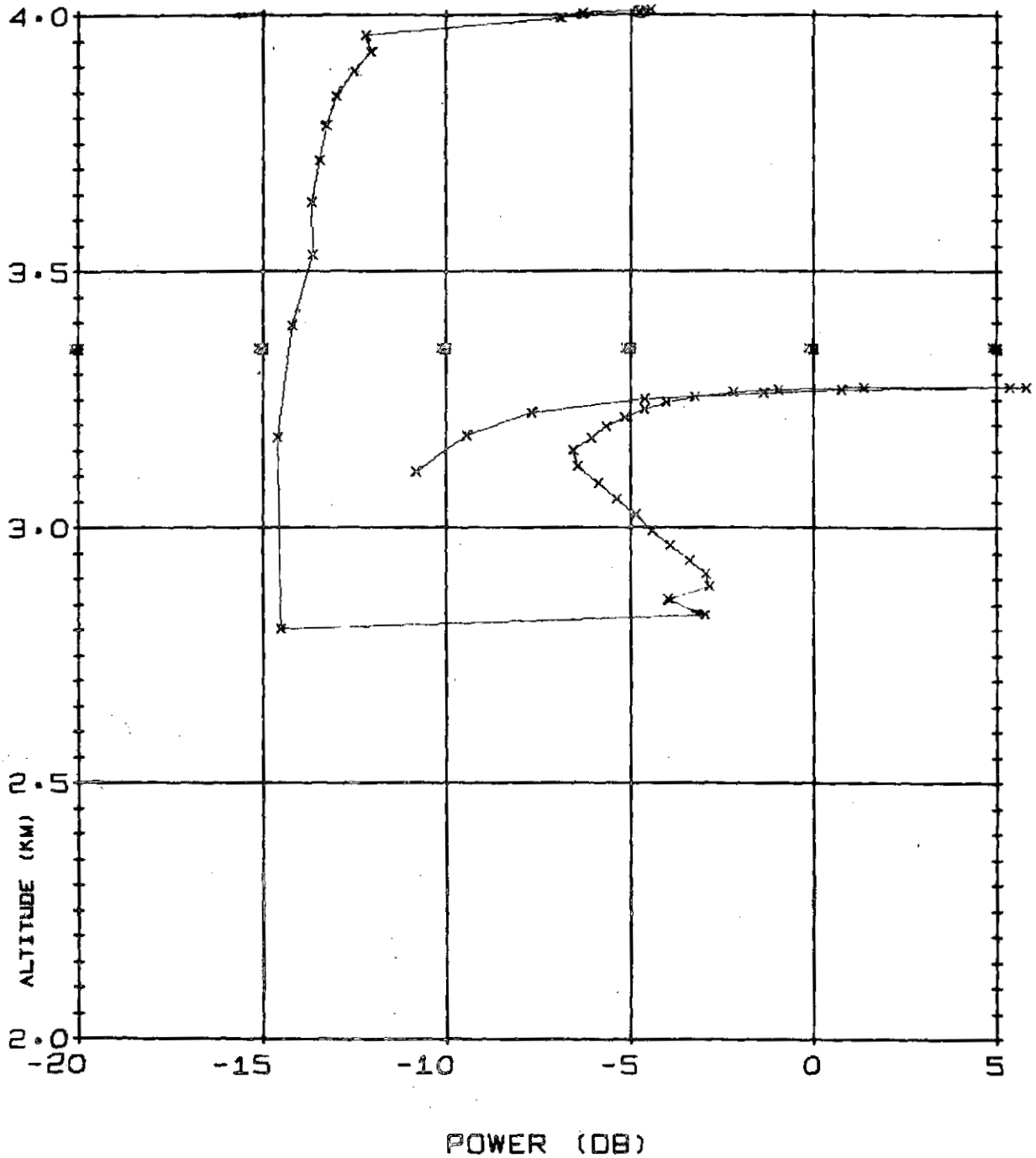

Fig. 32. POWER VS ALTITUDE AT THE RECEIVER RANGE FOR PROFILE 11D2. The double-valued nature of this curve clearly indicates the presence of multipath.

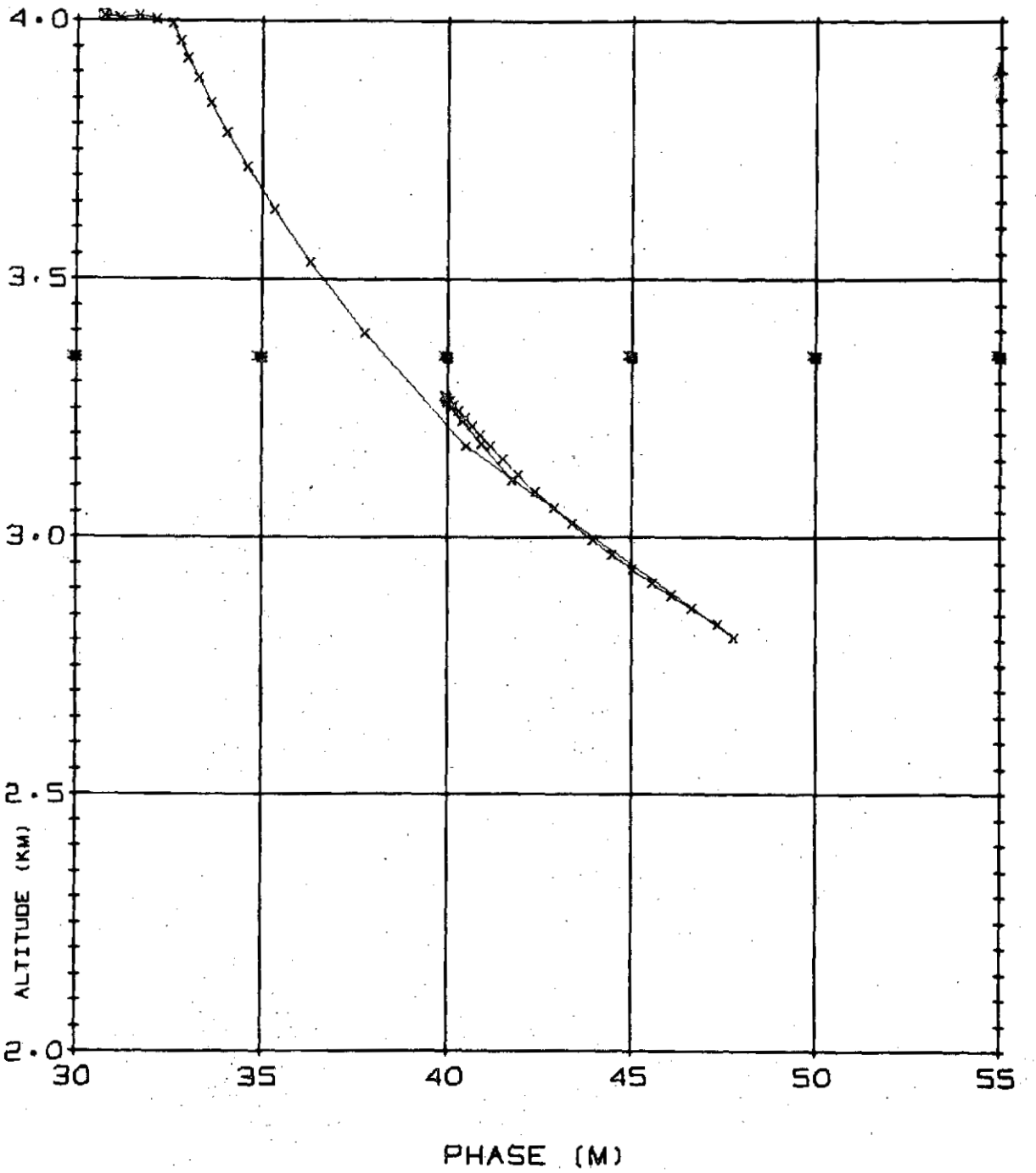

Fig. 33. PHASE VS ALTITUDE AT THE RECEIVER RANGE FOR PROFILE 11D2.

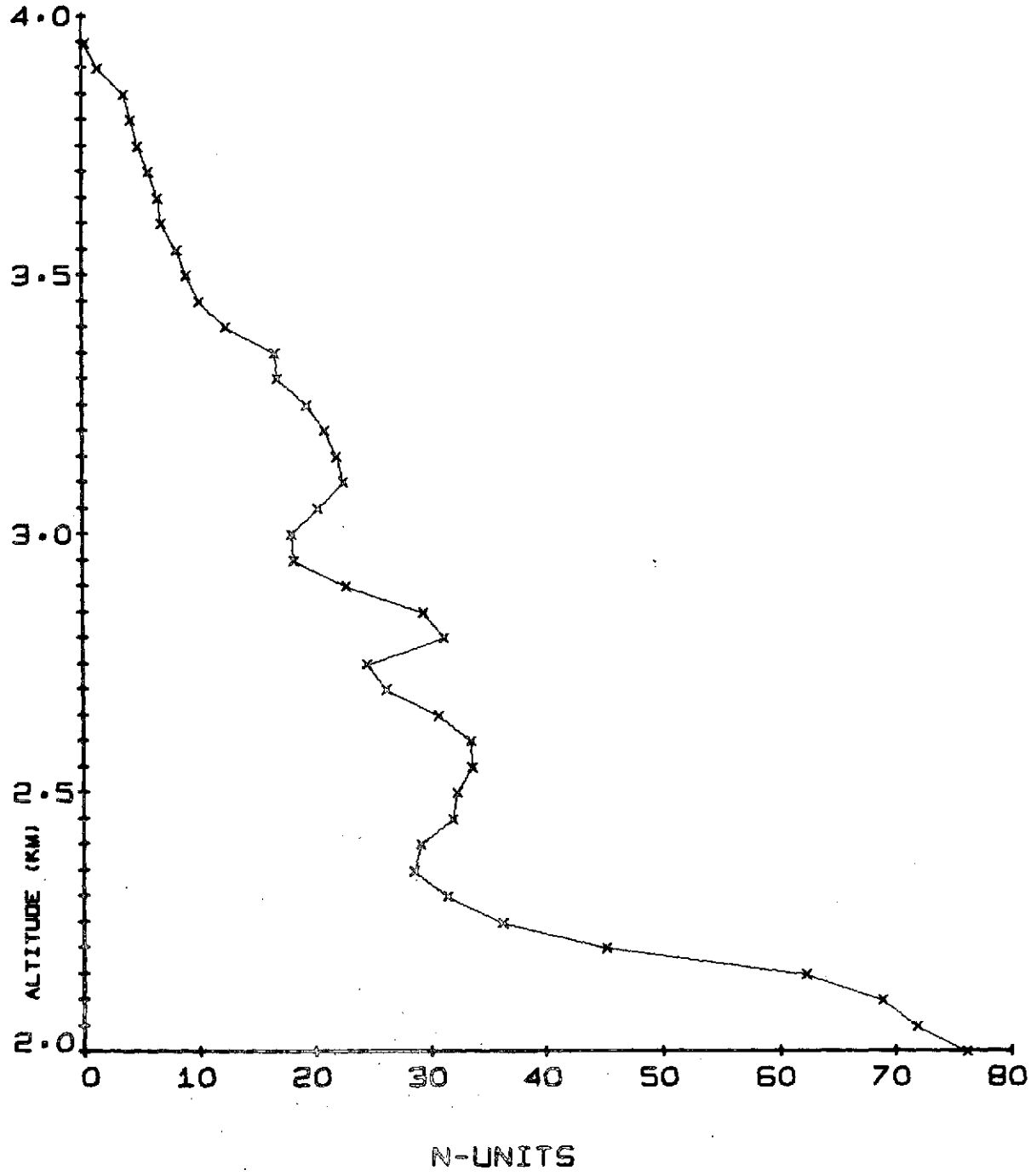

Fig. 34. N-PROFILE FOR FLIGHT 12D2, AS DRAWN BY THE SIGMA-5 COMPUTER. 12D2 refers to the second descent made on the twelfth flight. This profile was taken during a type-D period.

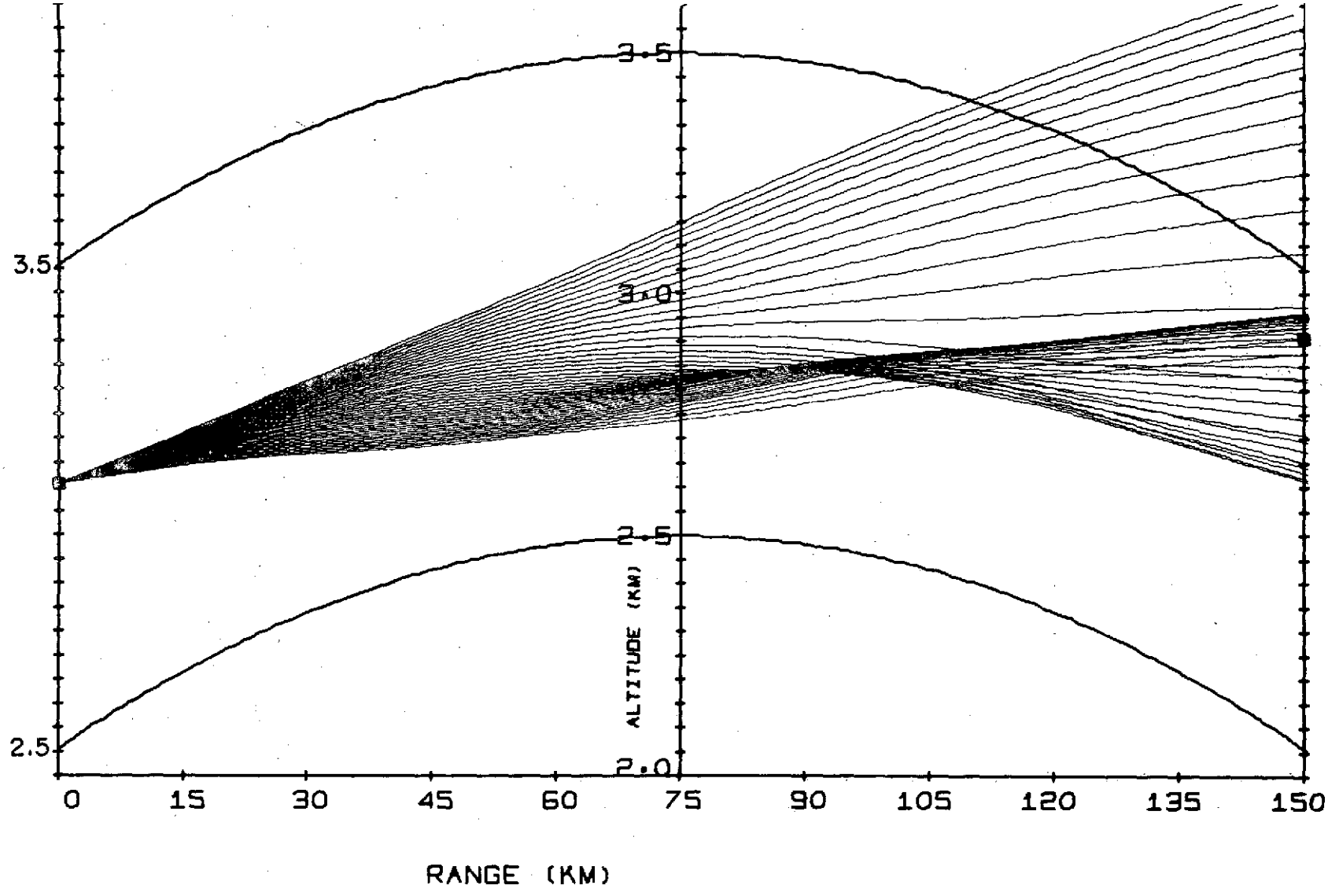

Fig. 35. COMPUTER-DRAWN RAYPATHS FOR PROFILE 12D2.

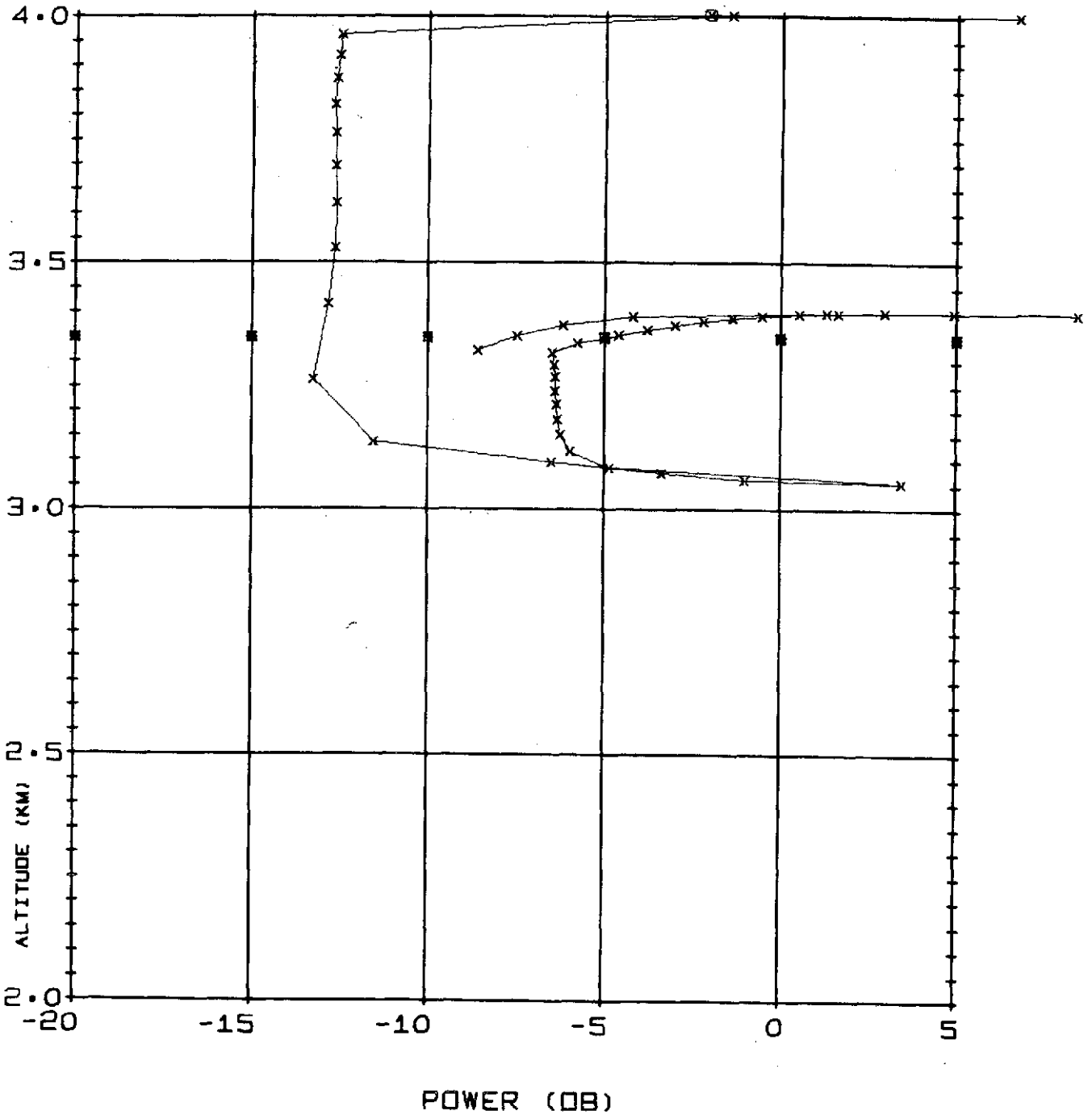

Fig. 36. POWER VS ALTITUDE AT THE RECEIVER RANGE FOR PROFILE 12D2.

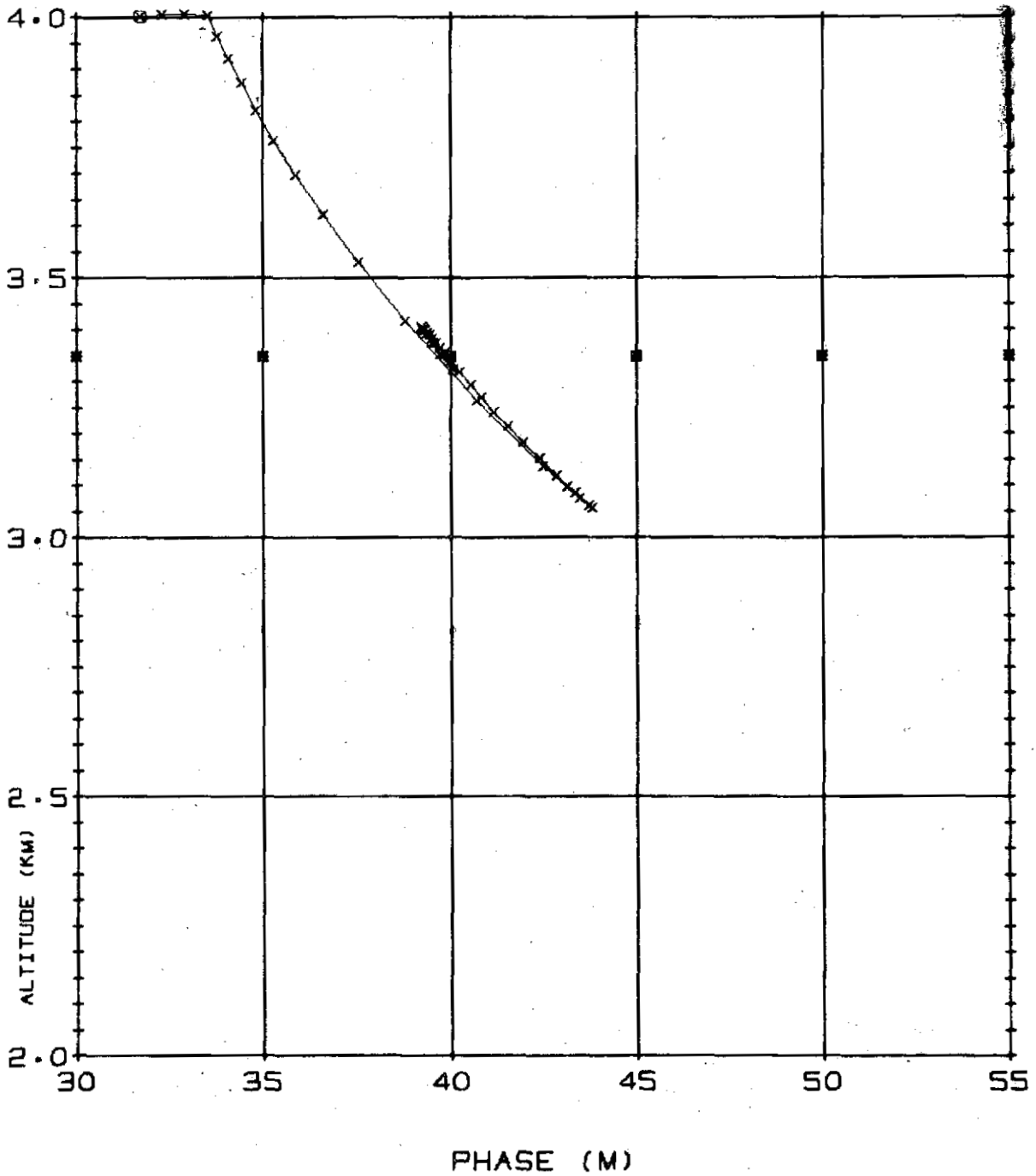

Fig. 37. PHASE VS ALTITUDE AT THE RECEIVER RANGE FOR PROFILE 12D2.

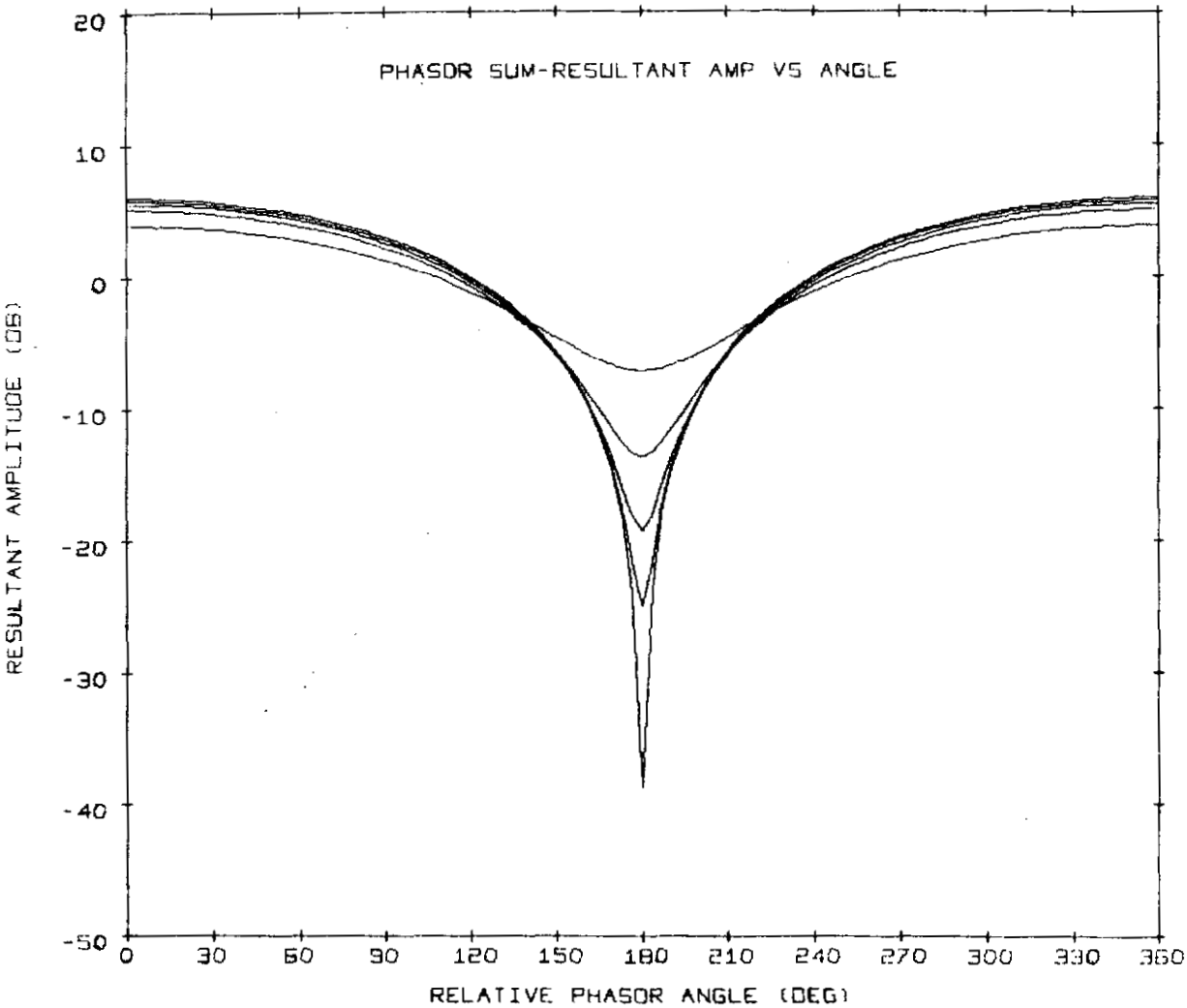

Fig. 38. RESULT OF ADDING TWO PHASORS. These curves represent five values of relative phasor amplitude. Reading upward at the 180° abscissa value, the phasors differ by 0.1, 0.5, 1.0, 2.0, and 5.0 dB, respectively.

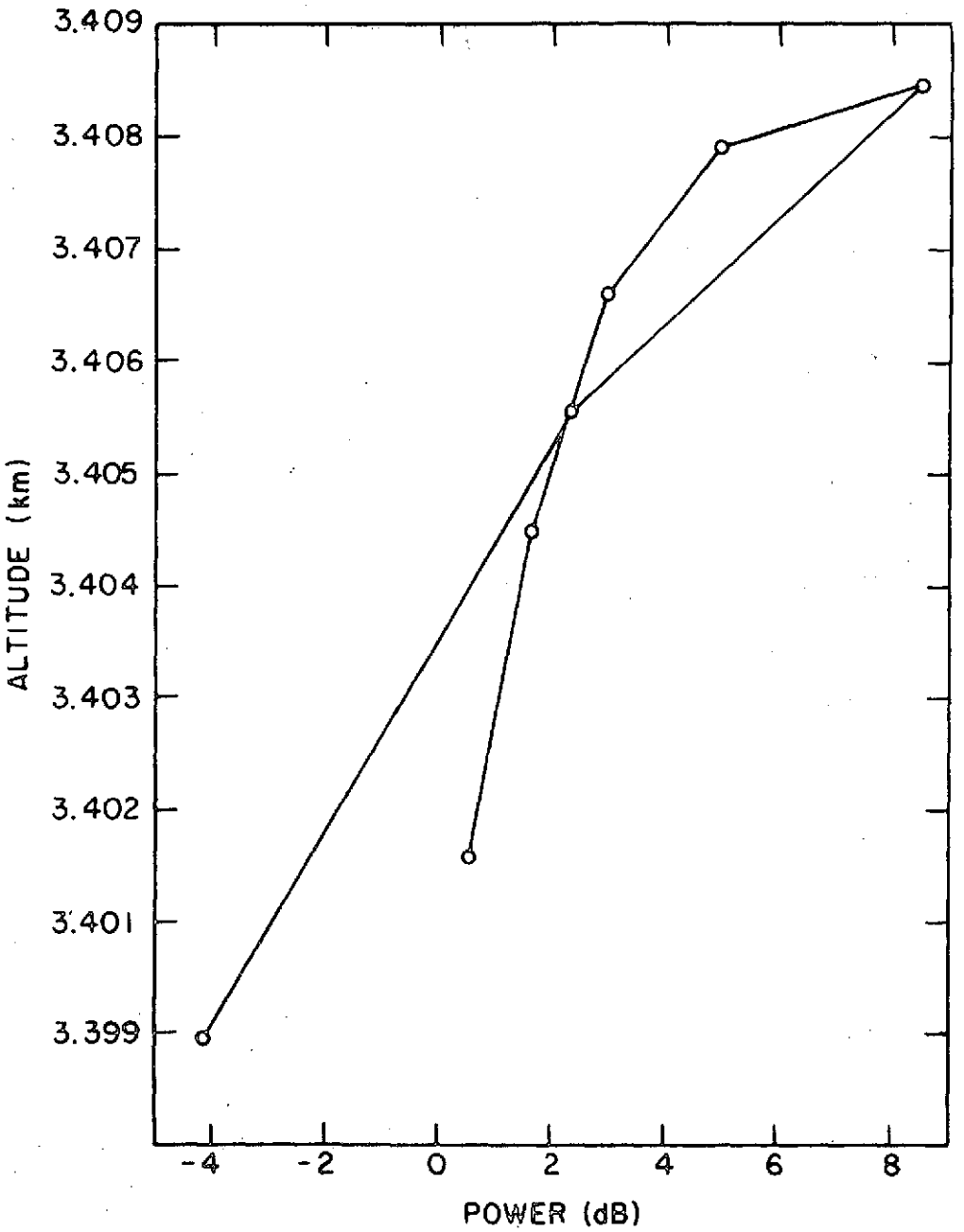

Fig. 39. POWER VS ALTITUDE AT THE RECEIVER RANGE FOR PROFILE 12D2. An expansion of a portion of Fig. 36.

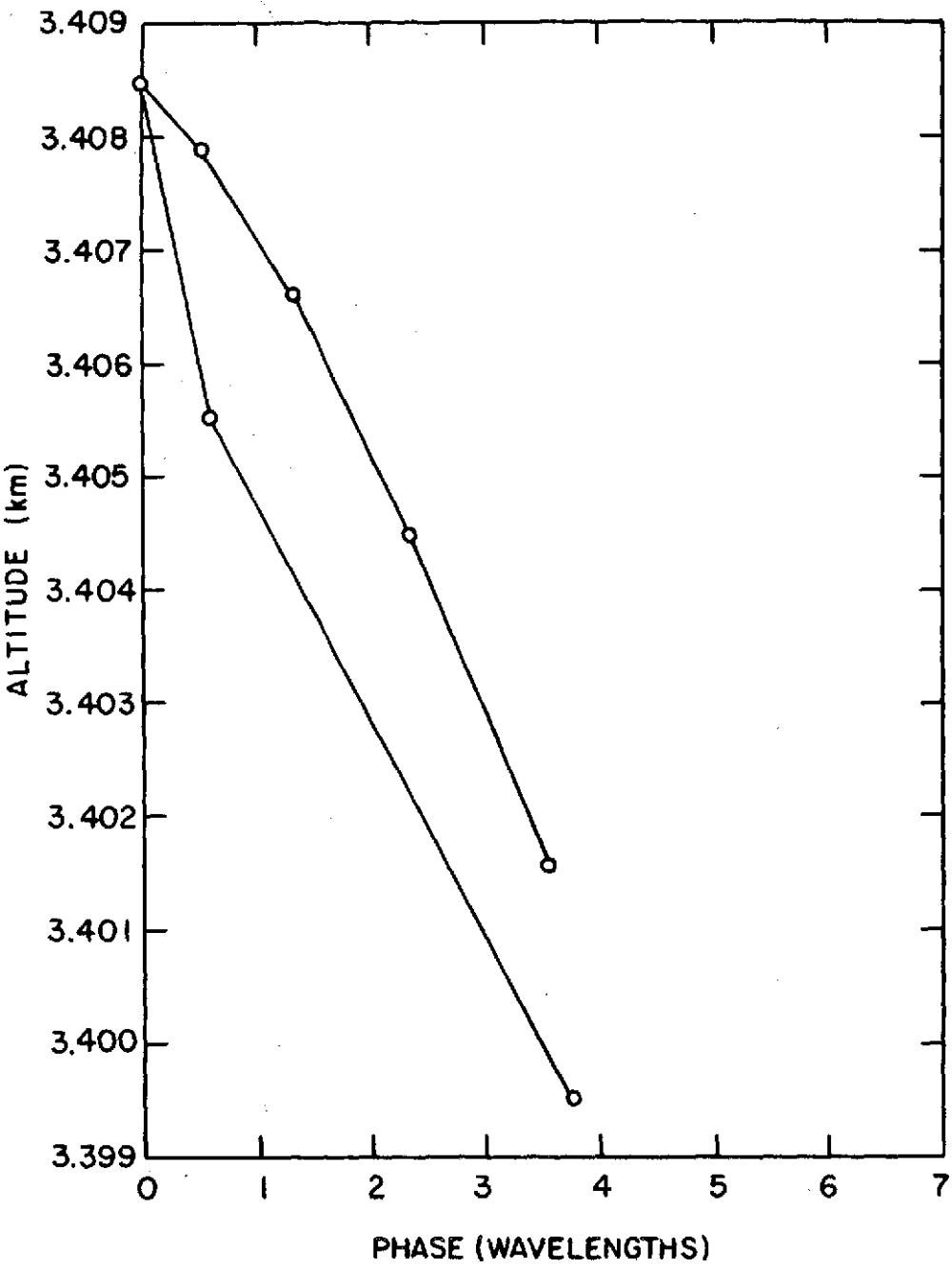

Fig. 40. PHASE VS ALTITUDE AT THE RECEIVER RANGE FOR PROFILE 12D2. An expansion of a portion of Fig. 37.

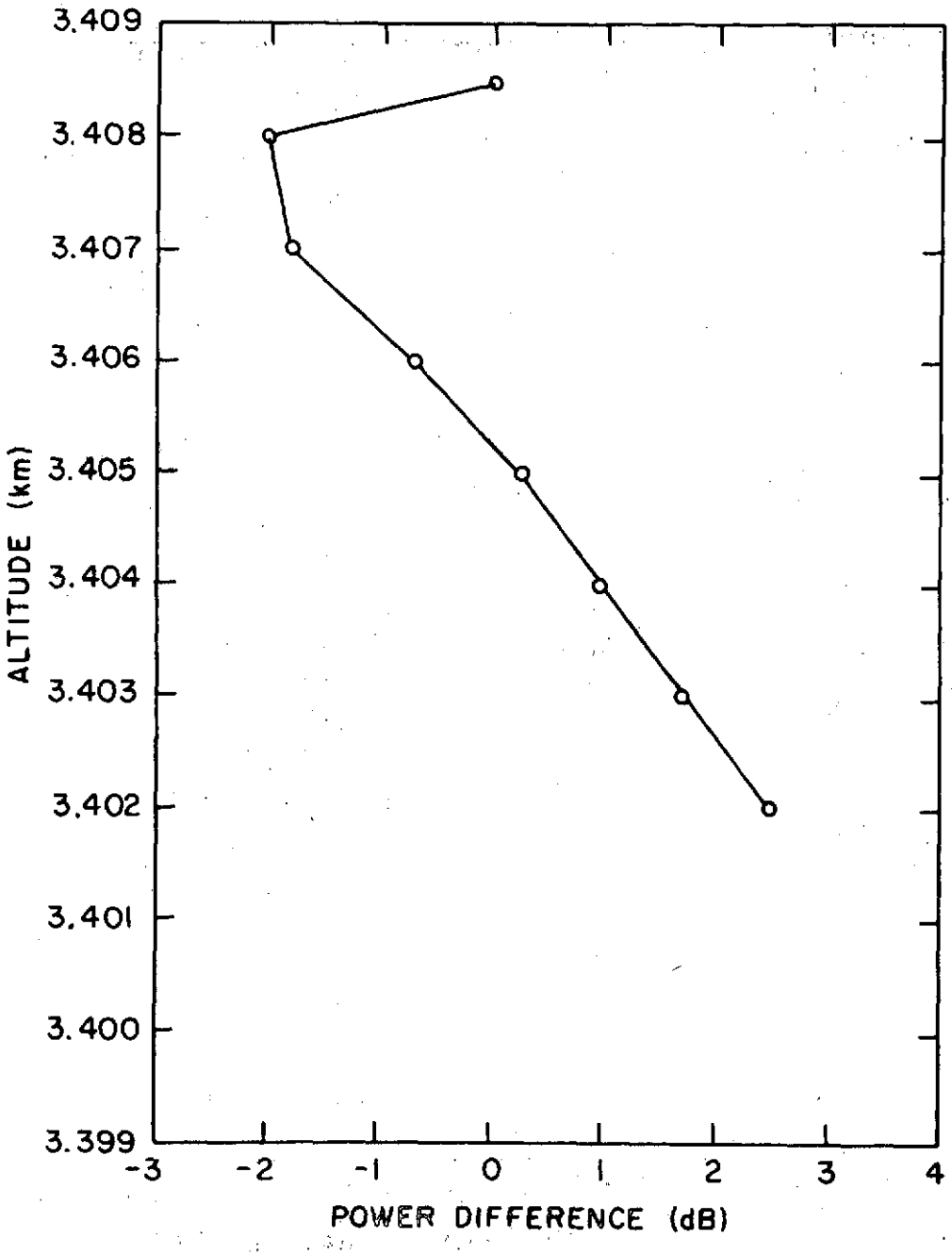

Fig. 41. POWER DIFFERENCE VS ALTITUDE AT THE RECEIVER RANGE FOR PROFILE 12D2. Derived from Fig. 40.

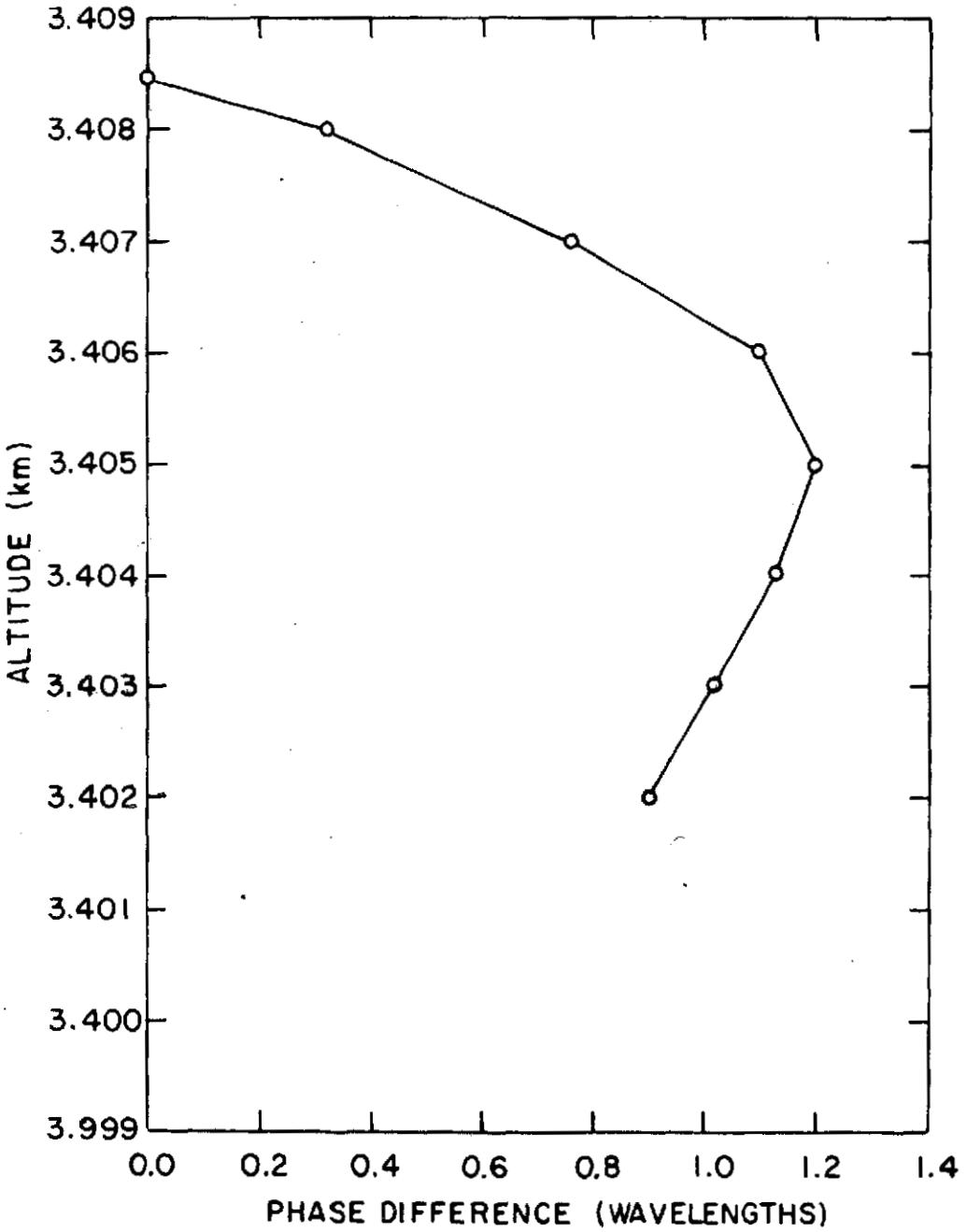

Fig. 42. PHASE DIFFERENCE VS ALTITUDE AT THE RECEIVER RANGE FOR PROFILE 12D2. Derived from Fig. 41.

Chapter VI

FURTHER ANALYSES OF THE HAWAII DATA

"One good turn deserves another."

--Gaius Petronius

In the foregoing computer analysis of the Hawaii N-profiles, each vertical profile obtained by the aircraft was expanded spherically symmetrically and then used as input for the raytracing routine; this was the most extensive analysis performed on the data. It is possible to use these data in other configurations, and these further analyses will be described in this chapter.

A. Nonsymmetric Raytracing

Because the aircraft recorded several vertical profiles on each of its runs, it is possible to combine the profiles to construct a single nonsymmetric N-profile for each flight (an N-profile with nonzero horizontal gradients). Hopefully, such a profile would be a more realistic representation of the conditions that existed along the transmission path when the flight was made.

To obtain N-profiles, the airplane flew two patterns (Chapter IV). Flight-pattern I was H-shaped, with two vertical profiles recorded on each flight; flight-pattern II was sawtoothed, with several vertical profiles recorded (see Fig. 19). It should be noted again that, even in pattern I, the "vertical" profile is not truly vertical because the plane cannot climb at an angle greater than a few degrees from the horizontal.

N-profiles from five representative flights were chosen for nonsymmetric analysis.

Type-A period: one flight, flight pattern I

Type-B: two flights, one each of patterns I and II

Type-C: one flight, pattern I

Type-D: one flight, pattern II

A type-A period is the "quietest" from the point of view of the number of incidents of intense radio fading, and type-D is the "noisiest."

The vertical profiles were used to construct a nonsymmetric atmosphere for each flight. This "atmosphere" consisted of a matrix of N-values, with 40 vertical points (spaced 0.05 km apart, as in the symmetric case described in Chapter V) and either 31 or 161 horizontal points (5 or 0.95 km, respectively), depending on the flight pattern. In the pattern-I data, each vertical profile was entered as a column of the matrix, the choice of column determined by the location of the aircraft when it made the vertical profile. In the pattern-II data, each vertical profile was read into the matrix in such a way as to simulate the sawtoothed configuration flown by the aircraft. This is the reason for the greater number of horizontal points used to represent flight-pattern II data (161 horizontal points are required to accommodate four 40-point profiles in a sawtooth arrangement; as in flight-pattern I data, 31 points would provide sufficient horizontal resolution.)

The points in the matrix not occupied by original data were filled by constructing simple linear gradients between points of the original profiles. A separate horizontal gradient was established for each of the 40 vertical levels and, in the flight-pattern II atmospheres, between each of the profiles. The result was an N-matrix with nonzero horizontal gradients. These nonsymmetric profiles (Fig. 43) were used as input to the HAWAII raytracing routine. The HAWAII program, based on a Snell's Law raytracing method, has the capability of raytracing through nonsymmetric atmospheres.

The results of this analysis are illustrated in Figs. 44 through 48. As can be seen, the results of nonsymmetric raytracing do not differ drastically from the results obtained in the spherically symmetric analysis.

Although this case of a simple linear gradient is interesting, it has certain shortcomings. It is very unlikely that the atmosphere along the transmission path in Hawaii consisted of one or two simple linear gradients. A more realistic picture would account for small pockets of high or low values of N, corresponding to small convective cells. The model described thus far is more sophisticated than a simple symmetric atmosphere; nonetheless it is a bit too simple to be real.

Another problem is that the N-data used to construct the vertical profiles prior to computing the horizontal gradients probably will contain features that look like horizontal layering but are, in fact, spurious. These "layers" are generated when the airplane hits an updraft or a downdraft and suddenly rises or falls. This vertical motion appears in the N-profile as a sudden decrease or increase in N; however, it merely represents the fact that the aircraft was not climbing or descending at a uniform rate. When linear gradients are constructed from this contaminated data, the spurious layer "stretches" out over scores of kilometers when, in fact, it might have a much smaller horizontal extent if it exists as a layer at all.

A statistical approach was applied to overcome these difficulties. Each of the vertical profiles was smoothed with a 0.1 km lowpass filter to remove the effects of spurious layering, and these smoothed profiles were used to construct linear horizontal gradients, as described above.

A random-number generator was employed to construct a matrix of random variates, with the same number of rows and columns as the N-matrix. This random-variate matrix was smoothed, first horizontally and then vertically, to eliminate any large gradients, and then adjusted to a mean of 0 and a standard deviation of 1.00. Each row was multiplied by a factor obtained by taking the rms value of the high-frequency component of the N-profiles for each flight.† The resulting matrix of smoothed, adjusted, and scaled random variates was added to the N-matrix constructed from the smoothed N-profiles.

Figures 45 and 46 are samples of the N-profiles from this matrix, before and after the random variates were added. Note the similarity between the N-profiles from the statistical atmosphere and those from the simple linear gradient atmosphere (Fig. 43). The difference, of course, is that the deviations from a smooth profile are regular, consistent, and relatively large-scale horizontal deviations in the case of the linear gradient; in the statistical case, the deviations are irregular and of a smaller horizontal scale because of the random nature of the added term.

† These high-frequency profiles, two of which are illustrated in Fig. 20, were provided along with the N-profiles by the Boulder group.

The results of raytracing through these nonsymmetric statistical profiles (Fig. 47) are very similar to those obtained from the simple linear gradient and, by extension, to those obtained from the simpler spherically symmetric expansions of the vertical profiles.

The similarity of these three cases illustrates the small effect that horizontal gradients have on ray propagation. Equally intriguing is the fact that, even in the presence of horizontal gradients, when a multipath situation exists, the excess path length (phase defect) appears to be dependent on the endpoints rather than on the raypath itself. Figure 48 presents some examples of the phase vs altitude record for nonsymmetric atmospheres that yield multipath.

B. Raytracing Satellite-to-Satellite

An operational occultation system will transmit signals between two satellites rather than between two ground stations. To determine how an occultation system would respond if it were to transmit through the N-profiles measured in the Hawaii experiment, the satellite-to-satellite raytracing routine THRUWAY was adapted to accommodate the Hawaii data. The Hawaii N-profiles provide data only between 2 and 4 km above sea level. Because THRUWAY requires data from 69 km down to the minimum altitude of the ray, it was necessary to "extend" the vertical range.

The U.S. Standard Atmosphere Supplement, 1966, 15° N Annual temperature profile [9] combined with a standard high-humidity water-vapor profile (the high humidity curve in Fig. 53) generated a "standard" profile of refractivity vs altitude (Fig. 49), and the Hawaii data were then merged into this profile. In the nonsymmetric data, the horizontal gradient existing at the 2 km level was carried through to the lower altitudes. The atmosphere was considered to be spherically symmetric above 4 km.

Four representative profiles (one from each of the "fading types") were chosen for symmetric raytracing in the satellite-to-satellite mode. Results of this experiment are shown in Fig. 50; only those portions of the raypath below the 16 km level are illustrated. The three parabolas

indicate the 0, 2, and 4 km levels. (Original data existed only between the 2 and 4 km levels. Between 0 and 2 km and above 4 km, the measurements were obtained from the Standard Atmosphere Supplement, as described above.) The satellite altitude is assumed to be 1110.0 km, and the transmitter is located 31.98° from the vertical, as measured from a position corresponding to the center of the diagram.

These diagrams illustrate the relative preponderance of multipath and defocusing, even in those cases that correspond to the very quiet well-behaved results obtained when raytracing in the station-to-station mode. Apparently, multipath is an unavoidable phenomenon in the satellite-to-satellite configuration, at least for those rays with closest approach altitude in the 2 to 4 km range. (N.B.: the pressure-reference-level system will have a closest approach altitude in the 6 to 9 km range.)

In addition to the four symmetric cases, the five nonsymmetric cases considered in the station-to-station mode were also analyzed with the satellite-to-satellite program. The results are shown in Figs. 51 and 52. The satellite altitude and position were the same as for the symmetric profiles. Once again, the measured data existed only between the 2 and 4 km levels; however, horizontal gradients at the 2 km level were carried through to the lower altitudes. In addition, because data exist only for a horizontal range of approximately 150 km and the ray travels approximately 500 km horizontally in the lower 3 km of its path, it was necessary to "extend" the Hawaii data horizontally. This was accomplished merely by "flipping" the atmosphere at each end of the 150 km range, changing negative gradients to positive gradients (and vice versa), but maintaining the statistical properties of the profile.

Once again, the preponderance of multipath and defocusing can be seen, as in the symmetric case. Similarly, as in the nonsymmetric station-to-station raytracing, there appears to be very little difference between the results obtained from the linear gradient profile and those obtained from the "statistical profile."

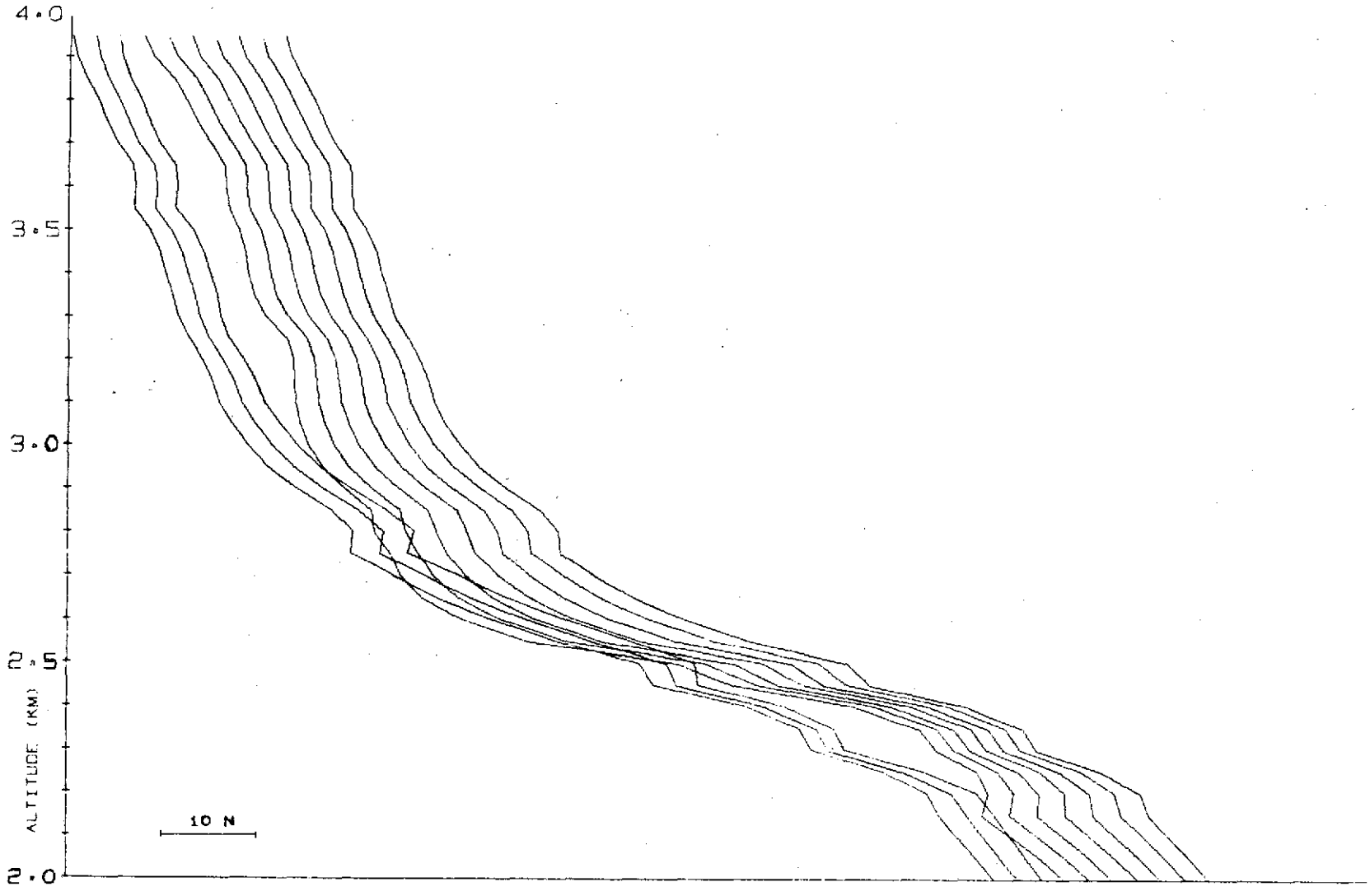

a. Flight 2: flight-pattern I, type-C fading

Fig. 43. NONSYMMETRIC LINEAR GRADIENT N-PROFILES. These vertical samples were generated from the data accumulated by the instrumented aircraft. Linear gradients were used to fill in points not represented by original data. For clarity, each of the succeeding profiles is shifted slightly to the right.

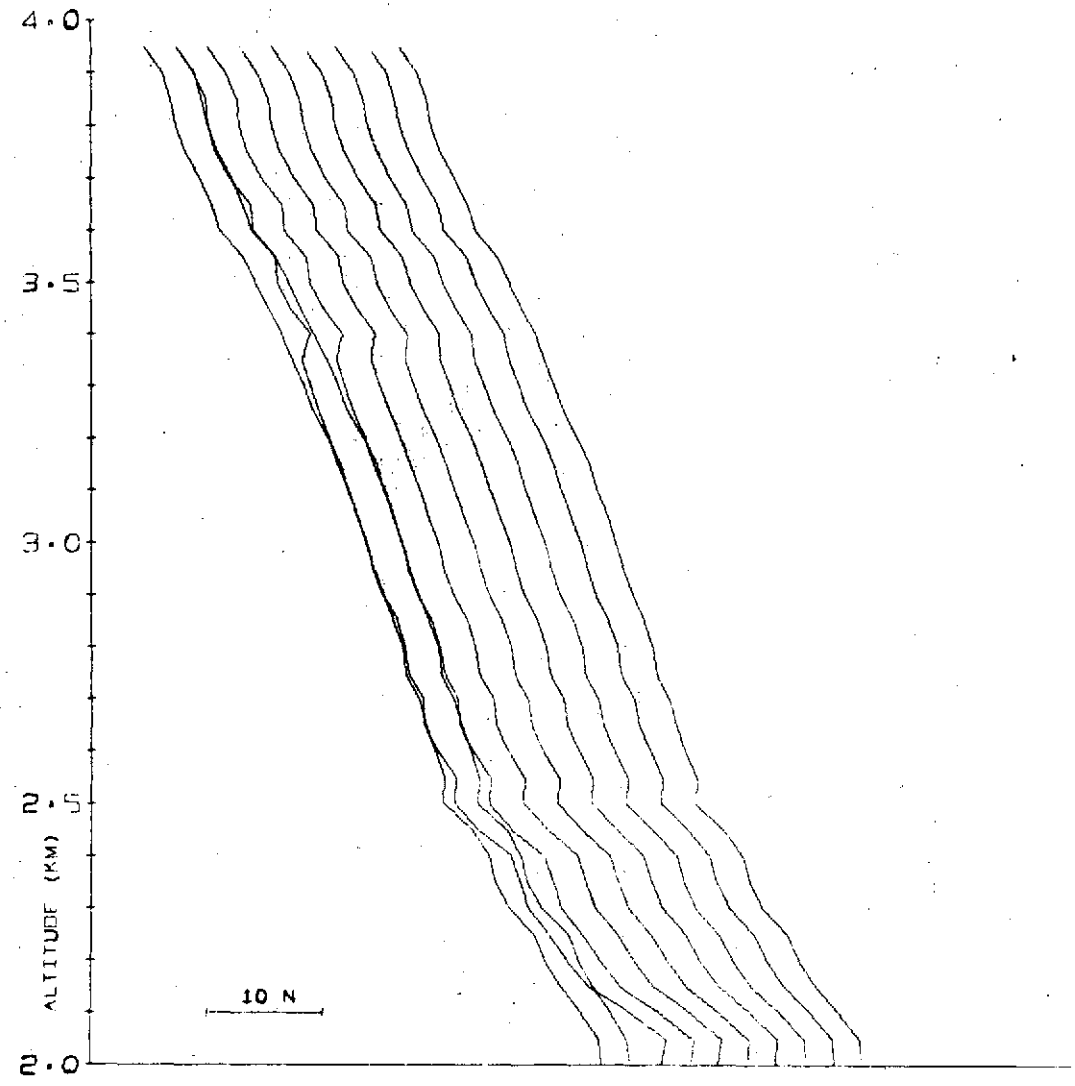

b. Flight 4: flight-pattern I, type-B fading

Fig. 43. CONTINUED.

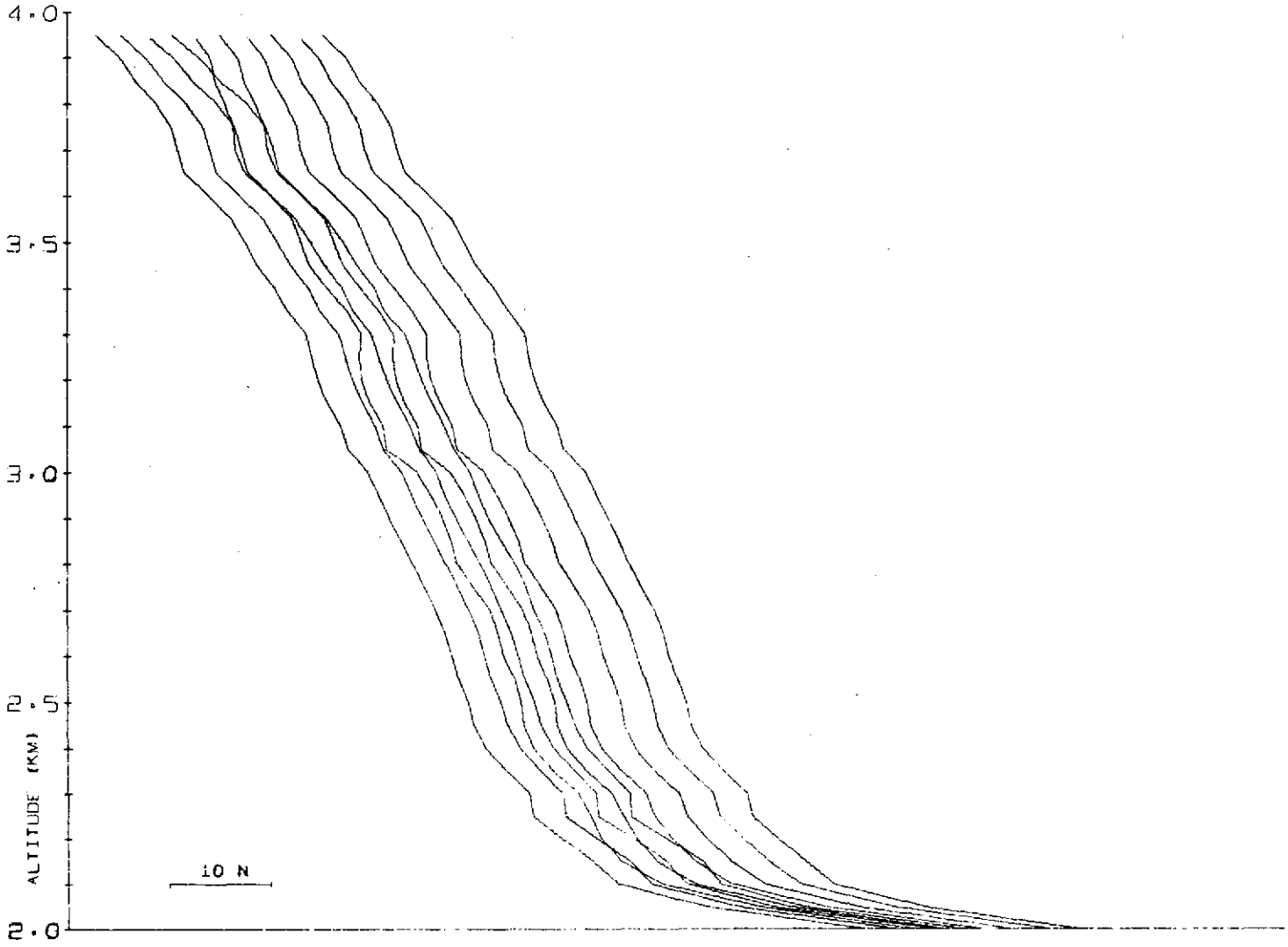

c. Flight 14: flight-pattern I, type-A fading

Fig. 43. CONTINUED.

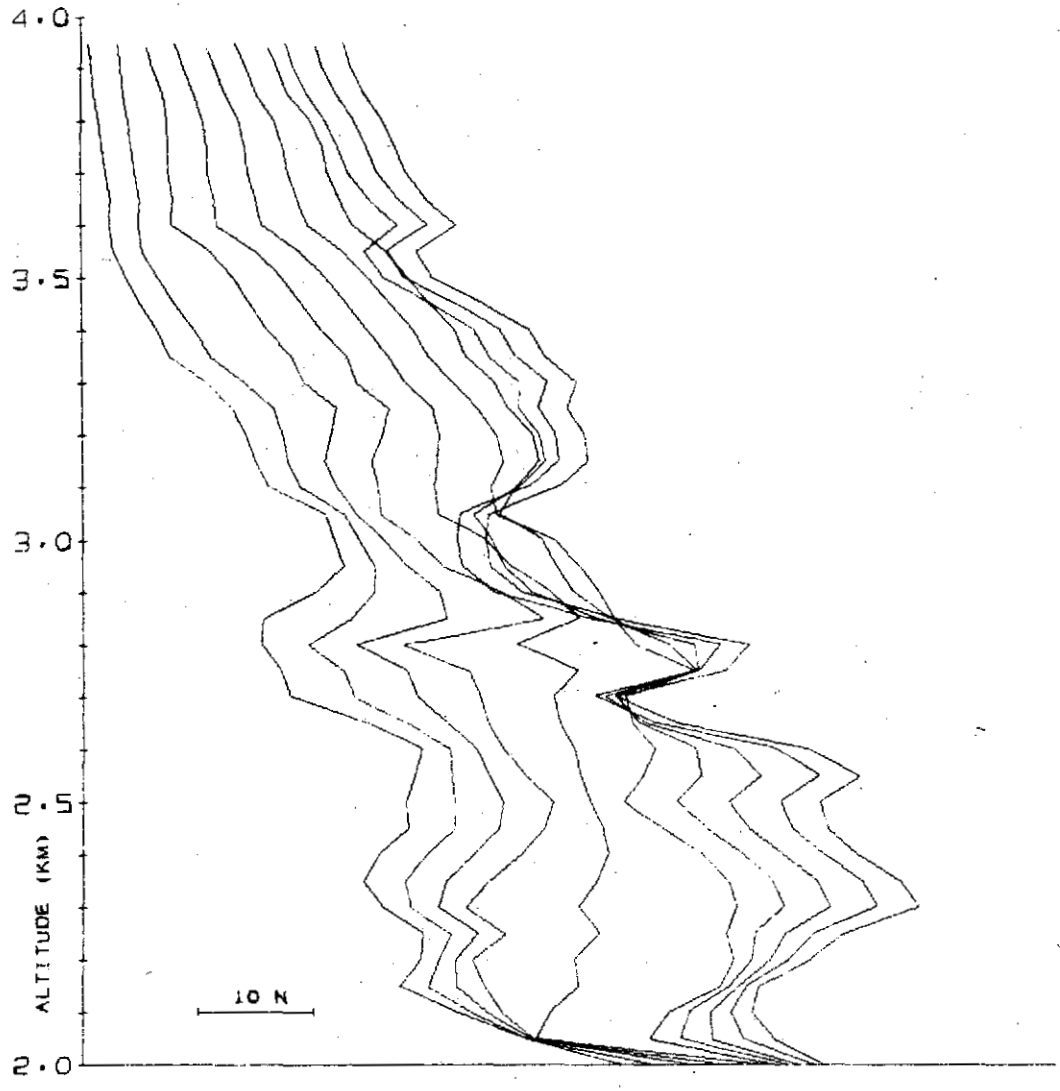

d. Flight 11: flight-pattern II, type-D fading

Fig. 43. CONTINUED.

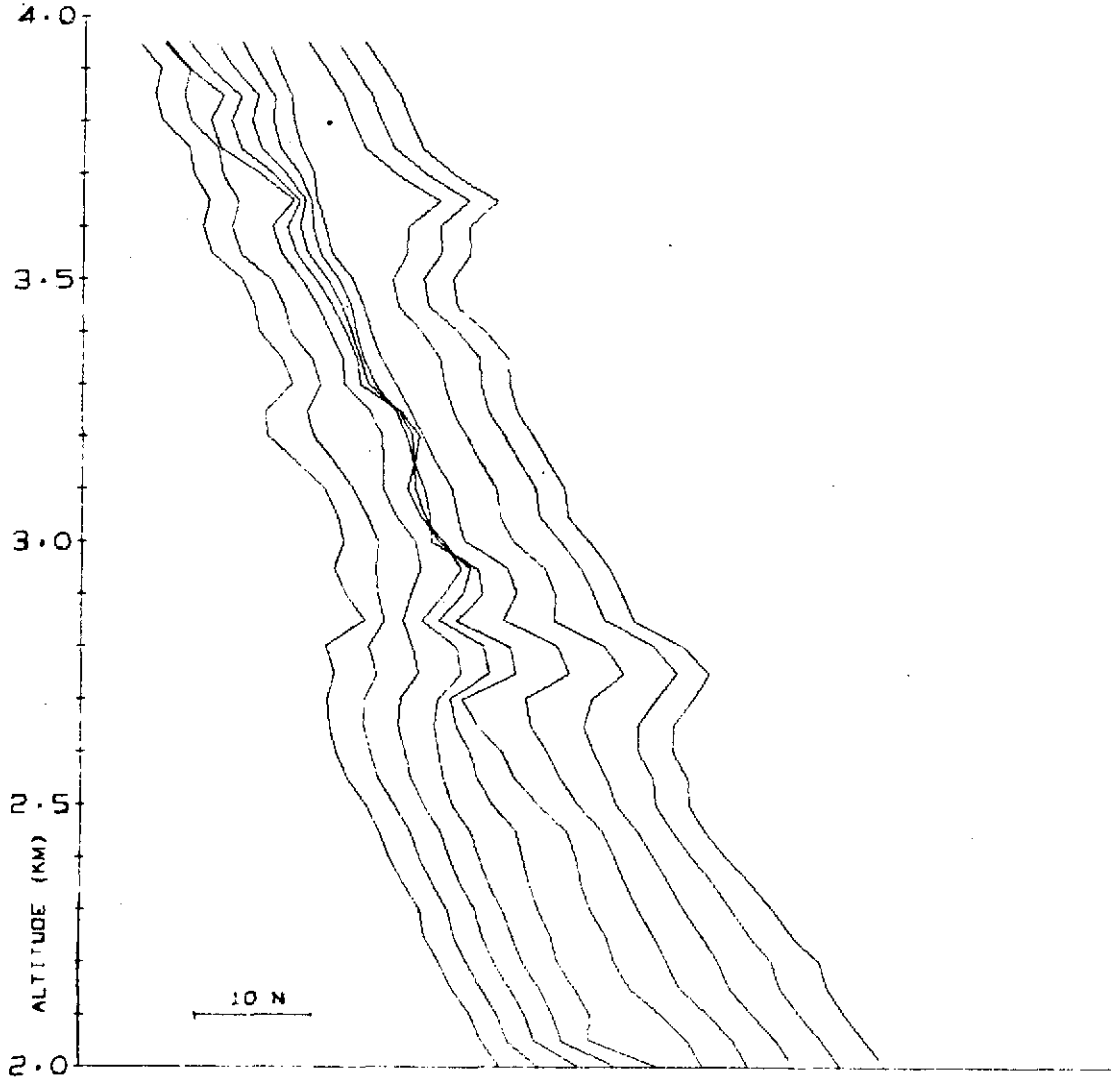

e. Flight 16: flight-pattern II, type-B fading

Fig. 43. CONTINUED.

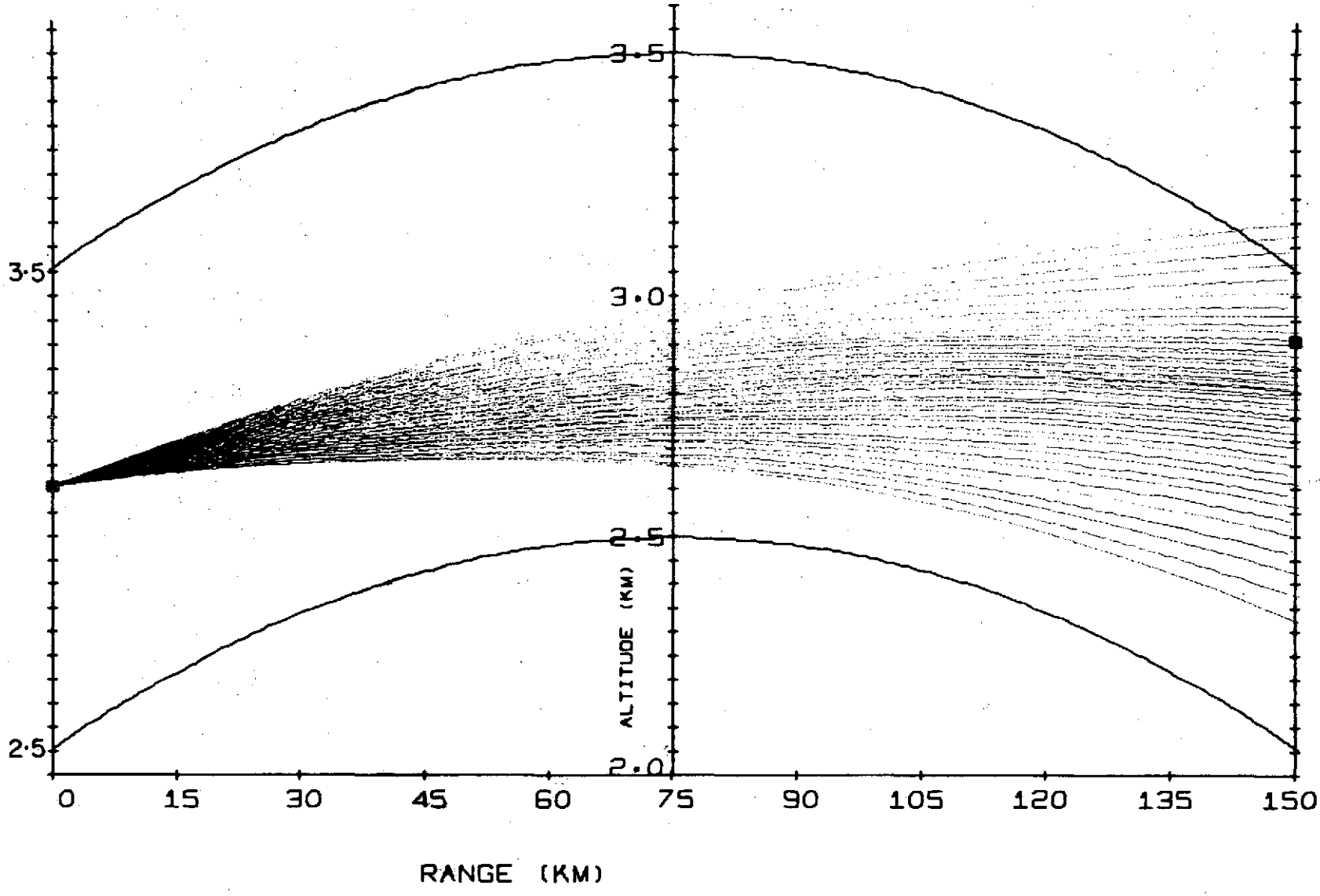

a. Flight 2

Fig. 44. COMPUTER-DRAWN RAYPATHS FOR THE NONSYMMETRIC PROFILES IN FIG. 43.

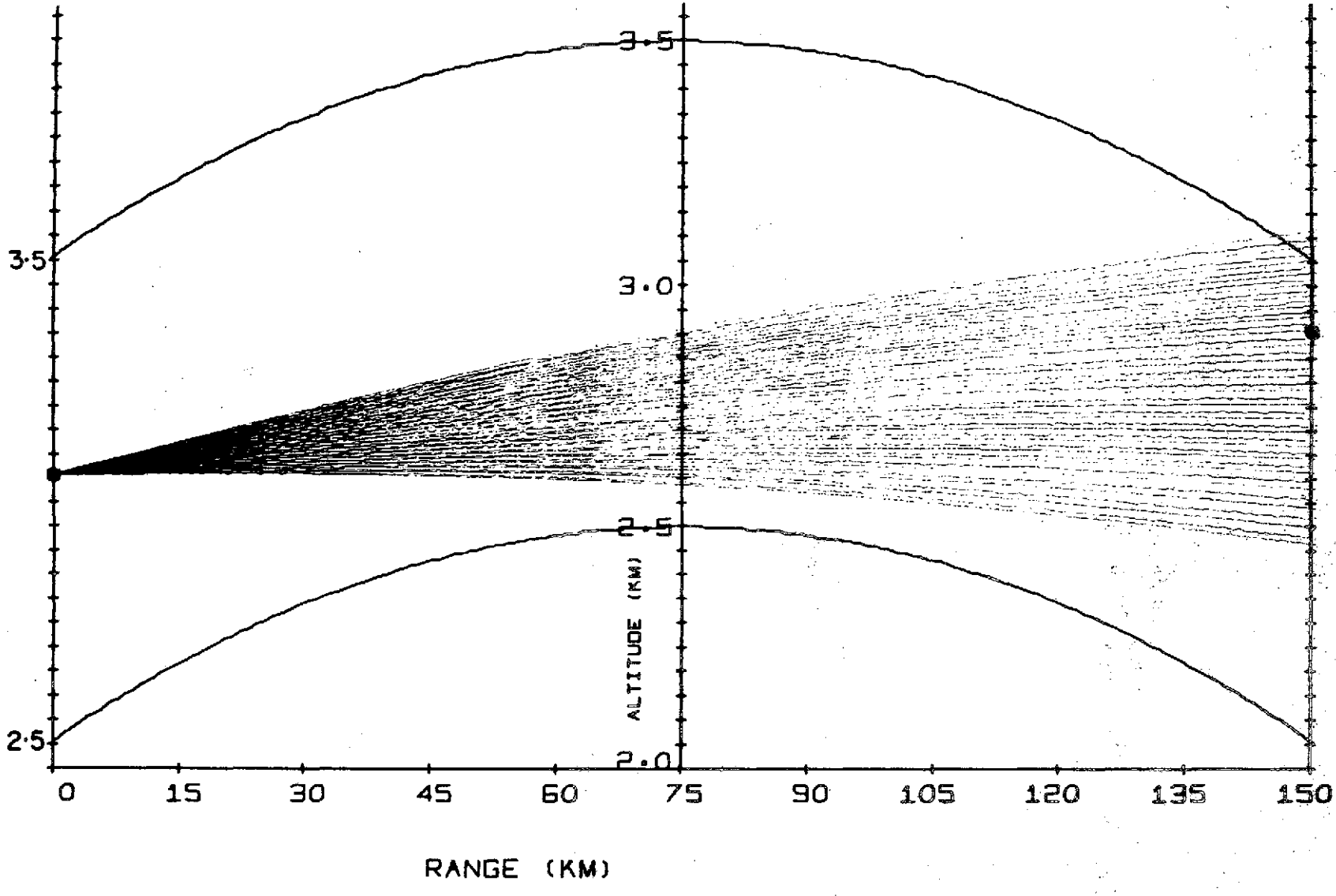

b. Flight 4

Fig. 44. CONTINUED.

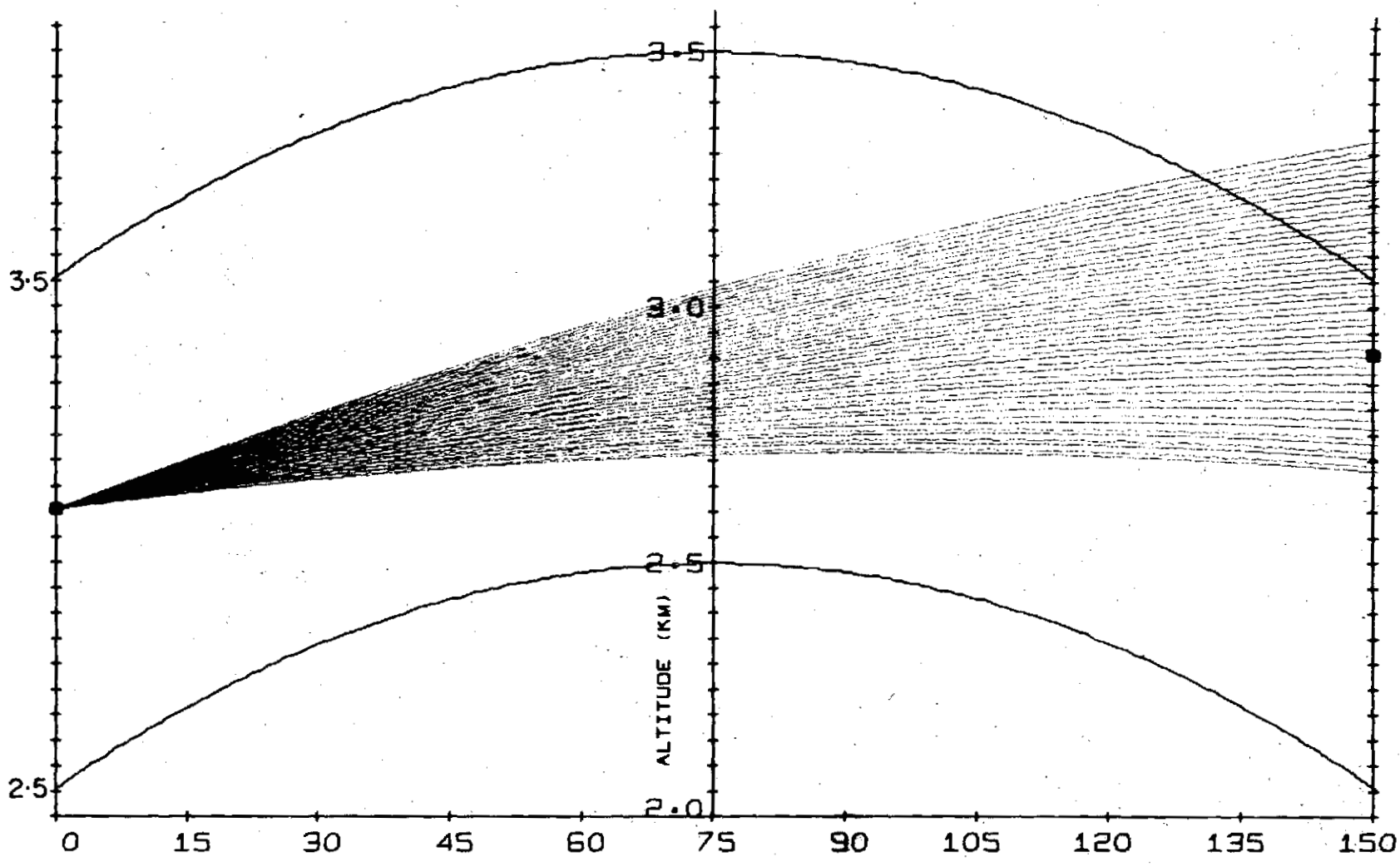

c. Flight 14

Fig. 44. CONTINUED.

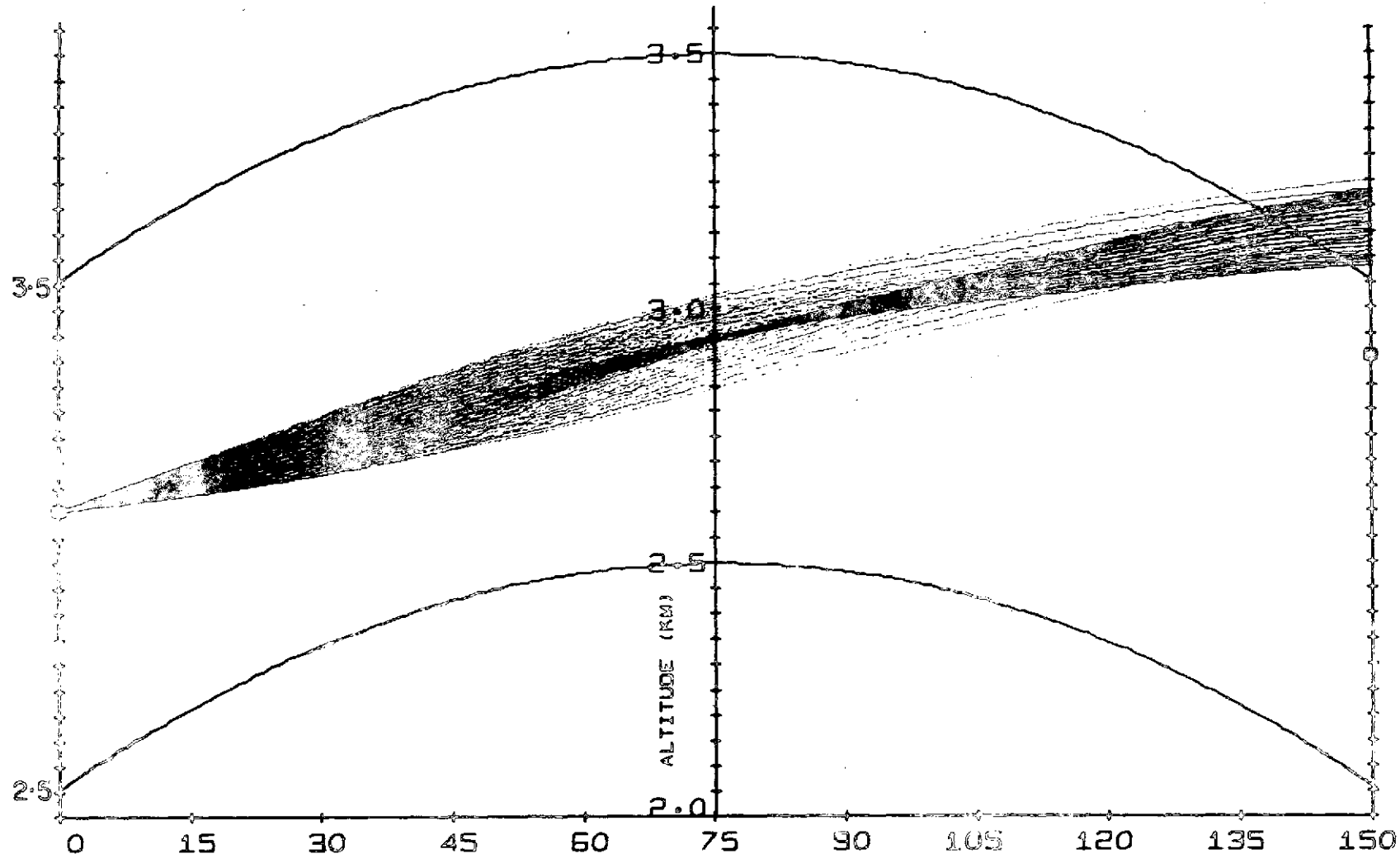

d. Flight 11

Fig. 44. CONTINUED.

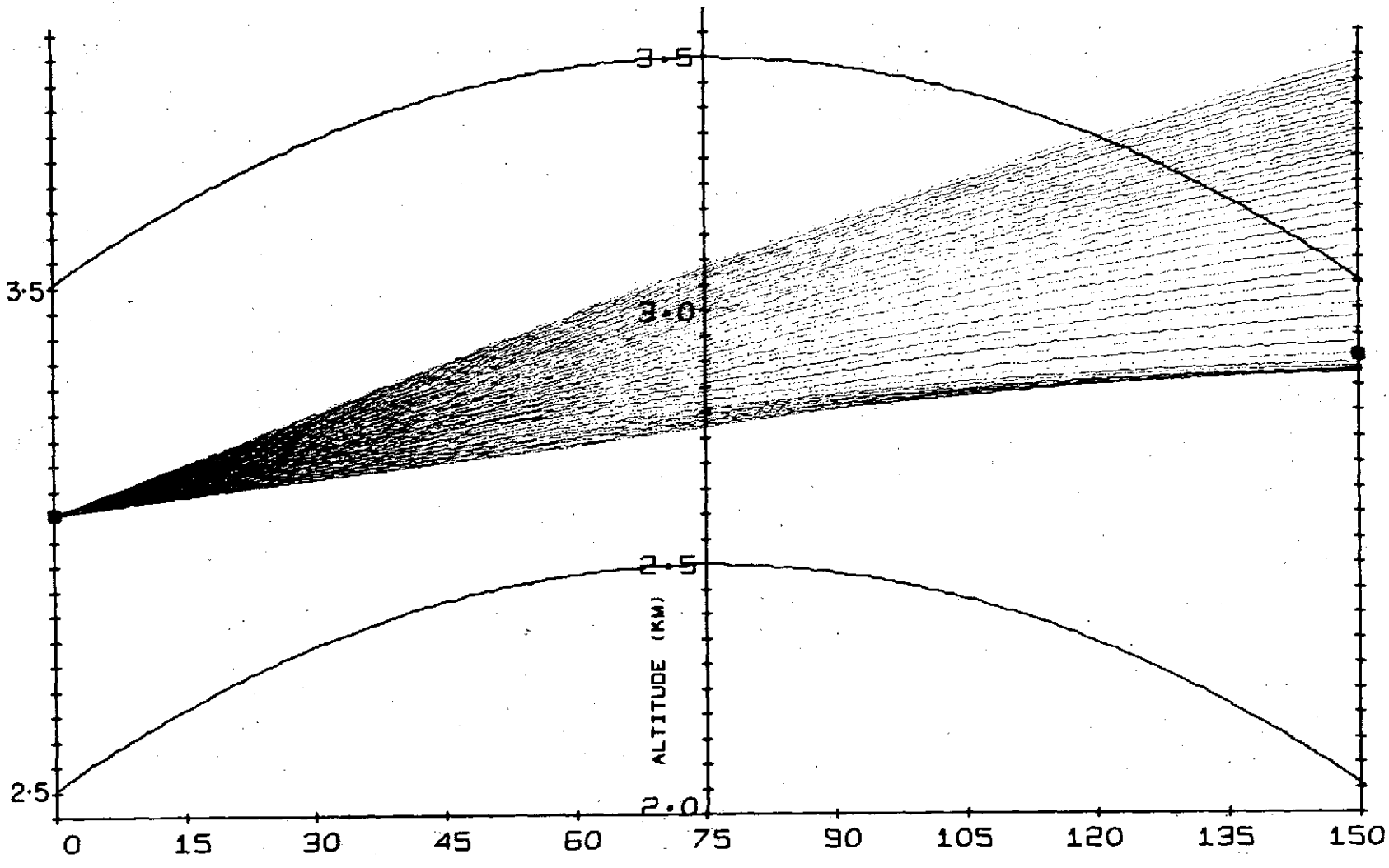

e. Flight 16

Fig. 44. CONTINUED.

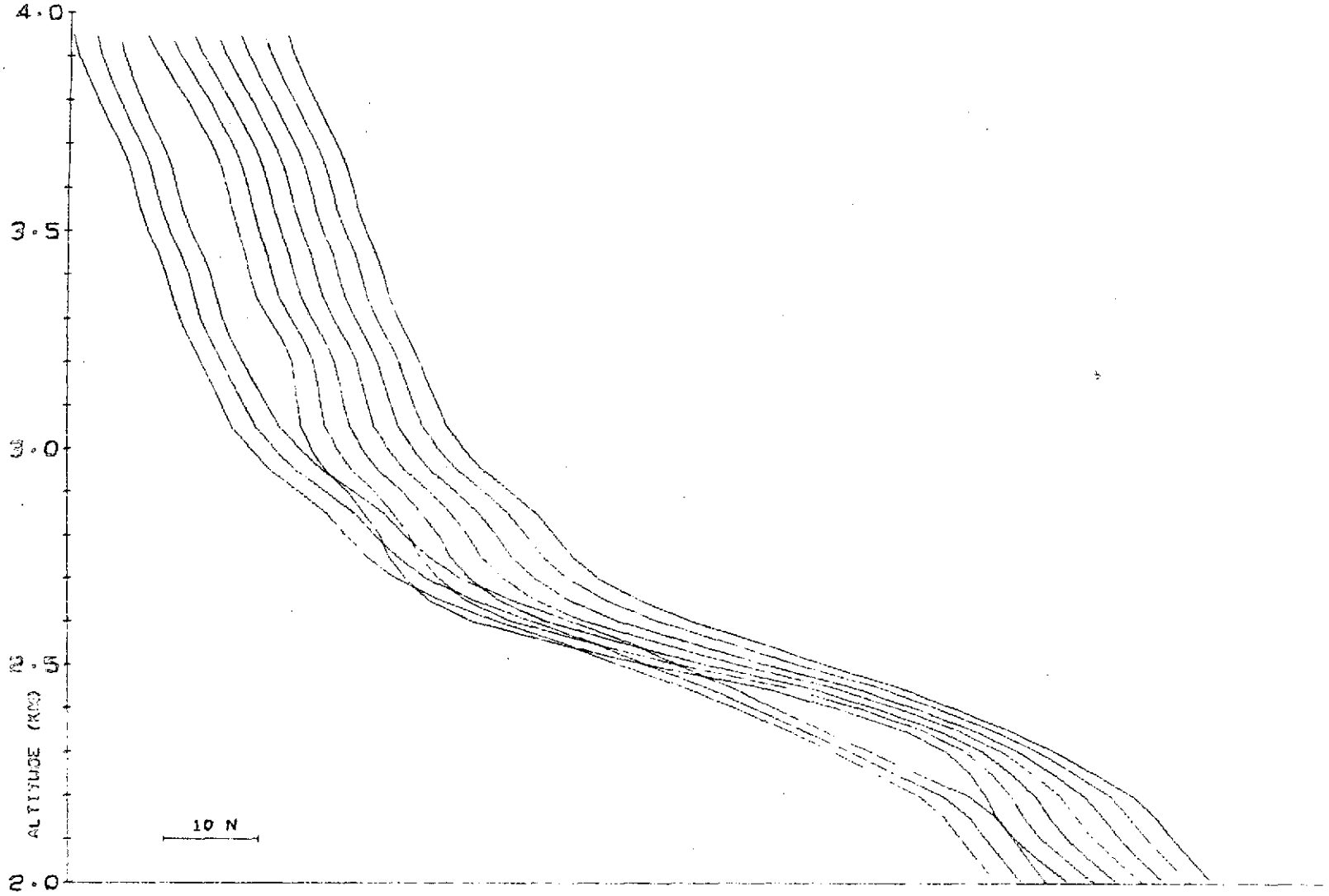

a. Flight 2: flight-pattern I, type-C fading

Fig. 45. NONSYMMETRIC SMOOTHED N-PROFILES. Generation of these samples was the same as for the profiles in Fig. 43, with the exception that the aircraft-originated data were run through a smoothing filter prior to generating the linear gradients.

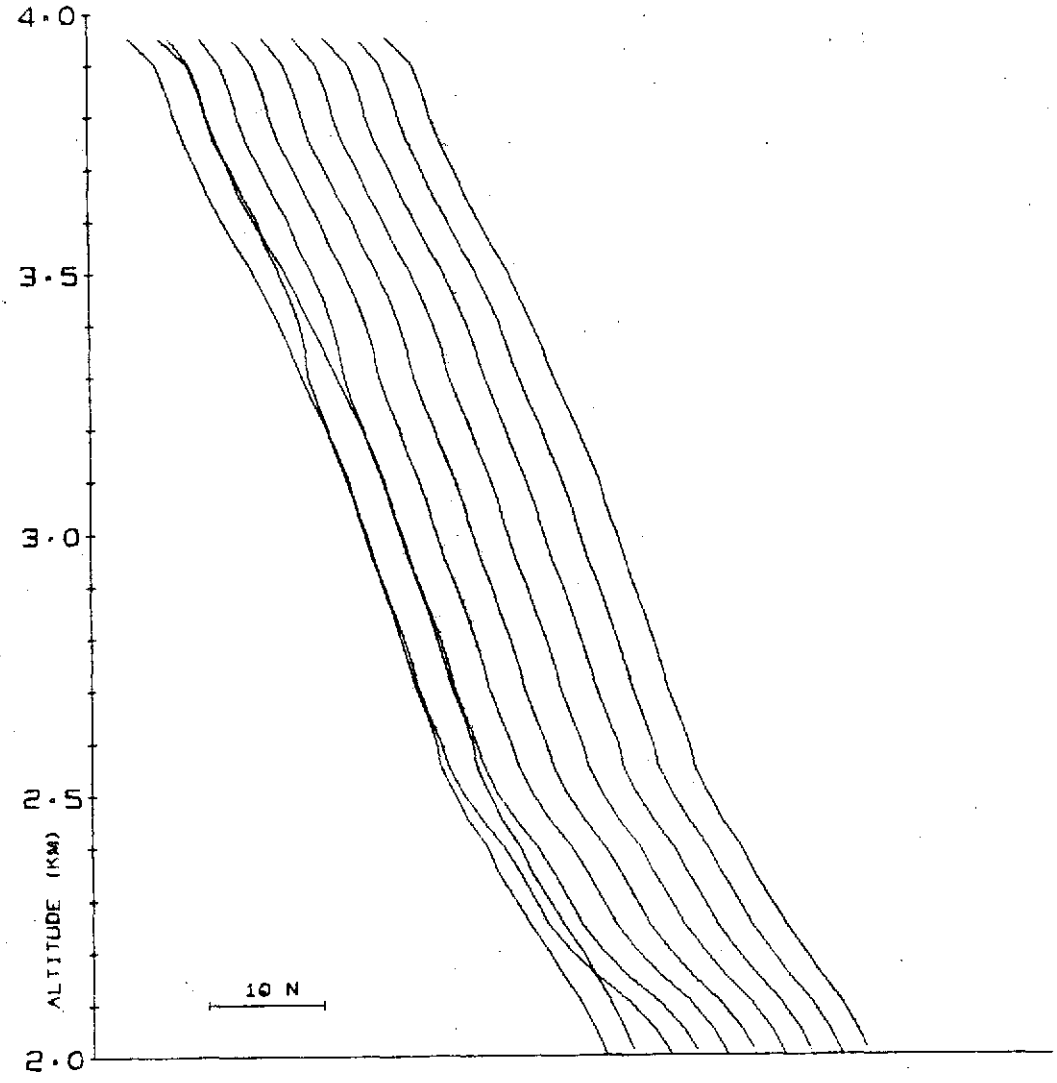

b. Flight 4: flight-pattern I, type-B fading

Fig. 45. CONTINUED.

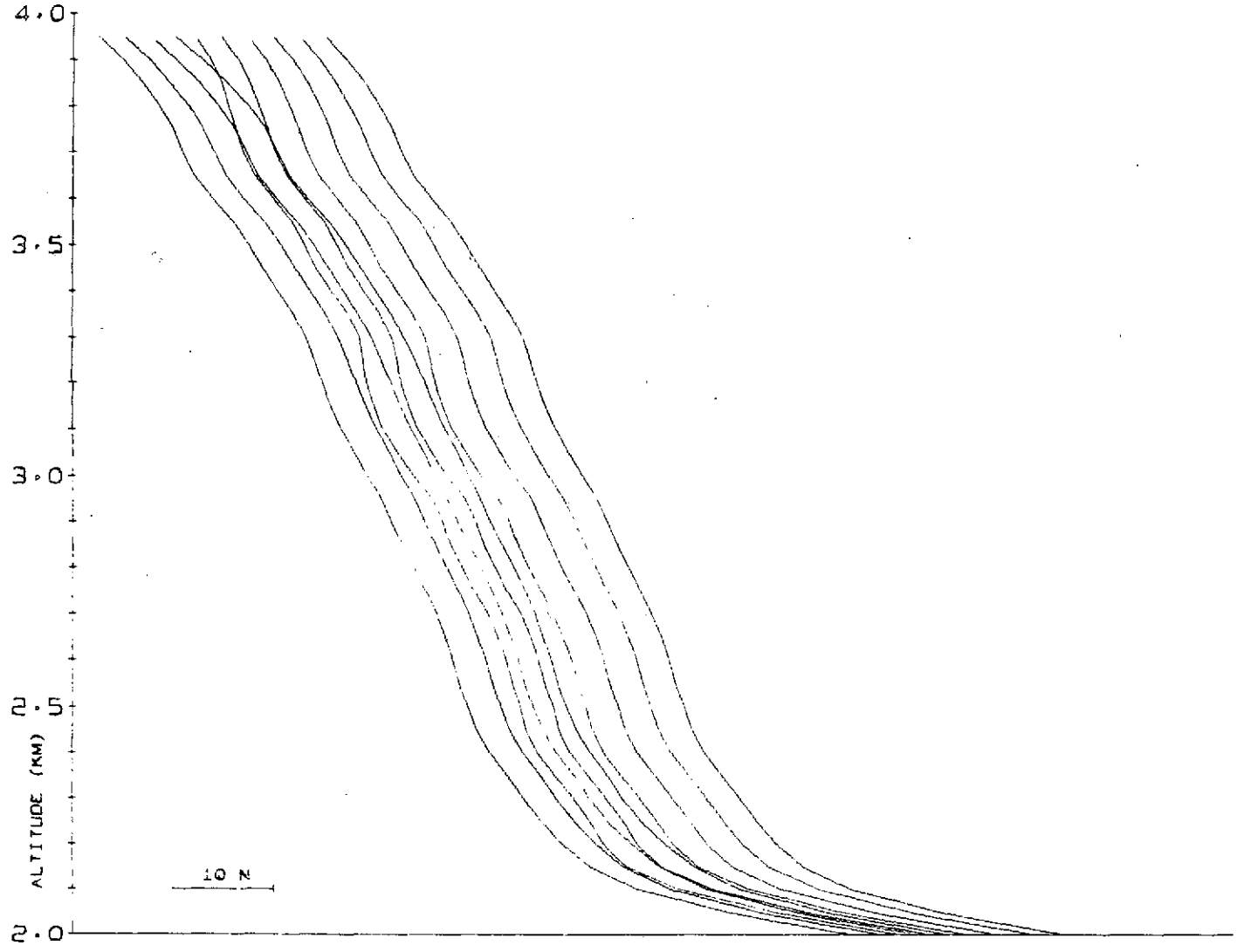

c. Flight 14: flight-pattern I, type-A fading

Fig. 45. CONTINUED.

d. Flight 11: flight-pattern II, type-D fading

Fig. 45. CONTINUED.

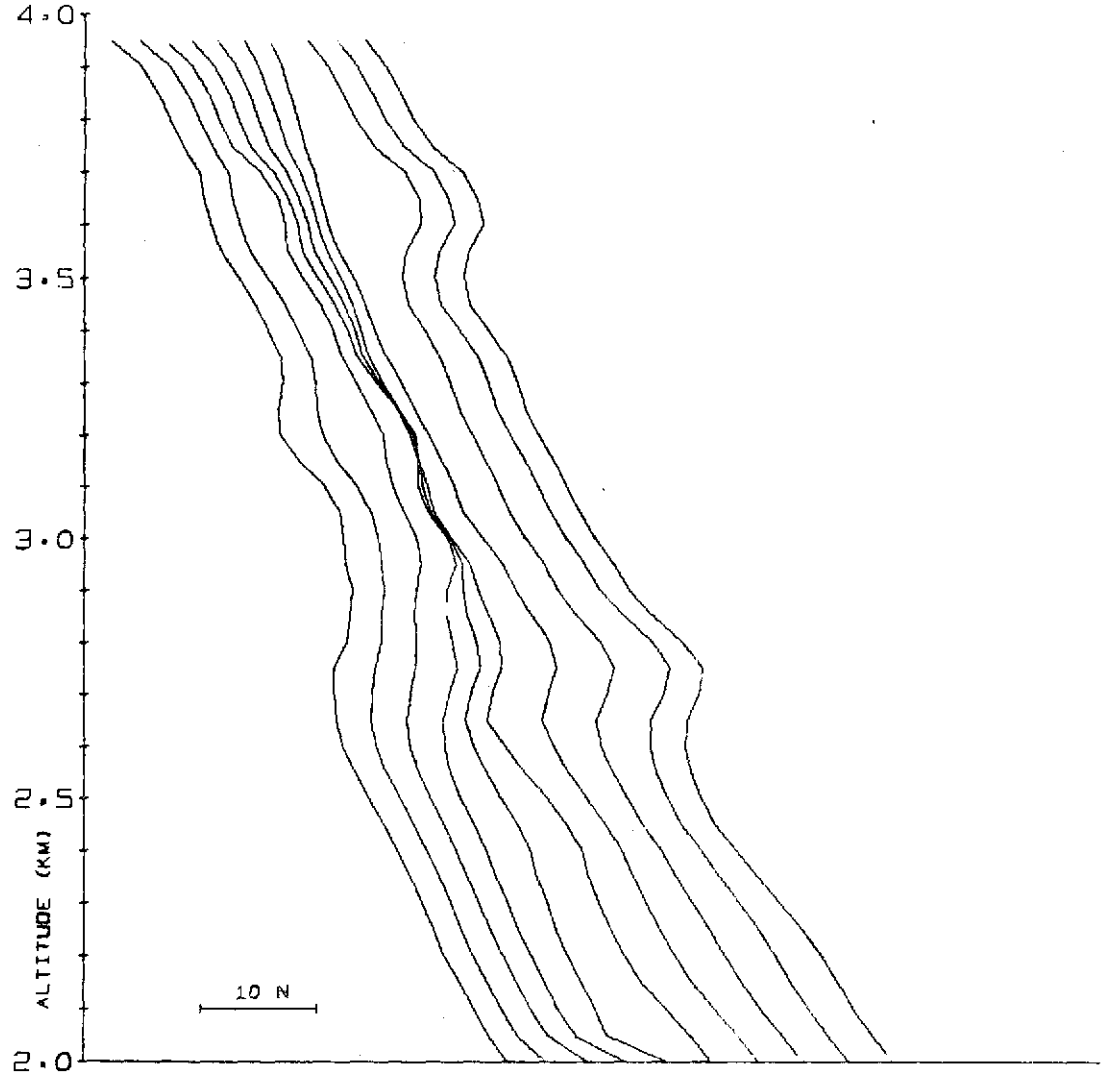

e. Flight 16: flight-pattern II, type-B fading

Fig. 45. CONTINUED.

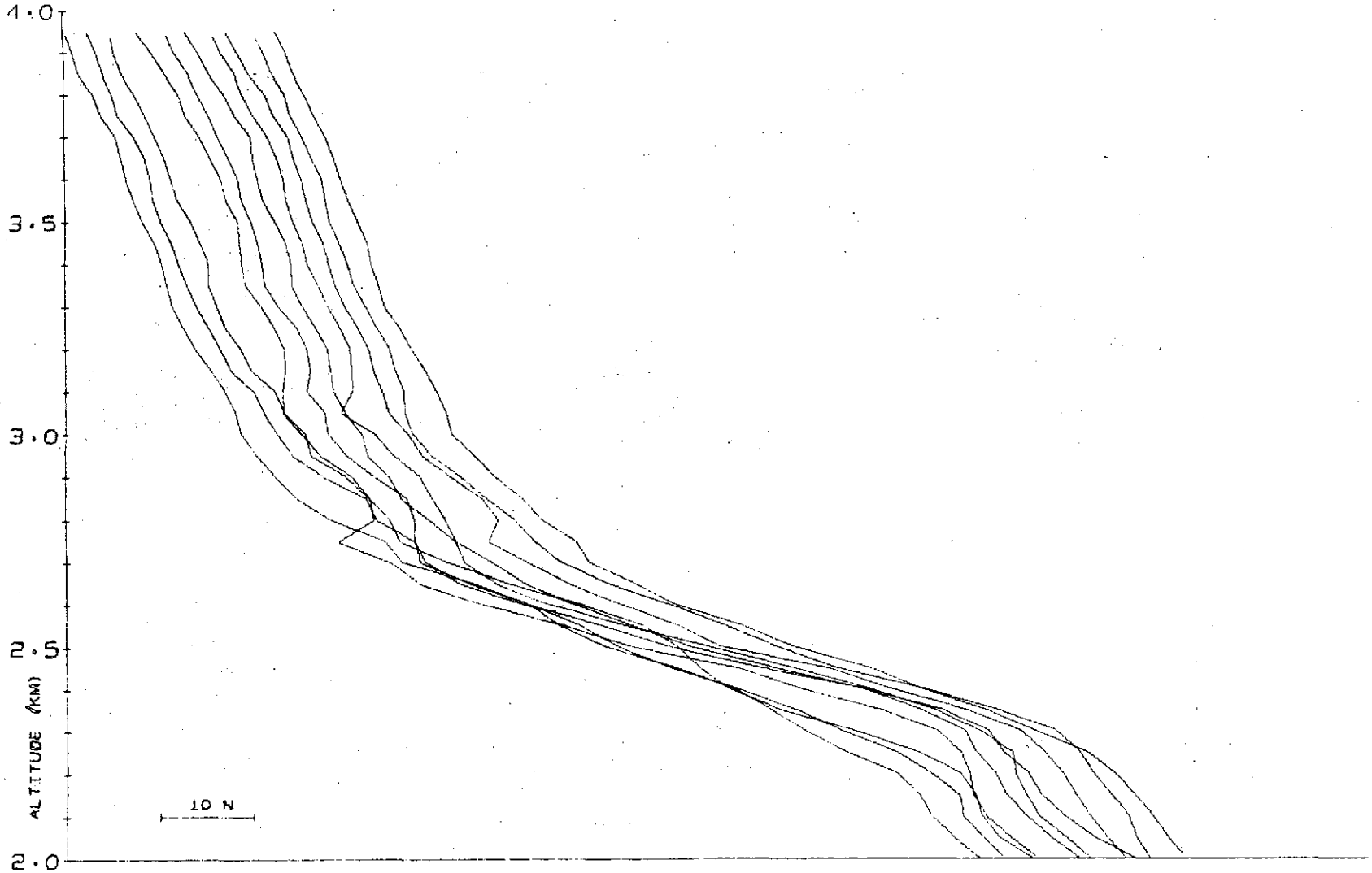

a. Flight 2: flight-pattern I, type-C fading

Fig. 46. NONSYMMETRIC STATISTICAL N-PROFILES. These samples were generated by adding a random variate to the profiles in Fig. 45.

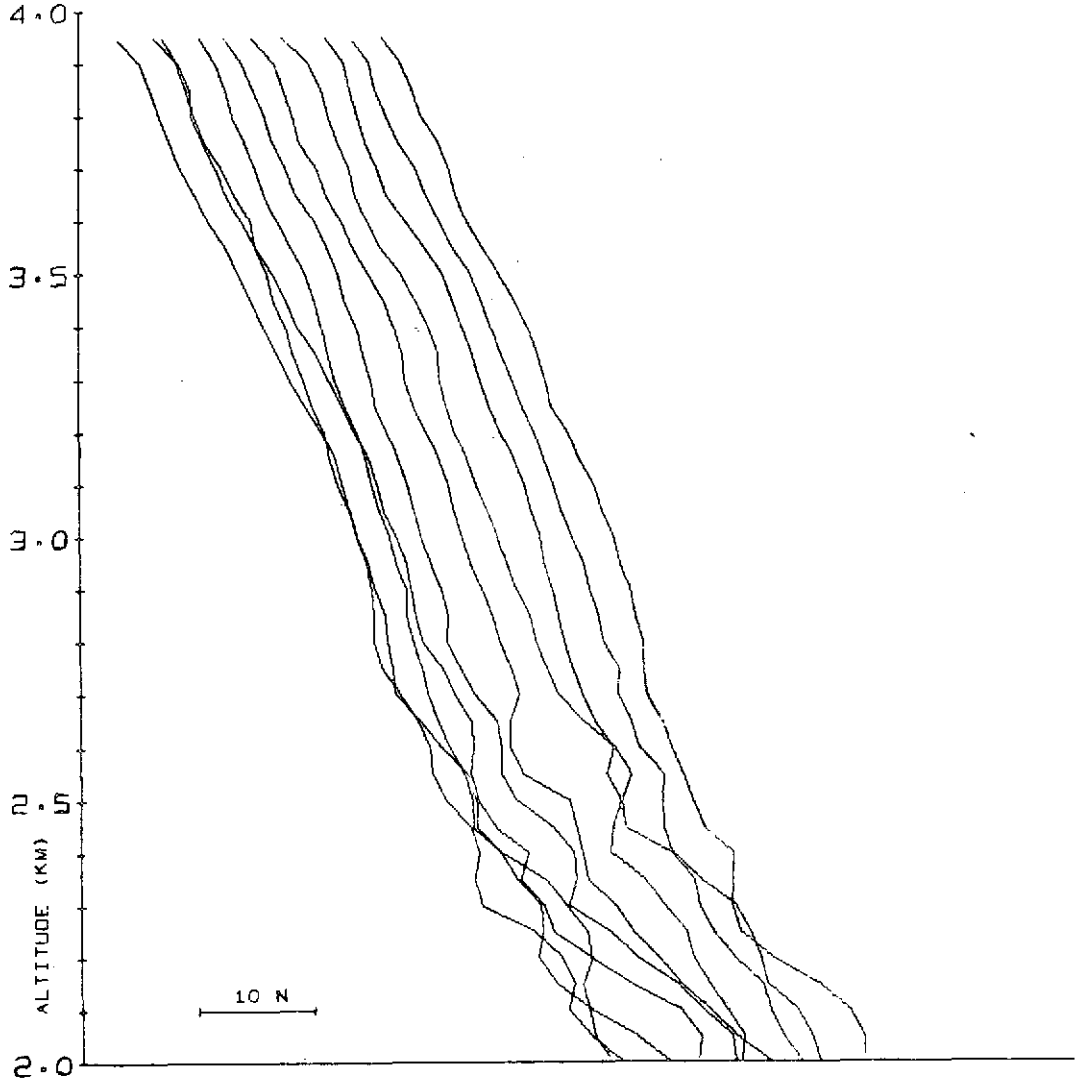

b. Flight 4: flight-pattern I, type-B fading

Fig. 46. CONTINUED.

c. Flight 14: flight-pattern I, type-A fading

Fig. 46. CONTINUED.

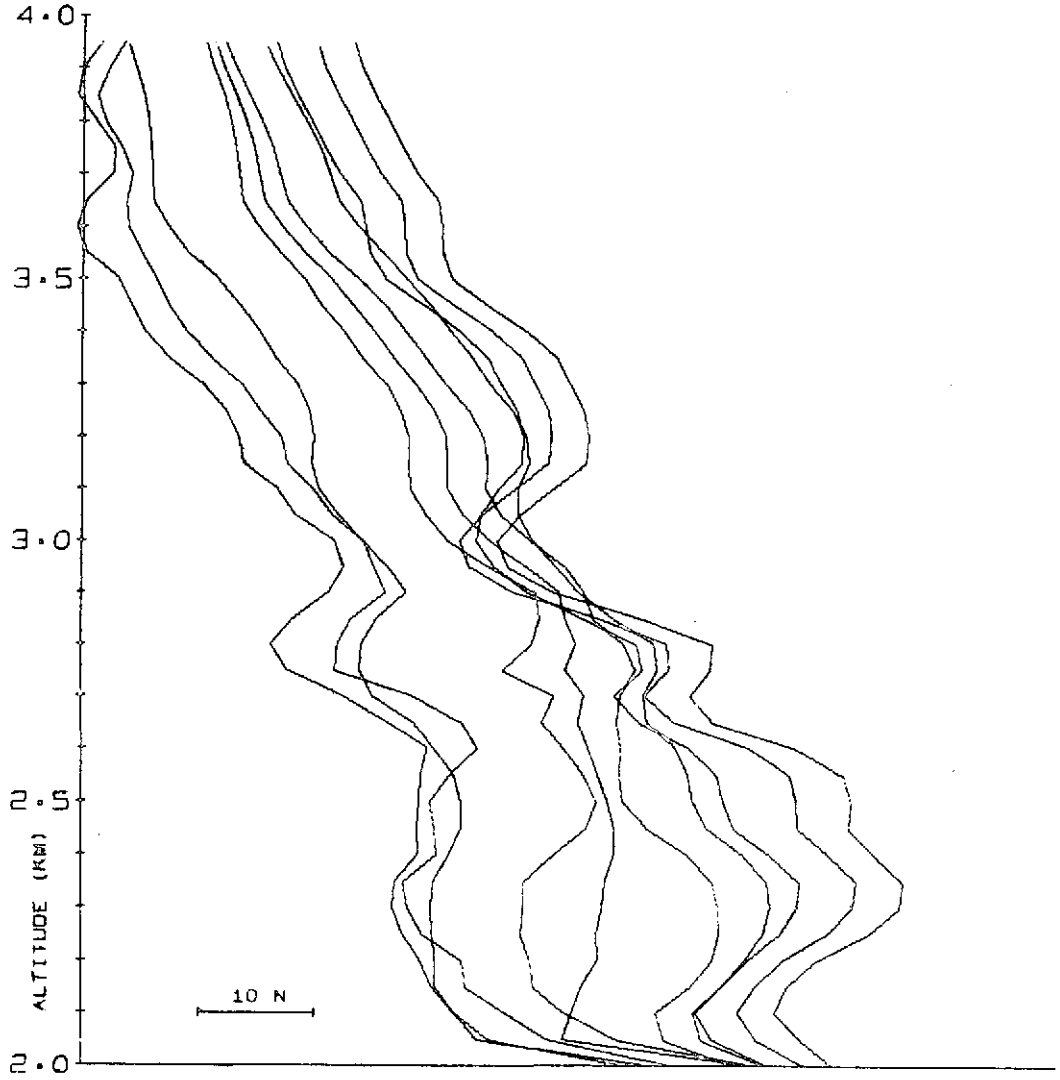

d. Flight 11: flight-pattern II, type-D fading

Fig. 46. CONTINUED.

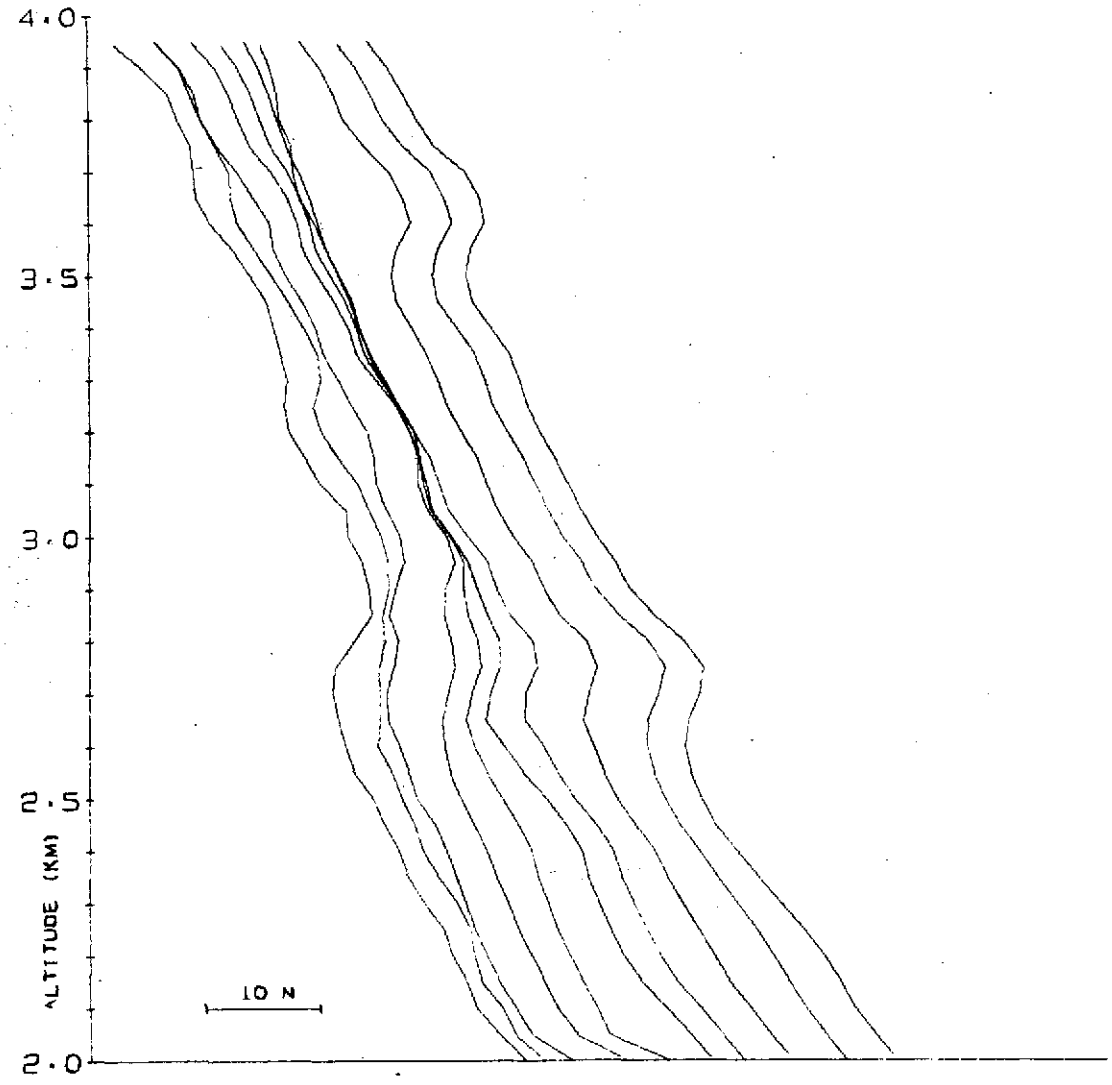

e. Flight 16: flight-pattern II, type-B fading

Fig. 46. CONTINUED.

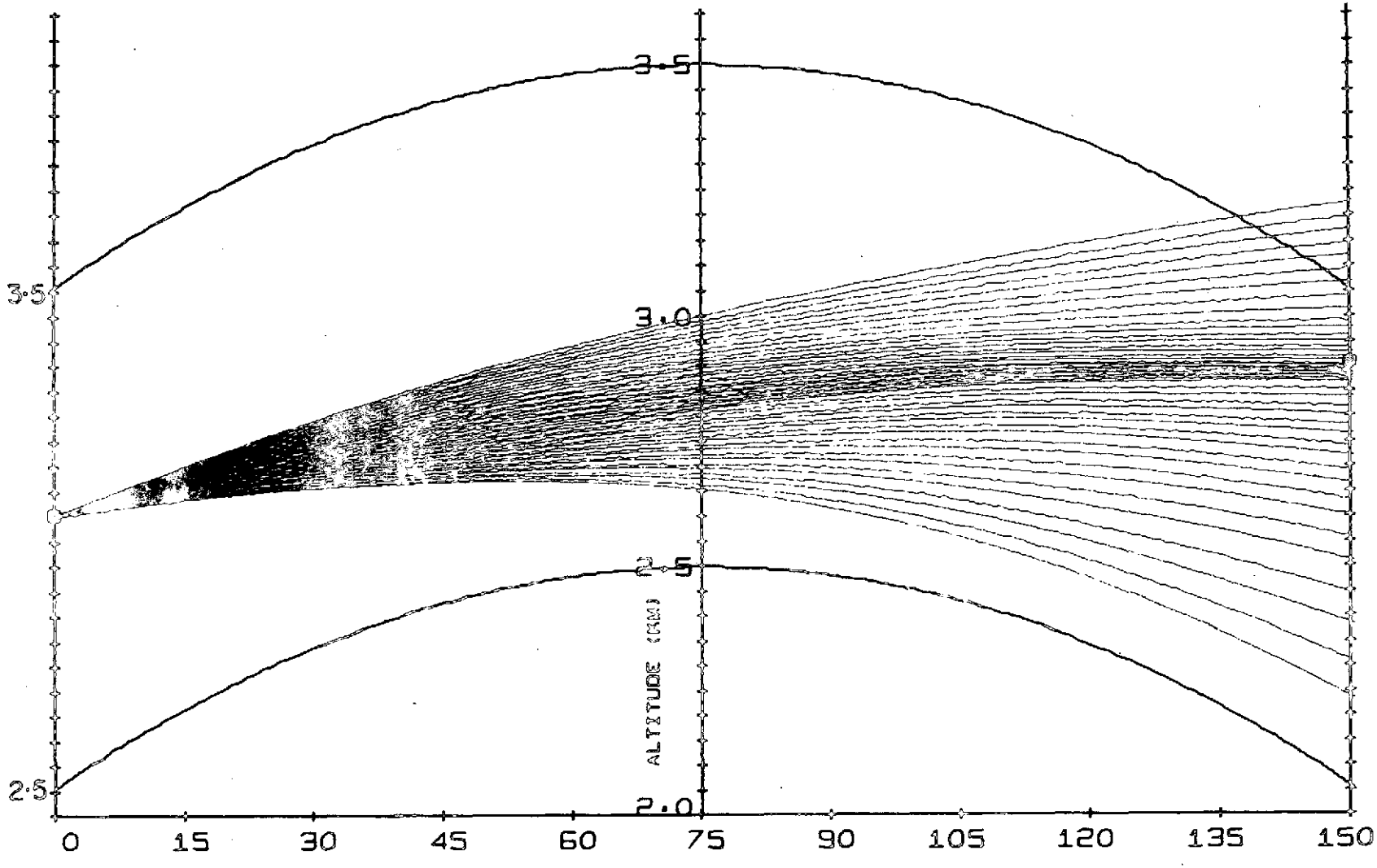

a. Flight 2

Fig. 47. COMPUTER-DRAWN RAYPATHS FOR THE NONSYMMETRIC STATISTICAL PROFILES IN FIG. 46.

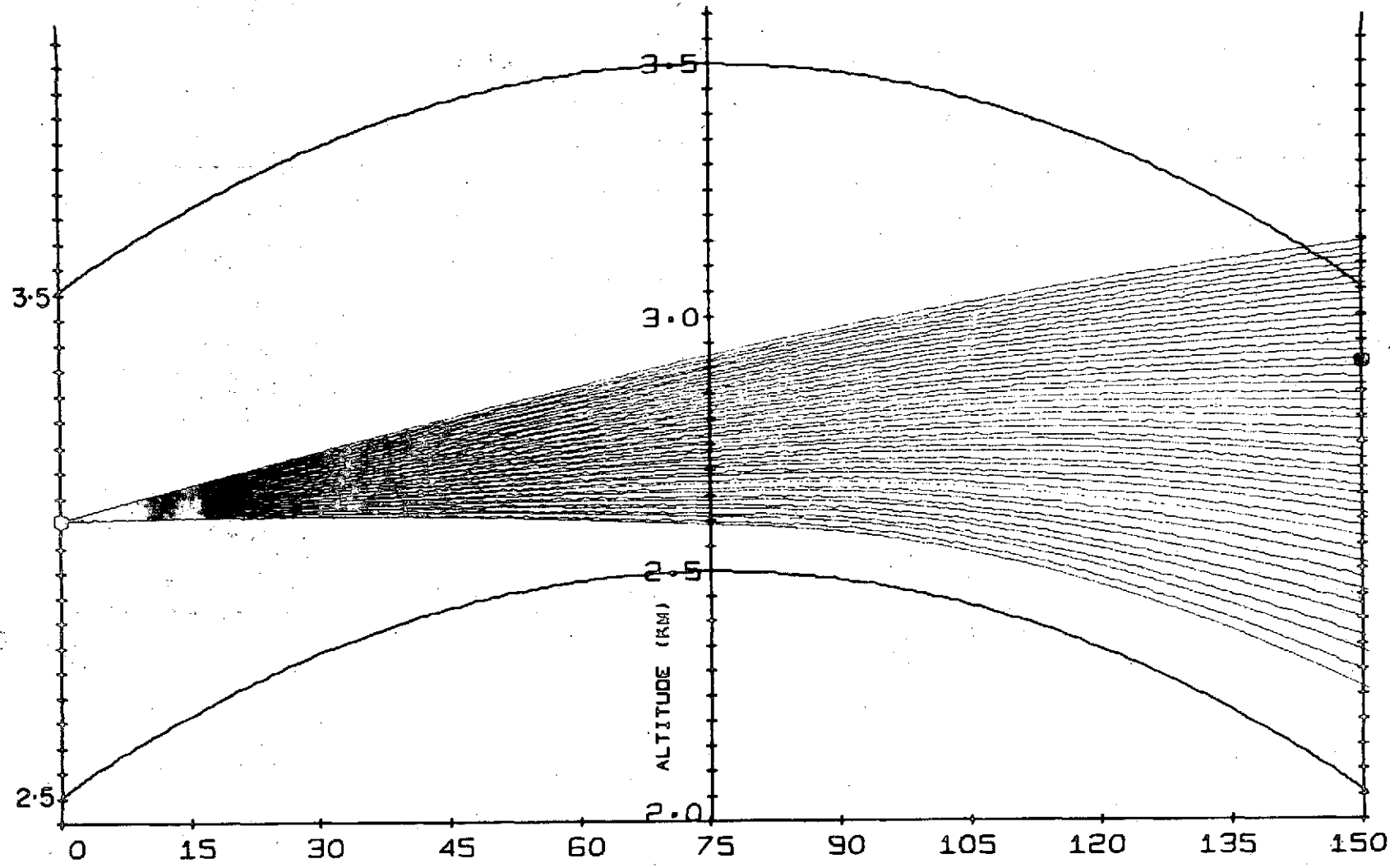

b. Flight 4

Fig. 47. CONTINUED.

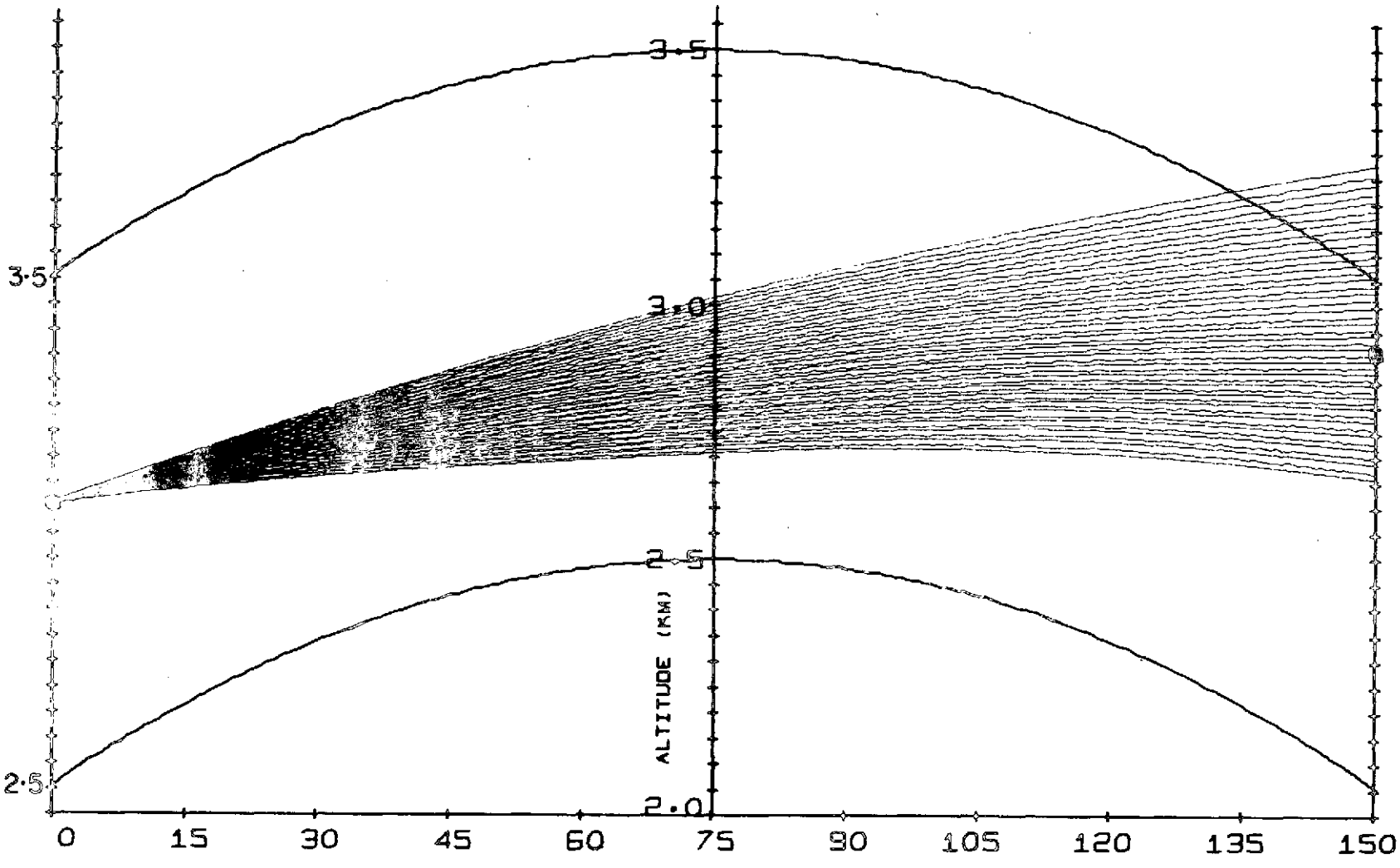

c. Flight 14

Fig. 47. CONTINUED.

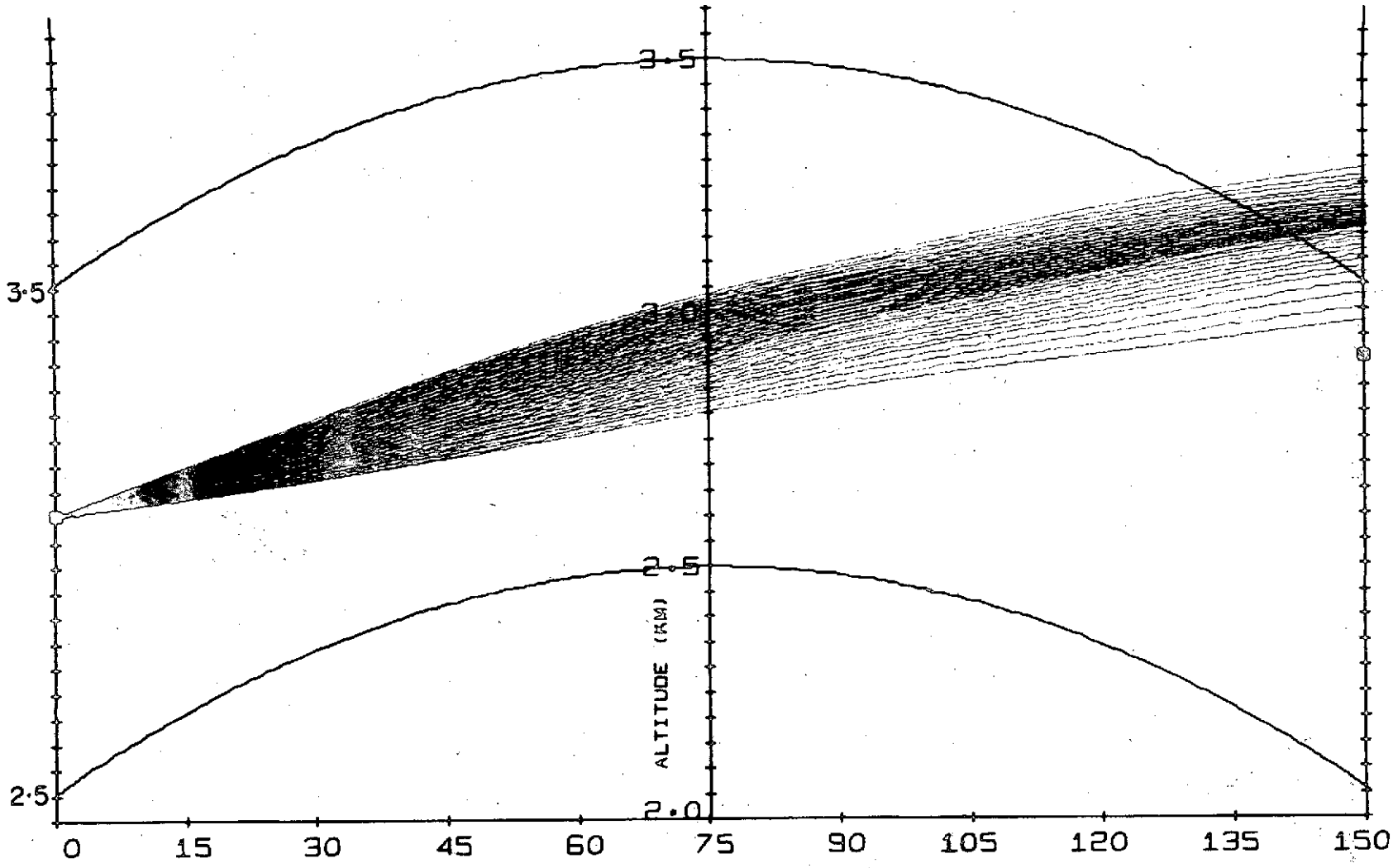

d. Flight 11

Fig. 47. CONTINUED.

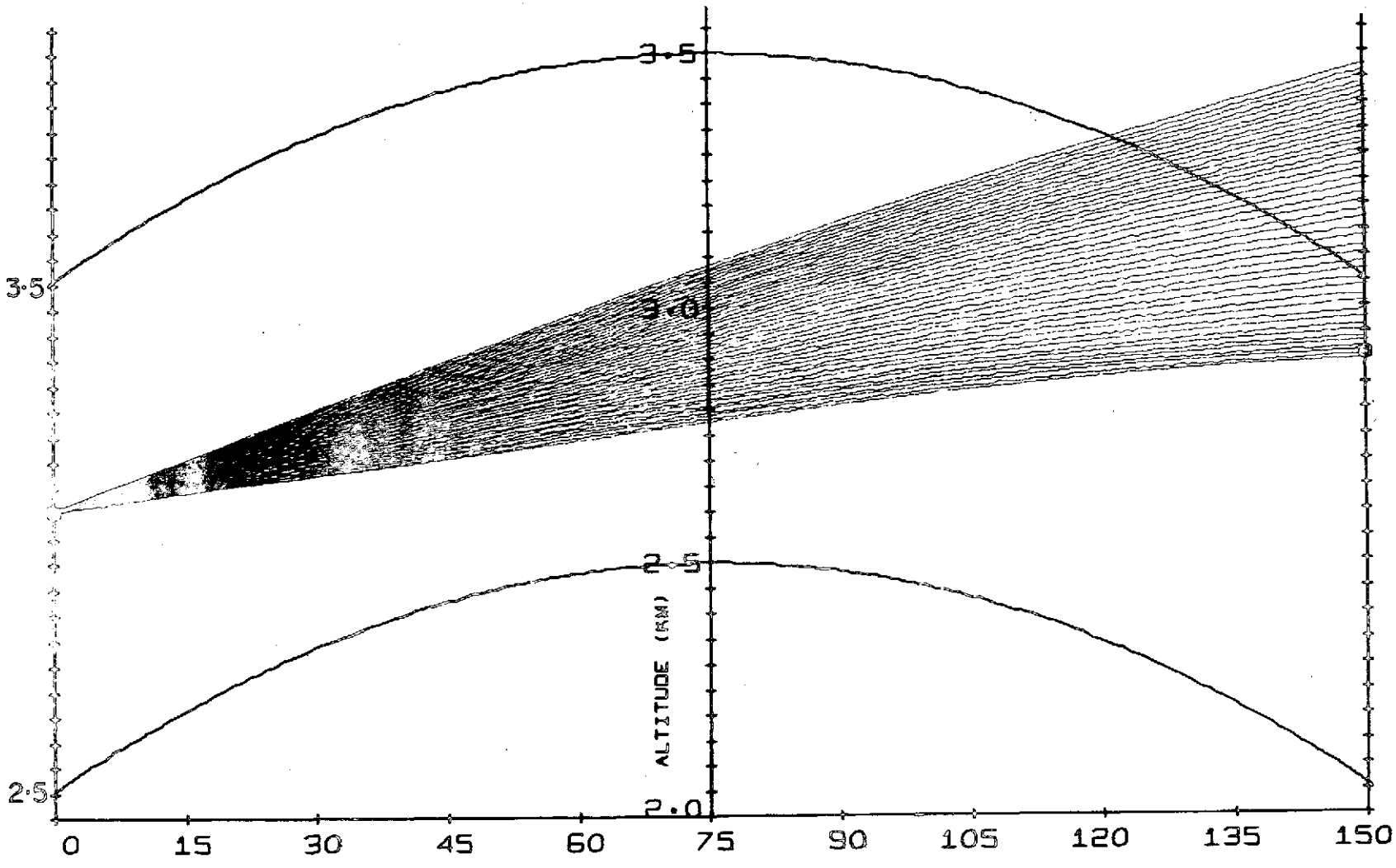

e. Flight 16

Fig. 47. CONTINUED.

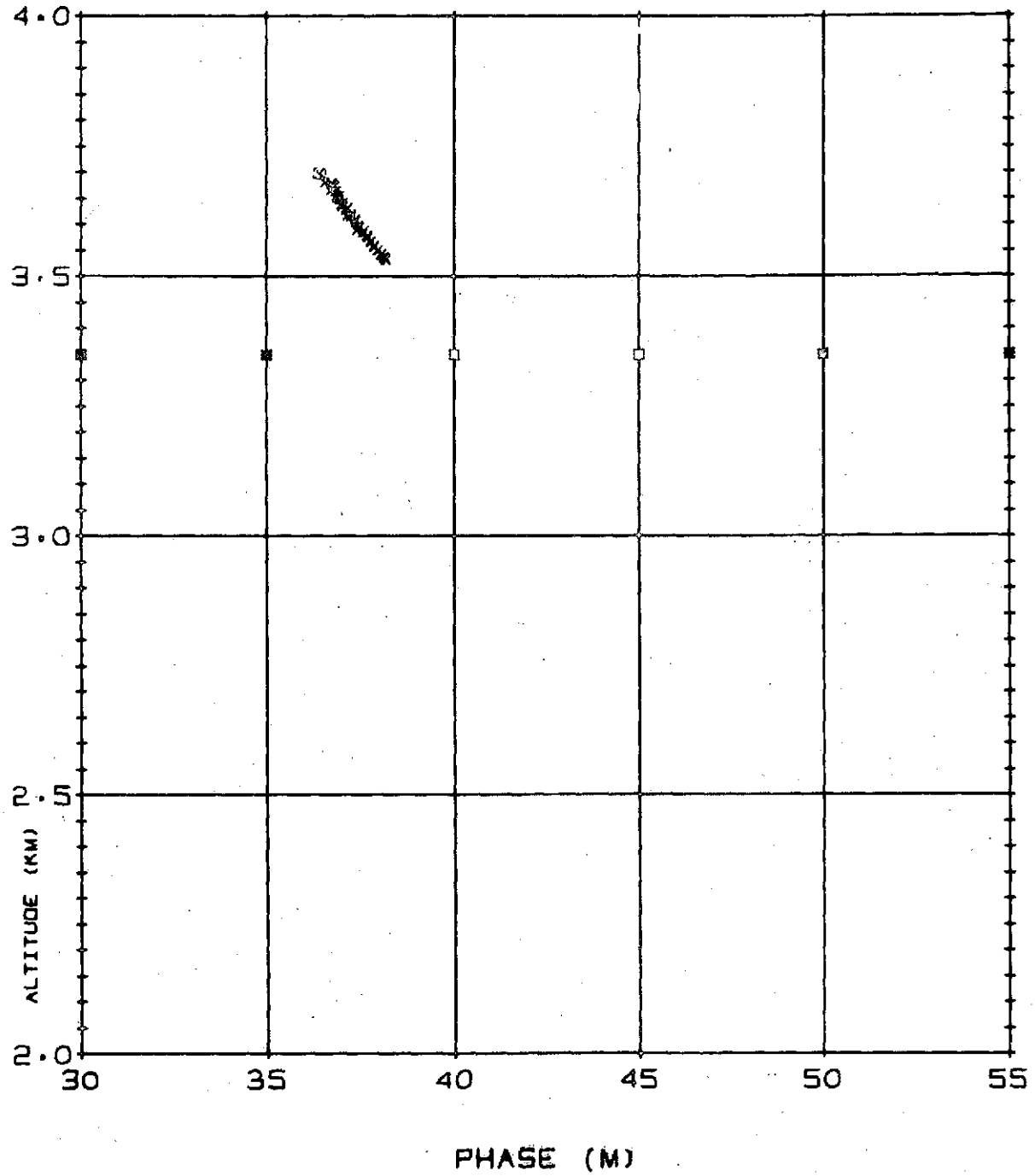

a. Flight 11, linear gradient (see Fig. 43d)

Fig. 48. PHASE VS ALTITUDE AT THE RECEIVER RANGE FOR TWO NONSYMMETRIC PROFILES.

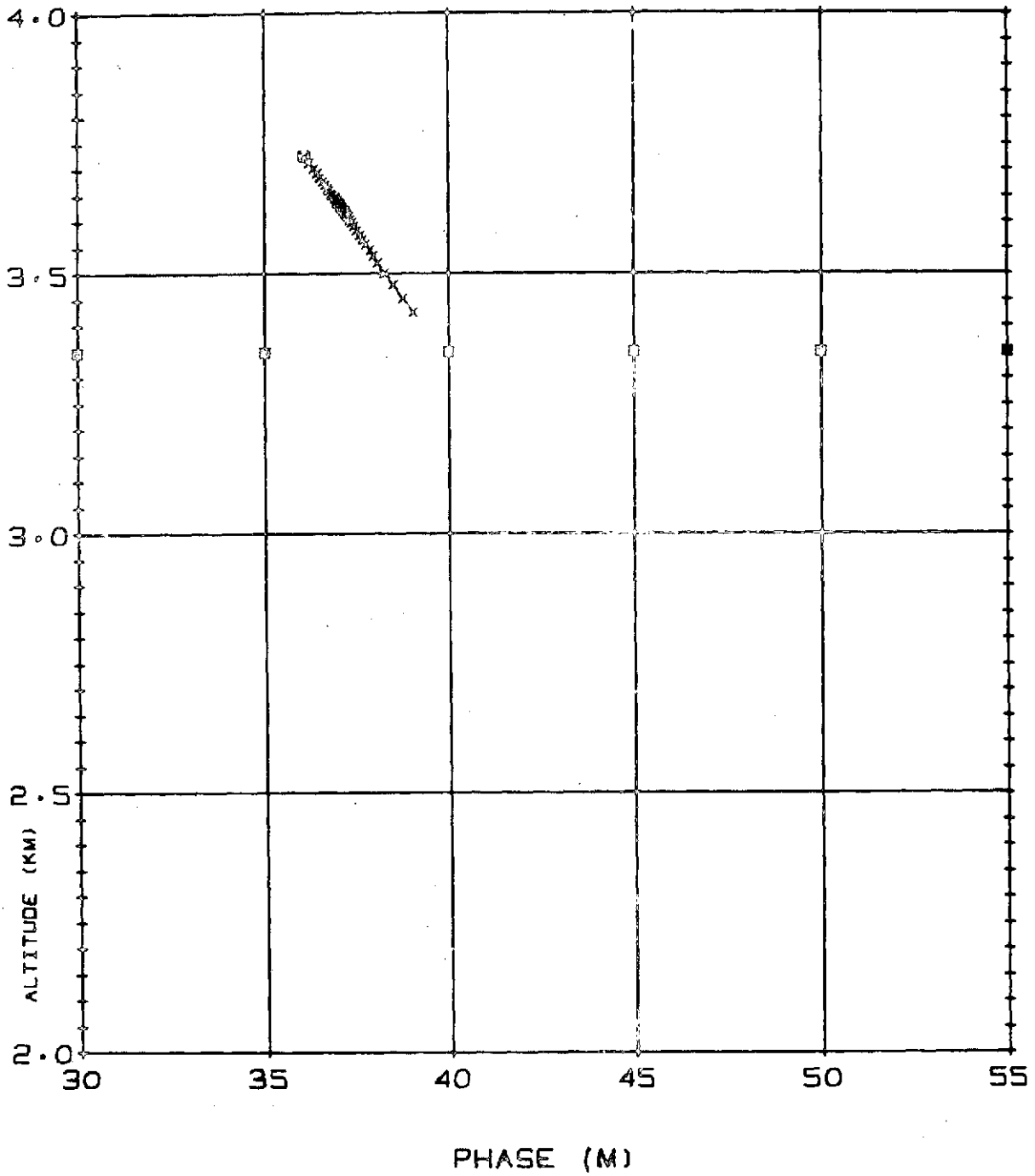

b. Flight 11, statistical gradient (see Fig. 47d)

Fig. 48. CONTINUED.

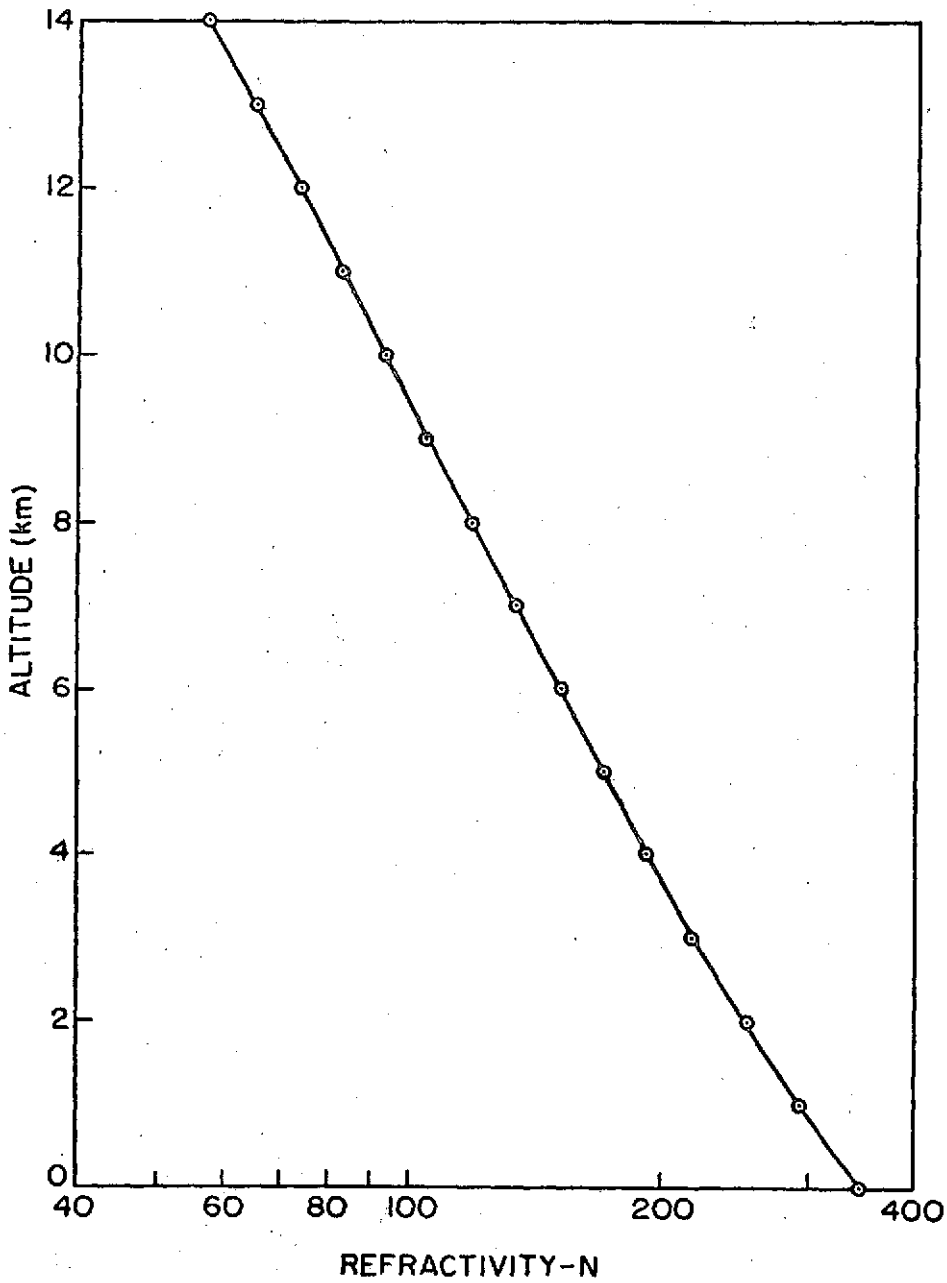

Fig. 49. STANDARD N-PROFILE.

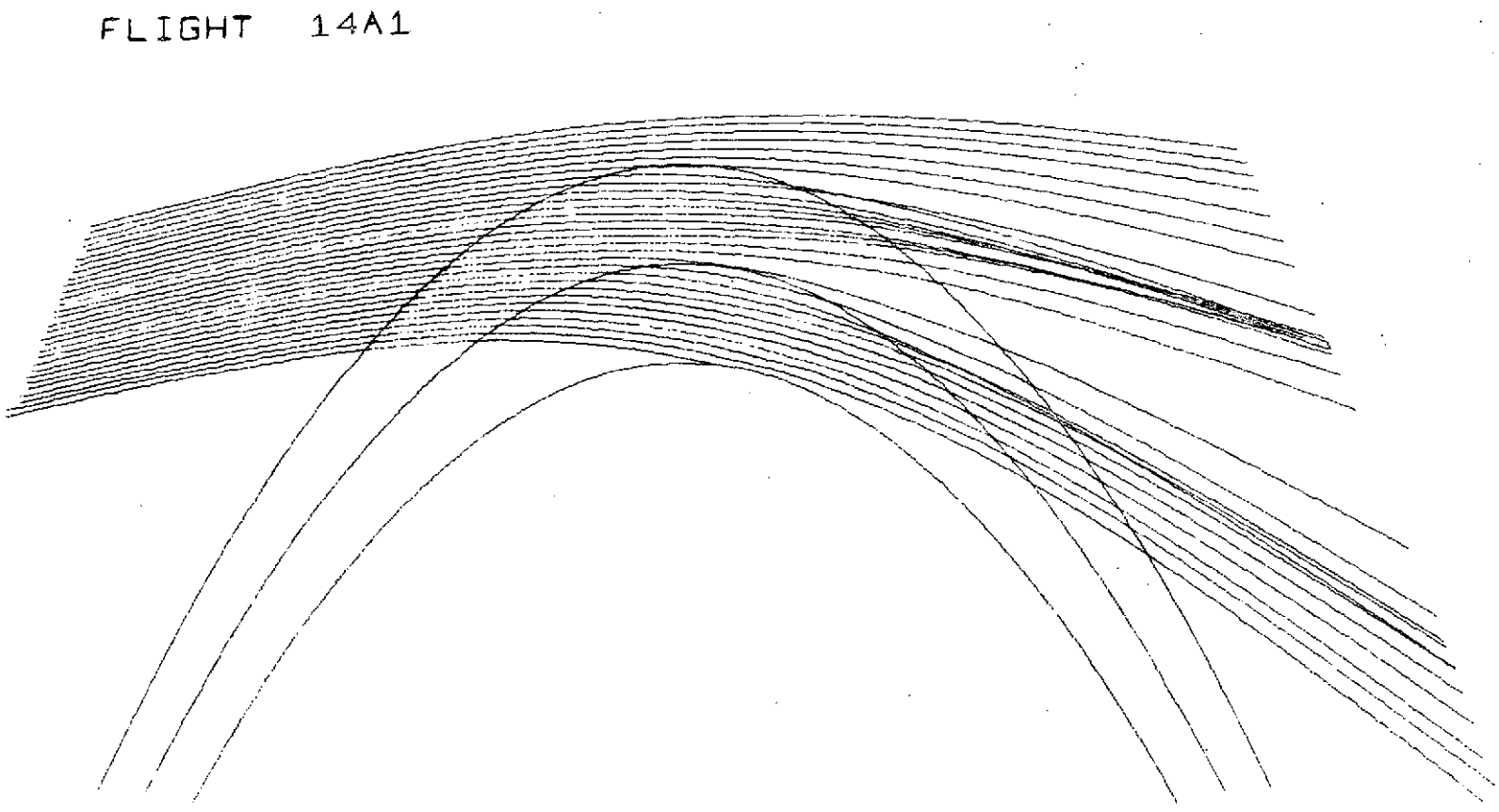

a. Profile 14A1: fading type-A

Fig. 50. COMPUTER-DRAWN RAYPATHS FOR SATELLITE-TO-SATELLITE PROPAGATION THROUGH SPHERICALLY SYMMETRIC HAWAII PROFILES. These figures show the lower 16 km of the raypaths as signals propagate between two co-orbiting satellites. The three parabolas represent (reading up) the surface of the Earth and the 2 and 4 km levels. The parabolic shape, rather than the customary circle, is the result of the exaggeration of the vertical scale.

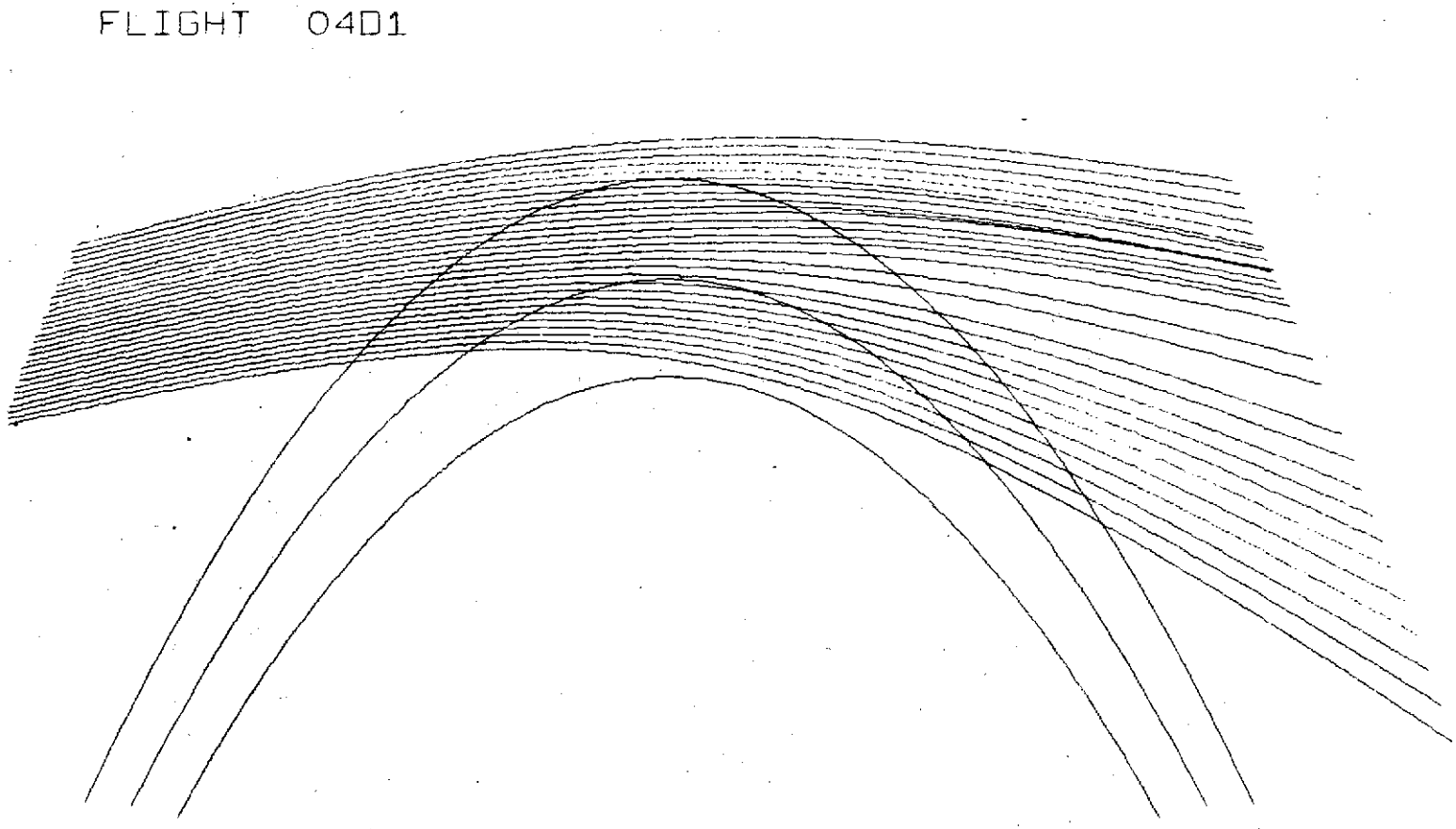

b. Profile 04D1: fading type-B

Fig. 50. CONTINUED.

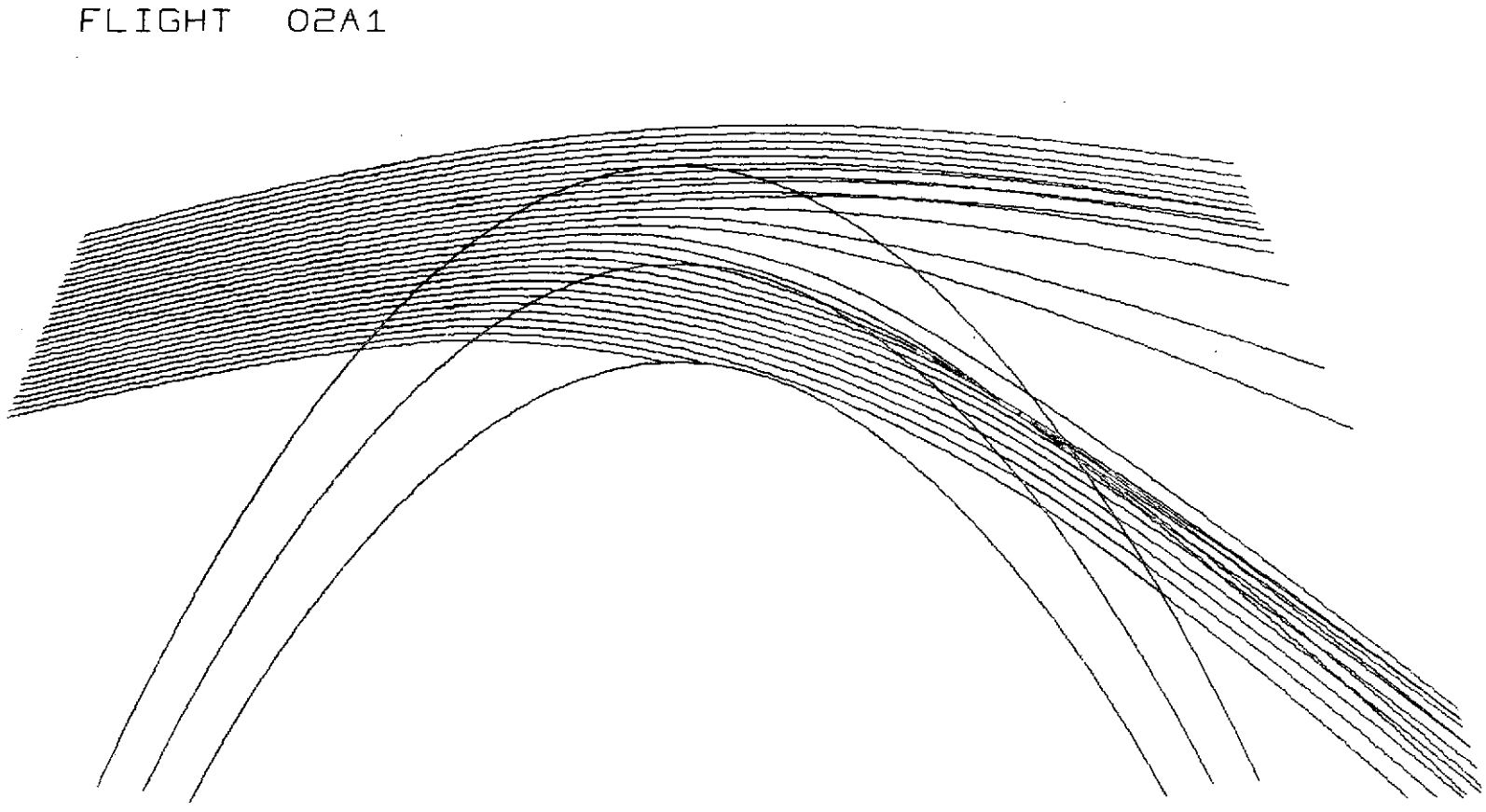

c. Profile 02A1: fading type-C

Fig. 50. CONTINUED.

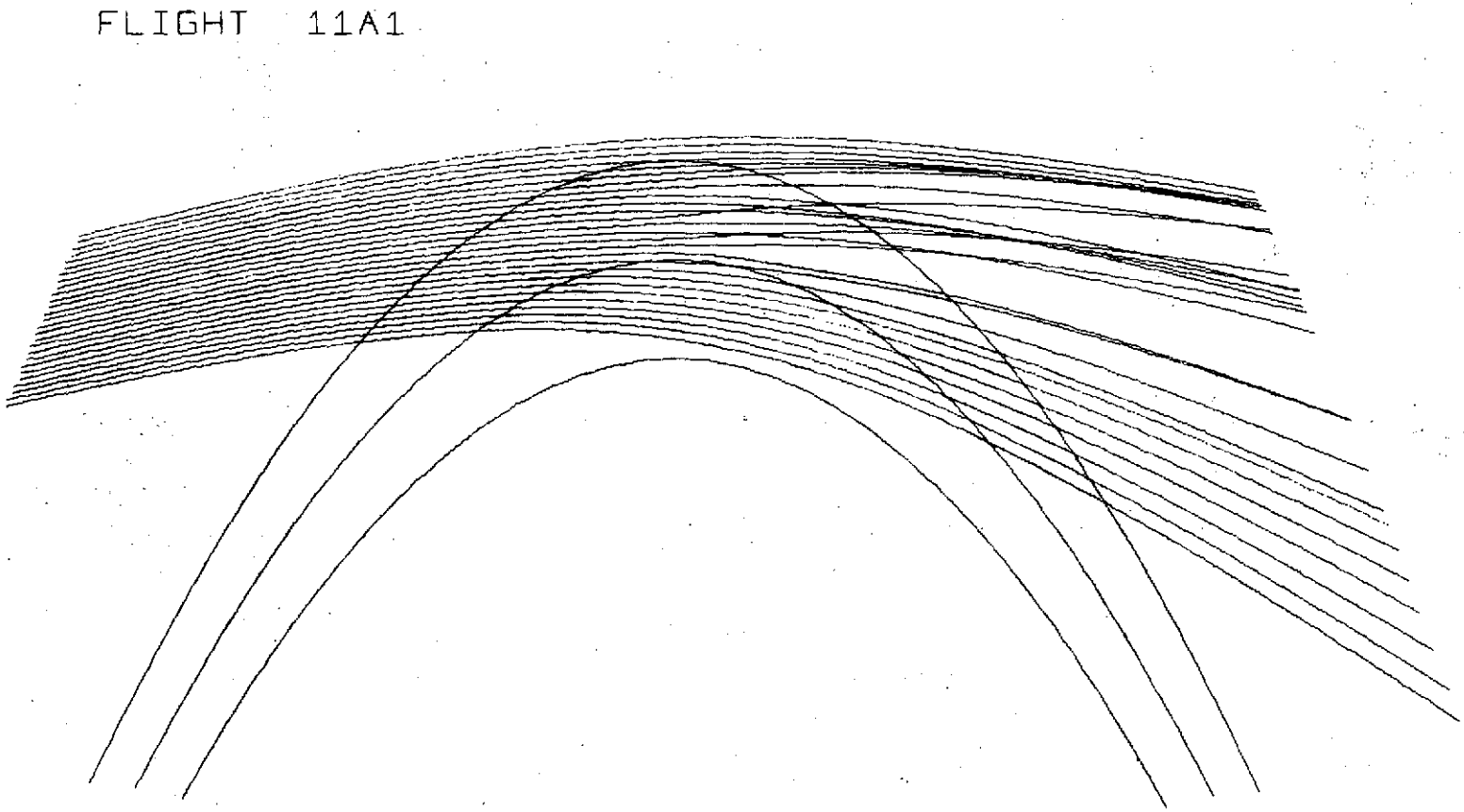

d. Profile 11A1: fading type-D

Fig. 50. CONTINUED.

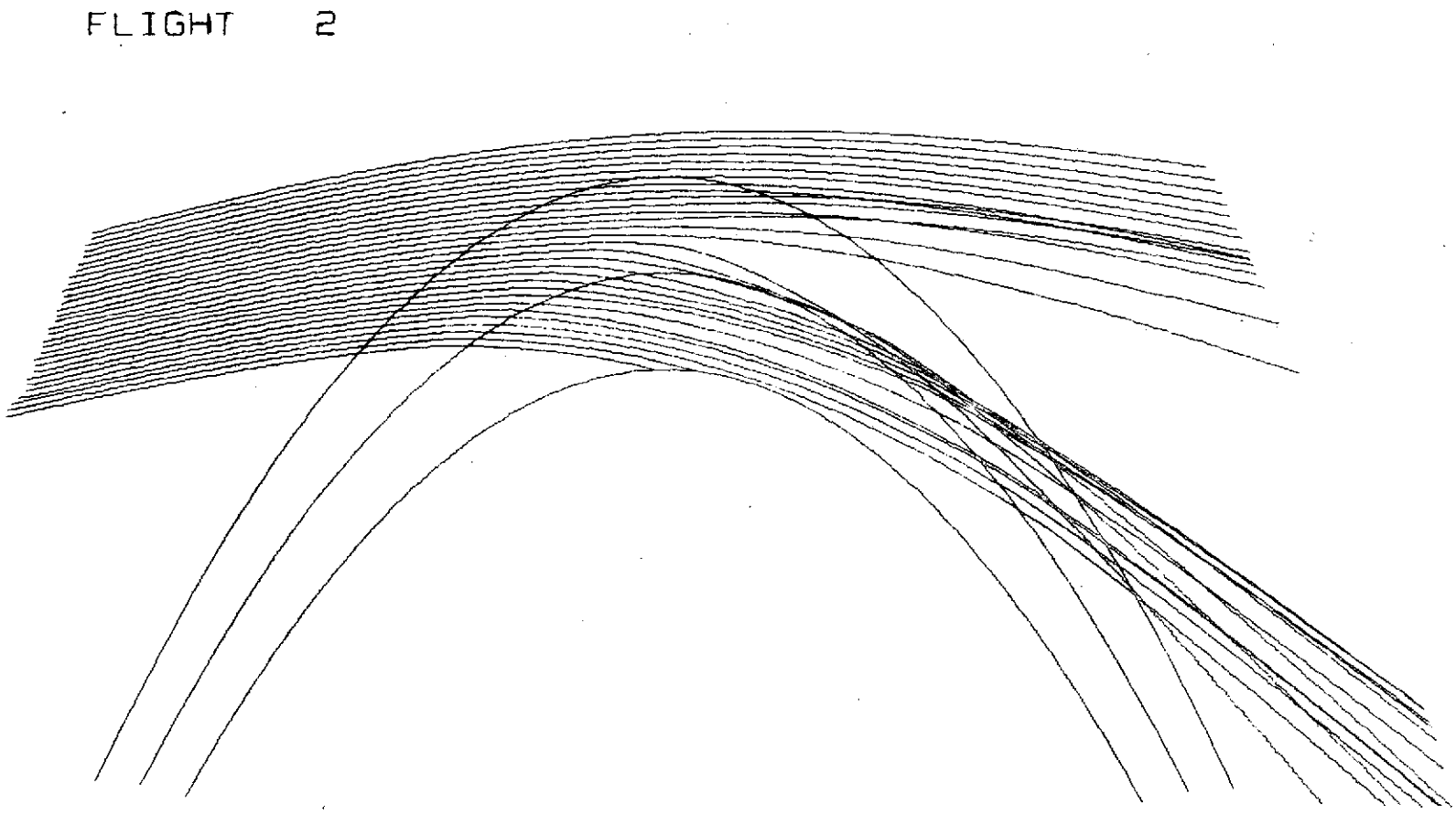

a. Flight 2

Fig. 51. COMPUTER-DRAWN RAYPATHS FOR SATELLITE-TO-SATELLITE PROPAGATION THROUGH NONSYMMETRIC LINEAR GRADIENT PROFILES. The lower 16 km of the raypaths generated by transmitting between two co-orbiting satellites through the nonsymmetric profiles of Fig. 43.

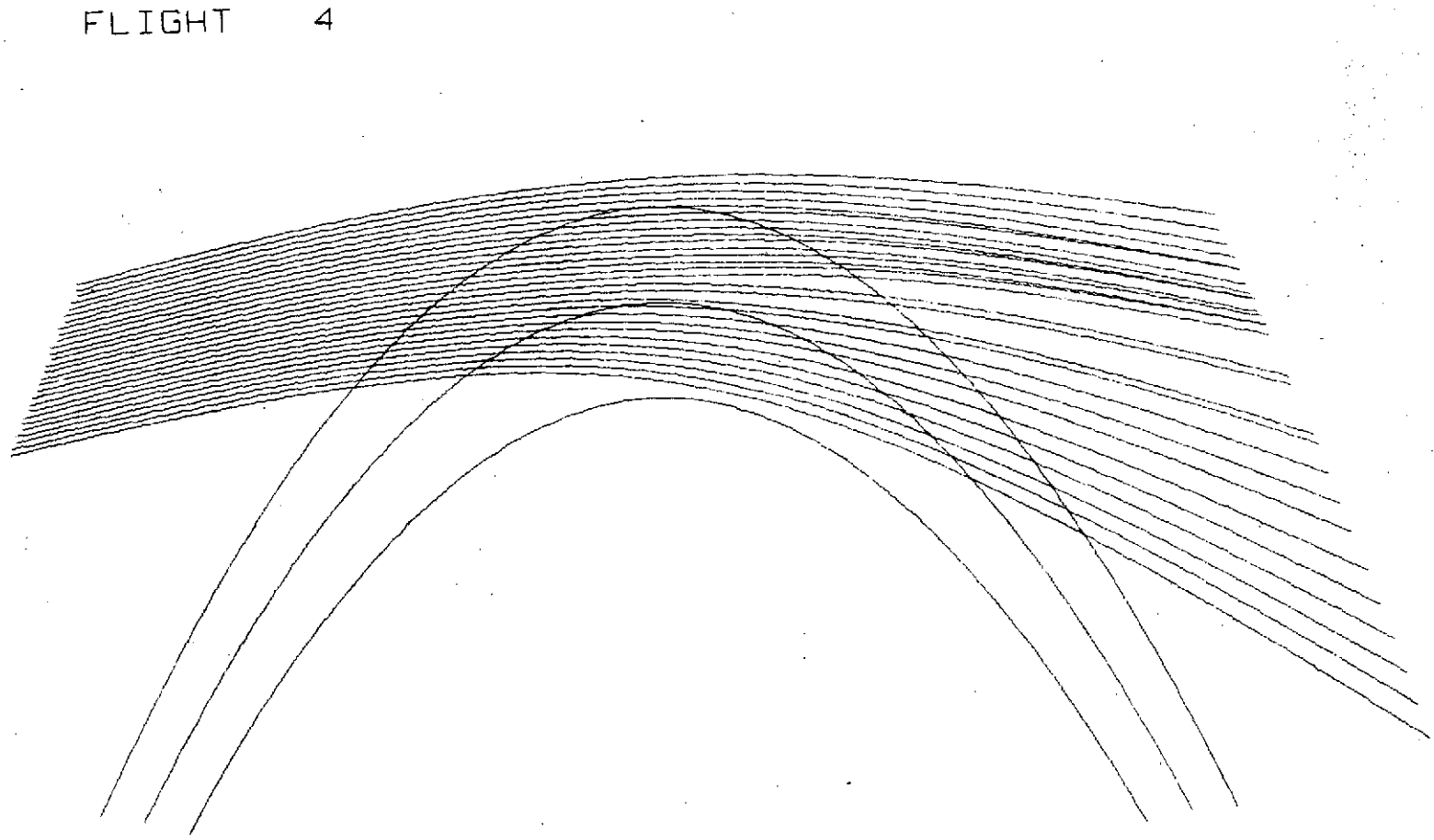

b. Flight 4

Fig. 51. CONTINUED.

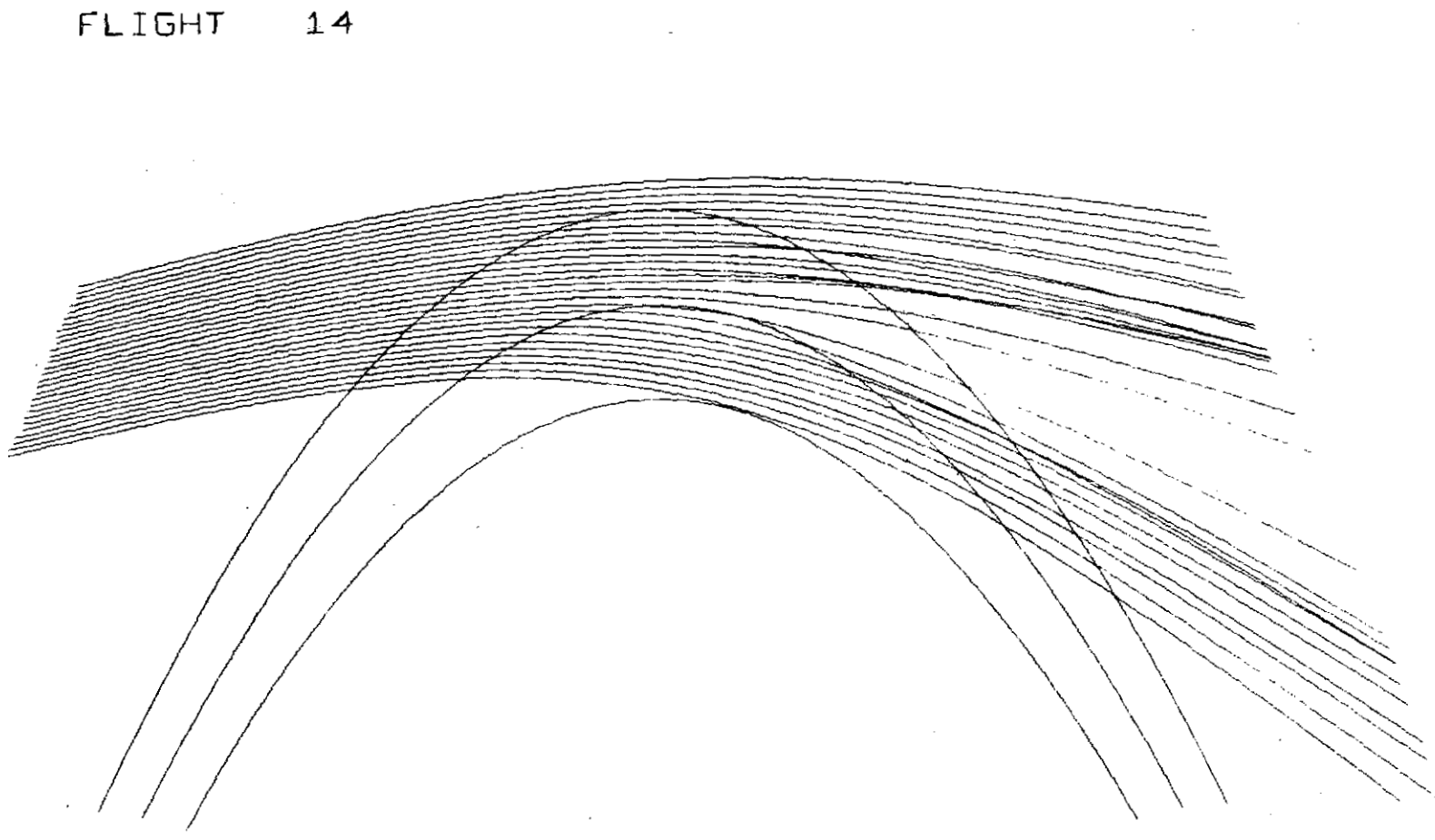

c. Flight 14

Fig. 51. CONTINUED.

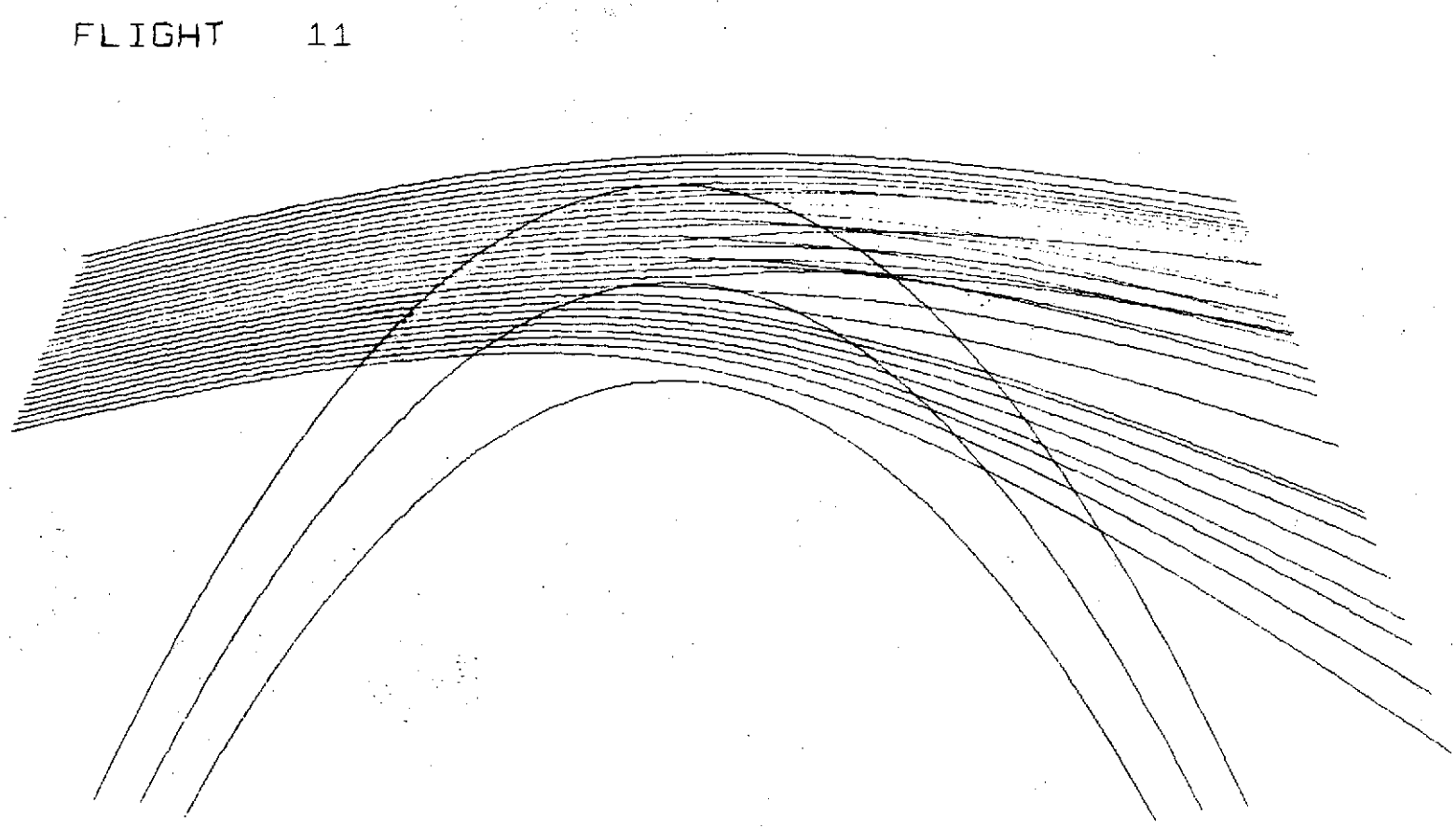

d. Flight 11

Fig. 51. CONTINUED.

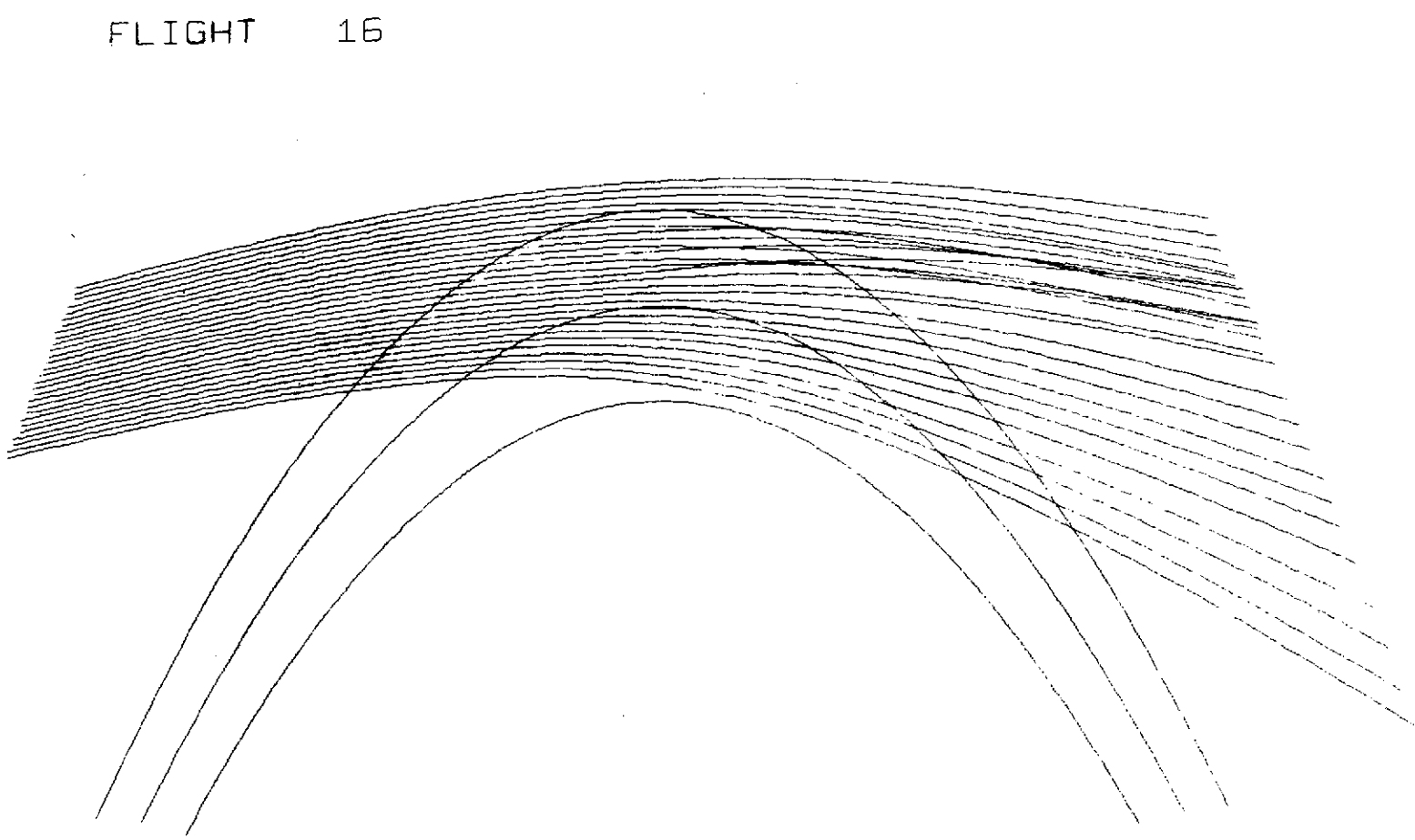

e. Flight 16

Fig. 51. CONTINUED.

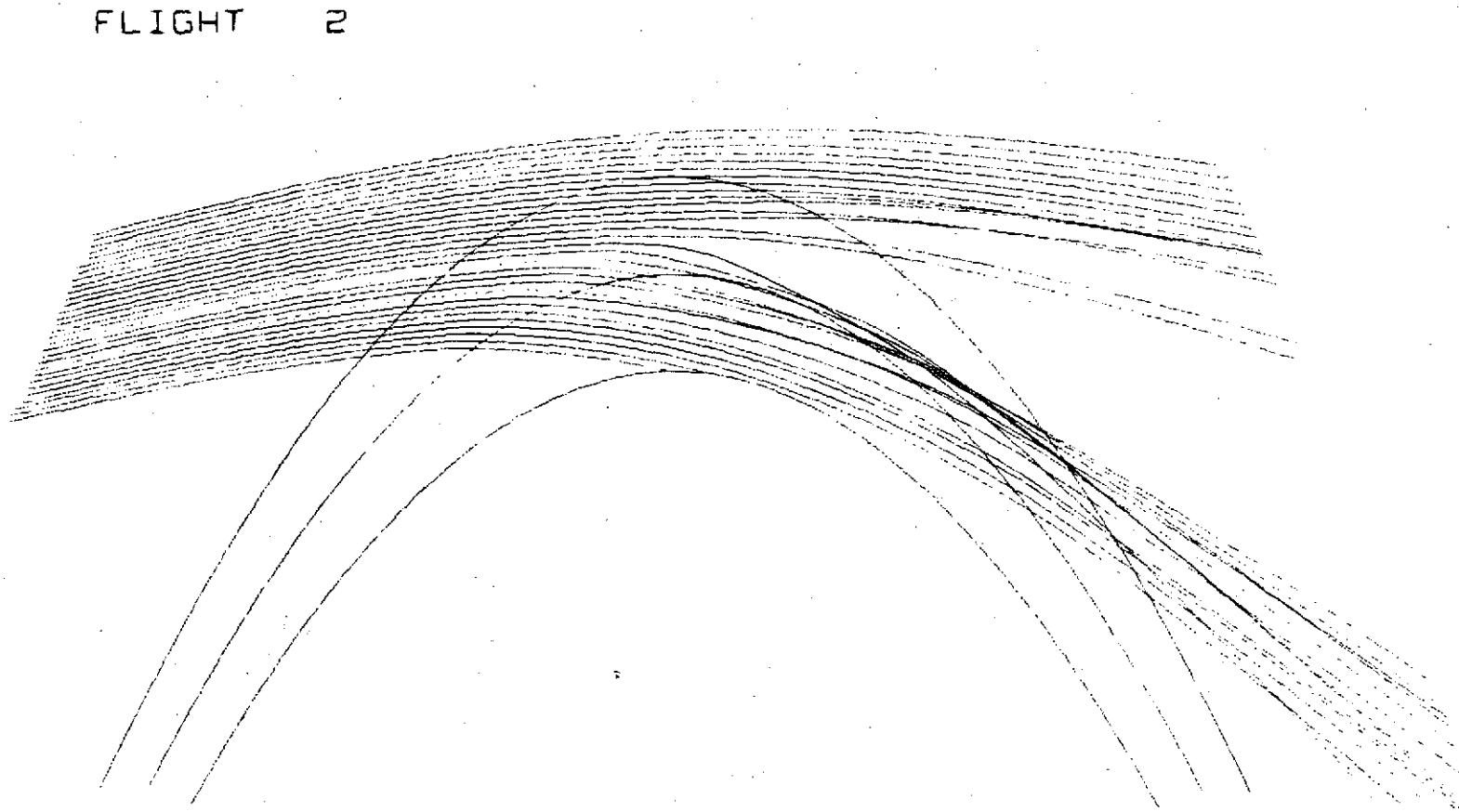

a. Flight 2

Fig. 52. COMPUTER-DRAWN RAYPATHS FOR SATELLITE-TO-SATELLITE PROPAGATION THROUGH NONSYMMETRIC STATISTICAL PROFILES. The lower 16 km of the raypaths generated by transmitting between two co-orbiting satellites through the nonsymmetric statistical profiles of Fig. 46.

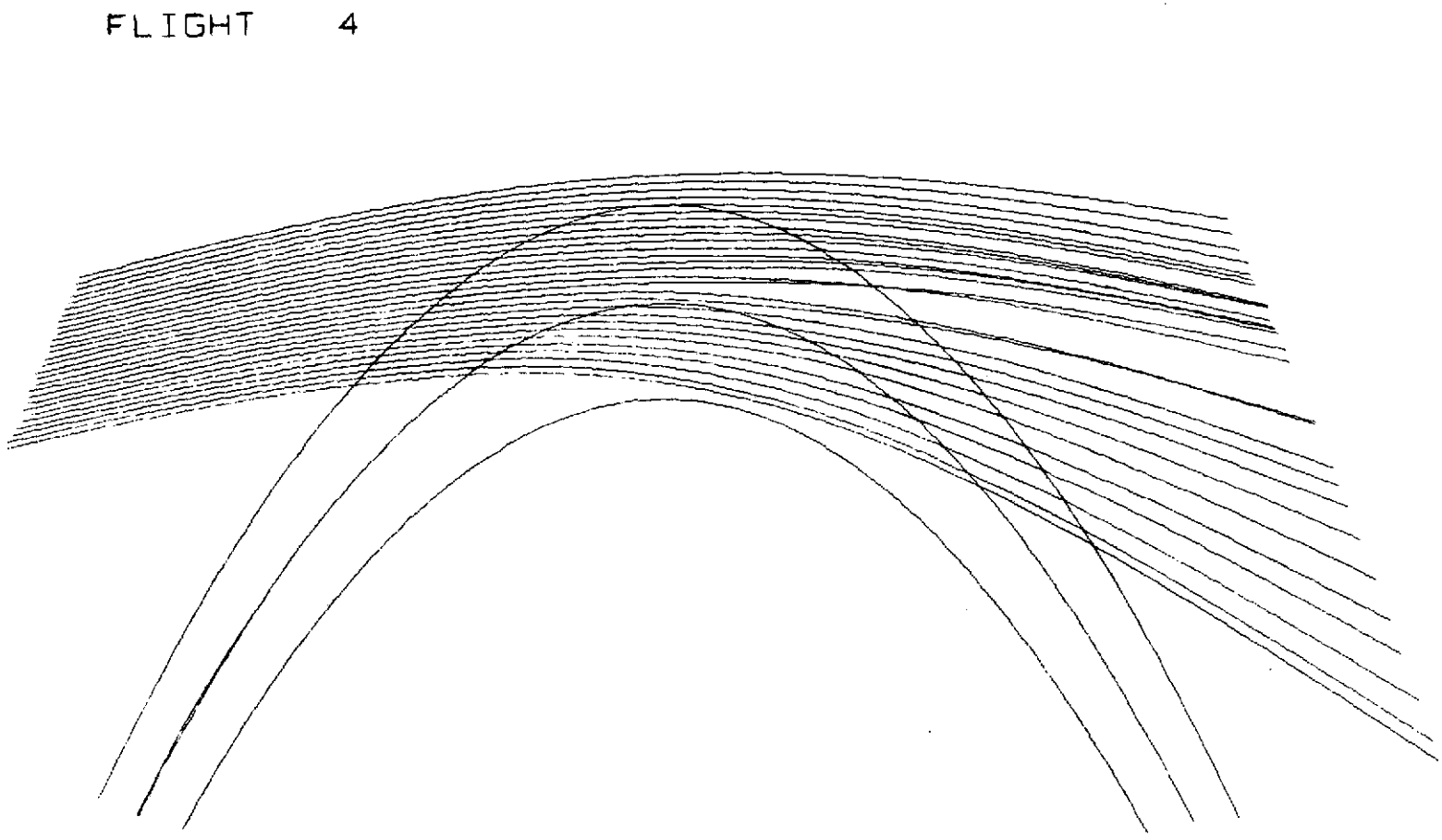

b. Flight 4

Fig. 52. CONTINUED.

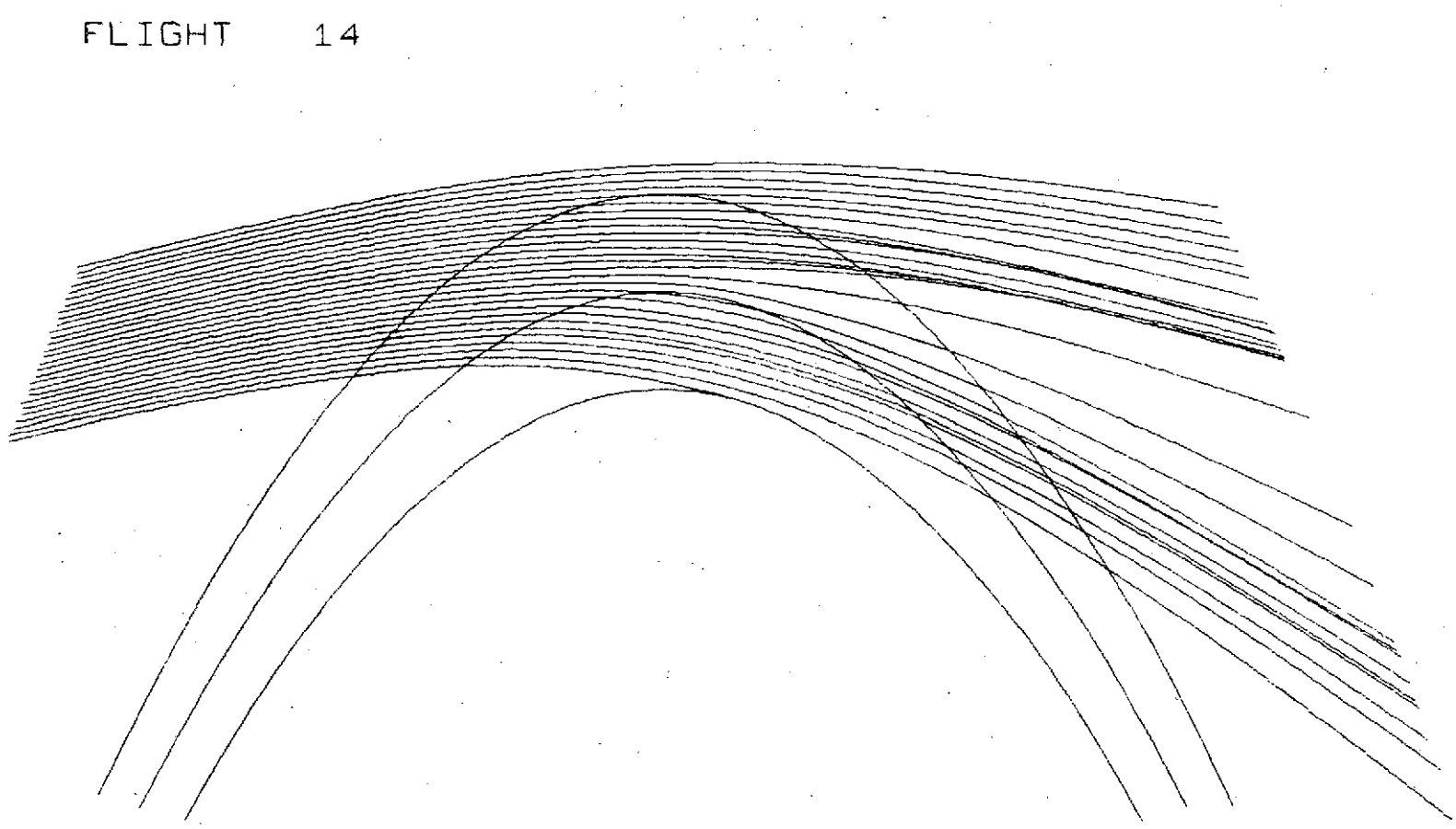

c. Flight 14

Fig. 52. CONTINUED.

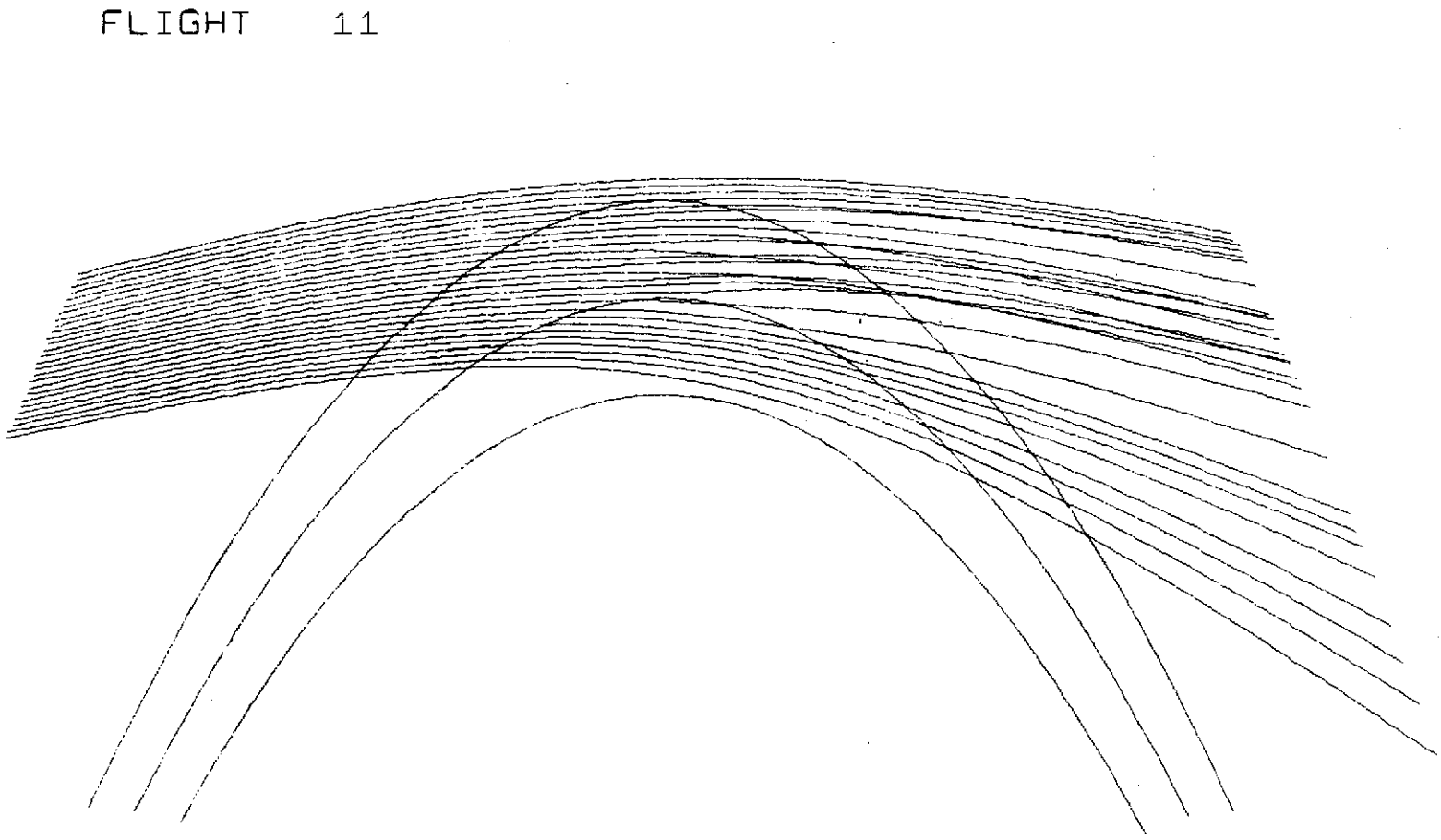

d. Flight 11

Fig. 52. CONTINUED.

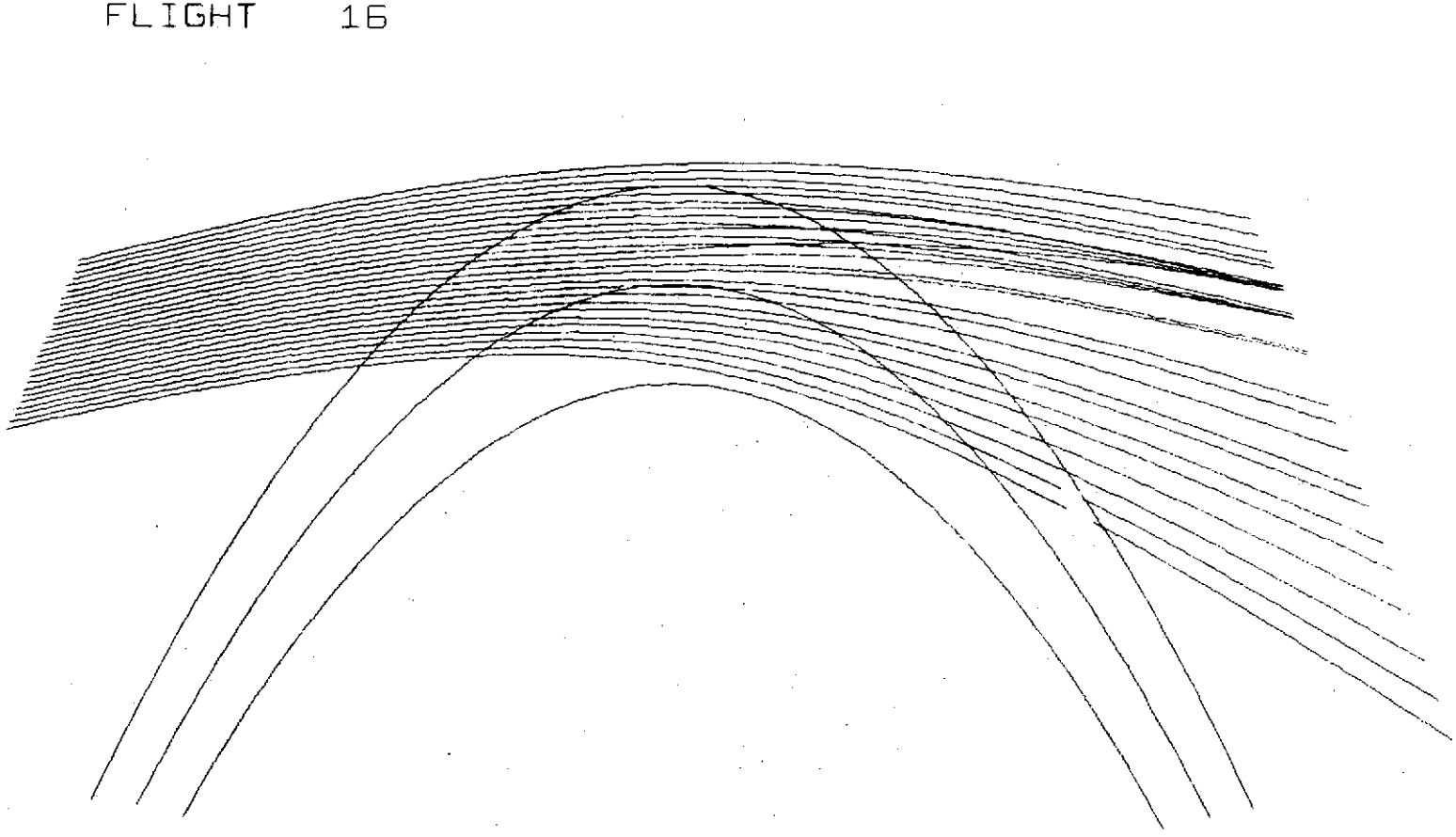

e. Flight 16

Fig. 52. CONTINUED.

Chapter VII

IMPLICATIONS OF THE HAWAII EXPERIMENT FOR AN OPERATIONAL OCCULTATION SYSTEM

"By a small sample we may judge of the whole piece."

--Miguel de Cervantes

The Hawaii microwave signal was characterized by periods of intense fading which, in an operational system, could result in loss of lock and subsequent loss of data. The Hawaii test results, however, were obtained at a relatively low altitude (3 km, as opposed to the operational closest approach altitude of 6 to 8 km) and over a tropical ocean where water-vapor content could be greater than over virtually any other terrain.

A. Water-Vapor Adjustments

To develop a more realistic picture of how an operational occultation satellite system would behave on a worldwide basis, a sample of the Hawaii test data was adjusted to simulate conditions typical of regions with lower water-vapor content than that of the Hawaii atmosphere. Although information was not available from which to state categorically that the anomalies in the measured N-profiles responsible for multipath were generated by water-vapor inhomogenities, it is certainly not unlikely. An attempt was made, therefore, to correct for the effect of water vapor by smoothing the N-profile over five vertical points (equivalent to 250 m). The smoothed profile was then subtracted from the unsmoothed profile, and the resulting high-frequency residual was assumed to be caused by water-vapor inhomogeneities. Of course, water vapor also contributes a low-frequency component to the N-profile but, for this study, only relative values were important.

To simulate different water-vapor conditions, the high-frequency residual was multiplied by a factor and then added to the smoothed profile. This factor was determined by assuming that the Hawaii data represented a typically "wet" atmosphere and then by taking the ratio of the water vapor on a typically "dry" day and a "normal" day to that on a "wet" day. The values for "wet," "dry," and "normal" water-vapor concentrations were obtained from the standard curves shown in Fig. 53.

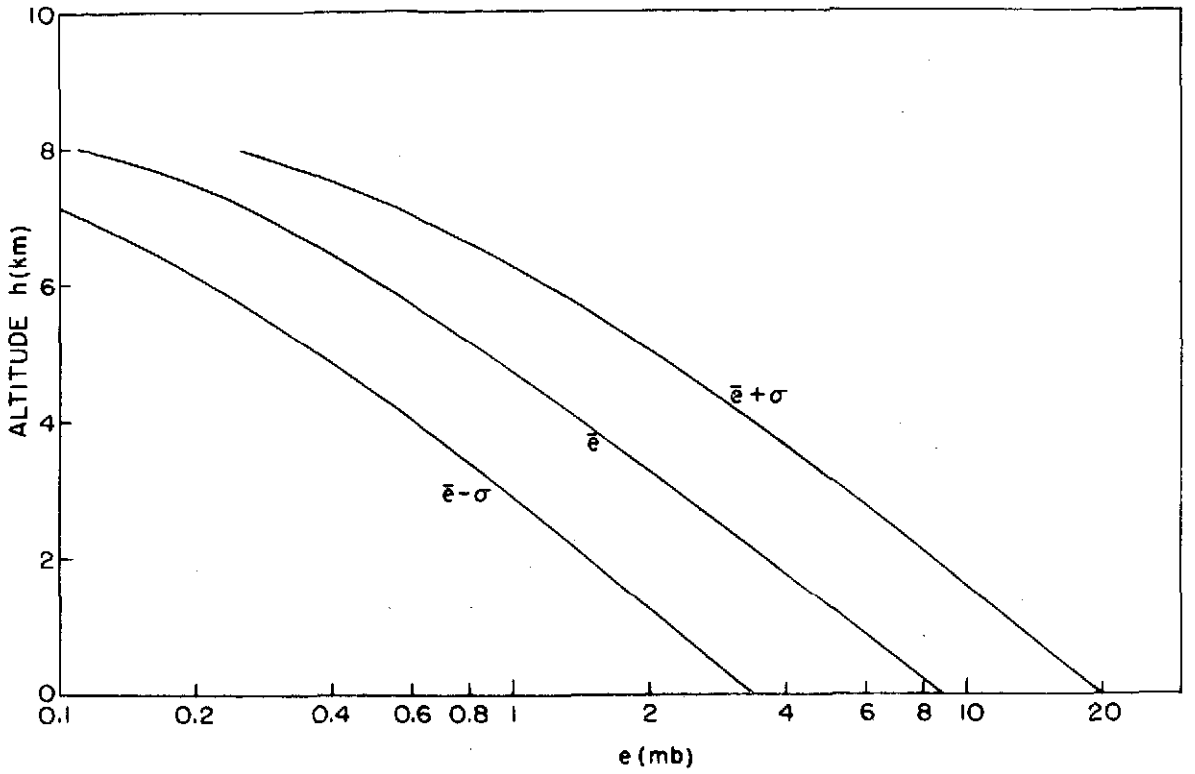

Fig. 53. STANDARD WATER-VAPOR PROFILES. The two curves on the left are the same as those in Fig. 10.

Note that the "dry" and "normal" curves correspond to the profiles in Fig. 10 and were derived from the same source. It should be noted also that the curves were derived from data applicable only to the middle-latitudes [10], where water-vapor concentrations are generally lower than over tropical seas, so the assumption that the Hawaii data represents conditions for a typical "wet" day is probably conservative.

The data sets chosen for adjustment were the same as those used in raytracing satellite-to-satellite in a symmetric mode (see Chapter VI). The four data sets (one for each fading type) were adjusted as described above and used for raytracing in the satellite-to-satellite symmetric mode. A brief examination of the results (Figs. 54 and 55) and those for the original data (Fig. 50) indicates that, as the high-frequency component of the N-profile is decreased, the incidence of multipath is slightly reduced. Figure 56 presents the smoothed and unsmoothed profiles for the type-D example which is the "noisiest" of the four.

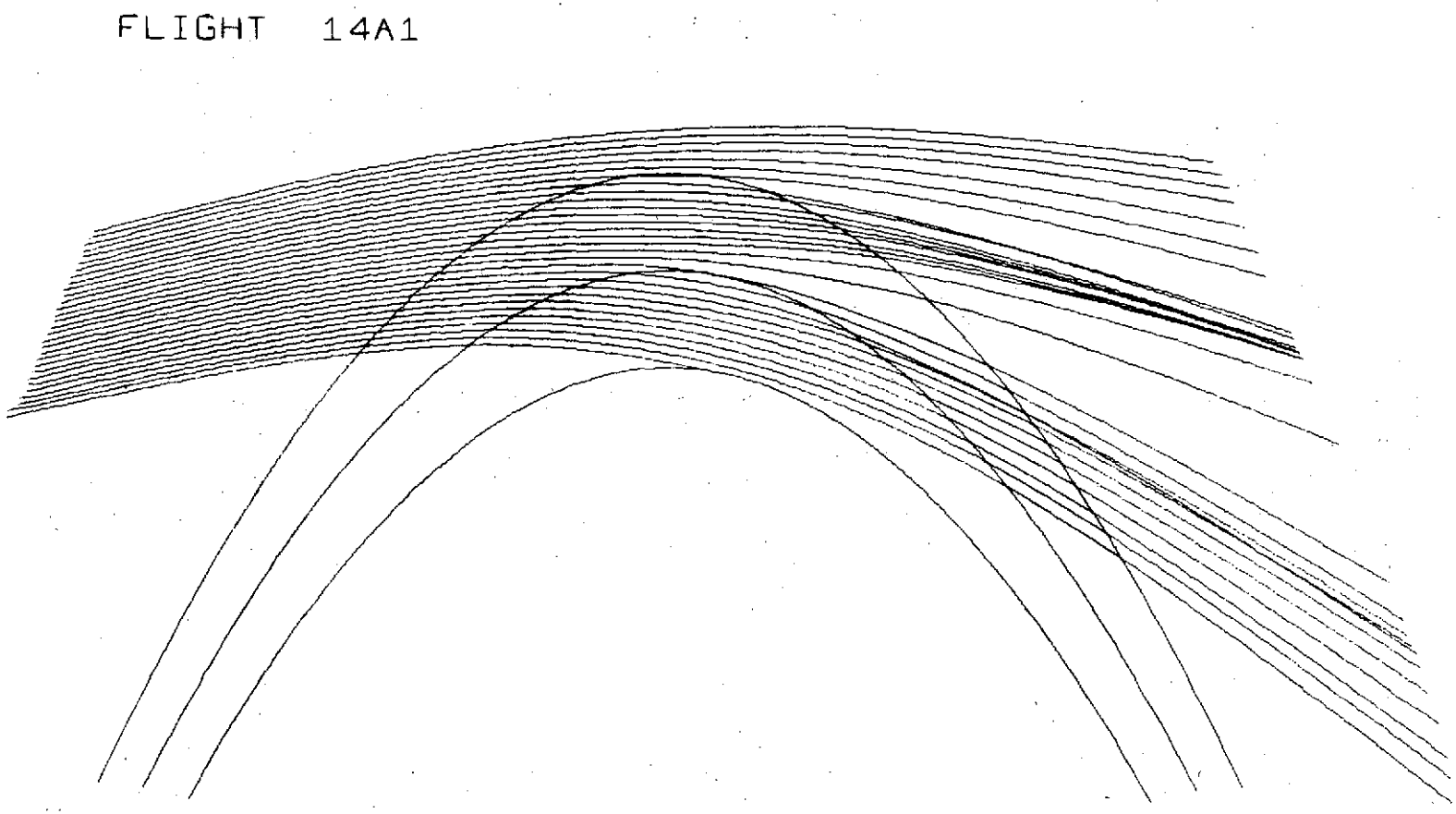

a. Profile 14A1

Fig. 54. COMPUTER-DRAWN RAYPATHS FOR SATELLITE-TO-SATELLITE PROPAGATION THROUGH SPHERICALLY SYMMETRIC ADJUSTED HAWAII PROFILES. Lower 16 km of the raypaths generated by transmitting between two co-orbiting satellites through symmetric N-profiles that have been adjusted to simulate the water-vapor conditions for a "normal" day.

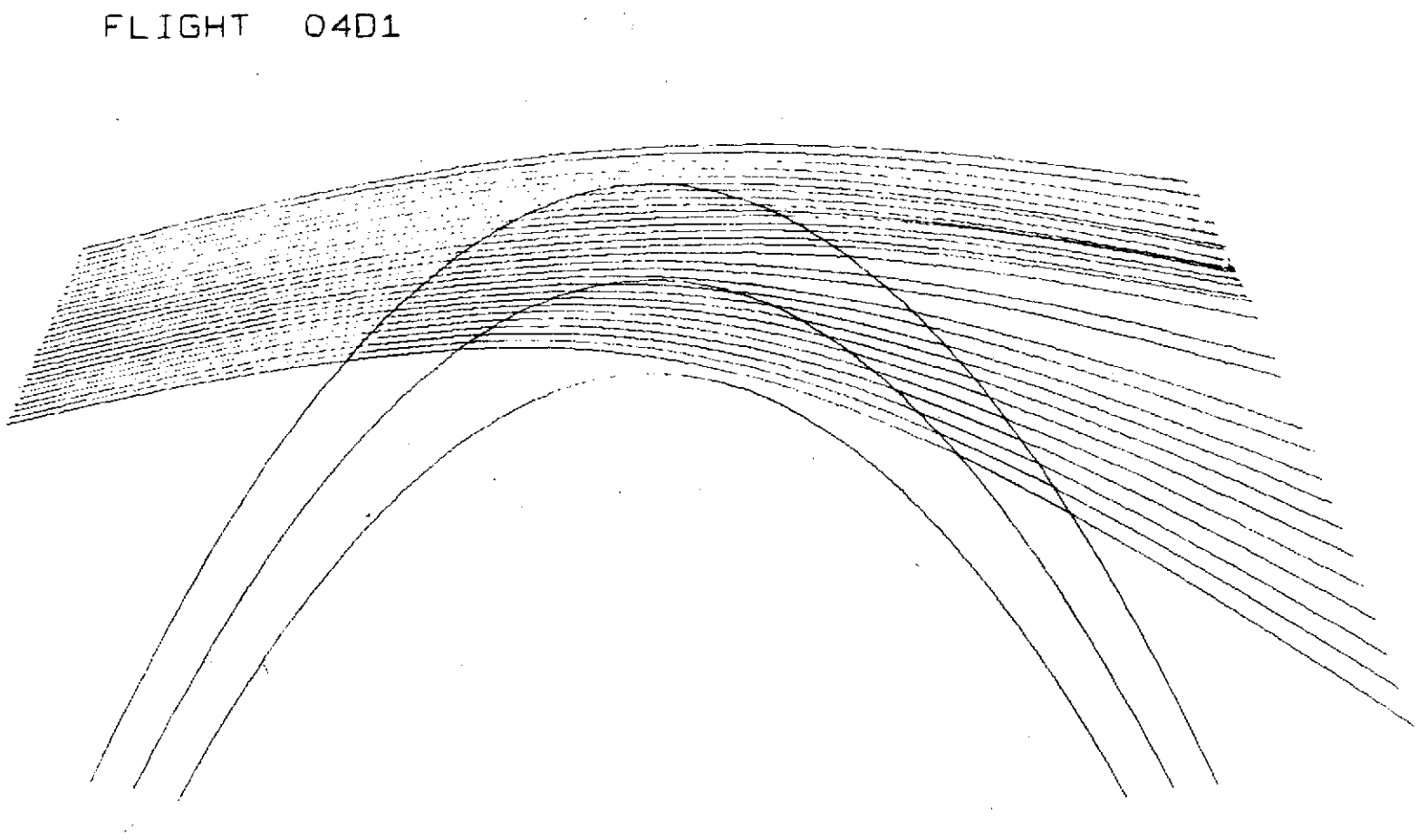

b. Profile 04D1

Fig. 54. CONTINUED.

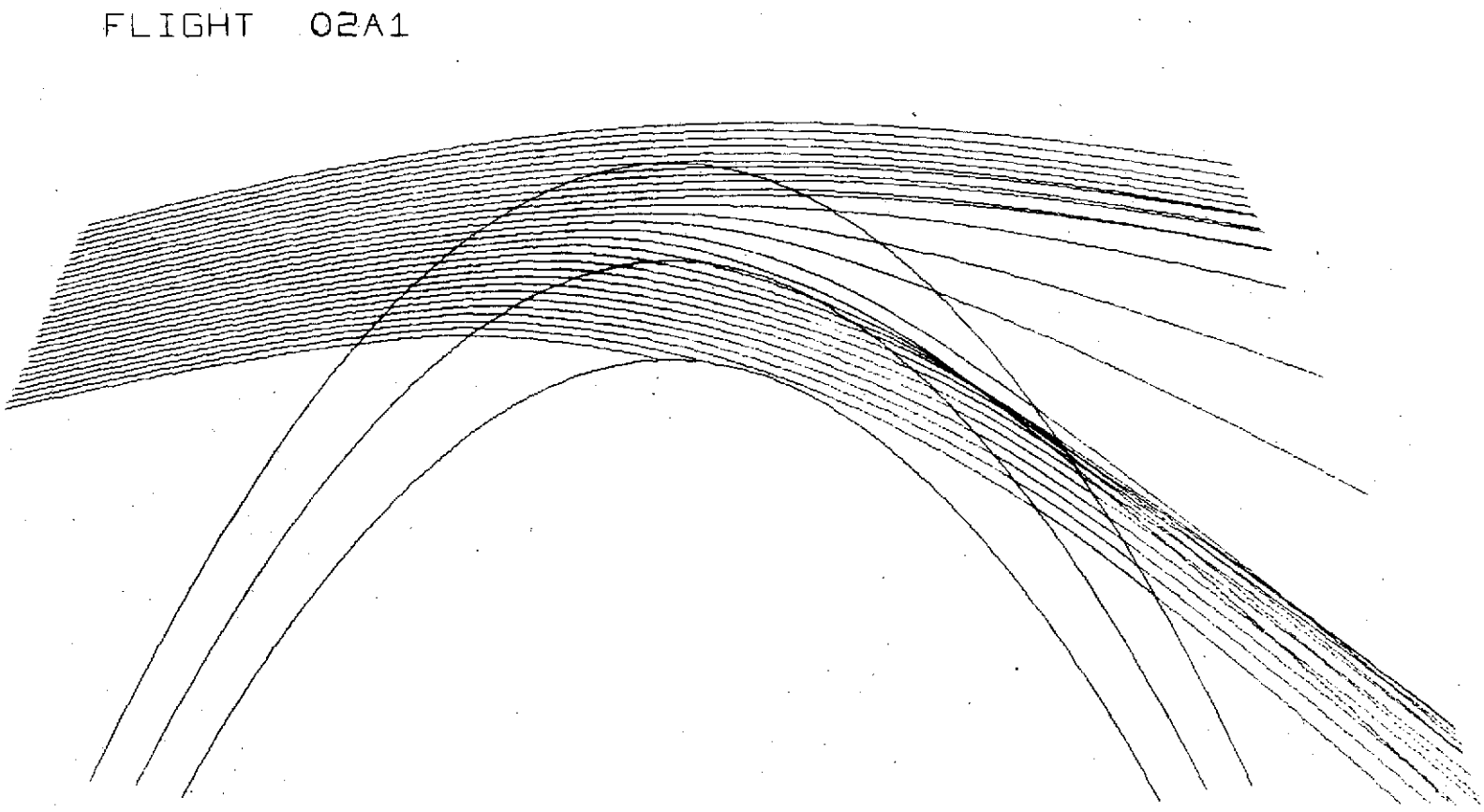

c. Profile 02A1

Fig. 54. CONTINUED.

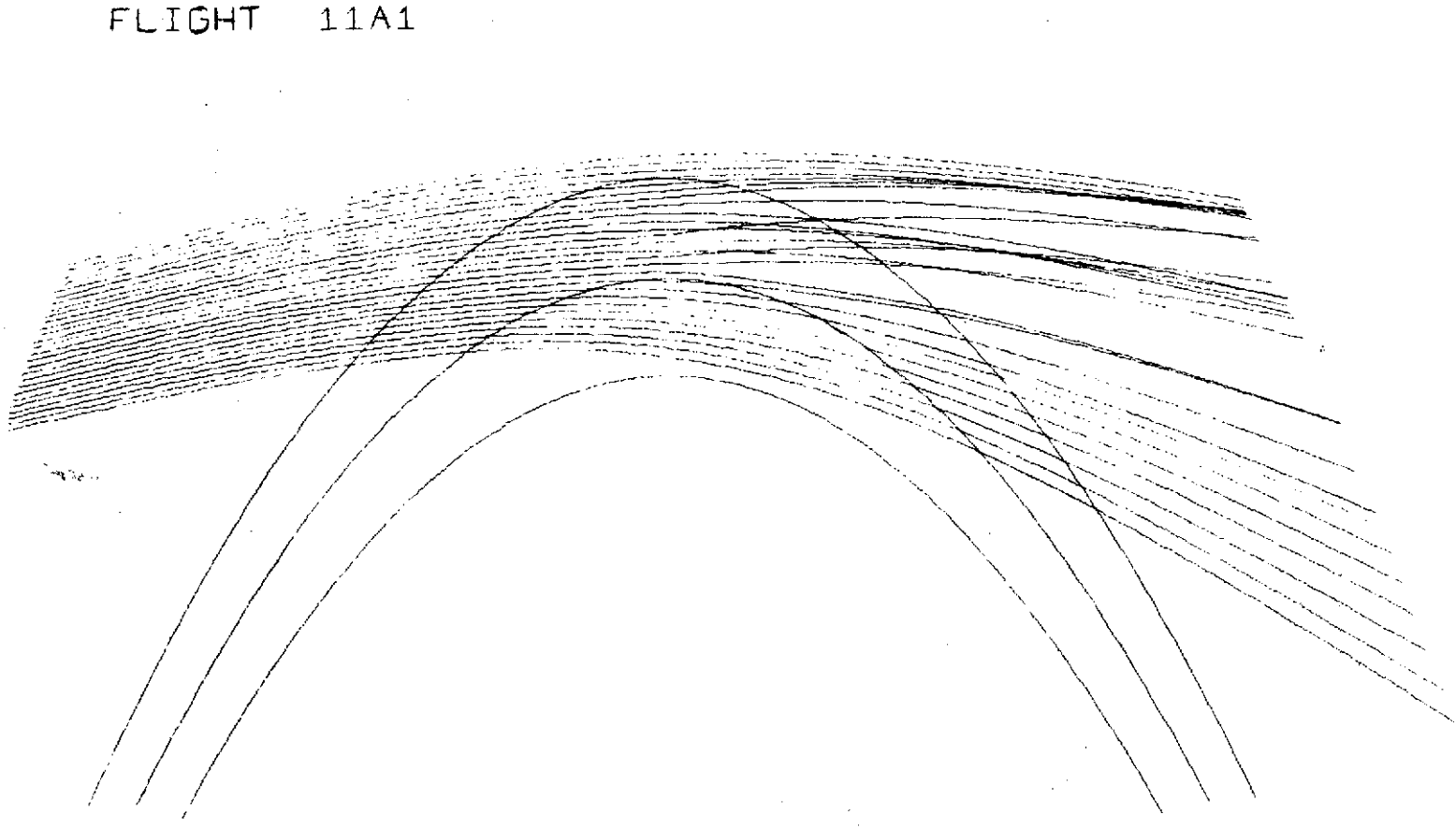

d. Profile 11A1

Fig. 54. CONTINUED.

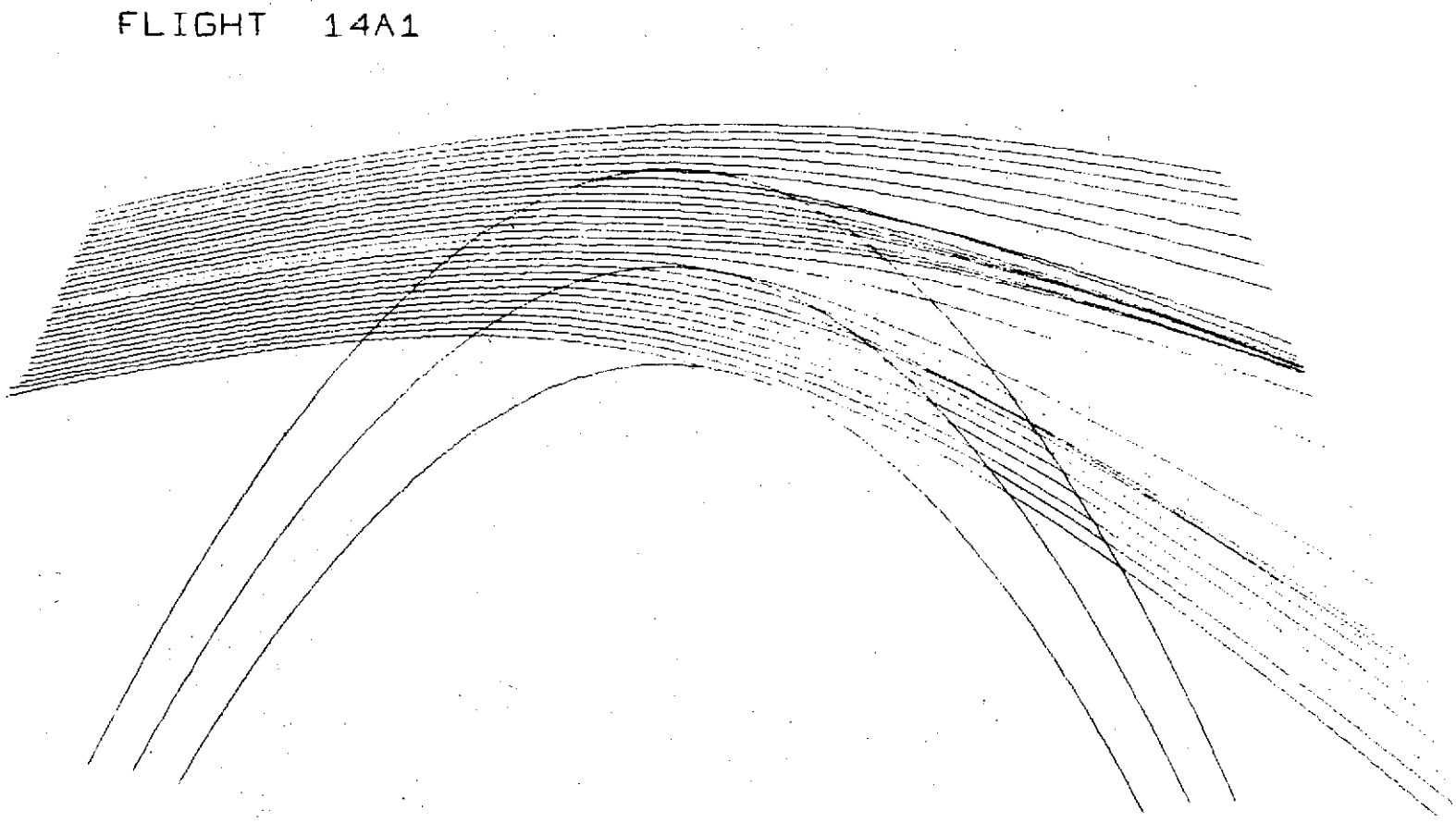

a. Profile 14A1

Fig. 55. COMPUTER-DRAWN RAYPATHS FOR SATELLITE-TO-SATELLITE PROPAGATION THROUGH SPHERICALLY SYMMETRIC ADJUSTED HAWAII PROFILES. Lower 16 km of the raypaths generated by transmitting between two co-orbiting satellites through symmetric N-profiles that have been adjusted to simulate the water-vapor conditions for a "dry" day.

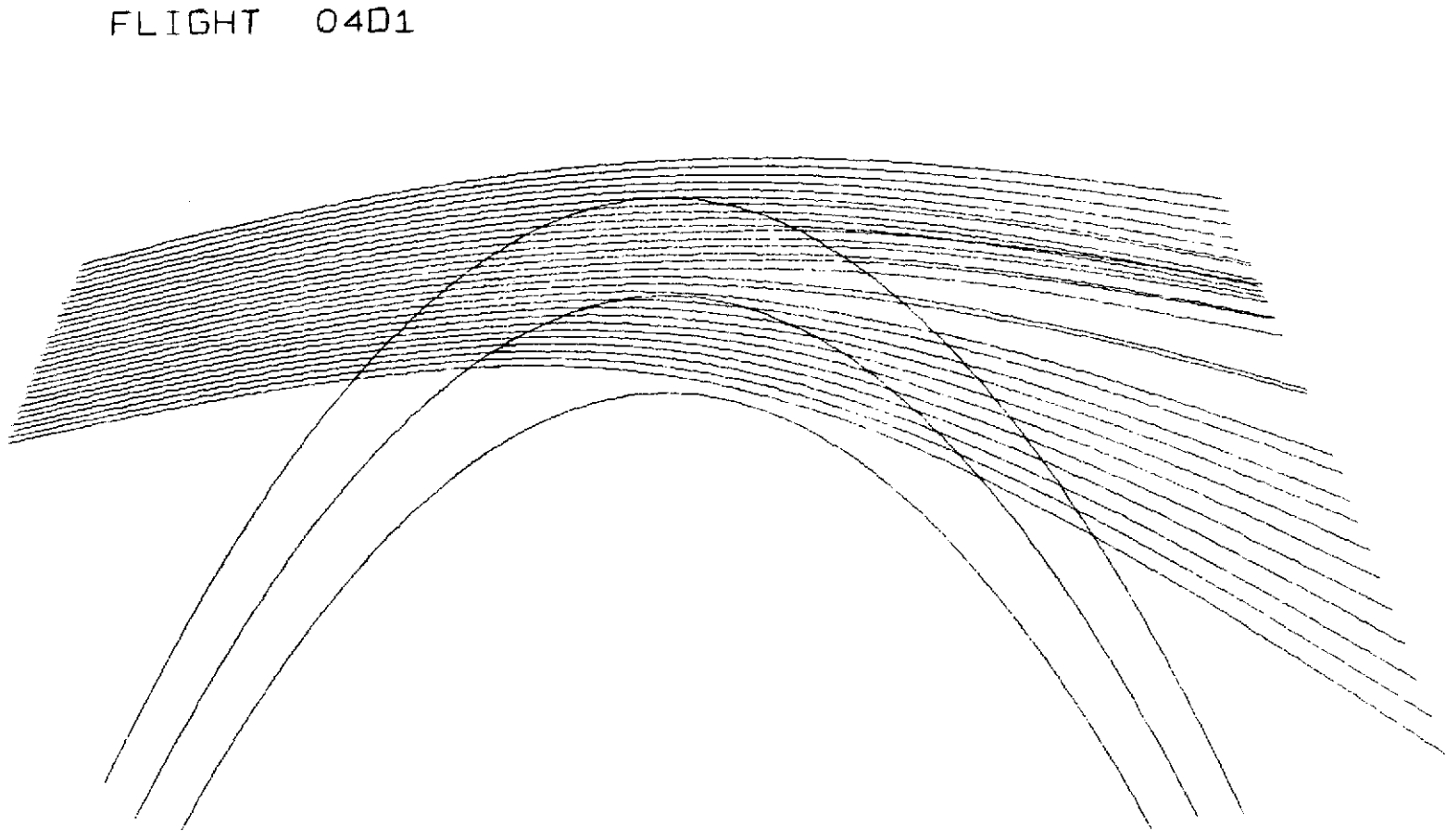

b. Profile 04D1

Fig. 55. CONTINUED.

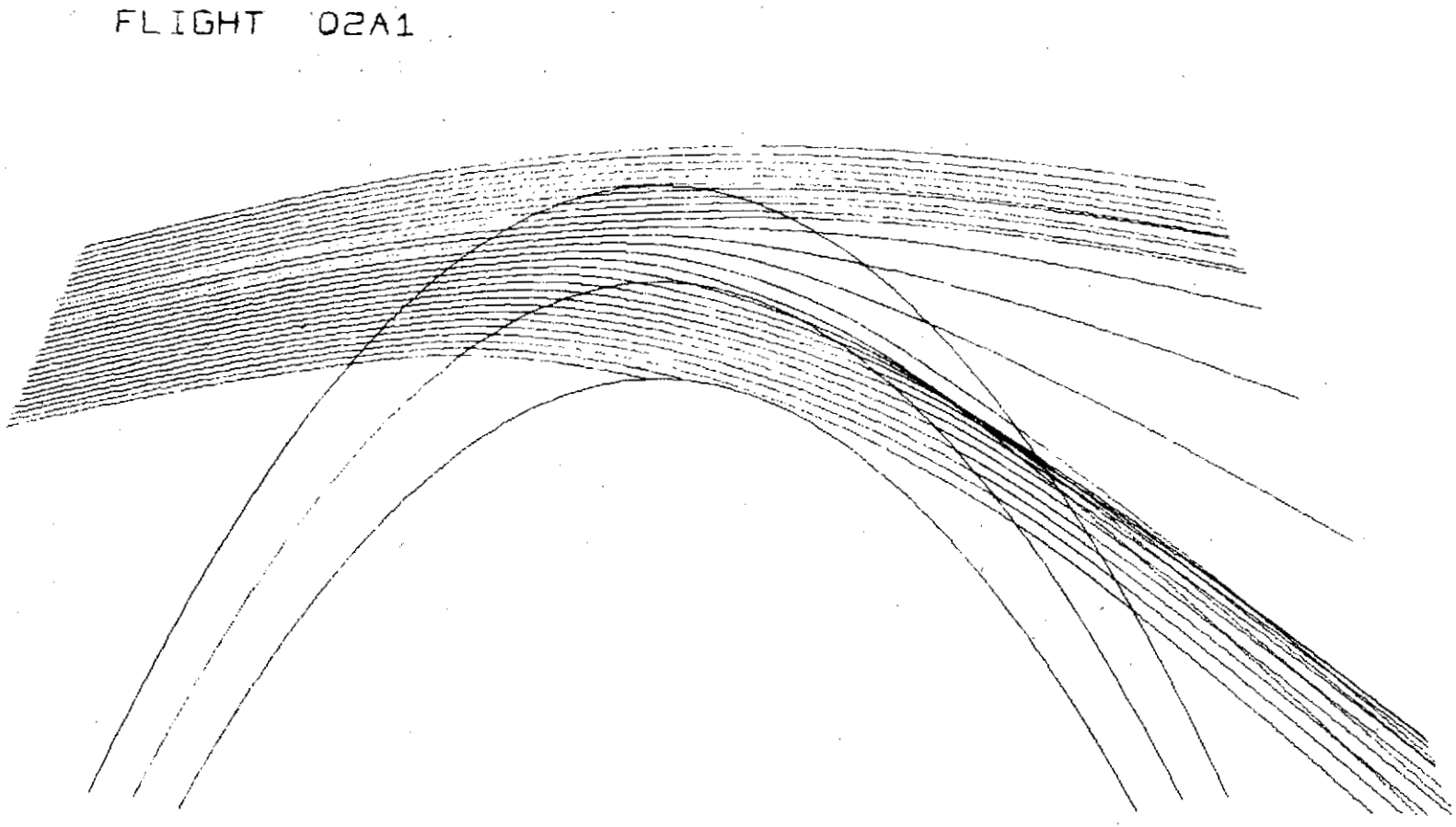

c. Profile 02A1

Fig. 55. CONTINUED.

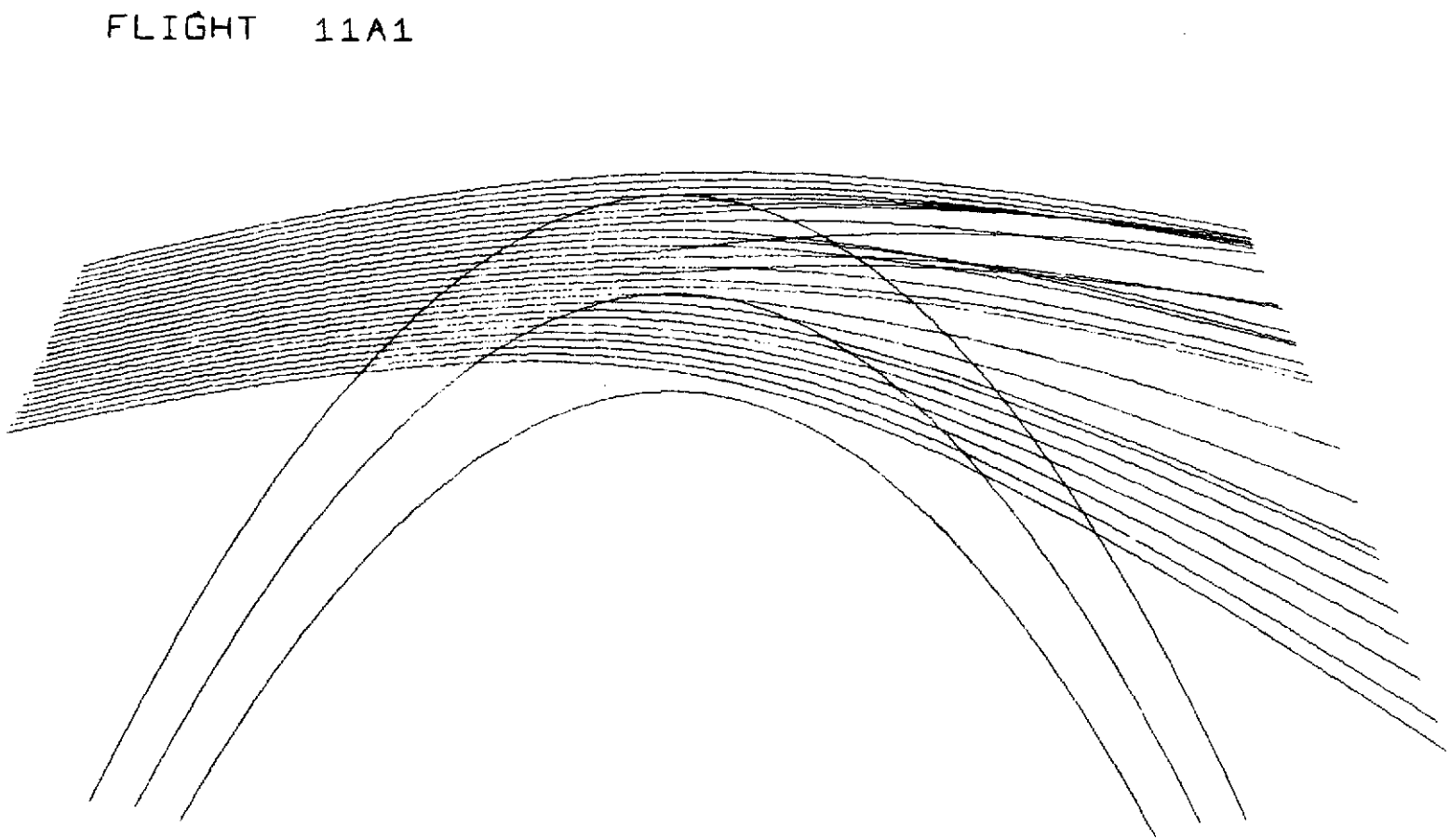

d. Profile 11A1

Fig. 55. CONTINUED.

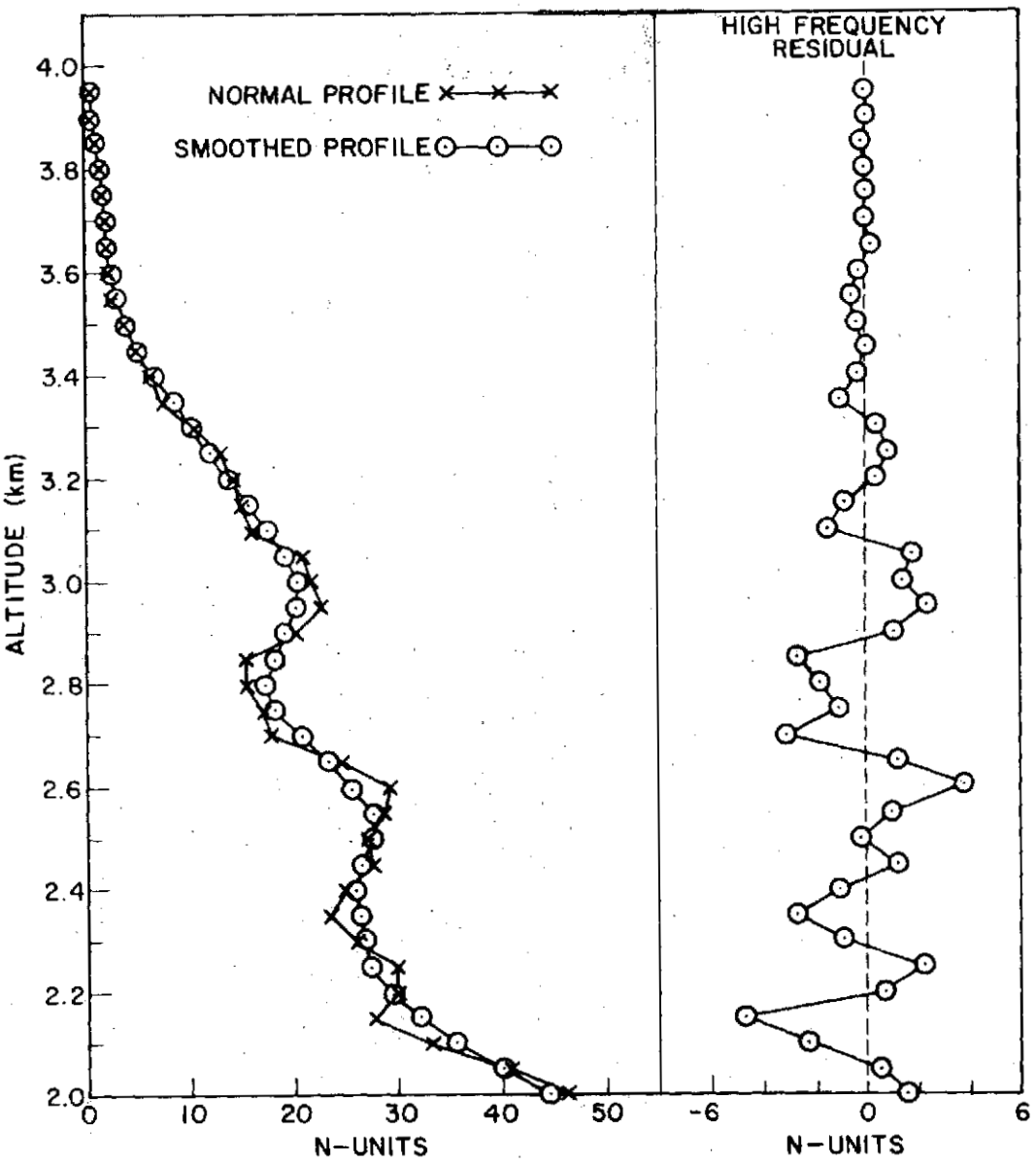

Fig. 56. SMOOTHED (5-point) AND NORMAL N-PROFILE 11A1.

There is reason to be concerned with whether this smoothing process actually eliminates the effect of water-vapor inhomogeneities in the N-profile. Too much smoothing could remove just those effects that should be revealed by adjusting the data; too little smoothing could result in unduly pessimistic results. To assess the efficacy of this process, the smoothed N-profile of Fig. 56 was "inverted" by assuming a dry-atmosphere and a standard-atmosphere pressure curve, resulting in a temperature profile that would generate the smoothed refractivity profile if water-vapor content were zero.

Figure 57 is the temperature profile corresponding to the smoothed curve in Fig. 56. It is clear that this equivalent temperature profile is not realistic and that a five-point smoothing, although obviously removing most of the effects of water-vapor inhomogeneity, does not remove them all. The results of this analysis, therefore, are rather conservative. If the curve were smoothed over a greater range so as to remove more of the water-vapor contribution, the multipath incidence would decrease further.

This point becomes significant when the next logical step is taken and the behavior of the system at 3 km is compared to that at 7 km. By following the "wet" curve in Fig. 53 from the 3 km to the 7 km level and

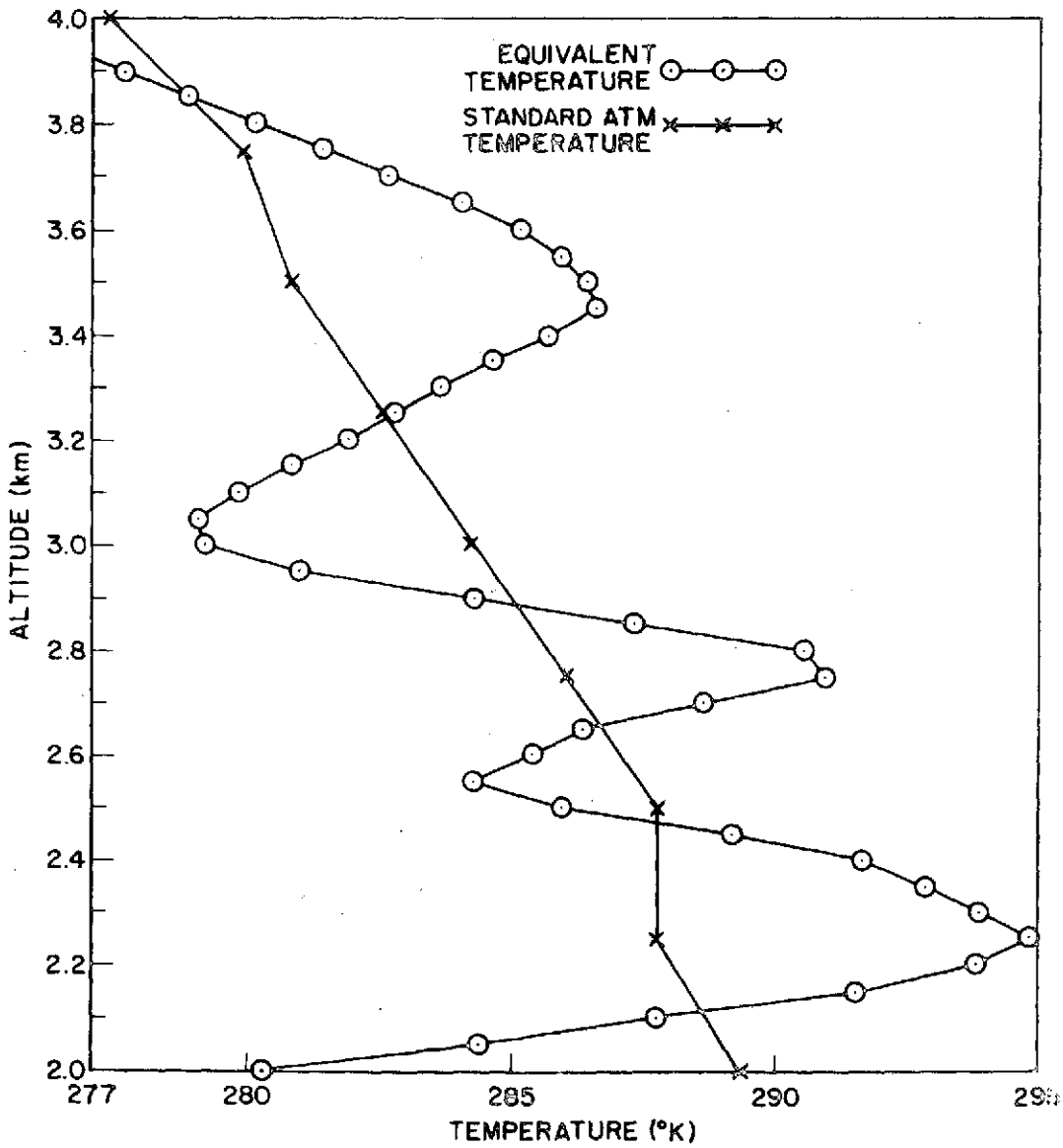

Fig. 57. EQUIVALENT TEMPERATURE PROFILE FOR SMOOTHED (5-point) N-PROFILE 11A1.

by taking the ratio of water-vapor concentration at 7 km to that at 3 km, the N-profile data can be adjusted, as described above, to simulate the water-vapor concentration at the higher altitude.

When raytracing satellite-to-satellite through this simulated high-altitude profile, the incidence of multipath is greatly reduced; in fact, in all four of the profiles tested, only eight satellite separations with multipath were recorded, as opposed to 60 multipath recordings when the profiles were run at the lower altitude without adjustment for water-vapor content. These high-level multipaths are caused by the unrealistic temperature profile in Fig. 57, which resulted from the insufficient five-point smoothing of the N-profiles. It appears, therefore, that the results of the Hawaii experiment produced a somewhat pessimistic picture of probable system performance.

It should be noted that there is a possibility that a system operating at the higher closest approach altitude (6 to 8 km, as described in Chapter III) might be affected by signals being deflected upward from a Hawaii-like atmosphere at a lower level (the antenna beamwidth will be such that the lower levels and the surface of the Earth will be illuminated). When the results of raytracing through the Hawaii profiles are examined, however, it can be seen that no signal is deflected to the extent that it would be detected by a receiver placed at the operational satellite separation (assuming that the greatest separation is 7888.0 km, as described in Chapter III). Although the possibility of interference from a low-level multipath does exist, none of the simulations indicates that the probability is significant that this situation will occur frequently or pose any real problems for the operational system. Should a low-level multipath occasionally interfere with system operation, the raytracing results indicate that the amplitude of the unwanted signal would be significantly less than that of the "direct," or desired signal and, therefore, would have little or no effect on system performance.

B. Other High-Altitude Effects

There are other reasons to believe that the results of the Hawaii experiment give a somewhat conservative picture of the performance to be expected from an operational satellite system. First, multipath

in the satellite-to-satellite mode will not necessarily have the same effect on the system (long and frequent deep fades) as it had in the station-to-station mode. Figure 58 plots the excess path length (phase defect) as a function of satellite separation; in other words, it plots the phase defect that would be measured by a receiving satellite located a given geometric distance from the transmitting satellite.

Once again, as in the station-to-station mode, phase defect is a function of endpoints rather than raypath. Phase defects of two signals received at the same satellite position due to multipath are likely to match to within 20 or 30 cm. Because satellite phase-path results are required only to approximately 50 cm, two such signals will be indistinguishable from one another (they are the same within the accuracy required by the experiment, as described in Chapter II).

If two or three of these signals are received at the daughter satellite, the deep fading associated with the station-to-station mode might occur also in the satellite-to-satellite mode. Inspection of the satellite-to-satellite results reveals, however, that 5, 7, or more signals appearing at the receiver is not uncommon; in fact, this situation exists in 49 percent of the resulting multipath configurations. Under this condition, the signals add as random phasors and, rather than resulting in deep fades, the power received is increased by several decibels. Because the phase defects are within a few tens of centimeters of each other, regardless of which signal is locked, the desired information is obtained. This multisignal multipath, in which more than three signals with comparable power appear at the receiver, is extremely rare in the station-to-station mode.

Second, there is a time factor that must be taken into account. The Hawaii receiver and transmitter were, of course, stationary. They sat still while the weather blew gently past them. The duration of a deep fade in the Hawaii data was typically much less than 30 sec, and the maximum wind velocity was on the order of 50 km/hr. If fading is ascribed to inhomogeneities traveling into the raypath with the wind, an estimate of the duration of a deep fade in the satellite-to-satellite configuration can be made. The satellites, in effect, move past the weather with a velocity on the order of 25×10^3 km/hr; therefore, the ratio of "velocities" between the station-to-station and satellite-to-satellite modes is roughly 0.002.

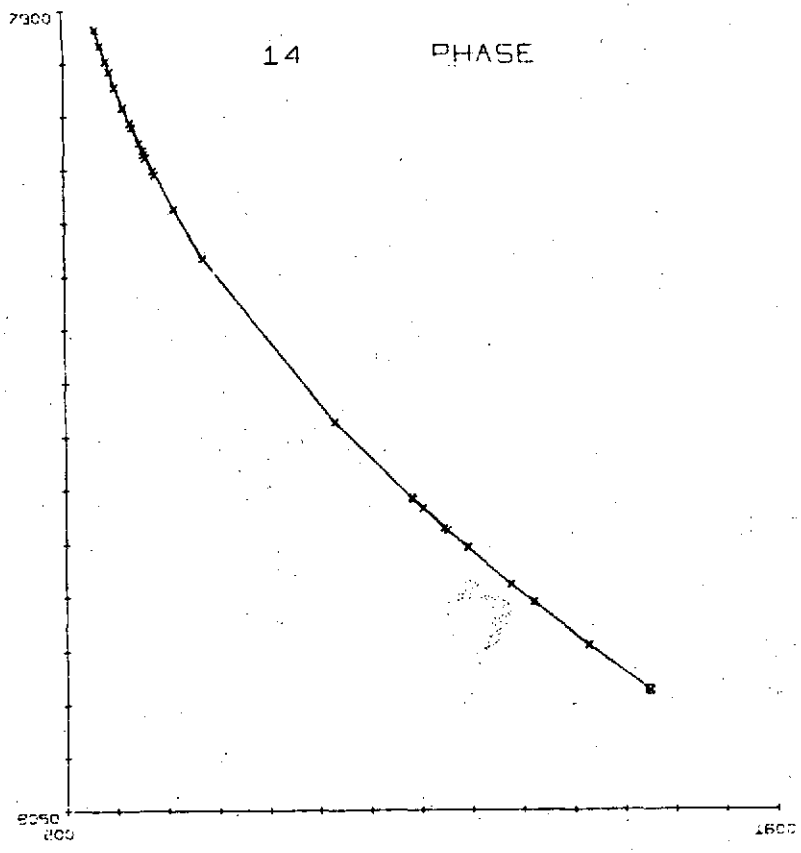

a. Flight 14; linear gradient

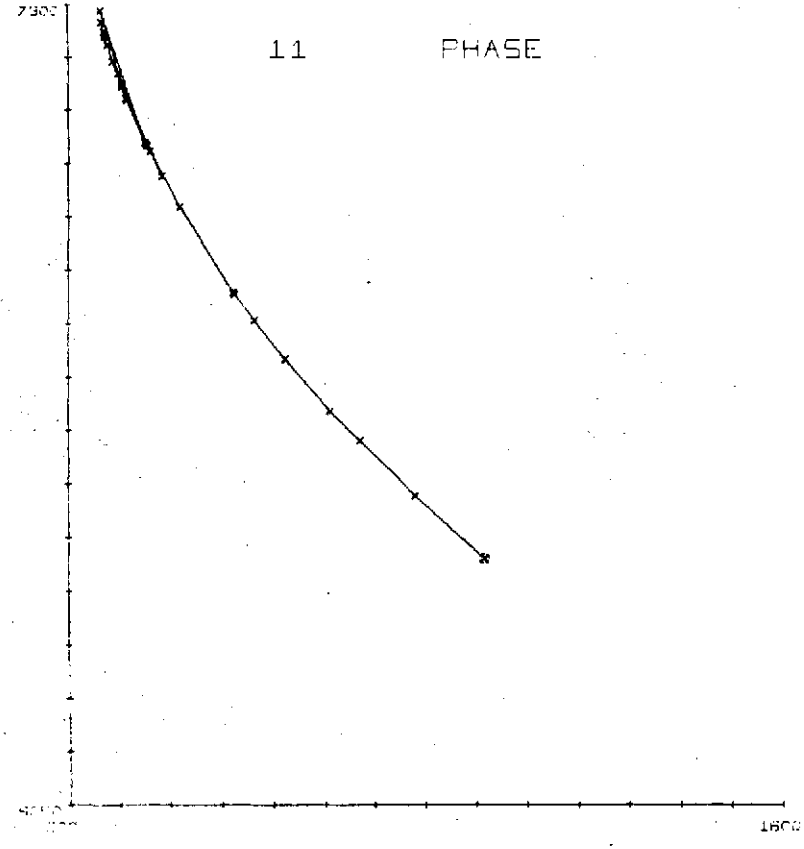

b. Flight 11; linear gradient

Fig. 58. PHASE AS A FUNCTION OF SATELLITE SEPARATION FOR FOUR NONSYMMETRIC PROFILES. The phase of the received signal appears as it would be recorded by the receiving satellite at the given separation from the transmitting satellite. The vertical scale shows separation in kilometers, with 7900 km at top and 8050 km at bottom. The scale is arranged this way because the greater separation corresponds to the lower closest approach altitude of the ray. The horizontal scale shows phase, in meters, with 200 m on the left and 1600 m on the right.

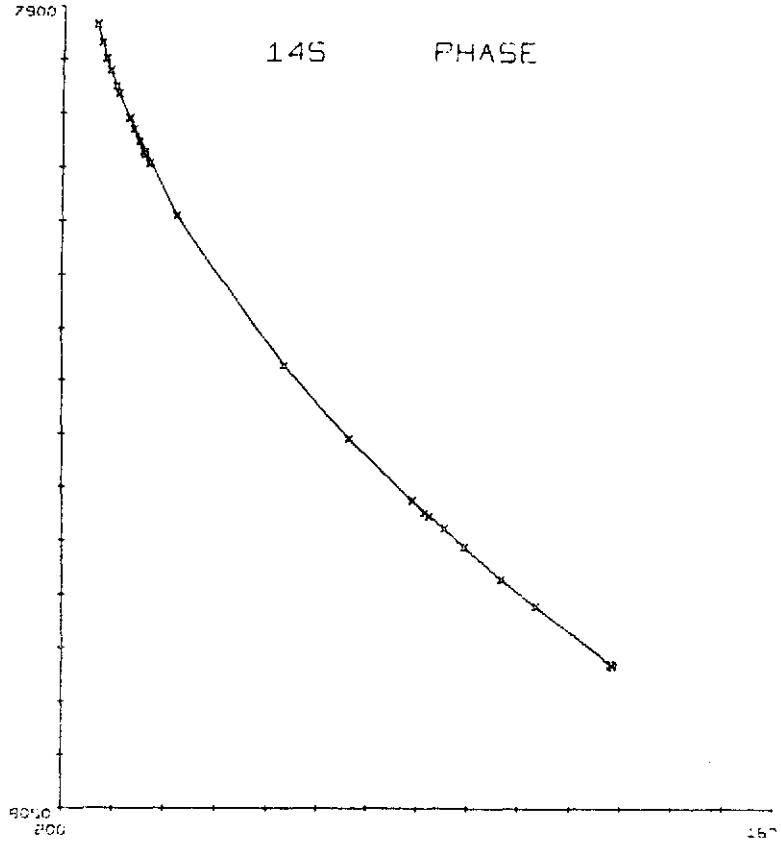

c. Flight 14; statistical

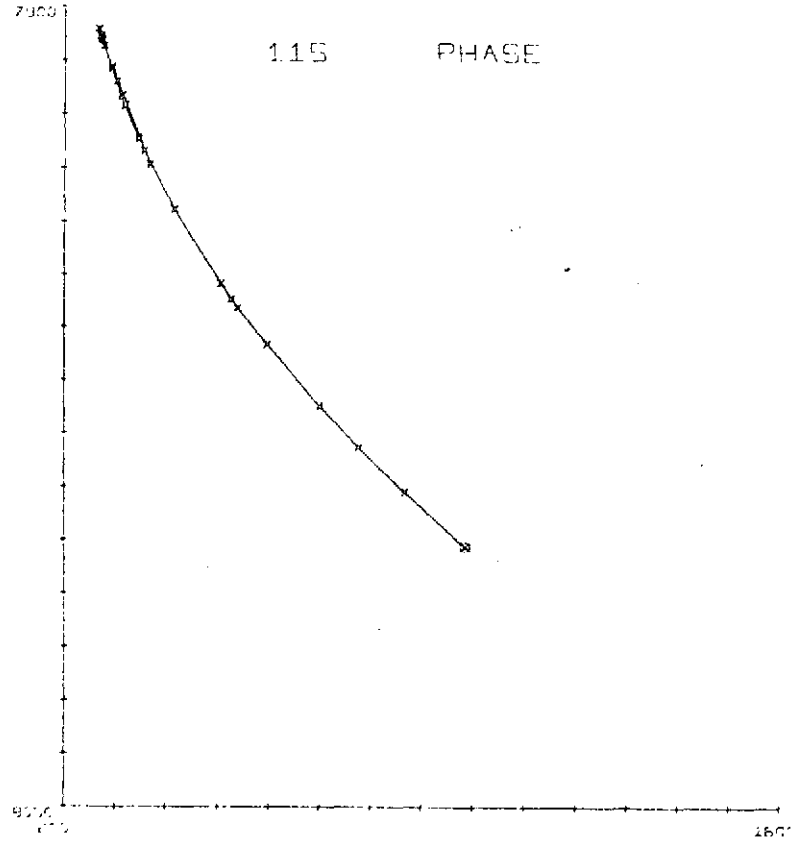

d. Flight 11; statistical

Fig. 58. CONTINUED.

The fading duration could be decreased by a similar factor, which would mean deep fades with a "duration" of perhaps 0.06 sec.

Assuming that this rough calculation is significant, the crucial question is the number of 60 msec fades that can be expected per second. The prevalence of multiple-ray multipath in the satellite-to-satellite raytracing suggests that these periods of deep fade are rather uncommon and occur far less often than in the case of the stationary Hawaii receiver and transmitter.

A third factor is the magnitude of the phase defect experienced by the satellite and ground systems. A typical phase defect in the satellite-to-satellite mode is on the order of 140 to 240 m (corresponding to approximately 8 and 6 km closest approach altitudes, respectively), whereas the phase defect experienced in the station-to-station mode is closer to 40 m; thus, there is a factor of approximately 5 between the phase-defect magnitudes of the satellite and ground systems.

This becomes significant when one realizes that the satellite system is not only sweeping through the weather at a much greater speed than is the ground system but also that, as it sweeps, the difference in phase defect is likely to be greater by a factor of approximately 5. This extra factor further reduces the expected fade duration from ≈ 60 to ≈ 12 msec.

To the extent that the Hawaii results can be extrapolated to the satellite-to-satellite configuration, there appears to be little reason to be pessimistic as to the potential dangers of fading caused by multipath in an operational microwave occultation system.

Chapter VIII

SUMMARY AND CONCLUSIONS

"It is better never to begin a good work than, having begun it, to stop."

--Bede

This research has investigated the feasibility of using a two-satellite occultation system to supplement the infrared sensor system (SIRS) by providing an accurate altitude reference that will serve to fix, as a function of height, the temperature-pressure profile of the SIRS instrument.

The final stage of the error analysis used simulated SIRS data to determine the behavior of the system over a realistic range of inputs. Based on this analysis, the microwave occultation system was found to be capable of establishing a 300 mb pressure reference level to within approximately 24 m. The effects of water vapor can be corrected by suitable climatological profiles. This work has shown that even the most simplistic climatological approach results in a dramatic improvement in accuracy; more sophisticated methods promise to be even more effective.

Improvements in the accuracy of the SIRS instrument will yield improvements in the performance of the occultation system. Most of the error in the output of the system (neglecting the component attributable to water vapor) was caused by error in the input temperature profile. As these input errors are reduced, system performance will be significantly improved. Even with the present SIRS instrumentation, however, the microwave occultation system produces results that are acceptable to, and badly needed by, the meteorological community.

Ground tests of a microwave link similar to that which would be employed in a pressure-reference-level system were described. These tests, conducted in June 1970, consisted of a continuous two-week monitoring of transmission between two mountain tops in Hawaii, with periodic flights of an instrumented aircraft along the radio path to measure the refractivity profile of the atmosphere.

The microwave signal was characterized by periods of intense fading. Using the refractivity profiles measured by the aircraft, an extensive computer analysis was performed to determine the probable cause of the observed fades. Results indicated that multipath interference, originating from anomalies in the N-profiles, was primarily responsible for the fading.

Multipath is a low-altitude phenomenon associated with water-vapor inhomogeneities. Extrapolating the results of the Hawaii experiment (performed at an altitude of ≈ 3 km) to the higher altitude of an operational occultation system (≈ 7 km), indicated that multipath was greatly reduced. It was concluded, therefore, that the fading observed on the Hawaii link will have little or no effect on an operational occultation system.

A microwave occultation system appears to be a feasible and useful technique for acquiring an important piece of data. Further work in this area should be directed toward the operational aspects of this system. For example, although this study has demonstrated that water-vapor effects can be corrected by the simplest of climatic methods, it would be of value to have a more accurate estimate of water vapor along the raypath. Several techniques have been proposed, such as passive microwave sounders or attenuation measurements of the signal. Tank [12] has suggested a dual-frequency occultation system that would determine water-vapor density by matching attenuation of the two signals to the water-vapor absorption line at 22.3 GHz.

Another area deserving further work is the inversion program that shifts the temperature-pressure profile to the proper altitude. The technique used in this study was a simple curve-fitting routine. The program can be speeded up somewhat by taking into account the climatology of the geographic area being sampled. Empirical orthogonal functions may be of some use.

Although the Hawaii study was intended to provide useful information for the occultation system design, it has generated some scientific results of its own. For example, it would be interesting to investigate how the periods of deep fade correlate with large-scale weather systems that were in the area at the time. It has been demonstrated that fading

is probably the result of multipath; however, no attempt was made to define the actual mechanism that produces the particular N-profiles responsible for the multipath. Presumably, water-vapor inhomogeneities are the cause, but this study has not attempted to correlate such factors as atmospheric conditions, wind, and sea state, in order to describe the physical phenomena that may be associated with the inhomogeneities.

It should be pointed out that the recent studies by Pirraglia and Gross [13] of errors inherent in the occultation technique seem not to apply to our proposed system. As they state in their conclusion, two orbiting satellites in a common plane will not be affected by the errors described in their paper. This is noted here to avoid possible confusion on the part of readers familiar with their work.

Appendix A

THE PRESSURE-REFERENCE PROGRAM

```
C
C
C*****************************************************************************
C
C
//LUDWIG JOB (N529,240,3,21,'STEVEN G. UNGAR'
// EXEC FURTHCG,PARM.FORT='OPT=2,MAP'
//FORT.SYSIN DD *
C
C*****************************************************************************
C
C     LUDWIG--A PROGRAM TO FIX A PRESSURE LEVEL IN THE ATMOSPHERE
C
C MEANING OF ARRAYS:
C   P(I) IS THE 100 PRESSURE LEVELS LISTED IN THE SIRS DATA; T(I) IS THE
C   ARRAY OF CORRESPONDING TEMPERATURE VALUES "MEASURED" BY THE SIRS INSTRUMENT;
C   TD(I) IS THE ARRAY OF TEMPERATURE ERRORS; THE "TRUE" TEMPERATURE,
C   T(I)-TD(I), IS STORED IN TR(I); Z(I) IS THE ARRAY OF ALTITUDE VALUES FOR
C   EACH OF THE 100 PRESSURE LEVELS; PW(I) HOLDS WATER VAPOR PRESSURE
C   VALUES FOR COMPUTING THE REFRACTIVITY PROFILE; EW(I,J) HOLDS THE TWO
C   STANDARD WATER VAPOR PROFILES (HIGH AND LOW); EPW(I) GIVES RAWINSONDE VALUES
C   OF WATER VAPOR PRESSURE MEASURED AT PRESSURES IPW(I); APW(I) IS EQUAL TO
C   IPW(I), BUT IN REAL, RATHER THAN INTEGER, FORMAT; TT(I) AND PP(I) ARE
C   STANDARD ATMOSPHERE VALUES OF TEMPERATURE AND PRESSURE; N(I) IS THE REFRAC-
C   TIVITY ARRAY ACTUALLY USED IN RAYTRACING; NL(I) IS THE "MEASURED" ATMOSPHERE
C   REFRACTIVITY PROFILE; NN(I) IS THE "REFERENCE" ATMOSPHERE N-PROFILE; PL(I)
C   IS THE ARRAY OF STANDARD PRESSURES FOR WHICH PRESSURE HEIGHTS ARE TO BE
C   COMPUTED; TL(I) AND PLW(I) ARE CORRESPONDING VALUES OF TEMPERATURE AND
C   WATER VAPOR PRESSURE; A(I) AND B(I) ARE CORRESPONDING HEIGHTS; FOR THE
C   "REFERENCE" ATMOSPHERE AND "MEASURED" ATMOSPHERE, RESPECTIVELY (THE LATTER
C   VALUE MEASURED PRIOR TO SHIFTING); W(I),X1(I),Z1(I),Y1(I),ZZ(I),N2(I) AND
C   EWW(I) ARE WORK VECTORS; LAT(I), LONG(I), STNAME(I), AND STNO(I) ARE USED
C   FOR IDENTIFICATION OF DATA SETS.
C
C MEANING OF SUBROUTINES:
C   ATSG AND ALI ARE A SORTING AND AN INTERPOLATION ROUTINE IN THE IBM
C   SCIENTIFIC SUBROUTINE PACKAGE (SSP).  SEE IBM MANUAL H20-0205-3 FOR DETAILS.
C   SE13 IS AN SSP SMOOTHING ROUTINE.  ATBILO, N, RAYTRA,STGEN,AND TALLY ARE
C   DESCRIBED UNDER THEIR RESPECTIVE LISTINGS.
C
C*****************************************************************************
C
      REAL P(100),T(100),Z(100),TT(91),PW(100),W(100),X1(100),Z1(100)
      DIMENSION TD(100),TR(100),LAT(2),LONG(2)
      DIMENSION Y1(100),EW(25,2),PL(9),TL(9),A(9),B(9)
      DIMENSION PLW(9),IPW(15),EPW(15),EWW(25),APW(15),ZZ(25)
      REAL*8 SS,STNAME(8),RE,STNO(10)
      REAL PP(91),N(91),NN(100),N2(10),ITYPE,NL(100)
      COMMON Z,PP,TT,VL,MAX
      COMMON /A/ RE,IH
      COMMON /RAYT/ N
C
C INITIALIZATION OF CONSTANTS
C
      DATA PL/500.,400.,300.,200.,140.,100.,70.,50.,30./
      LEVELS=9
      DATA PI/3.1415926/,AR/6378.15/,BR/6356.77/,LEVELS/9/,PW/100*0.0/
      F=1.0-BR/AR
C
C READ DATA COMMON TO ALL DATA SETS
C
      READ (5,11) (P(I),I=1,100)
      WRITE (6,116) (P(I),I=1,100)
      WEIGHT = 1.0
C   (G IS THE CONSTANT IN THE EXPONENT OF THE HYPSOMETRIC FORMULA)
      G=28.9644*9.80665/8.31432
      READ (5,102) PP
      WRITE (6,102) PP
```

```
      READ (5,102) TT
      WRITE (6,102) TT
      DO 920 J=1,2
      READ (5,114) (EW(I,J),I=1,8)
      WRITE (6,114) (EW(I,J),I=1,8)
      DO 920 I=9,25
C     (0.5476 IS THE INVERSE OF THE WATER VAPOR SCALE HEIGHT)
920   EW(I,J)=EW(8,J)*EXP(-.5476*(I-8))
      WRITE (6,114)((EW(I,J),I=1,25),J=1,2)
C     (MIX IS THE NUMBER OF PRESSURE LEVELS IN THE INPUT DATA (100); H IS THE
C     STARTING HEIGHT FOR THE RAYTRACING ROUTINE; ERS IS THE ERROR IN SATELLITE
C     POSITION; EPPH IS THE MAXIMUM PERMISSABLE ERROR IN PHASE DEFECT; SS IS THE
C     SATELLITE SEPARATION.)
      READ (5,100) MIX,H,ERS,EPPH,SS
      WRITE(6,103) MIX,H,ERS,EPPH,SS
      ITOP=0
      ERS=ERS/7481.0
      SS=SS/2
      IH=1
C
C READ INPUT DATA FOR SPECIFIC DATA SET
C
27    READ (5,113,END=999) STNO
      WRITE (6,113) STNO
      READ (5,117) LAT,LONG,MINALT,STNAME
      WRITE (6,117) LAT,LONG,MINALT,STNAME
      PHI=(LAT(2)/60.0+LAT(1))*PI/180
C     (RE IS THE RADIUS OF THE EARTH AT THE GIVEN LAT)
      RE=AR*(1.0-(F-3.0/2*F*F)*SIN(PHI)*SIN(PHI))
      WRITE (6,118) PHI,RE
      MAX = MIX
C     (DH IS THE AMOUNT OF VERTICAL SHIFT IN KM)
      DH=1
      Z300=0
      READ (5,102) (T(I),I=1,100)
      WRITE (6,102) (T(I),I=1,100)
      READ (5,102) (TD(I),I=1,100)
      WRITE (6,102) (TD(I),I=1,100)
C     (ITOP IS THE NUMBER OF DATA SETS READ)
      ITOP=ITOP+1
      DO 400 I=1,100
400   TR(I)=T(I)-TD(I)
      WRITE (6,102) (TR(I),I=1,100)
C     (NPW IS THE NUMBER OF WATER VAPOR DATA POINTS. JW=1 OR 2, CORRESPONDING TO)
C     LOW OR HIGH STANDARD WATER VAPOR PROFILE.)
      READ (5,122) NPW,JW
      WRITE (6,122) NPW,JW
      READ (5,123) (IPW(I),EPW(I),I=1,NPW)
      WRITE (6,121) (IPW(I),EPW(I),I=1,NPW)
C
C*************************************************************************
C
C "REFERENCE ATMOSPHERE" PORTION OF PROGRAM
C
C INTERPOLATE NPW WATER VAPOR VALUES AT 100 INPUT PRESSURES
C
      DO 80 I=1,NPW
80    APW(I)=IPW(I)
      PWMIN=APW(NPW)
      DO 81 I=1,MAX
      IPWMAX=I
      IPWM=IPWMAX-1
      IF (P(I).LT.PWMIN) GO TO 82
      CALL ATSG (P(I),APW,EPW,W,NPW,1,Z1,X1,NPW)
      CALL ALI (P(I),Z1,X1,PW(I),NPW,.01,IER)
      IF (IER.GE.2) WRITE (6,106) IER,I
81    CONTINUE
82    CONTINUE
C
C CALCULATE REFRACTIVITY AND ALTITUDE PROFILES FOR "REFERENCE ATMOSPHERE"
C
      Z(1)=0
      PL1=ALOG(P(1))
      TS1=TR(1)
```

```
143.            NN(1)=77.6*(P(1)-PW(1))/TS1+3.75E5/TS1*PW(1)/TS1
144.            WRITE (6,100) IH,Z(1),NN(1)
145.            DO 1 I=2,MAX
146.            PL2=ALOG(P(I))
147.            TS2=TR(I)
148.            Z(I)=Z(I-1)+(TS1+TS2)/2*(PL1-PL2)/G
149.            PWW=0.0
150.      C     (WATER VAPOR=0 ABOVE 20 KM, CALCULATED ACCORDING TO EXPONENTIAL
151.      C     BETWEEN MAXIMUM HEIGHT OF DATA AND 20 KM.)
152.            IF (I.EQ.IPWM) ZPW=Z(I)
153.            IF (Z(I).LT.20.0.AND.I.GE.IPWMAX) PW(I)=PW(IPWM)*EXP(-.5476*(Z(I)-
154.           *ZPW))
155.            IF (Z(I).LT.20.0) PWW=PW(I)
156.            NN(I)=77.6*(P(I)-PWW)/TS2+3.75E5/TS2*PWW/TS2
157.            WRITE (6,100) I,Z(I),NN(I)
158.            PL1=PL2
159.      1     TS1=TS2
160.      C
161.      C INTERPOLATE VALUES OF TEMPERATURE (TL), ALTITUDE (A), AND WATER VAPOR
162.      C   PRESSURE (PLW) FOR 9 STANDARD PRESSURES (PL)
163.      C
164.            DO 2 I=1,LEVELS
165.            CALL ATSG (PL(I),P,TR,W,MAX,1,Z1,X1,MAX)
166.            CALL ALI(PL(I),Z1,X1,TL(I),MAX,.01,IER)
167.            CALL ATSG (PL(I),P, Z,W,MAX,1,Z1,X1,MAX)
168.            CALL ALI(PL(I),Z1,X1,A(I),MAX,.01,IER)
169.            CALL ATSG (PL(I),P,PW,W,MAX,1,Z1,X1,MAX)
170.            CALL ALI (PL(I),Z1,X1,PLW(I),MAX,.01,IER)
171.      2     CONTINUE
172.            DO 667 I=1,LEVELS
173.      667   WRITE (6,100) I,PL(I),A(I),TL(I),PLW(I)
174.      C     (Z300 IS THE HEIGHT OF THE 300 MB LEVEL)
175.            Z300=A(3)
176.      4     WRITE (6,101) Z300
177.            IMAX=Z(MAX)
178.      C
179.      C SET N(I)=REFRACTIVITY OF STANDARD DRY ATMOSPHERE
180.      C
181.            DO 5 I=1,91
182.            N(I)=77.6*PP(I)/TT(I)
183.      5     CONTINUE
184.      C
185.      C INTERPOLATE DATA REFRACTIVITY PROFILE AT 1 KM INTERVALS, AND REPLACE
186.      C   STANDARD ATMOSPHERE REFRACTIVITY VALUES WITH THESE VALUES
187.      C
188.            DO 7 I=1,IMAX
189.            X=I-1
190.            CALL ATSG (X,Z,NN,W,MAX,1,Z1,X1,MAX)
191.            CALL ALI (X,Z1,X1,N(I),MAX,1.E-4,IER)
192.            IF (IER.GE.2) GO TO 303
193.      7     CONTINUE
194.      C
195.      C SMOOTH PROFILE IN NEIGHBORHOOD OF TRANSITION BETWEEN DATA REFRACTIVITY
196.      C   PROFILE AND STANDARD ATMOSPHERE REFRACTIVITY PROFILE (TRANSITION
197.      C   OCCURS NEAR 70 KM ALTITUDE)
198.      C
199.            DO 30 I=1,10
200.            II=IMAX-5+I
201.      30    N2(I)=N(II)
202.            CALL SEIS (N2,N2,10,IER)
203.            IF (IER.NE.0) GO TO 304
204.            DO 31 I=1,10
205.            II=IMAX-5+I
206.      31    N(II)=N2(I)
207.      C
208.      C RAYTRACE THROUGH REFERENCE ATMOSPHERE PROFILE
209.      C
210.            CALL RAYTRA (SS,ERS,H,SR)
211.      C   (PHASE EFFECT=SR)
212.      C
213.      C**********************************************************************
214.      C
```

```
C "MEASURED ATMOSPHERE" PORTION OF PROGRAM
C
C SET EWW=APPROPRIATE STANDARD WATER VAPOR PROFILE
C
      DO 87 I=1,25
      EWW(I)=EW(I,JW)
87    ZZ(I)=I-1
      WRITE (6,115) EWW
C
C CALCULATE REFRACTIVITY AND ALTITUDE PROFILES FOR "MEASURED ATMOSPHERE"
C
      Z(1)=0.0
      PL1=ALOG(P(1))
      TS1=T(1)
      PW(1)=EWW(1)
      NL(1)=77.6*(P(1)-PW(1))/TS1+3.73E5/TS1*PW(1)/TS1
      WRITE (6,100) IH,Z(1),NL(1)
      DO 85 I=2,MAX
      PL2=ALOG(P(I))
      TS2=T(I)
      Z(I)=Z(I-1)+(TS1+TS2)/2*(PL1-PL2)/G
      PL1=PL2
85    TS1=TS2
      DO 86 I=2,MAX
      PW(I)=0.0
      IF (Z(I).GE.20.0) GO TO 86
      CALL ATSG (Z(I),ZZ,EWW,W,25,1,Z1,X1,25)
      CALL ALI (Z(I),Z1,X1,PW(I),25,.01,IER)
      IF (IER.GE.2) WRITE (6,104) IER,I
      IF (IER.EQ.3) WRITE (6,116) ZZ
      IF (IER.EQ.3) WRITE (6,116) Z1
      IF (IER.EQ.3) STOP
86    NL(I)=77.6*(P(I)-PW(I))/T(I)+3.73E5/T(I)*PW(I)/T(I)
      DO 88 I=1,LEVELS
C
C INTERPOLATE VALUES OF TEMPERATURE (TL), ALTITUDE (B), AND WATER VAPOR
C   PRESSURE (PLW) FOR 9 STANDARD PRESSURES (PL)
C
      CALL ATSG (PL(I),P, T,W,MAX,1,Z1,X1,MAX)
      CALL ALI(PL(I),Z1,X1,TL(I),MAX,.01,IER)
      CALL ATSG (PL(I),P, Z,W,MAX,1,Z1,X1,MAX)
      CALL ALI(PL(I),Z1,X1,B(I),MAX,.01,IER)
      CALL ATSG (PL(I),P,PW,W,MAX,1,Z1,X1,MAX)
      CALL ALI (PL(I),Z1,X1,PLW(I),MAX,.01,IER)
88     CONTINUE
C   (ZZ300 IS ALTITUDE OF THE 300 MB LEVEL)
      ZZ300=B(3)
      DO 16 I=1,LEVELS
16    WRITE (6,100) I,PL(I),B(I),TL(I),PLW(I)
C
C MERGE REFRACTIVITY PROFILE WITH STANDARD ATMOSPHERE REFRACTIVITY
C PROFILE, AND RAYTRACE
C
      CALL ATBILD
      CALL RAYTRA (SS,ERS,H,PD1)
C   (PHASE DEFECT=PD1)
C
C SHIFT PROFILE UP 1 KM (DH=1)
C
C MERGE REFRACTIVITY PROFILE WITH STANDARD ATMOSPHERE REFRACTIVITY
C PROFILE, AND RAYTRACE
C
      DO 83 I=1,MAX
93    Z(I)=Z(I)+DH
      ZZ300=ZZ300+DH
      CALL ATBILD
      CALL RAYTRA (SS,ERS,H,PD2)
      DPHDZ=PD2-PD1
      WRITE (6,202) DPHDZ
      DPHI=SR-PD2
C   (IF ERROR IN PHASE DEFECT IS SUFFICIENTLY SMALL, CEASE ITERATION)
      IF (ABS(DPHI).LE.ERPH) GO TO 91
C
C CALCULATE NEW DH, SHIFT PROFILE, MERGE WITH STANDARD ATMOSPHERE
C   PROFILE, AND RAYTRACE
```

```
290.      C
291.      12     DH=   DPHI/DPHDZ*WEIGHT
292.             WRITE (6,201) DH,DPHI,Z(IH)
293.             DO 13 I=1,MAX
294.      13     Z(I)=Z(I)+DH
295.             ZZ300=ZZ300+DH
296.      C    (PHASE DEFECT=PD2)
297.      C
298.      C CALCULATE DPHDZ, DPHI
299.      C
300.             CALL ATBILD
301.             CALL RAYTRA (SS,ERS,H,PD2)
302.      15     DPHI=SR-PD2
303.      C    (IF ERROR IN PHASE DEFECT IS SUFFICIENTLY SMALL, LEAVE ITERATION)
304.             IF(ABS(DPHI).LE.ERPH) GO TO 91
305.      C
306.      C**********************************************************************
307.      C
308.      C PRINT RESULTS
309.      C
310.      C    (ZDIF=ERROR, IN METERS, AT 300 MB LEVEL)
311.             GO TO 12
312.      91     ZDIF =1000*(ZZ300-Z300)
313.             WRITE (6,113) STNO
314.             WRITE (6,103) ZZ300,Z300,ZDIF
315.             WRITE (6,111)
316.             MAX=MIX
317.             DH=1
318.             ANS=ZZ300
319.      77     CONTINUE
320.             WRITE (6,113) STNO
321.             WRITE (6,119) STNAME,LAT,LONG,RE
322.      C
323.      C PRINT ALTITUDE ERRORS FOR EACH OF 9 PRESSURES
324.      C
325.             CALL STGEN(A,B,PL,ANS,ITOP,LEVELS)
326.             WRITE (6,111)
327.             GO TO 27
328.      999    CONTINUE
329.      C
330.      C CALCULATE AND PRINT STATISTICS FOR ENTIRE RUN.  "COUNT" IS AN ENTRY
331.      C    IN "STGEN."
332.      C
333.             SS=2*SS
334.             WRITE (6,120) ITOP,SS
335.             CALL COUNT (ITOP,LEVELS)
336.             STOP
337.      303    WRITE (6,107) IER,I
338.             STOP
339.      304    WRITE (6,109) IER
340.             STOP
341.      100    FORMAT (I4,5F8.3)
342.      101    FORMAT (2F8.3)
343.      102    FORMAT (10F8.3)
344.      103    FORMAT ('0300 MB. PRESSURE LEVEL:  CALC. VALUE =',F8.3,' KM.  TRUE
345.             * VALUE =',F8.3,' KM.'//' DIFFERENCE =',F12.3,' METERS')
346.      104    FORMAT (' ERROR IN ALI,EW.  IER=',I4,' I=',I4)
347.      105    FORMAT (' ERROR IN ALI,T400.  IER=',I4,' I=',I4)
348.      106    FORMAT (' ERROR IN ALI,PW. IER=',I4,' I=',I4)
349.      107    FORMAT (' ERROR IN ALI,N.      IER=',I4,' I=',I4)
350.      108    FORMAT (' ',2F8.3)
351.      109    FORMAT (' ERROR IN SEI3,N.      IER=',I4)
352.      110    FORMAT (9F8.3)
353.      111    FORMAT ('1')
354.      112    FORMAT (4(5X,F12.6))
355.      113    FORMAT (10A8)
356.      114    FORMAT (9F10.6)
357.      116    FORMAT (' ',9F8.3)
358.      117    FORMAT (2(2I3,1X),I5,7A8,A5)
359.      118    FORMAT (' LAT=',F10.4,' RADIANS   RE=',F10.4,' KM.')
360.      119    FORMAT ('0',7A8,A5//2X,2I3,' N   ',2I3,' W    RADIUS OF EARTH',
361.             *' AT THIS LATITUDE',F10.4,' KM.')
362.      120    FORMAT ('1STATISTICS FOR',I4,' STATIONS'/' SATELLITE SEPARATION'
363.             *,F10.4,' KM.')
364.      121    FORMAT (I5,F10.6)
```

```
      122   FORMAT (2I3)
      123   FORMAT (I4,F11.6)
      200   FORMAT ('1DSOH=',E20.8)
      201   FORMAT (4E20.8)
      202   FORMAT (' DOHOZ=',E20.8)
            END
      C
      C
      C*****************************************************************************
      C
      C
            SUBROUTINE ATBILD
      C
      C THIS SUBROUTINE MERGES THE "MEASURED ATMOSPHERE" N-PROFILE WITH A STANDARD
      C   ATMOSPHERE REFRACTIVITY PROFILE
      C
            REAL Z(100),PP(91),TT(91),N2(100),N(91),PW(100)
            REAL T(100),P(100),Z1(100),X1(100),NL(100)
            REAL W(100)
            REAL*8 RE
            COMMON Z,PP,TT,NL,MAX
            COMMON /A/RE,IH
            COMMON /RAYT/N
            IMAX=Z(MAX)
            DO 12 I=1,70
     12     N(I)=77.6*PP(I)/TT(I)
            JMAX=MAX
            DO 3 I=IH,IMAX
            X=I-1
            CALL ATSG (X,Z,NL,W,MAX,1,Z1,X1,JMAX)
            CALL ALI (X,Z1,X1,N(I),JMAX,1.E-4,IER)
            IF(IER.GE.2) WRITE (6,100) IER,I
            IF (IER.GE.2) WRITE (6,102) Z1
      C     WRITE (6,105) I,X,N(I)
      3     CONTINUE
            DO 4 I=1,10
            II=IMAX-5+I
      4     N2(I)=N(II)
            CALL SE13 (N2,N2,10,IER)
            IF (IER.NE.0) WRITE (6,101) IER
            DO 5 I=1,10
            II=IMAX-5+I
      5     N(II)=N2(I)
            RETURN
      100   FORMAT (' ERROR IN ALI.    IER=',I5,' I=',I5)
      101   FORMAT (' ERROR IN SE13.     IER=',I5)
      102   FORMAT (' ',8E10.4)
      105   FORMAT (I5,F9.4,5X,F12.8)
            END
      C
      C
      C*****************************************************************************
      C
      C
            REAL FUNCTION N*8(R)
      C
      C THIS SUBROUTINE IS CALLED BY RAYTRA.  IT INTERPOLATES IN THE REFRACTIVITY
      C ARRAY AT A GIVEN VALUE OF R (DISTANCE FROM THE CENTER OF THE EARTH).
      C
            REAL*8 R
            REAL N2(91)
            COMMON /RAYT/N2
            COMMON /A/RE,IH
            RA=R-RE
            I=INT(RA)+1
            IF (I.LT.1) WRITE (6,1) RA
            I=MAX0(I,1)
            RAP=AINT(RA)
            J=I+1
            I=MIN0(I,91)
            J=MIN0(J,91)
            N=N2(I)+(RA-RAP)*(N2(J)-N2(I))
```

```
      N = N*1.00-6 + 1.D00
      RETURN
    1 FORMAT (' RA LESS THAN RE.  RA=',F15.7)
      END
C
C
C*****************************************************************************
C
C
      SUBROUTINE RAYTRA (ACL,ACC,H,PHDFT)
C
C THIS IS A FERMAT'S PRINCIPLE RAYTRACING ROUTINE WRITTEN BY DR. JOSE
C   ROMALAZA-DIAZ.  ACL IS HALF THE SATELLITE SEPARATION, IN KM; ACC IS
C   THE ERROR IN SATELLITE SEPARATION; H IS A STARTING VALUE FOR THE
C   CLOSEST APPROACH ALTITUDE OF THE RAY; PHDFT IS THE RESULTING PHASE
C   DEFECT.  THE PROGRAM BEGINS AT HEIGHT H, RAYTRACES TO SATELLITE
C   ALTITUDE, AND THEN ADJUSTS H SO THAT THE RESULTANT SATELLITE HALF-
C   SPACING EQUALS ACL TO WITHIN ACC.
C
      REAL*8 DCOS,DSIN,DATAN,DSQRT,DARSIN
      REAL*8 RI,R2,N,C,SN,RN,DELR,R,RR,DELS,DELSN,DELC,RI,PI,BET,GAM
      REAL*8 NP,TTHP,X1,Y1,X2,Y2,THP,TH,TH1,TH2,Y,RD,RDP,DELT,ACL,DELTH
      REAL*4 P(1001),T(1001),PW(1001),PL(9)
      REAL*4 PHDFT,E,L
      REAL*8 R3,RE,Z
      COMMON /A/RE,IH
      PI=3.14159265359
      ER2=0
      ER1=0
      ER=0
      DELTH =0.0005
      RDP = 1100.0
      RDP=RDP+6378.15
      RI = RE+H
      E = -.847E-3
      II=0
      IF (II.EQ.0) RI=RI+1.D00
       KKO=0
       K1O=0
       PHDI=0.0
       III=II
       HR=RI-RE
       II3=II
       I2=4
       IF (III.GT.0) I2=3
   50 RMAX=RE+87.0
       SEP=100.0
       SEN=-100.0
       FACT1=1.0
       K8=0
       STU1=0.0
      Y=DELTH
      K=0
   23 STU=0.000
      C1=STU
    4 C=0.000
        ATTN=0.0
       ATTN2=0.0
       ATO6=0.0
       ATW6=0.0
       ATWV6=0.0
       ATO=0.0
       ATWV=0.0
       ATW=0.0
       DAT1=0.0
      SN=0.000
      TH=0.000
       CONST=RE
      INDICE=0
      R=RI
      J=0
       Y1=RI-0.25
       Y2=RI+0.25
```

```
510.            DNDR=N(Y2)-N(Y1)
511.             DNDR=[illegible]/2.5
512.            RHO=N(R1)/DNDR
513.            RN=N(R1)*RI
514.             RHO=ABS(RHO)
515.             RR=RHO-RI
516.             GAM=RR*DSIN(PI-DELTH)/RHO
517.             GAM=DARSIN(GAM)
518.             BET=DELTH-GAM
519.             DELR=RHO*DSIN(BET)/DSIN(PI-DELTH)-RI
520.             DELS=RHO*BET
521.             R=R+DELR/2.0
522.             RR=RI
523.            NP=N(R)
524.             GO TO 51
525.       5     CONTINUE
526.            NP=N(R)
527.            DELR=R*DSQRT((R*NP/RN)**2-1.0D0)*DELTH
528.       20   RR=R
529.            J=J+1
530.            R=R+DELR/2
531.            NP=N(R)
532.            DELR=R*DSQRT((R*NP/RN)**2-1.0D0)* DELTH
533.            DELS=R*R*NP*DELTH/RN
534.       51    CONTINUE
535.            TH=TH+DELTH
536.             IF (III.GT.0) GO TO 69
537.            DELSN=(NP-1.0D0)*DELS
538.            DELC=DELS-(DSQRT(DELS*DELS-DELR*DELR)*DCOS(TH)+DELR*DSIN(TH))
539.             H=R-RE
540.       18    CONTINUE
541.            C=C+DELC
542.            SN=SN+DELSN
543.       69     CONTINUE
544.            DELTH=Y
545.            R=RP
546.            R=R+DELR
547.            IF (R.GE.RMAX) GO TO 6
548.            GO TO 5
549.       6    N2=INDICE-1
550.            IF (INDICE.NE.0) GO TO 7
551.            R1=R
552.            TH1=TH
553.            INDICE=INDICE+1
554.            GO TO 5
555.       7    IF (N2) 8,9,9
556.       8    INDICE=INDICE+1
557.            GO TO 5
558.       9    R2=R
559.            TH2=TH
560.            X1=R1*DSIN(TH1)
561.            Y1=R1*DCOS(TH1)
562.            X2=R2*DSIN(TH2)
563.            Y2=R2*DCOS(TH2)
564.            TTHP=-(Y2-Y1)/(X2-X1)
565.            THP=DATAN(TTHP)
566.            X1=(Y1+X1*TTHP)*DCOS(THP)/ROP
567.            X1=(DSQRT(-X1*X1+1.0D0))/X1
568.            TH=DATAN(X1)+THP
569.            X1=ROP*DSIN(TH)
570.            C=C+(X1-X2)*(1.0D0/DCOS(THP)-1.0D0)
571.            Y1=DSQRT(ROP**2-X1*X1)
572.            TTHP=ACL/(DSQRT(ROP*ROP-ACL**2))
573.            THP=DATAN(TTHP)
574.             IF ((K.GT.8).OR.(FACT1.LT.0.1)) FACT1=1.0
575.             IF (K.LT.40) GO TO 55
576.             K=0
577.             II=0
578.             STU=C1
579.             K8=0
580.             SFP=100.0
581.             SEN=-100.0
582.       55    CONTINUE
```

```
      IF (STU1.GT.0) K=0
      IF (STU1.GT.0) II=0
     IF (K.GT.0) GO TO 24
     IF (STU.NE.C1) GO TO 19
      IF (II.GT.0) GO TO 25
     Z=TH
     RO=RI
     RI=RI-1.0D0
     STU=1.001
     GO TO 4
19   STU=(Z-TH)/(RO-RI)
     GO TO 26
25   STU=E
26   EP=STU
24    CONTINUE
     E=EP
     EPS=TH-THP
      IF (K8.EQ.0) EPI=EPS
     X=ABS(EPS)
     STU=EP
      STU1=STU
      K8=K8+1
      IF (III.GT.0) GO TO 68
     PHDFT=2000.0*(C+SN)
      DA2=2.0*DAT1
     WRITE(6,35) PHDFT,DA2
      WRITE(6,39) STU,HP,HN,SEP,SEN,EPS
      K10=K10+1
68    CONTINUE
     IF (X.LE.ACC) GO TO 22
      FACT2=ABS(EPS)
      FACT3=ABS(EPI)
      IF (FACT2.GE.FACT3) FACT1=FACT1*0.75
      H=RI-RE
      IF (EPS.GT.0) GO TO 67
      IF (SEN.LT.EPS) HN=H
      IF (SEN.LT.EPS) SEN=EPS
      GO TO 62
67    IF (SEP.GT.EPS) HP=H
      IF (SEP.GT.EPS) SEP=EPS
62    CONTINUE
      IF ((SEP.LT.100.0).AND.(SEN.GT.-100.0)) GO TO 60
      R3=RI
      RI=RI-FACT1*EPS/STU
      K=K+1
      GO TO 61
60    FAC=(HP-HN)/(SEP-SEN)
      K=K+1
      R3=RI
      XP=ABS(SEP)
      XN=ABS(SEN)
      IF(XP.LT.XN) RI=RE+HP-SEP*FAC*FACT1
      IF (XN.LE.XP) RI=RE+HN-SEN*FAC*FACT1
61    CONTINUE
      H=RI-RE
      KKO=KKO+1
      IF (KKO.GT.50) RI=-10.0D0
      PHO1=PHDFT
      EP1=EPS
      DA1=2.0*DAT1
      H=RI-RE
      IF ((KKO.LT.40).OR.(H.LE.0)) GO TO 500
       WRITE(6,41) HN,SEN,HP,SEP
     WRITE(6,14)
      WRITE(6,15) EPS,STU1,H,FACT1
500   CONTINUE
     IF (X.GT.ACC) GO TO 23
22    CONTINUE
      IF (K10.GT.0) GO TO 70
      III=0
      GO TO 23
70    CONTINUE
     HO=ROP*DCOS(TH)-RE
     RF=ROP-RE
```

```
      TH=TH*57.2957800
      H=RI-RE
      DELH=H-HO
       ATO=2.0*ATO
       ATWV=2.0*ATWV
       ATW=2.0*ATW
       DAT1=2.0*DAT1
       ATTN=ATWV
       ATTN2=DAT1
       WRITE(6,37) ATTN,ATTN2
       II=II3
      DIST=0.0
      DELL=2000.0*C
      RD=2000.0*SN
      PHDFT=DELL+RD
       IF (EPS.NE.EP1) ER1=(PHDFT-PHD1)/(EPS-EP1)
       IF ((II.EQ.0).AND.(EPS.NE.EP1)) ER=ER1
       IF ((II.EQ.0).AND.(EPS.NE.EP1)) ER2=(DAT1-DA1)/(EPS-EP1)
       DAT1=DAT1-EPS*ER2
       ATTN2=DAT1
       WRITE(6,37) ATTN,ATTN2
      PHDFT=PHDFT-EPS*ER
       ER1=ABS(ER1)
       WRITE(6,36) ER1,ER2
      WRITE(6,11) RE,TH,ACL,DELL,RD,PHDFT,H,HO,DELH,E,ATTN,DIST
      RETURN
 11   FORMAT(     'ORBIT ALTITUDE=',F11.4,' KM.',10X,'CENTRAL ANGLE=',F12
     1.5,' DEG.',10X,'ST. LINE PATH=',F12.5,' KM.',/' BENDING=',F9.3,'
     2M.',19X,'RETARDATION=',F9.3,' M.',17X,'PHASE DEFECT=',F9.3,' M.',/
     3' ACTUAL RAY HEIGHT=',F8.3,' KM.',10X,'APPARENT RAY HEIGHT=',F8.3,
     4' KM.', 9X,'DELTA H=',F9.3,' KM.',/' BENDING ANGLE=',F12.8,' DEG.'
     5,9X,'SIGNAL ATTENUATION=',F8.4,' DB.',10X,'SURFACE DISTANCE=',F9.3
     6,' KM.')
 14    FORMAT(' ','EPS','STU1','H','FACT1')
 15    FORMAT(' ',F12.7,E16.6,2F12.7)
 16    FORMAT(' ',D16.6)
 17   FORMAT(8D16.7)
 30   FORMAT(I12)
 35   FORMAT(2X,'PHASE DEFECT=',F12.6,1X,'ATTN=',F12.6)
 36    FORMAT(' ','ERR=',E12.5,1X,'ER2=',E12.5)
 37    FORMAT(' ','ATTN6=',F12.7,2X,'ATTN1=',F12.7)
 39     FORMAT(' ',6E16.7)
 41    FORMAT(' ',4F13.7)
      END
C
C
C***********************************************************************
C
C
      SUBROUTINE STGEN (A,B,D,ANS,NUM,LEVELS)
C
C THIS SUBROUTINE CALCULATES AND PRINTS THE AVERAGE, STANDARD DEVIATION,
C   RMS, MINIMUM AND MAXIMUM VALUES OF ALTITUDE ERROR AT THE 9 PRESSURE
C   LEVELS.  ACTUAL CALCULATIONS ARE PERFORMED BY SUBROUTINE TALLY.
C
      REAL A(9),C(120,9),D(9),B(9),RMS(9)
      DIMENSION AVER(9),SD(9),VMIN(9),VMAX(9),R(9,1)
      DATA C/1080*0.0/
      DIF=ANS- B(3)
      DO 1 J=1,LEVELS
      C(NUM,J)=(B(J)+DIF-A(J))*1.E3
      R(J,1)=C(NUM,J)
 1    CONTINUE
      WRITE (6,107)
      DO 3 J=1,LEVELS
      WRITE (6,106) D(J), R(J,1)
 3    CONTINUE
      CALL TALLY (R,AVER,SD,RMS,VMIN,VMAX,LEVELS,1)
      WRITE (6,100) LEVELS
      WRITE (6,101) AVER(1)
      WRITE (6,102) SD(1)
      WRITE (6,105) RMS(1)
```

```
      WRITE (6,103) VMIN(I)
      WRITE (6,104) VMAX(I)
      RETURN
      ENTRY COUNT (NUM,LEVELS)
      CALL TALLY (C,AVER,SD,RMS,VMIN,VMAX,NUM,LEVELS)
      WRITE (6,108)
      DO 5 J=1,LEVELS
      WRITE (6,106) D(J),AVER(J),SD(J),RMS(J),VMIN(J),VMAX(J)
5     CONTINUE
      RETURN
100   FORMAT (//1OX,'STATISTICS FOR LOWER',I4,'  PRESSURE LEVELS'/)
101   FORMAT (' MEAN',6X,10(F9.2,2X))
102   FORMAT (' ST. DEV.',2X,10(F9.2,2X))
103   FORMAT (' MIN',7X,10(F9.2,2X))
104   FORMAT (' MAX',7X,10(F9.2,2X))
105   FORMAT (' RMS',7X,10(F9.2,2X))
106   FORMAT (' ',F10.3,10(F9.2,2X))
107   FORMAT (//' LEVEL(MB)'/)
108   FORMAT (//' LEVEL(MB)',5X,'MEAN',6X,'ST. DEV.',
     *5X,'RMS',8X,'MIN',8X,'MAX'/)
      END
C
C
C*****************************************************************************
C
C
      SUBROUTINE TALLY (A,AVER,SD,RMS,VMIN,VMAX,NO,NV)
C
C SEE STGEN FOR DESCRIPTION
C
      REAL A(120,9),AVER(9),SD(9),VMIN(9),VMAX(9),TOTAL(10),RMS(9)
      DO 1 K=1,NV
      TOTAL(K)=0.0
      AVER(K)=0.0
      SD(K)=0.0
      RMS(K)=0.0
      VMIN(K)=1.0E75
      VMAX(K)=-1.0E75
1     CONTINUE
      DO 7 J=1,NO
      DO 7 I=1,NV
      AA=A(J,I)
      TOTAL(I)=TOTAL(I)+AA
      IF (AA-VMIN(I)) 3,4,4
3     VMIN(I)=AA
4     IF (AA-VMAX(I)) 6,6,5
5     VMAX(I)=AA
6     SD(I)=SD(I)+AA*AA
7     CONTINUE
      DO 8 I=1,NV
      AVER(I)=TOTAL(I)/NO
      SD(I)=SQRT(ABS((SD(I)-TOTAL(I)*TOTAL(I)/NO)/(NO-1)))
      RMS(I)=SQRT(AVER(I)*AVER(I)+SD(I)*SD(I))
8     CONTINUE
      RETURN
      END
C
C
C*****************************************************************************
C
C
/*
//GO.SYSIN DD *
1000.00  967.57  935.91  904.98  874.80  845.34  816.60  788.56  761.22
734.56  709.57  683.25  658.58  634.55  611.16  588.39  566.23  544.67
523.71  503.33  483.52  464.28  445.59  427.44  409.83  392.74  376.16
360.10  344.53  329.44  314.83  300.70  287.02  273.79  261.00  248.65
236.72  225.20  214.09  203.38  193.05  183.11  173.53  164.32  155.47
146.96  138.78  130.94  123.42  116.22  109.32  102.71   96.40   90.37
 84.61   79.12   73.89   68.91   64.18   59.68   55.41   51.37   47.54
 43.92   40.50   37.27   34.24   31.38   28.70   26.18   23.83   21.63
 19.58   17.68   15.91   14.27   12.75   11.36   10.07    8.90    7.82
  6.84    5.95    5.15    4.43    3.78    3.21    2.70    2.25    1.85
```

```
802.    1.51     1.22     0.97     0.75     0.58     0.43     0.32     0.22     0.15
803.    0.10
804.    1013.50  902.2    801.6    710.5    628.0    553.6    486.6    426.4    372.4    324.0
805.    284.9    242.6    208.6    178.6    152.5    130.3    111.3    95.03    81.21    69.46
806.    59.47    50.96    43.70    37.52    32.23    27.71    23.85    20.54    17.71    15.29
807.    13.22    11.45    9.922    8.613    7.488    6.519    5.684    4.963    4.339    3.799
808.    3.330    2.923    2.569    2.261    1.992    1.757    1.552    1.371    1.214    1.075
809.    .951     .842     .755     .660     .583     .515     .455     .401     .353     .310
810.    .272     .239     .209     .183     .160     .139     .121     .105     .091     .078
811.    .067     .057     .049     .042     .035     .030     .025     .021     .018     .015
812.    .012     .010     .008     .007     .005     .004     .004     .003     .002     .002
813.    .002
814.    296.22   291.14   286.20   279.79   273.57   267.45   261.33   254.81   248.28   241.77
815.    235.27   228.77   222.37   215.82   215.65   215.65   215.65   215.65   216.79   217.98
816.    219.17   220.37   221.56   222.75   223.94   225.13   226.32   227.51   229.69   231.57
817.    233.65   235.73   237.81   240.22   242.70   245.17   247.64   250.11   252.58   255.05
818.    257.52   259.99   262.46   264.93   267.39   269.86   272.32   274.79   275.65   275.65
819.    275.65   275.65   275.65   274.24   271.79   269.33   266.87   264.42   261.96   259.51
820.    257.05   254.60   252.15   248.93   244.52   240.11   235.70   231.29   226.89   222.48
821.    218.08   213.68   209.28   204.88   200.48   196.09   191.69   187.30   182.90   178.51
822.    174.12   169.72   165.33   165.12   165.10   165.09   165.08   165.07   165.06   165.05
823.    165.04
824.     3.30      2.33      1.48      0.96      0.60      0.375     0.217     0.110
825.     8.85      5.42      3.60      2.28      1.42      0.865     0.515     0.288
826.     100       5.0     .04      .0100 7888.00      01.
827.  1  STATION NO. 72202  PROFILE NO.  2  CASE NO. 2  SET NO. 2
828.    25 48  80 16     3  MIAMI/INT FLORIDA
829.    290.93   286.82   286.04   285.26   284.54   283.86   283.19   282.72   281.05   279.30
830.    277.60   275.99   274.41   272.83   271.21   269.57   267.92   266.26   264.57   262.86
831.    261.05   259.19   257.27   255.33   253.36   251.32   249.15   246.93   244.56   242.15
832.    239.70   237.21   234.67   232.13   229.57   226.97   224.30   221.56   218.80   216.09
833.    214.36   212.83   211.32   209.85   208.65   207.10   205.84   204.62   203.50   202.47
834.    201.53   200.63   199.82   199.09   199.14   199.37   200.01   201.44   202.92   204.39
835.    205.90   207.45   209.00   210.59   212.16   213.81   215.55   217.21   218.86   220.45
836.    222.02   223.55   225.05   226.50   227.92   229.30   230.65   231.97   233.28   234.56
837.    236.84   239.75   242.64   245.52   248.40   251.26   254.12   256.97   259.80   262.61
838.    265.43   269.25   269.49   269.40   267.05   262.27   257.50   252.26   241.42   230.54
839.     -0.17    -2.24    -0.97     0.30     1.63     2.97     4.24    -0.74    -1.42    -1.30
840.     -1.13    -0.97    -0.84    -0.72    -0.63    -0.56    -0.50    -0.45    -0.42    -0.43
841.     -0.24     0.08     0.41     0.71     0.98     1.30     1.66     1.91     2.08     2.19
842.      2.25     2.29     2.31     1.37    -0.39    -2.40    -4.15    -4.25    -4.33    -4.37
843.     -3.32    -2.28    -2.27    -2.23    -2.12    -1.81    -1.19    -0.49     0.30     1.16
844.      2.03     2.19     2.66     3.39     4.40     4.03     4.07     4.83     5.36     3.25
845.      1.08    -1.06    -3.27    -3.09    -2.92    -2.67    -2.36    -2.08    -1.12     0.52
846.      1.17     0.83     0.44     0.07     0.19     0.27     0.33     0.35     0.36    -0.45
847.     -0.31     0.46     1.20     1.55     2.14     2.18     2.24     2.04     1.71     1.17
848.      0.28    -0.59    -2.51    -1.94    -1.43    -2.40    -2.32    -1.68    -6.12   -10.46
849.    11  2
850.    1023  1.403870
851.    1000  1.080260
852.     850  7.889437
853.     810  6.739714
854.     800  4.956509
855.     782  2.775787
856.     700  1.756351
857.     500  0.487902
858.     478  0.429759
859.     400  0.299725
860.     300  0.260981
```

Subroutine RAYTRA by Dr. Jose Pomalaza.

Appendix B

SATELLITE-TO-SATELLITE RAYTRACING PROGRAM THRUWAY

THRUWAY raytraces between two satellites. The "atmosphere" is divided into four regions.

(1) The region between 4 km and RO (69 km) consists of spherically symmetric standard-atmosphere data.

(2) Above RO km, the medium is assumed to be vacuum.

(3) Between 2 and 4 km, the atmosphere consists of non-symmetric Hawaii data.

(4) Below 2 km, standard-atmosphere data are again used, but the horizontal gradients at 2 km are carried through to the lower altitudes.

Because the XDS Sigma-5 computer does not have sufficient core storage for all the Hawaii data, it is stored on a disk (called the RAD, for Rapid Access Device) and pulled when necessary.

```
1.      C
2.      C
3.      C*************************************************************************
4.      C
5.      C
6.       JOB 3657,UNGAR
7.       ALLOBT (FILE,60),(FSIZE,500),(FORMAT,8),(RSIZE,30),(SAVE)
8.       FORTRAN RO
9.      C
10.     C
11.     C*************************************************************************
12.     C
13.     C
14.     C                  *****THRUWAY*****
15.     C       NON-SYMMETRIC ATMOSPHERE
16.             IMPLICIT REAL*8(A,O,R)
17.             REAL*8 SINPHI,TH,COSPHI,N,C,SN,SN1,C1,PHDET,KON,SLOPE,EP,THP,THO
18.             REAL*8 NI,PH,THI,THI,THPREC,TH2,U,THO,PSI,THOIS,NN
19.             REAL*4 DUM,DELH,SEP(2,30)
20.             REAL*4 B(50),RO2(50),DB(50)
21.             REAL N2(40,20)
22.             INTEGER PNT,TIMES
23.             LOGICAL HORAD
24.             LOGICAL       PLOTR,BEGIN,PLOTP,DERIV,PLOTPH,PLOTDB
25.             COMMON      THOIS,THMIN/FLY/IFLY,PLOTR,PLOTP,PLOTPH,PLOTDB
26.             COMMON N2
27.             COMMON SEP,B,RO2,DB
28.              DSEC(U)=1/DCOS(U)
29.             DARSIN(U)=DATAN(U/DSQRT(1-U*U))
30.     C
31.     C  INITIALIZE CONSTANTS
32.     C
```

```
      C  DPSI IS THE INCREMENT IN STARTING ANGLE PSI.  RE IS THE RADIUS OF THE EARTH.
      C  ROP IS THE SATELLITE ALTITUDE.  DBIG IS A BIG NUMBER, USEFUL TO HAVE AROUND.
           DPSI=0.000173
           CALL PIOCS(14)
           DBIG=1.D50
           RE=6371.
           PI2=3.14159265/2
           ROP=1110.0
           ROP=ROP+RE
      C
      C  READ INPUT DATA
      C
      C  RO IS THE HEIGHT OF THE "TOP" OF THE ATMOSPHERE, SS IS SATELLITE SEPARATION,
      C  PSI IS THE INITIAL STARTING ANGLE, AND NUM IS THE NUMBER OF RAYS TO BE
      C  LAUNCHED.  NREAD IS A SUBROUTINE THAT READS THE N-PROFILE DATA.  K IS THE
      C  NUMBER OF RAYS SO FAR LAUNCHED.
           READ (5,500) RO,THPREC
           WRITE(6,500) RO,THPREC
           READ (5,500) SS,PSI
           WRITE(6,500) SS,PSI
           READ (5,160) NUM
           WRITE (6,160) NUM
           CALL NREAD
           RO=RO+RE
           RPSI=PSI
           R1=RE+80.0
           R2=RE+16.0
           K=1
     1     CONTINUE
           ACL1=0.0
           ABC1=0.0
      C  NCONT IS AN ENTRY IN NREAD.
           IF (K.NE.0) CALL NCONT
           PSI=RPSI
           K=0
      C  DELTH IS THE STEPPING VALUE IN THE RAYTRACING ROUTINE.
           DELTH=.0005
           WRITE (6,501) SS,RO,THPREC,PSI,DELTH
      C  THO IS THE LEFT-HALF CENTRAL ANGLE MEASURED AT THE SURFACE OF THE EARTH.
           THO= DARSIN(SS/(2*ROP*2))
      C
      C  DETERMINE RAYPATH PARAMETERS BETWEEN TRANSMITTING SATELLITE AND TOP EDGE OF
      C  ATMOSPHERE
      C
     4     CONTINUE
           BEGIN=.TRUE.
           DC=DCOS(THO-PSI)
           WRITE (6,43) ROP,RO,THO,PSI
           BANGO=ROP/RO*DC
           WRITE (6,44) BANGO
     43    FORMAT (' ',' ROP=',F12.7,'  RO=',F12.7,'  THO=',F12.7,
          *'  PSI=',F12.7)
     44    FORMAT (' TERM=',F12.7)
           TH1=-PI2-PSI+DARSIN(ROP/RO*DC)
           WRITE (6,45) TH1
     45    FORMAT (' TH1=',F12.7)
           AB=RO*DSIN(THO+TH1)/DC
      C
      C  RAYTRACING ROUTINE
      C
      C
      C  INITIALIZE RAYTRACING PARAMETERS
      C
      C  R AND TH ARE POLAR COORDINATES WITH ORIGIN AT THE CENTER OF THE EARTH.  H IS
      C  THE CLOSEST APPROACH ALTITUDE OF THE RAY.  SN IS THE EXCESS PATH LENGTH DUE
      C  TO RETARDATION.  C IS THE EXCESS PATH LENGTH DUE TO BENDING.  PH IS THE
      C  ANGLE BETWEEN THE POSITION VECTOR R AND THE RADIUS OF CURVATURE VECTOR RCU.
      C  NSTART IS AN ENTRY IN SUBROUTINE VNREAD.  NSET IS AN ENTRY IN SUBROUTINE
      C  NREAD.
           C=0.0D0
           PH=+TH1+PSI
           WRITE (6,616) PH
     616   FORMAT (' PH=',F12.7)
```

```
106.            R=R0
107.            TH=TH1
108.            H=R0
109.            SN = 0.0D0
110.            DELR = 0.0D0
111.            CALL NSTART(TH,THINDX)
112.            COSPHI = DCOS (PH)
113.            SINPHI = DSIN (PH)
114.            RS=RE+0.50
115.            CALL NSET
116.      C
117.      C  MAIN RAYTRACING LOOP
118.      C
119.      C  NSHIFT IN AN ENTRY IN SUBROUTINE NNREAD.  THINDX IS A PARAMETER ASSOCIATED
120.      C  WITH CALLING DATA FROM THE DISK.  N(R,TH) IS A CALL TO FUNCTION SUBROUTINE
121.      C  N, WHICH COMPUTES THE INDEX OF REFRACTION AT POSITION (R,TH) IF R IS GREATER
122.      C  THAN 4 KM OR LESS THAN 2 KM.  NN(R,TH) PERFORMS THE SAME FUNCTION FOR
123.      C  2<R<4 KM.
124.      20    CONTINUE
125.            IF (TH.GE.THINDX.AND. R.LE.6375.0) CALL NSHIFT (THINDX)
126.            DERIV=.FALSE.
127.            RDIS=0.50
128.      C
129.      C  COMPUTE DNDR AND DNDTH.  DNDTH=0 ABOVE 4 KM.
130.      C
131.            HGRAD = R.LE.6375.AND.R.GE.6373.
132.            IF (HGRAD) GO TO 40
133.            NI=N(R,TH)
134.            DNDTH=0.0D0
135.            IF (R.GE.RS) GO TO 50
136.            DNDR=(N(R,TH)-N(R+RDIS,TH))/RDIS
137.            GO TO 8
138.      40    NI=NN(R,TH)
139.            DNDTH=(NN(R,TH+THDIS)-NN(R,TH-THDIS))/(2*THDIS)
140.      50    CONTINUE
141.            IF (R.GE.6375.5.OR.R.LE.6372.5) GO TO 51
142.            IF (R.LE.6374.9.AND.R.GE.6373.1) GO TO 52
143.            IF (R.GE.6374) GO TO 54
144.            DNDR=(N(R-RDIS,TH)-NN(R+RDIS,TH))/(2*RDIS)
145.            GO TO 8
146.      54    DNDR=(NN(R-RDIS,TH)-N(R+RDIS,TH))/(2*RDIS)
147.            GO TO 8
148.      52    RDIS=1.0E
149.            DNDR=(NN(R-RDIS,TH)-NN(R+RDIS,TH))/(2*RDIS)
150.            GO TO 8
151.      51    DNDR=( N(R-RDIS,TH)- N(R+RDIS,TH))/(2*RDIS)
152.      8     CONTINUE
153.            DNDTH=0.0D0
154.      C
155.      C  COMPUTE ROH
156.      C  SPECIAL CASES EXIST FOR DNDR=0, IN WHICH CASE ROH=0.1E+8, AN APPROXIMATION TO
157.      C  INFINITY, AND FOR PH=0, A HORIZONTAL RAY, IN WHICH CASE DELR, THE INCREMENT
158.      C  IN R, MUST BE COMPUTED ACCORDING TO A SECOND-ORDER APPROXIMATION.  VARIABLES
159.      C  T AND P ARE DUMMY PARAMETERS FOR THE PLOTTING ROUTINE PLOT.
160.      C
161.            IF (DABS(DNDR).LE.1.0D-20) DERIV=.TRUE.
162.            RN = R*NI
163.            IF (C.NE.0) GO TO 2
164.            IF (DERIV) GO TO 62
165.            ROH = NI/(DNDR*COSPHI-SINPHI*DNDTH/R)
166.            GO TO 61
167.      60    ROH=0.1E+8
168.            WRITE (6,730) R,TH
169.      61    CONTINUE
170.            C=AH*(1.0-DCOS(PSI))
171.            WRITE (6,180) C
172.      2     CONTINUE
173.            IF (PH.NE.0.0D0) GO TO 22
174.            IF (DERIV) GO TO 62
175.            ROH = NI/(DNDR*COSPHI - SINPHI*DNDTH/R)
176.            GO TO 63
177.      62    ROH=0.1E+8
178.            WRITE (6,730) R,TH
```

```
      63    CONTINUE
            DELP = (R*DELTH**2)/2*(1.0D0-R/ROH)
            R = R + DELP
            TH = TH + DELTH
            IF (.NOT.PLOTR.OR.R.GT.R2) GO TO 20
            T=R*DSIN(TH)/R1
            P=R*DCOS(TH)-RE
            IF (P.GT.12.0.OR.P.LT.- 9.0) GO TO 20
            CALL PLOT (2,T,P)
            GO TO 20
      C
      C  CALCULATE DELPHI, ROH, DELSN, DELR, AND DELC
      C
      22    DELPHI = DELTH*(1.000-R/(COSPHI*ROH))
            IF (PGRAD) GO TO 21
            DELTH=0.0005
            GO TO 221
      21    DELTH=0.0001
      221   CONTINUE
            PH  = PH  + DELPHI
            COSPHI = DCOS(PH )
            SINPHI = DSIN(PH )
            IF (DERIV) GO TO 64
            ROH = NI/(ONDR*COSPHI + SINPHI*ONDTH/R)
            GO TO 65
      64    ROH=ORIG
            WRITE (6,730) R,TH
      65    CONTINUE
            DELS = R*DELTH/COSPHI
            DELC = DELS*(1.0D0-DCOS(TH-PH))
            DELR = DELS*SINPHI
            DELSN = (NI - 1.000) * DELS
            IF (DELS.EQ.0.0)  GO TO 23
      513   FORMAT (' ',3D15.7)
            TH = TH + DELTH
      615   FORMAT (' TH=',F12.7,'   P=',F12.7)
            C = C + DELC
            R = R + DELR
      C
      C  IF THE RAY STRIKES THE SURFACE OF THE EARTH, STOP RAYTRACING
      C
            IF (R.GE.RE) GO TO 300
            PSI=PSI+DPSI
            NUM=NUM-1
            WRITE (6,103) R,NUM
            GO TO 4
      C
      C  CALL PLOTTING ROUTINES
      C
      300   CONTINUE
            IF (.NOT.PLOTR.OR.R.GT.R2) GO TO 5
            IF (.NOT.BEGIN) GO TO 10
            T=R*DSIN(TH)/R1
            P=R*DCOS(TH)-RE
            IF (P.GT.12.0.OR.P.LT.- 9.0) GO TO 5
            CALL PLOT(1,T,P)
            BEGIN=.FALSE.
            GO TO 5
      10    CONTINUE
            T=R*DSIN(TH)/R1
            P=R*DCOS(TH)-RE
            IF (P.GT.12.0.OR.P.LT.- 9.0) GO TO 5
            CALL PLOT (2,T,P)
      5     CONTINUE
            SN = SN + DELSN
      C
      C  IF THE RAY IS AT THE TOP OF THE ATMOSPHERE, STOP RAYTRACING AND PROCEED
      C  WITH LINEAR INTERPOLATION
      C
            IF (R.GE.RO) GO TO 6
            IF (R.GE.H) GO TO 20
            THC=TH
            H=R
```

```
      GO TO 20
C
C  END OF RAYTRACING ROUTINE
C
C
C  CALCULATE RAYPATH PARAMETERS BY LINEAR INTERPOLATION FROM POINT AT WHICH
C  RAY LEAVES ATMOSPHERE TO POINT AT WHICH IT INTERSECTS SATELLITE ORBIT
C
23    TH = TH + DELTH
      WRITE (6,720) DELS
      R = R + DELR
      C = C + DELC
      SN = SN + DELSN
6     R1=R-DELR
      R=R-DELR
      TH=TH-DELTH
      SN1=SN-DELSN
      C1=C-DELC
      THI=TH-DELTH
      SLOPE=(DELR*DCOS(THI)-R*DELTH*DSIN(THI))
      SLOPE=SLOPE/(R*DELTH*DCOS(THI)+DELR*DSIN(THI))
      WRITE (6,175) R1,THI
175   FORMAT (' R1=',F12.6,5X,'THI=',F12.6)
      ABE=DELR*DCOS(THI)
      ABF=R*DELTH*DSIN(THI)
      ABG=R*DELTH*DCOS(THI)
      ABH=DELR*DSIN(THI)
      ABI=ABE-ABF
      ABJ=ABG+ABH
      WRITE (6,173) ABE,ABF,ABG,ABH,ABI,ABJ
      DELRP=R0-R1
      DELTHP=DELTH*(DELRP/DELR)
      RP=R1+DELRP/2.
      DELSP=RP*RP*N(RP,THI)*DELTHP/RN
      C=N(RP,THI)
      DELSNP=(N(RP,THI)-1.000)*DELSP
      THP=THI+DELTHP
      DELCP=DELSP-(DSQRT(DELSP**2-DELRP**2)*DCOS(THP)+DELRP*DSIN(THP))
      EP=DATAN(-SLOPE)
      KON=(RP*(DCOS(THP)-SLOPE*DSIN(THP)))/RDP
      THD=DARSIN((DSQRT(1.DO+SLOPE**2-KON**2)-KON*SLOPE)/(1.+SLOPE**2))
      DLP=(RDP*DSIN(THD)-RP*DSIN(THP))*((1.DO/DCOS(EP))-1.DO)
      WRITE (6,180) C1,DELCP,DLP
      DELL=1000.*(C1+DELCP+DLP)
      WRITE (6,173) THD,EP,SLOPE,KON,THP,DELTHP
      ABA=DSIN(THD)
      ABB=DSIN(THP)
      ABC=RDP*ABA-RP*ABB
      ABD=1.DO/DCOS(EP)-1.DO
      WRITE (6,173) ABA,ABB,ABC,ABD,R,DELR
      ABE=DCOS(THI)
      ABF=DSIN(THI)
      WRITE (6,173) ABE,ABF,DELRP
173   FORMAT (6(D12.5,5X))
180   FORMAT ('DC1=',D12.5,'    DELCP=',D12.5,'    DLP=',D12.5)
      RD=1000.*(SN1+DELSNP)
      E=EP
      IF (E.LE.0.0) DELL=0.0
      IF (RD.LE.0.0) RD=0.0
      IF (E.LE.0.0) E=0.0
      TD1=THD*57.29578
      TD2=THD*57.29578
      ED1=PSI*57.29578
      ED2=E*57.29578
      ACL=2*RDP*DSIN(0.5*(THD+THD))
      HD=RDP*DCOS(0.5*(THD+THD)) - RE
      PHDFT=DELL+RD
      H=H-9E
      DELH=H-HD
      ET=(E+PSI)*3000.
      I=K+1
C
C  SAVE AND WRITE RESULTS
C
```

```
            B(I)=PHDFT
            RD2(I)=ACL
            DELR=ACL-ACL1
            ABC=ACL+DELL/1000.0
            IF (ACL1.EQ.0) GO TO 24
            DELS=(ABC+ABC1)/2
            DB(I)=  -10*DLOG10(DABS(DELR)/(DELS*DPSI))
            WRITE (6,102) I,DB(I)
   24       CONTINUE
            ACL1=ACL
            ABC1=ABC
            WRITE (6,100) IFLY,PSI
            WRITE (6,110) TD1,TD2,ACL,DELL,RD,PHDFT,H,HO,DELH,ED1,ED2,ET,THC
            IF (.NOT.PLOTP) GO TO 3
            SEP(1,K+1)=H
            SEP(2,K+1)=ACL
    3       CONTINUE
            PSI=PSI+DPSI
            TH2=THO
            K=K+1
C
C  REPEAT RAYTRACING AT NEW STARTING ANGLE PSI
C
            IF (K.LT.NUM) GO TO 4
            IF (.NOT.PLOTP) GO TO 7
            TH=0.070+4/85.5
            R=6410.0
            T=R*DSIN(TH)/RI
            P=R*DCOS(TH)-RE
            CALL PLOT (1,T,P)
    7       CONTINUE
C
C  SEARCH FOR MULTIPATH
C
            CALL PHASOR (RD2,DB,B,NUM)
            IF (.NOT.PLOTP) GO TO 11
            CALL RAMR
            XS=9.5/120
            YS=8.0/5
            CALL SCALE (XS,YS,7900.0,-1.25)
            CALL CHAR (7900.0,-1.0,0.10,0.10,0)
            WRITE (14,101) IFLY
            CALL PLOT (1,7900.0,0.0)
            CALL PLOT (2,7900.0,5.0)
            CALL PLOT (1,SEP(2,NUM),SEP(1,NUM))
            DO 9 I=1,NUM
            K=NUM-I+1
    9        CALL PLOT (2,SEP(2,K),SEP(1,K))
            CALL PLOT (1,8040.0,0.0)
   11       CONTINUE
            IF (PLOTPH) CALL PHPLOT (RD2,B,NUM)
            IF (PLOTDB) CALL DBPLOT (RD2,DB,NUM)
            GO TO 1
  100       FORMAT ('0FLIGHT NO.',A4,'  STARTING ANGLE',F10.6,' RAD.')
  101       FORMAT (A4)
  102       FORMAT (I5,F15.6)
  103       FORMAT (' R LESS THAN RE'//' R=',F12.6/' NEW NUM=',I6)
  110       FORMAT('0CENTRAL ANGLE 1='F10.5,' DEG.',9X, 'CENTRAL ANGLE 2=',F10
           #.5,' DEG.',10X,'ST. LINE PATH=',F12.5,' KM.',/' BENDING=',F9.3,'
           #M.',10X,'RETARDATION=',F9.3,' M.',17X,'PHASE DEFECT=',F9.3,' M.',/
           #' ACTUAL RAY HEIGHT=',F8.3,' KM.',10X,'APPARENT RAY HEIGHT=',F8.3,
           #' KM.', 9X,'DELTA H=',F9.3,' KM.',/' BENDING ANGLE1=',F11.8,' DEG.
           #',9X,'BENDING ANGLE2=',F11.8,' DEG.',10X,'TOTAL BENDING ANGLE=',F1
           #1.5,' MR. ',/' ANGULAR ERROR=     ',F8.4,' MR.'/)
  160       FORMAT (I2,2I3)
  500       FORMAT (5F10.6)
  501       FORMAT ('1SS=',F15.8,'  RO=',F18.8,'   THPREC=',F15.8,
           *'  PSI=',F15.8,' DELTH=',F15.8//)
  502       FORMAT (' ITERATION NO.',I4,'  U=',F15.8,'  TH1=',F15.8)
  503       FORMAT (5F15.6)
  720       FORMAT ('0DELS=',D20.13)
  730       FORMAT (' DNDR=',D20.13,  R=',F15.8,'  TH=',F15.8)
            END
C
```

```
      C
      C*****************************************************************************
      C
      C
            SUBROUTINE NREAD
      C
      C  THIS SUBROUTINE INPUTS DATA TO THE PROGRAM AND INITIALIZES SOME
      C  VARIABLES
      C
            REAL*8 RRDIS
            REAL N1(125),H(3),HR(3)
            REAL RL(4)
            INTEGER IH(3)
            LOGICAL PLOTR,PLOTP,PLOTPH,PLOTDB
            COMMON /FLY/IFLY,PLOTR,PLOTP,PLOTPH,PLOTDB
            COMMON /NTRAN/N1,H,HR,RMIN,RDIS,R,IH,INDEX
            DATA R1/6379.0/,RE/6371.0/
            DATA RL/6371.0,6373.0,6375.0,6387.0/
      C
      C  READ STANDARD ATMOSPHERE N-PROFILE, N1(I)
      C
      C  H(I) GIVES THE LOWER ALTITUDE AT WHICH THE VERTICAL RESOLUTION OF THE
      C  DATA CHANGES.  HR(I) GIVES THE RESOLUTION ABOVE ALTITUDE H(I).
      C  IH(I) GIVES THE INDEX NUMBER OF ARRAY N1(I) AT WHICH THE RESOLUTION
      C  CHANGES.
            READ (5,101) (H(I),HR(I),IH(I),I=1,3)
            WRITE(6,101) (H(I),HR(I),IH(I),I=1,3)
            READ (5,100) (N1(I),I=1,125)
            WRITE(6,102) (N1(I),I=1,125)
            A=N1(17)
            B=N1(9)
      C
      C
            ENTRY NCONT
      C  PLOTR, PLOTP, PLOTPH AND PLOTDB CONTROL PLOTTING ROUTINES.
            READ (5,105,END=2) PLOTR,PLOTP
            WRITE (6,105) PLOTR,PLOTP
            READ (5,105) PLOTPH,PLOTDB
            WRITE (6,105) PLOTPH,PLOTDB
      C  SUBROUTINE NNREAD INPUTS AND MANIPULATES THE HAWAII DATA.
            CALL NNREAD(A)
            IF (.NOT.PLOTR) GO TO 3
            CALL PAML
            CALL SCALE (25.5,1.43,-0.07),12.0)
            CALL CHAR (-0.065,9.1,0.25,0.29,0)
            WRITE (14,104) IFLY
            DO 12 J=1,3
            THT=-0.07
      10    THT=THT+0.001
            RT=RL(J)
            T=RT*SIN(THT)/R1
            P=RT*COS(THT)-RE
            IF (P.GT.12.0.OR.P.LT.-9.0) GO TO 10
            CALL PLOT(1,T,P)
            DO 12 I=1,140
            THT=THT+0.001
            T=RT*SIN(THT)/R1
            P=RT*COS(THT)-RE
            IF (P.GT.12.0.OR.P.LT.-9.0) GO TO 12
            CALL PLOT (2,T,P)
      12    CONTINUE
      3     CONTINUE
      C
      C
            ENTRY NSET
            RMIN=H(3)
            RDIS=HR(3)
            INDEX=IH(3)
            RETURN
      2     CONTINUE
            REWIND 80
            STOP
      100   FORMAT (8E10.6)
      101   FORMAT (2E10.6,I5)
```

```
      102   FORMAT (' ',8F10.6)
      104   FORMAT ('FLIGHT  ',A4)
      105   FORMAT (2L10)
            END
C
C
C*************************************************************************
C
C
            REAL FUNCTION N*8(R,TH)
C
C  THIS SUBROUTINE COMPUTES THE INDEX OF REFRACTION FOR THE REGION
C  ABOVE 4 KM AND BELOW 2 KM
C
            REAL*8 R,TH,RA,RAP,RDIS,RR/6373.000/,NN
            REAL N2(125),H(3),HR(3),RE/6371.0/
            INTEGER IH(3)
            COMMON /NTRAN/N2,H,HR,RMIN,RDIS,R,IH,INDEX
            RA=R-RE
            J=1
            DO 2 I=1,2
            II=4-I
            IF (RA.LT.H(II)) GO TO 2
            J=II
            GO TO 3
      2     CONTINUE
      3     CONTINUE
            RMIN=H(J)
            RDIS=HR(J)
            INDEX=IH(J)
      1     CONTINUE
            I=IDINT((RA-RMIN)/RDIS)+INDEX
            RAP=RDIS*(I-INDEX)+RMIN
            J=I+1
            N=N2(I)+(RA-RAP)*(N2(J)-N2(I))/RDIS
C
C  IF ALTITUDE LESS THAN 2 KM, OFFSET N-VALUE WITH VALUE AT 2 KM
C
            IF (RA.GT.2.0) GO TO 4
            N=N-R+(NN(RR,TH)-1.0D0)*1.D6
      4     CONTINUE
            N=1.000+N*1.D-6
            RETURN
            END
C
C
C*************************************************************************
C
C
            REAL FUNCTION NN*8(R,TH)
C
C  THIS SUBROUTINE COMPUTES THE INDEX OF REFRACTION FOR THE REGION
C  BETWEEN 2 AND 4 KM
C
            REAL*8 R,TH,N21,N22,THDIS,RDIS,RMIN,N
            REAL*8 RA,RAP,CBLE
            REAL N2(40,20),RRIS/0.05/
            INTEGER PNT,TIMES
            COMMON      THDIS,THMIN,N2
            THA=TH-THMIN
            RA=R-6373.0
            I=IDINT(RA/RRIS)+1
            RAP=RRIS*(I-1)
            J=I+1
            I=MIN0(I,40)
            J=MIN0(J,40)
            K=IDINT(THA/THDIS)+1
            K=MAX0(K,1)
            K=MIN0(K,20)
            N21=N2(I,K)+(RA-RAP)*(N2(J,K)-N2(I,K))/RRIS
            K1 = K + 1
            K1 = MIN0(K1,20)
            N22=N2(I,K1)+(RA-RAP)*(N2(J,K1)-N2(I,K1))/RRIS
            N=N21+(N22-N21)*(THA-(K-1)*THDIS)/THDIS
```

```
548.      100   FORMAT (3020.6)
549.            NN=1.000+N*1.D-6
550.            RETURN
551.            END
552.      C
553.      C
554.      C*****************************************************************************
555.      C
556.      C
557.            SUBROUTINE NNREAD(NBASE)
558.      C
559.      C  THIS SUBROUTINE INPUTS AND MANIPULATES HAWAII DATA.  THE HAWAII
560.      C  DATA IS READ FROM TAPE, WRITTEN ON DISK, AND ACCESSED FROM DISK
561.      C  WHEN REQUIRED.  UNIT NO. 80 REFERS TO 9-TRACK MAG TAPE.  UNIT
562.      C  NOS. 20 AND 21 REFER TO DISK (CALLED "RAD" IN SIGMA 5 TERMINOLOGY)
563.      C
564.            REAL*8 RDIS,THDIS,RMIN,TH
565.            REAL N1(40,20),NBASE
566.            REAL N(40,20)
567.            LOGICAL PRINT
568.            EQUIVALENCE (N1,N),(LRANGE,NUM)
569.            COMMON      THDIS,THMIN,N1
570.            COMMON /FLY/IFLY
571.            WRITE (1,100)
572.            WRITE (6,108) NBASE
573.      C  IFLY IDENTIFIES FLIGHT NUMBER.  MRANGE IS THE HORIZONTAL NUMBER OF
574.      C  DATA POINTS IN THE HAWAII DATA ARRAY.  LRANGE IS THE TOTAL NUMBER
575.      C  OF HORIZONTAL DATA POINTS.
576.      8     READ (80,107,END=9) IFLY
577.            WRITE (6,107) IFLY
578.            READ(80,100) MRANGE
579.            WRITE (6,100) MRANGE
580.            READ(80,100) LRANGE
581.            WRITE (6,100) LRANGE
582.            RDIS=.05
583.            THDIS=150/(5371.*MRANGE)
584.            THMIN=-THDIS*LRANGE/2
585.            WRITE (6,103)
586.            READ (1,110) PRINT
587.            READ(80,101) ((N(I,J),I=1,40),J=1,20)
588.            IF (PRINT) WRITE (6,101) ((N(I,J),I=1,40),J=1,20)
589.            DO 3 I=1,40
590.            DO 3 J=1,20
591.      3     N(I,J)=N(I,J)+NBASE
592.      C  RADREW, RADWRT AND RADRD REWIND, WRITE ON AND READ FROM, RESPECTIVELY,
593.      C  THE DISK
594.            CALL RADREW(20)
595.            CALL RADWRT (20,N,800,0,&500,&501)
596.            INDEX=(NUM-20)/17
597.            IF (INDEX.LT.1) GO TO 12
598.            CALL RADREW(21)
599.            DO 11 K=1,INDEX
600.            DO 21 I=1,40
601.            N(I,1)=N(I,18)
602.            N(I,2)=N(I,19)
603.      21    N(I,3)=N(I,20)
604.            READ(80,101) ((N(I,J),I=1,40),J=4,20)
605.            IF (PRINT) WRITE (6,101) ((N(I,J),I=1,40),J=4,20)
606.            DO 5 I=1,40
607.            DO 5 J=4,20
608.      5     N(I,J)=N(I,J)+NBASE
609.      11    CALL RADWRT (21,N,680,0,&502,&503)
610.      12    KREM=NUM-(INDEX*17+20)
611.            IF (KREM.EQ.0) RETURN
612.            DO 4 I=1,40
613.            N(I,1)=N(I,18)
614.            N(I,2)=N(I,19)
615.      4     N(I,3)=N(I,20)
616.              KREM=KREM+3
617.            READ(80,101) ((N(I,J),I=1,40),J=4,KREM)
618.            IF (PRINT) WRITE (6,101) ((N(I,J),I=1,40),J=4,KREM)
619.            KKK=KREM+1
620.            DO 7 I=1,40
621.            DO 7 J=KKK,20
```

```
      7     N(I,J)=NBASE
            DO 6 I=1,40
            DO 6 J=4,KREM
      6     N(I,J)=N(I,J)+NBASE
            CALL RADWRT (21,N,680,0,&504,&505)
            RETURN
      500   NN=1
            GO TO 600
      501   NN=1
            GO TO 601
      502   NN=2
            GO TO 600
      503   NN=2
            GO TO 601
      504   NN=3
            GO TO 600
      505   NN=3
            GO TO 601
      600   WRITE (6,200) NN
            STOP
      601   WRITE (6,201) NN
            STOP
      C
      C
            ENTRY NSTART (TH,THINDX)
      C  NSTART READS THE INITIAL SET OF N-VALUES FROM THE DISK INTO CORE.
            THMIN=-THDIS*LRANGE/2
            THA=17*THDIS
            THINDX=THMIN+THA
            IF (TH.GE.THINDX) GO TO 1
            CALL RADREW (21)
            CALL RADRD (20,N,800,0,&400,&401)
            CALL RADREW (21)
            GO TO 13
      1     CALL RADREW (21)
            IND=(TH-THMIN)/THA
            DO 2 I=1,IND
      2     CALL RADRD (21,N,680,0,&400,&401)
            THINDX=THINDX+THA*IND
            THMIN=THINDX-THA
            GO TO 13
      400   WRITE (6,300)
            RETURN
      401   WRITE (6,301)
            RETURN
      C
      C
            ENTRY NSHIFT(THINDX)
      C NSHIFT READS THE NEXT SET OF N-VALUES FROM THE DISK INTO CORE
            THMIN=THINDX
            THINDX=THINDX+THDIS*17
            CALL RADRD  (21,N,680,0,&506,&507)
      13    CONTINUE
            RETURN
      506   WRITE (6,202)
            RETURN
      507   WRITE (6,203)
            RETURN
      100   FORMAT (I4)
      101   FORMAT (2(16F5.1/),8F5.1)
      102   FORMAT  (I5,5X,F10.6)
      103   FORMAT ('1',10X,'INPUT DATA'//)
      104   FORMAT (F10.6)
      106   FORMAT ('1',40(' ',5(F10.6,5X)/))
      107   FORMAT (A4)
      108   FORMAT (' NBASE=',F12.6)
      109   FORMAT ('PRINT?  FORMAT L2')
      110   FORMAT (L2)
      200   FORMAT (' ERROR IN RADWRT STATEMENT  NO.',I4)
      201   FORMAT (' EOF ENCOUNTERED IN RADWRT STATEMENT NO.',I4)
      202   FORMAT (' ERROR IN RADRD')
      203   FORMAT (' EOF ENCOUNTERED IN RADRD')
      300   FORMAT (' ERROR IN INITIAL RADRD')
```

```
      301   FORMAT (' EOF ENCOUNTERED IN INITIAL RADPD')
            END
      C
      C
      C*****************************************************************************
      C
      C
            SUBROUTINE PHASOR (H,DB,PH,ITER)
      C
      C  THIS SUBROUTINE INTERPOLATES RECEIVED PHASE DEFECT AND POWER AT
      C  1 KM INTERVALS IN SATELLITE SEPARATION.  IF A MULTIPATH IS DETECTED,
      C  THE SEPARATE AND COMBINED VALUES AT EACH 1 KM INTERVAL ARE PRINTED.
      C
            DIMENSION H(ITER),DB(ITER),PH(ITER),PHD(14),DBD(14)
            COMPLEX E,ET
            REAL TWOPI/6.283185/
            COMMON /FLY/ IFLY
            PHASE(P)=AMOD(P,0.032)/0.032*TWOPI
            DB(1)=DB(2)
            DO 10 I=1,ITER
      10    WRITE (6,104) I,H(I),DB(I),PH(I)
            HMIN=1.E9
            HMAX=-1.E8
            DO 1 I=1,ITER
            HH=H(I)
            IF (HH.LE.HMIN) HMIN=HH
      1     IF (HH.GE.HMAX) HMAX=HH
            GH=AINT(HMAX)
            WRITE (6,105) HMIN,HMAX,GH
            WRITE (6,100) IFLY
            WRITE (6,102)
            WRITE (6,103)
      7     HH=H(1)
            NN=0
            ET=0.0
            DO 4 I=2,ITER
            HM=H(I)
            IF (HH.LT.HM) GO TO 5
            IF (GH.GT.HH.OR.GH.LT.HM) GO TO 6
      8     CONTINUE
            NN=NN+1
            PP1=PH(I-1)
            PP2=PH(I)
            DB1=DB(I-1)
            DB2=DB(I)
            FAC=(GH-HH)/(HM-HH)
            DBD(NN)=DB1+(DB2-DB1)*FAC
            VOLT=10**(DBD(NN)/20)
            P1=PHASE(PP1)
            P2=PHASE(PP2)
            P=P1+(P2-P1)*FAC
            E=CMPLX(VOLT*COS(P),VOLT*SIN(P))
            ET=ET+E
            PHD(NN)=PP1+(PP2-PP1)*FAC
      6     HH=HM
            GO TO 4
      5     IF (GH.LT.HH.OR.GH.GT.HM) GO TO 6
            GO TO 8
      4     CONTINUE
            IF (CABS(ET).LE.0) GO TO 3
            VOLT=20*ALOG10(CABS(ET))
            GO TO 9
      3     VOLT=1.E-8
      9     CONTINUE
            P=ATAN2(AIMAG(ET),REAL(ET))
            P=P*180/3.1415926
            IF (NN.LE.1) GO TO 2
            WRITE (6,101) GH,VOLT,P,NN,(PHD(I),I=1,NN)
            WRITE (6,106) (DBD(I),I=1,NN)
      2     GH=GH-1
            IF (GH.GE.HMIN) GO TO 7
            RETURN
      100   FORMAT ('1',22X,'RECEIVED SIGNAL',5X,A4//)
      101   FORMAT (F6.1,5X,F11.5,4X,F6.2,I9,5X,7F10.3/46X,7F10.3)
```

```
      102   FORMAT ('   SAT SEP    REL SIG AMP  ANGLE   NO. OF RAYS',
     *10X,'PHASE DEFECT (ABOVE) AND POWER (BELOW)')
      103   FORMAT  ('      (KM)   ',7X,'(DB)',5X,'(DEG)',35X,'(METERS AND DB)')
      104   FORMAT (I5,3F15.4)
      105   FORMAT (' HMIN=',F10.4,' HMAX=',F10.4,' GH=',F10.4)
      106   FORMAT (2(46X,7F10.3))
      107   FORMAT (' ')
            END
C
C
C*****************************************************************************
C
C
            SUBROUTINE PHPLOT (RD,B,J)
C
C  THIS SUBROUTINE PLOTS PHASE DEFECT AS A FUNCTION OF SATELLITE
C  SEPARATION
C
            DIMENSION RD(J),B(J)
            COMMON /FLY/ IFLY
            X0=8.0/1400
            Y0=9.0/150
            YY=7900.0+8050.0
            CALL RAML
            CALL SCALE (X0,Y0,100.0,8050.0)
            CALL CHAR (300.0,8040.0,.2,.2,0)
            WRITE (14,104) IFLY
            CALL CHAR (100.0,8040.0,.1,.1,0)
            WRITE (14,101)
            CALL GRID (3,200.0,8050.0,10.0,15)
            CALL CHAR (100.0,7898.0,.1,.1,0)
            WRITE (14,100)
            CALL CHAR (150.0,7895.0,.1,.1,0)
            WRITE (14,102)
            CALL GRID (0,200.0,7900.0,100.0,14)
            CALL CHAR (1550.0,7895.0,.1,.1,0)
            WRITE (14,103)
            Y=YY-B(1)
            IF (Y.LT.7900.0) Y=7900.0
            IF (Y.GT.8050.0) Y=8050.0
            CALL PLOT (1,B(1),Y)
            CALL POINT (9)
            DO 1 I=2,J
            Y=YY-B(I)
            IF (Y.LT.7900.0) Y=7900.0
            IF (Y.GT.8050.0) Y=8050.0
            CALL PLOT (0,B(I),Y)
            CALL POINT(2)
    1       CONTINUE
            X=1600.0*2.0/X0
            CALL PLOT (1,X,8050.0)
            RETURN
      100   FORMAT ('8050')
      101   FORMAT ('7900')
      102   FORMAT ('200')
      103   FORMAT ('1600')
      104   FORMAT (A10,5X,'PHASE')
            END
C
C
C*****************************************************************************
C
C
            SUBROUTINE DBPLOT (RD,DB,J)
C
C  THIS SUBROUTINE PLOTS RECEIVED POWER AS A FUNCTION OF SATELLITE
C  SEPARATION
C
            DIMENSION RD(J),DB(J)
            COMMON /FLY/ IFLY
            X0=8.0/30
            Y0=9.0/150
            YY=7900.0+8050.0
            CALL RAML
```

```
843.            CALL SCALE (XO,YO,-30.0,8050.0)
844.            CALL CHAR (-25.0,8040.0,.2,.2,0)
845.            WRITE (14,104)IFLY
846.            CALL CHAR (-32.0,8048.0,.1,.1,0)
847.            WRITE (14,101)
848.            CALL GRID (3,-30.0,8050.0,10.0,15)
849.            CALL CHAR (-32.0,7898.0,.1,.1,0)
850.            WRITE (14,100)
851.            CALL CHAR (-30.5,7895.0,.1,.1,0)
852.            WRITE (14,102)
853.            CALL GRID (0,-30.0,7900.0,5.0,6)
854.            CALL CHAR (-0.5,7895.0,.1,.1,0)
855.            WRITE (14,103)
856.            Y=YY-80(2)
857.            IF (Y.LT.7900.0) Y=7900.0
858.            IF (Y.GT.8050.0) Y=8050.0
859.            CALL PLOT (1,DB(2),Y)
860.            CALL POINT (9)
861.            DO 1 I=3,J
862.            Y=YY-80(I)
863.            IF (Y.LT.7900.0) Y=7900.0
864.            IF (Y.GT.8050.0) Y=8050.0
865.            CALL PLOT (0,DB(I),Y)
866.            CALL POINT (2)
867.    1       CONTINUE
868.            X=2.0/XO
869.            CALL PLOT (1,X,8050.0)
870.            RETURN
871.    100     FORMAT ('8050')
872.    101     FORMAT ('7900')
873.    102     FORMAT ('-30')
874.    103     FORMAT ('  0')
875.    104     FORMAT (A10,5X,'POWER')
876.            END
877.    C
878.    C
879.    C*****************************************************************************
880.    C
881.    C
882.     OLOAD (GO),(MAP,PROG),(UDC#,2)
883.    :INCLUDE (P:XYPLT)
884.    :ASSIGN (F:20,BT,X1)
885.    :ASSIGN (F:21,BT,X2)
886.     ALLOBT (FILE,X1),(FSIZE,1),(RSIZE,800)
887.     ALLOBT (FILE,X2),(FSIZE,46),(RSIZE,680)
888.     RUN
889.    69.0            1.0-7
890.    7925.000   .007
891.    30
892.    0.000      0.250          1
893.    11.000     0.500          45
894.    32.000     1.000          87
895.        0.0000   341.3928    0.2500   327.3831    0.5000   314.5356    0.7500   302.4658
896.        1.0000   292.0496    1.2500   282.0127    1.5000   271.5203    1.7500   262.3286
897.        2.0000   253.1508    2.2500   244.3950    2.5000   236.6477    2.7500   226.9707
898.        3.0000   219.8244    3.2500   212.6913    3.5000   205.5858    3.7500   199.4466
899.        4.0000   192.8675    4.2500   186.7807    4.5000   181.2256    4.7500   175.7153
900.        5.0000   170.2479    5.2500   165.0793    5.5000   160.2175    5.7500   155.4059
901.        6.0000   151.3403    6.2500   146.1870    6.5000   141.7899    6.7500   137.6058
902.        7.0000   133.4915    7.2500   129.4621    7.5000   125.6156    7.7500   121.9384
903.        8.0000   118.1977    8.2500   113.5425    8.5000   110.4382    8.7500   107.4028
904.        9.0000   104.4268    9.2500   101.5135    9.5000    98.6651    9.7500    95.8756
905.       10.0000    93.1453   10.2500    90.4742   10.5000    87.8614   10.7500    85.3063
906.       11.0000    82.8077   11.5000    77.9737   12.0000    73.3565   12.5000    68.9497
907.       13.0000    64.7463   13.5000    60.7403   14.0000    56.9248   14.5000    53.2913
908.       15.0000    49.8390   15.5000    46.5588   16.0000    43.4429   16.5000    40.4898
909.       17.0000    36.8699   17.5000    33.4527   18.0000    30.3727   18.5000    27.6086
910.       19.0000    25.1183   19.5000    22.8748   20.0000    20.8505   20.5000    19.0221
911.       21.0000    17.3683   21.5000    15.8726   22.0000    14.5178   22.5000    13.3285
912.       23.0000    12.2555   23.5000    11.2736   24.0000    10.3747   24.5000     9.5514
913.       25.0000     8.7970   25.5000     8.1059   26.0000     7.4716   26.5000     6.8898
914.       27.0000     6.3557   27.5000     5.8653   28.0000     5.4148   28.5000     5.0011
915.       29.0000     4.6205   29.5000     4.2704   30.0000     3.9150   30.5000     3.7321
916.       31.0000     3.4531   31.5000     3.1962   32.0000     2.9595   33.0000     2.5401
917.       34.0000     2.1830   35.0000     1.8787   36.0000     1.6190   37.0000     1.3971
```

```
916.        38.0000     1.2071    39.0000     1.0442    40.0000     0.9045    41.0000     0.7845
919.        42.0000     0.6811    43.0000     0.5921    44.0000     0.5153    45.0000     0.4490
920.        46.0000     0.3917    47.0000     0.3421    48.0000     0.3002    49.0000     0.2646
921.        50.0000     0.2331    51.0000     0.2054    52.0000     0.1816    53.0000     0.1611
922.        54.0000     0.1427    55.0000     0.1264    56.0000     0.1118    57.0000     0.0988
923.        58.0000     0.0872    59.0000     0.0769    60.0000     0.0679    61.0000     0.0601
924.        62.0000     0.0531    63.0000     0.0468    64.0000     0.0412    65.0000     0.0362
925.        66.0000     0.0317    67.0000     0.0278    68.0000     0.0243    69.0000     0.0212
926.        70.0000     0.0184
927.   PLOT        NO
928.   PLOT        PLOT
929.   PLOT        NO
930.   PLOT        PLOT
931.   PLOT        NO
932.   PLOT        PLOT
933.   PLOT        NO
934.   PLOT        PLOT
935.   PLOT        NO
936.   PLOT        PLOT
937.    FIN
```

Appendix C

DESCRIPTION OF RAYTRACING PROGRAMS

1. Description of RAYTRACE

The technique used in RAYTRACE is based on Snell's Law, which can be written as [5]

$$\frac{\lambda}{\rho} = \frac{d\lambda}{d\rho} \tag{C.1}$$

where λ is the wavelength in the medium and ρ is the radius of curvature of the path followed by the ray through the medium. Now,

$$\lambda = \frac{c}{n\nu} \tag{C.2}$$

where n is the index of refraction of the medium, c is the speed of light in a vacuum, and ν is the frequency of the wave. Therefore,

$$d\lambda = -\frac{c}{n^2\nu}\, dn \tag{C.3}$$

and

$$\frac{\lambda}{\rho} = \frac{c}{n\nu\rho} = -\frac{c}{n^2\nu}\frac{dn}{d\rho} = \frac{d\lambda}{d\rho}$$

$$\frac{1}{\rho} = -\frac{1}{n}\frac{dn}{d\rho}$$

$$\rho = -\frac{n}{dn/d\rho} \tag{C.4}$$

The total derivative $dn/d\rho$ can be written as (see Fig. 59)

$$\frac{dn}{d\rho} = \vec{\nabla}n \cdot \frac{\vec{\rho}}{|\rho|} = -\left|\frac{dn}{dr}\right| \cos \phi + \frac{1}{r}\frac{dn}{d\theta} \sin \phi$$

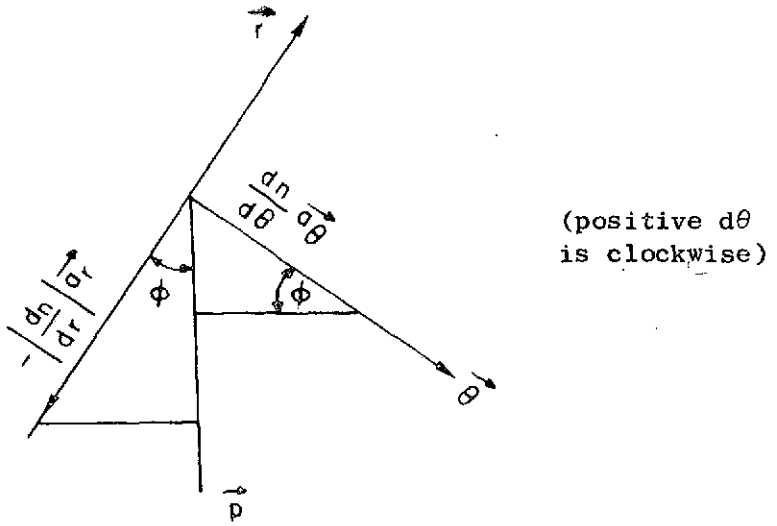

Fig. 59. COORDINATE SYSTEM AND RELATIONSHIP OF ρ TO dn/dr AND $dn/d\theta$.

where r and θ are polar coordinates with origin at the center of the Earth, and ϕ is the angle between $\vec{\rho}$ (the radius of curvature) and $\vec{r}$ (the radius vector). Note that, for $\vec{r}$ pointed outward, dn/dr is negative for a normal atmosphere. Now, ρ can be written as

$$\rho = \frac{n}{|dn/dr| \cos \phi - (1/r)(dn/d\theta) \sin \phi} \qquad (C.5)$$

The first term in the denominator is the effect of vertical gradients on the raypath; the second term is the effect of horizontal gradients and is usually much smaller than the first term.

The program operates as follows. An "atmosphere" is given to the computer in the form of a temperature profile (temperature vs altitude) and surface values of total pressure and water-vapor pressure. From this information, the program calculates values of N (the refractivity) for a grid representing a vertical slice of atmosphere. Grid points are spaced vertically 1 km apart to a height of 90 km and horizontally every 15 mrad for a total horizontal spread of 300 mrad, centered at $\theta = 0$.

Starting at $\theta = 0$, the program calculates the values of the derivatives dn/dr and $dn/d\theta$, determines the angle ϕ between the

radius of curvature $\vec{\rho}$ and the radius vector $\vec{r}$, and uses this information to calculate the magnitude of the radius of curvature ρ. The program steps off an increment $d\theta$ of 0.5 mrad, with ρ held constant, and computes the resulting increment in r. The new values of r and θ are then used to calculate a new ρ, and the process is repeated until the ray reaches a height of approximately 65 km. At this point, a linear approximation is used to complete the raypath to the satellite altitude. The program returns to the $\theta = 0$ position and repeats its calculations for the other half of the raypath. A running tally of path length and deviation of path length from that of a straight line is maintained. These tallies are used at the end of the run to calculate the phase defect that would result from such a raypath. The above procedure is repeated in each run for starting altitudes (at $\theta = 0$) of 0 to 30 km, at 1 km intervals.

The equations used to determine ϕ, r, S (path length) and C (path deviation) are given below.

For the first step (at $\theta = \phi = 0$), a second-order approximation is necessary:

$$\Delta r_1 = \frac{r_o(\Delta\theta)^2}{2\left[1 - (r_o/\rho_o)\right]} \qquad (C.6)$$

The program now steps to the point $(r + \Delta r, \theta + \Delta r)$ and computes dn/dr and $dn/d\theta$ at this point (using linear interpolation between the points on the N-grid). The value for ϕ at this new point is computed by assuming that the raypath is a smooth curve, which implies that the new value of ρ to be computed at this point will pass through the center of curvature for the previous value of ρ (see Fig. 60). This leads to

$$\phi_n = \phi_{n-1} + \left(1 - \frac{r_n}{\rho_{n-1}} \sec \phi_{n-1}\right)\Delta\theta \qquad (C.7)$$

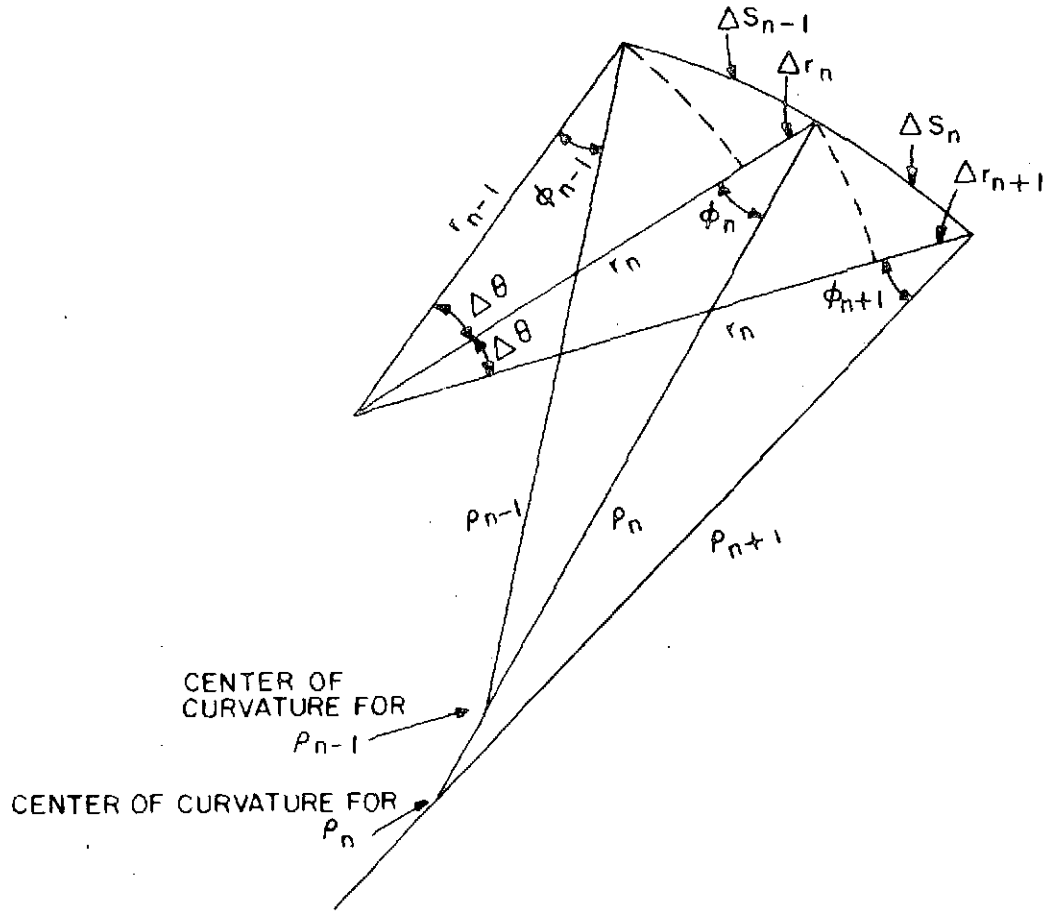

Fig. 60. RELATIONSHIP OF ϕ, ρ, $\Delta\theta$, r, AND Δr. Note ρ_n and ρ_{n+1} pass through the same center of curvature.

The value of ρ_{n+1} is calculated from (C.5) for the next step. The incremental path length ΔS_n is given by

$$\Delta S_n = r_n \Delta\theta \sec \phi_n \tag{C.8}$$

and the incremental path deviation ΔC_n is given by

$$\Delta C_n = \Delta S_n [1 - \cos (\theta_n - \phi_n)] \tag{C.9}$$

Finally, the new value of Δr_{n+1} is calculated from

$$\Delta r_{n+1} = r_n \Delta\theta \tan \phi_n \qquad (C.10)$$

and, using $r_{n+1} = r_n + \Delta r_{n+1}$ and $\theta_{n+1} = \theta_n + \Delta\theta$, the program begins the new iteration.

These equations are derived in the next section.

2. Derivation of RAYTRACE Equations

Derivation of the first-step equation [Eq. (C.6)].

In the beginning, $\theta_o = \phi_o = 0$, and $\vec{\rho}$ lies along $\vec{r}$:

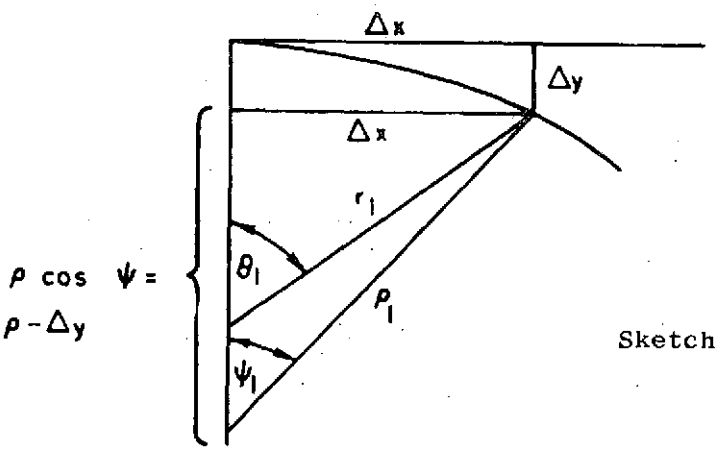

Sketch 1

Because θ_1 and ψ_1 are very small,

$$\Delta x = r_1\theta_1 = \rho_1\psi_1 \qquad (C.11)$$

and

$$\Delta y = \rho_1 - \rho_1 \cos \psi_1 = \rho_1(1 - \cos \psi_1)$$

Because ψ_1 is also very small, $\cos \psi_1 \approx 1 - (\psi_1^2/2)$, therefore,

$$\Delta y \cong \rho_1 \frac{\psi_1^2}{2}$$

Now,

$$\Delta x = (\rho_1 - \Delta y) \tan \psi_1$$

$$\Delta x \doteq \left(\rho_1 - \frac{\rho_1 \psi_1^2}{2}\right) \tan \psi_1 = \rho_1 \left(1 - \frac{\psi_1^2}{2}\right) \tan \psi_1$$

$$\Delta x \doteq \rho_1 \cos \psi_1 \tan \psi_1 = \rho_1 \sin \psi_1$$

so

$$\Delta x \doteq \rho_1 \psi_1$$

and

$$\frac{\Delta y}{\Delta x} \doteq \frac{\psi_1}{2}$$

Now, if $\Delta y = \Delta x(\psi_1/2)$, then from Eq. (C.11),

$$\Delta y = \frac{r_1 \theta_1}{2\rho_1} \Delta x = \frac{r_1^2 \theta_1^2}{2\rho_1}$$

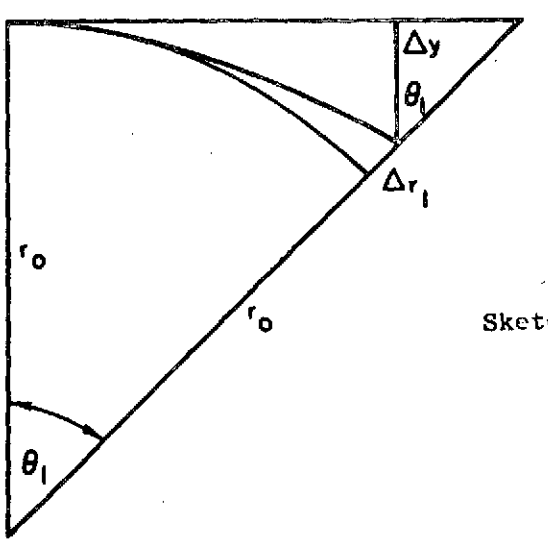

Sketch 2

As a result,

$$\frac{\Delta y}{\cos \theta_1} + \Delta r_1 + r_1 = \frac{r_1}{\cos \theta_1}$$

$$\Delta r_1 = \frac{r_1}{\cos \theta_1} - r_1 - \frac{\Delta y}{\cos \theta_1}$$

$$\Delta r_1 \doteq r_1 \left(\frac{\theta_1^2}{2} \right) - \frac{r_1^2 \theta_1^2}{2\rho_1}$$

Because $\theta_1 = \Delta\theta$,

$$\Delta r_1 \doteq \frac{r_1 (\Delta\theta)^2}{2} \left(1 - \frac{r_1}{\rho_1} \right)$$

which is Eq. (C.6).

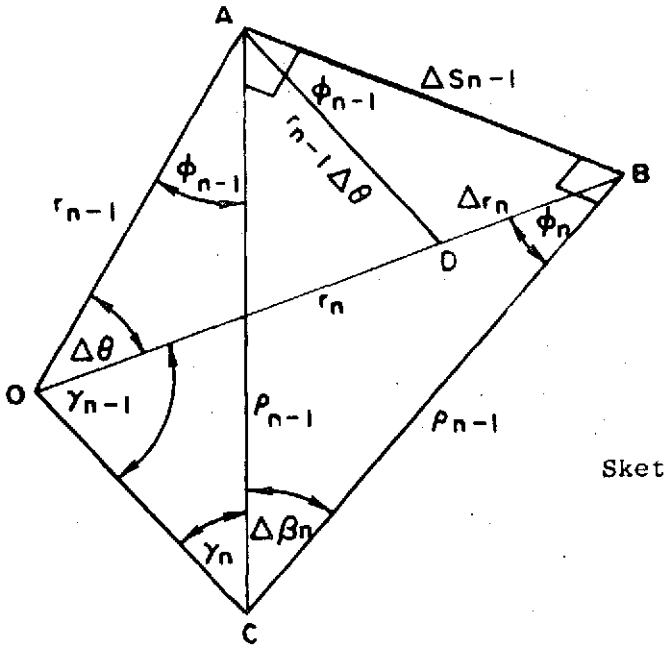

Sketch 3

Equation (C.10) is derived directly from Sketch 3:

$$\Delta r_n = r_{n-1} \tan \phi_{n-1} \Delta\theta$$

Equation (C.9) is derived using

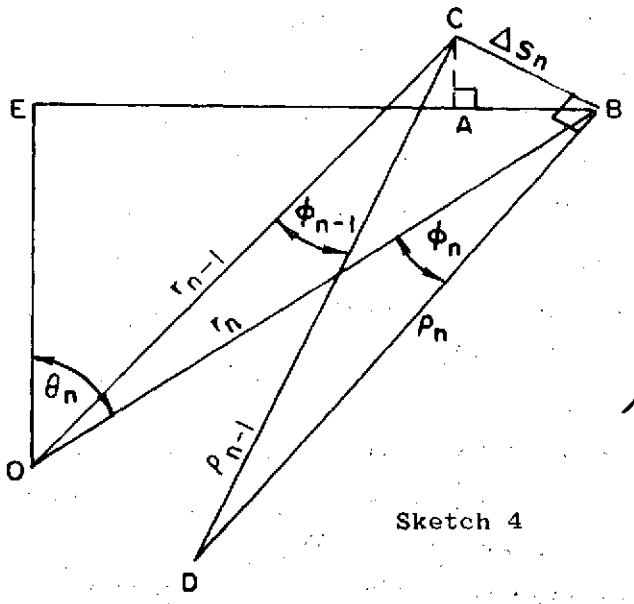

Sketch 4

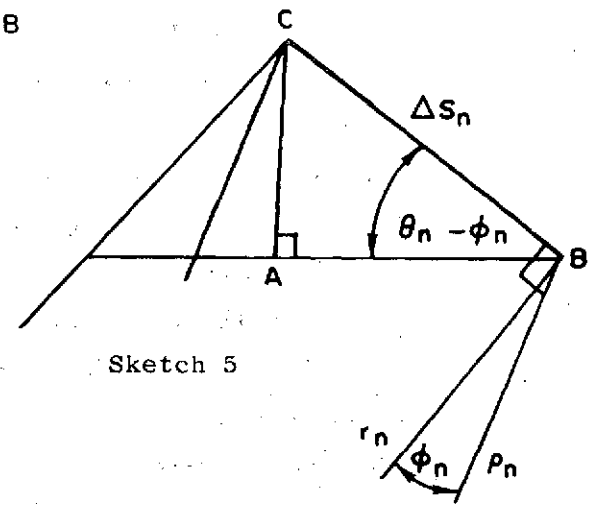

Sketch 5

The quantity ΔC_n represents the difference between ΔS_n and the length $\overline{AB}$ which can be found as follows. The angle OBE is given by $90° - \theta_n$. Because OBD = ϕ_n and CBD = 90°, by simple arithmetic ABC = $\theta_n - \phi_n$. Thus,

$$\overline{AB} = \Delta S_n \cos (\theta_n - \phi_n)$$

and

$$\Delta C_n = \Delta S_n \left[1 - \cos (\theta_n - \phi_n)\right]$$

which is Eq. (C.9).

3. Description of THRUWAY

THRUWAY is a program that traces a raypath between two satellites in Earth occultation configuration. It differs from its predecessor RAYTRACE in that it begins the raypath at one satellite, follows it through space to the atmosphere, traces the path through the atmosphere, and then out to the second satellite. RAYTRACE began at what was arbitrarily designated the center of the raypath, at a specific altitude. It traced the raypath in one direction to satellite altitude, returned to start, and then traced the raypath in the opposite direction out to satellite altitude. The intersections of the satellite orbit with the raypath gave the satellite location that would result in a raypath with that specific starting altitude. By starting the ray at different altitudes, it was possible to interpolate the results to find the characteristics (phase defect, bending angle, minimum altitude) of a raypath for a given satellite separation.

THRUWAY does the same job, but a bit differently. In RAYTRACE, the independent parameter is the minimum ray altitude; in THRUWAY, the independent parameter is the starting angle of the ray. A ray is "launched" at a particular starting angle, and its path is traced to and through the atmosphere and out to satellite altitude again. The straight-line distance between the starting point and the intersection of the ray and the satellite orbit is designated satellite separation (SS). The starting angle is then stepped 1 mrad, a new path is calculated, and the derivative $d(SS)/d\alpha$ is calculated (where α is the starting angle). This derivative is then used in an iteration scheme to calculate the correct starting angle:

$$\alpha_{n+1} = \frac{d\alpha}{d(SS)} (SS_{true} - SS_n) + \alpha_n$$

Iteration continues until the error term $SS_{true} - SS_n$ is acceptably small.

The advantage of THRUWAY is that it is no longer necessary to stipulate that the center of the raypath must coincide with the center of the available data set. The satellites can be positioned anywhere,

and the resultant ray will be traced regardless of where the minimum altitude of the path may fall.

A program such as THRUWAY became desirable with the acquisition of the Hawaii data. With such a data set, it is unrealistic to arbitrarily define the center of the raypath as the center of the profile; in fact, the information for which we were searching might be masked entirely by such an assumption. Thus, a program which could start at a well-defined transmitter and trace its way through to a well-defined receiver was required. THRUWAY was developed to meet this need.

Two forms of THRUWAY exist. One version (called HAWAII) is used on the XDS Sigma-5 computer to raytrace mountain-to-mountain through the Hawaii data. In addition to raytracing, this program also computes power densities at the receiver distance, draws plots of index of refraction, power, and phase at the receiver distance, and traces the raypaths themselves. The second version raytraces from satellite-to-satellite through the same low-resolution atmosphere as does RAYTRACE, with high-resolution Hawaii data superimposed at the lower altitudes.

4. Mathematics of THRUWAY

All of THRUWAY is divided into three parts (Fig. 61):

(a) the section of raypath between the transmitting satellite and the upper edge of the atmosphere

(b) the portion of the raypath actually in the atmosphere

(c) the path traversed by the ray on its way to the receiver after it has left the atmosphere.

In the first and third sections of the raypath, the ray travels in a straight line at the speed of light in a vacuum. The ray slows down or bends only in the second portion of the path.

Because the raypath in (a) is a straight line, no real "raytracing" is involved. One begins at a given position in space, say (r_s, θ_s), and launches a ray at a starting angle α which is the angle between the tangent to the satellite orbit at (r_s, θ_s) and the raypath. The problem is then to determine at what point (r_o, θ_o) does the ray encounter

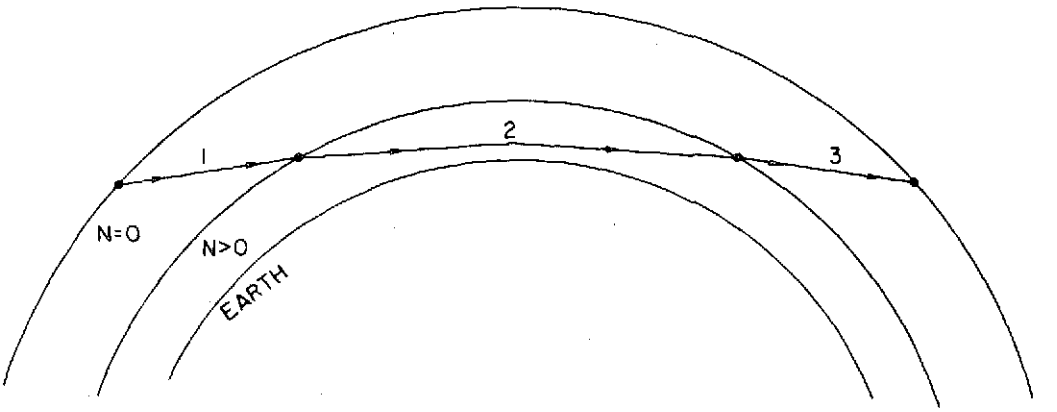

Fig. 61. THE THREE PORTIONS OF THRUWAY. Portions 1 and 3 are straight-line segments that lie outside the atmosphere. Portion 2 is within the atmosphere, where the refractivity is greater than zero.

the atmosphere and what is the initial radius of curvature vector $(\rho, \emptyset)$ at that point. These are the initial values for the actual raytracing procedure of part two of the raypath. In addition, although the ray does not actually bend while it is in free space, it does acquire "bending" which is defined as the excess path length caused by the raypath being longer than a straight-line path between the satellites. These parameters are illustrated in Fig. 62, and the equations relating them are derived in Section 5.

In (b), the ray is in the atmosphere, and THRUWAY, like RAYTRACE, uses Snell's Law to raytrace through the atmosphere. Snell's Law can be written as [5]

$$\frac{\lambda}{\rho} = \frac{d\lambda}{d\rho}$$

where λ is the wavelength in the atmosphere and ρ is the radius of curvature of the raypath. For this portion of the program, therefore, THRUWAY uses essentially the same equations as does RAYTRACE. The difference lies in how the parameters are initialized. The important parameters for raytracing using Snell's Law are

r, θ = position coordinates of the ray

ρ = radius of curvature

ϕ = angle between the radius of curvature vector and the position vector

The origin of the coordinate system is the center of the Earth.

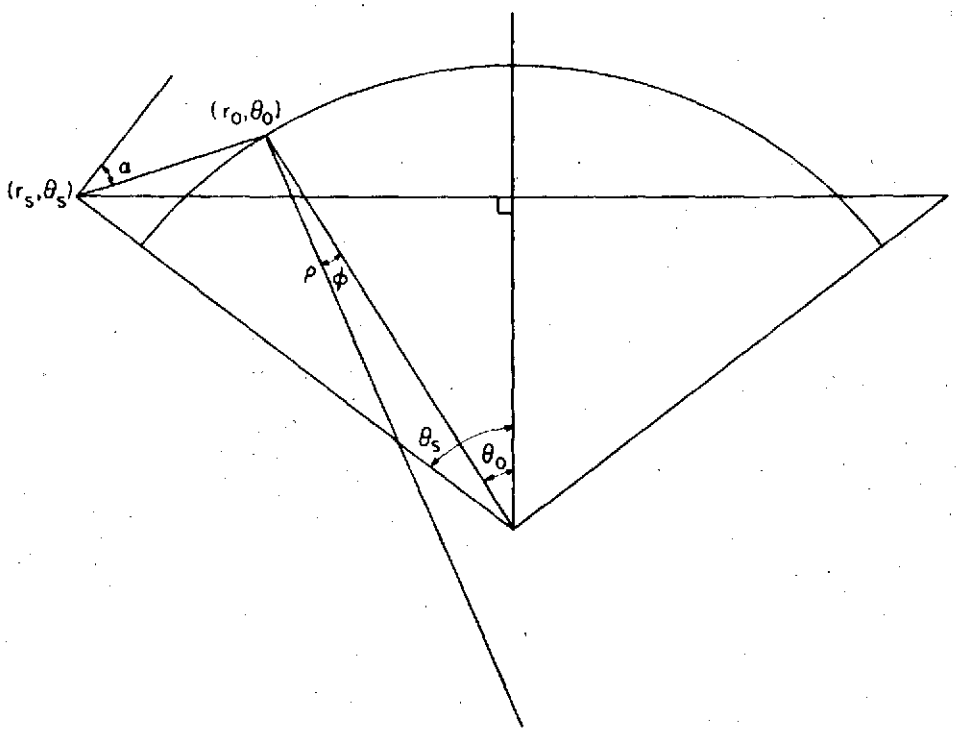

Fig. 62. SIGNIFICANT PARAMETERS OF THRUWAY.

In RAYTRACE, initializing these parameters is not difficult. Because the starting position of the ray is an independent parameter, r and θ are determined immediately. Similarly, because the ray is constrained to start out horizontally, the angle between the radius of curvature vector and the position vector is zero ($\phi = 0$). The radius of curvature is computed immediately by use of Eq. (C.5). Although the actual initialization of parameters poses no problems, the first step in the raytracing does. It is necessary to go to a second-order approximation for Δr because the first-order expression used to compute Δr along the raypath yields a value of zero if $\phi = 0$.

In both RAYTRACE and THRUWAY, the independent parameter in the raytracing is the coordinate θ, and $\Delta\theta$ is set to some constant value (usually 0.5 mrad). Because of this finite step size, THRUWAY does not have to use second-order approximations for Δr, unless, of course, the ray enters the atmosphere at a value of θ which is an integer multiple of the step size; this is an extremely remote possibility.

In (c), the raypath is the segment between the edge of the atmosphere and the receiving satellite. As in (a), the ray travels in a straight line, and one must determine how much bending is accumulated as the ray approaches satellite altitude. This segment of the program is identical to the corresponding segment of RAYTRACE.

5. Derivation of THRUWAY Equations

The equation relating r_s, θ_s, r_o, θ_o, ρ, and ϕ, and the expression for bending in part one of the raypath, can be derived from Fig. 63, which is a segment of Fig. 62.

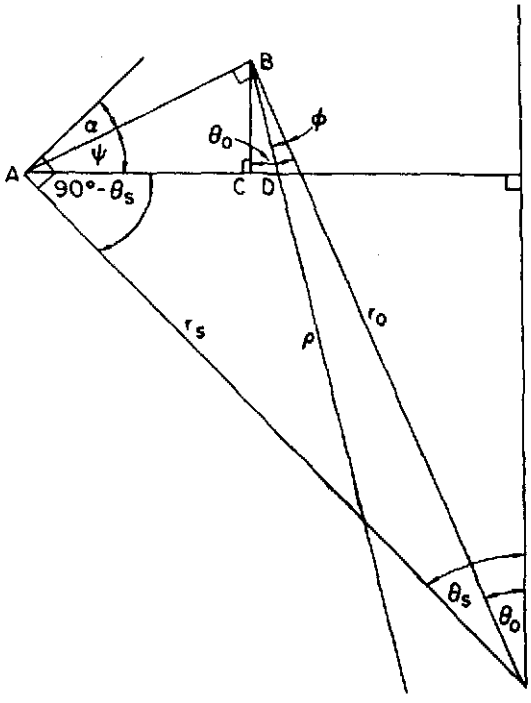

Fig. 63. A SEGMENT OF FIG. 62, SHOWING THE PARAMETERS IN GREATER DETAIL.

It is useful to establish a relationship between θ_o, ϕ, and ψ (which is the angle between the raypath and the line connecting the satellites). From Fig. 63,

$$\measuredangle \text{CBD} = \theta_o - \phi$$

$$\measuredangle \text{ABD} = 90°$$

Now,

$$\measuredangle \text{ABC} = \measuredangle \text{ABD} - \measuredangle \text{CBD}$$

so

$$\measuredangle \text{ABC} = 90° - \theta_o + \phi$$

Because

$$\psi = 90° - \measuredangle \text{ABC}$$

we have

$$\psi = \theta_o - \phi \qquad \text{(C.12)}$$

Also,

$$\alpha = 90° - (90° - \theta_s) - \psi$$

or

$$\alpha = \theta_s - \psi \qquad \text{(C.13)}$$

Now, from the law of sines,

$$\frac{r_o}{r_s} = \frac{\sin (90° - \theta_s + \psi)}{\sin (90° + \phi)}$$

or

$$\sin (90° + \phi) = \frac{r_s}{r_o} \sin \left[90° - (\theta_s - \psi)\right]$$

$$\sin (90° + \phi) = \frac{r_s}{r_o} \cos (\theta_s - \psi)$$

where

$$90^\circ + \phi = \sin^{-1}\left[\frac{r_s}{r_o}\cos\ (\theta_s - \psi)\right]$$

Because

$$\alpha = \theta_s - \psi \tag{C.14}$$

and

$$\phi = \theta_o - \psi \tag{C.15}$$

we have

$$90^\circ + \theta_o - \psi = \sin^{-1}\left(\frac{r_s}{r_o}\cos\ \alpha\right)$$

or

$$\theta_o = -90^\circ + \psi + \sin^{-1}\left(\frac{r_s}{r_o}\cos\ \alpha\right)$$

where r_s is the satellite altitude, r_o is the altitude of the upper layer of the atmosphere, α is the "bending angle" or "starting angle" of the ray, and ψ is given by Eq. (C.2).

REFERENCES

1. SPINMAP Final Report, School of Engineering, Stanford University, Stanford, Calif., 1966.

2. G. Fjeldbo and V. R. Eshleman, "The Atmosphere of Mars Analyzed by Integral Inversion of the Mariner IV Occultation Data," Planetary and Space Science, 16, 1968, pp. 1035-1059.

3. J. C. Pomalaza, "Remote Sensing of the Atmosphere by Occultation Satellites," TR No. 3670-1, Stanford Electronics Laboratories, Stanford University, Stanford, Calif., 1969.

4. B. R. Bean and E. J. Dutton, Radio Meteorology, National Bureau of Standards Monograph 92, Washington, D. C., 1966.

5. N. F. Mott, Elements of Wave Mechanics, Cambridge University Press, Cambridge University, 1960, pp. 11-12.

6. A. R. Morrison, private communication.

7. William Smith, private communication.

8. M. C. Thompson, Jr., H. B. Janes, L. E. Wood, and D. Smith, "Phase and Amplitude Scintillations of Microwave Signals over an Elevated Atmospheric Path," U. S. Department of Commerce, Office of Telecommunications, Institute for Telecommunication Sciences, Boulder, Colo., May 1971.

9. U. S. Standard Atmosphere Supplements, 1966, United States Committee on Extension to the U. S. Standard Atmosphere, Washington, D.C., 1966.

10. D. C. Hutcherson, "Water Vapor in the Atmosphere," Humidity and Moisture, 2, 1965, pp. 486-494.

11. M. Born and E. Wolf, Principles of Optics, Pergamon Press, Oxford, 1965, p. 128.

12. W. G. Tank, "An On-Board Technique for Estimating the Effect of Water Vapor in Radio Occultation Measurements of Atmospheric Density," J. Geophys. Res., Space Physics, 74, 16, Aug 1969, pp. 4147-4156.

13. J. Pirraglia and S. H. Gross, "Latitudinal and Longitudinal Variation of a Planetary Atmosphere and the Occultation Experiment," Planetary and Space Science, 18, 1970, pp. 1769-1784.